AD NUMBER
ADB008209
LIMITATION CHANGES

TO:

Approved for public release; distribution is unlimited.

FROM:

Distribution authorized to U.S. Gov't. agencies only; Test and Evaluation; DEC 1975. Other requests shall be referred to Air Force Armament Lab., Eglin AFB, FL 32542.

AUTHORITY

USADTC ltr, 21 May 1979

MAGNUS AND ROLL-DAMPING CHARACTERISTICS OF THE FIXED-FIN AND INFLATABLE STABILIZER RETARDER CONFIGURATIONS OF THE MK-82 STORE AT TRANSONIC SPEEDS

PROPULSION WIND TUNNEL FACILITY
ARNOLD ENGINEERING DEVELOPMENT CENTER
AIR FORCE SYSTEMS COMMAND
ARNOLD AIR FORCE STATION, TENNESSEE 37389

December 1975

Final Report for Period May 21 — 27, 1975

TECHNICAL REPORTS
FILE COPY

Air Force
AEDC LIBRARY
F40600-75-C-0001

Prepared for

AIR FORCE ARMAMENT LABORATORY (DLJC)
EGLIN AFB, FLORIDA 32542

NOTICES

When U. S. Government drawings specifications, or other data are used for any purpose other than a definitely related Government procurement operation, the Government thereby incurs no responsibility nor any obligation whatsoever, and the fact that the Government may have formulated, furnished, or in any way supplied the said drawings, specifications, or other data, is not to be regarded by implication or otherwise, or in any manner licensing the holder or any other person or corporation, or conveying any rights or permission to manufacture, use, or sell any patented invention that may in any way be related thereto.
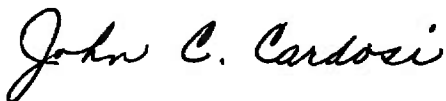
Qualified users may obtain copies of this report from the Defense Documentation Center.

References to named commercial products in this report are not to be considered in any sense as an endorsement of the product by the United States Air Force or the Government.

APPROVAL STATEMENT

This technical report has been reviewed and is approved for publication.

FOR THE COMMANDER

JOHN C. CARDOSI
Lt Colonel, USAF
Chief Air Force Test Director, PWT
Directorate of Test

CRAIG E. MAHAFFY
Colonel, USAF
Director of Test

REPORT DOCUMENTATION PAGE		READ INSTRUCTIONS BEFORE COMPLETING FORM
1 REPORT NUMBER AEDC-TR-75-163 AFATL-TR-75-159	2 GOVT ACCESSION NO.	3. RECIPIENT'S CATALOG NUMBER
4 TITLE (and Subtitle) MAGNUS AND ROLL-DAMPING CHARACTERISTICS OF THE FIXED-FIN AND INFLATABLE STABILIZER RETARDER CONFIGURATIONS OF THE MK-82 STORE AT TRANSONIC SPEEDS		5 TYPE OF REPORT & PERIOD COVERED Final Report- May 21 - 27, 1975
		6 PERFORMING ORG. REPORT NUMBER
7 AUTHOR(s) A. R. Wallace and T. O. Shadow, ARO, Inc.		8 CONTRACT OR GRANT NUMBER(s)
9 PERFORMING ORGANIZATION NAME AND ADDRESS Arnold Engineering Development Center (XO) Arnold Air Force Station, Tennessee 37389		10. PROGRAM ELEMENT, PROJECT, TASK AREA & WORK UNIT NUMBERS Program Element 64602F Project 5613-02
11. CONTROLLING OFFICE NAME AND ADDRESS Air Force Armament Laboratory (DLJC) Eglin AFB, Florida 32542		12. REPORT DATE December 1975
		13. NUMBER OF PAGES 140
14 MONITORING AGENCY NAME & ADDRESS(if different from Controlling Office)		15 SECURITY CLASS. (of this report) UNCLASSIFIED
		15a. DECLASSIFICATION/DOWNGRADING SCHEDULE N/A

16 DISTRIBUTION STATEMENT (of this Report)

Distribution limited to U.S. Government agencies only; this report contains information on test and evaluation of military hardware; December 1975; other requests for this document must be referred to Air Force Armament Laboratory (DLJC), Eglin AFB, Florida 32542.

17. DISTRIBUTION STATEMENT (of the abstract entered in Block 20, if different from Report)

1. Magnus force
2. Store - roll damping
3. Magnus force

18 SUPPLEMENTARY NOTES

Available in DDC

19 KEY WORDS (Continue on reverse side if necessary and identify by block number)

Magnus	flaps (control surfaces)	store
damping	stabilizer (inflatable)	transonic flow
roll	retarder fins	
characteristics	MK-82	

20 ABSTRACT (Continue on reverse side if necessary and identify by block number)

Wind tunnel tests to measure the Magnus and roll-damping characteristics of a bomb shape, which is a candidate for replacement of the MK-82 Snakeye Bomb, were conducted at Mach numbers from 0.4 to 1.3 and Reynolds numbers, based on model diameter from 0.54×10^6 to 1.0×10^6. Two basic fin configurations, the fixed fin (FF) and the inflatable stabilizer retarder with extender (ISRE), were tested with and without wedge-shaped tabs and slots.

DD $\underset{1 \text{ JAN } 73}{\text{FORM}}$ 1473 EDITION OF 1 NOV 65 IS OBSOLETE

20. ABSTRACT (Continued)

The Magnus coefficients for all configurations were often nonlinear
with spin rate, particularly at Mach number 0.4 and the larger
roll rates, and were very nonlinear at the higher angles of attack
(α) where the magnitude of the Magnus coefficient derivatives
increased greatly with α.   The roll-damping characteristics were
mostly linear except for the FF configuration at Mach number 0.4.
The ISRE configuration, because of its larger fin area and span,
produced over twice the damping and static rolling moment as did
the FF configuration.

AFSC
Arnold AFB Tenn

PREFACE

The work reported herein was conducted by the Arnold Engineering Development Center (AEDC), Air Force Systems Command (AFSC), for the Air Force Armament Laboratory (AFATL), AFSC, under Program Element 64602F, Project 5613-02. The AFATL project monitor was Mr. Paul D. Shirey. The results presented herein were obtained by ARO, Inc. (a subsidiary of Sverdrup & Parcel and Associates, Inc.), contract operator of AEDC, AFSC, Arnold Air Force Station, Tennessee. The tests were conducted under ARO Project No. P41C-86A. The authors of this report were A. R. Wallace and T. O. Shadow, ARO, Inc. The final data package was completed on July 25, .1975, and the manuscript (ARO Control No. ARO-VKF-TR-75-146) was submitted for publication on September 25, 1975.

CONTENTS

ILLUSTRATIONS

Figure | Page

TABLE

1.0 INTRODUCTION

This test was conducted as part of the Inflatable Retarder Development Program for the Air Force Armament Laboratory (AFATL), Eglin Air Force Base, Florida and the Naval Surface Weapons Center (NSWC), Dahlgren, Virginia. The tests were conducted in the Aerodynamic Wind Tunnel (4T), Propulsion Wind Tunnel Facility (PWT) to determine the Magnus and roll-damping characteristics of two basic fin configurations of a bomb which is a candidate for replacement of the MK-82 Snakeye. Both fin configurations were tested with and without slots and wedge-shaped tabs. The static stability and pitch-damping tests are reported in Reference 1.

The Mach number ranged from 0.4 to 1.3. The tunnel stagnation pressure was maintained at 1,200 psfa resulting in Reynolds numbers based on model diameter from 0.54×10^6 for $M_\infty = 0.4$ to 1.0×10^6 for the supersonic Mach numbers. The angle of attack was varied from -2 to 26 deg, and the spin parameter ($pd/2V_\infty$) ranged from zero to 0.16 radians.

2.0 APPARATUS

2.1 WIND TUNNEL

The PWT Aerodynamic Wind Tunnel (4T), Tunnel 4T, is a closed-circuit, continuous flow, variable density tunnel capable of being operated at Mach numbers from 0.1 to 1.3. At all Mach numbers, the stagnation pressure can be varied from about 290 to 3,700 psfa. The test section is 48 in. square and 150 in. long with perforated, variable porosity (0 to 10 percent) walls that can be diverged or converged (±0.5 deg). The test section is completely enclosed in a plenum chamber from which the air can be evacuated, allowing part of the tunnel airflow to be removed through the perforated walls of the test section. This design allows control of wave attenuation and blockage effects. A schematic of the test section with model and balance installed is shown in Fig. 1. Additional information concerning this tunnel may be found in Ref. 2.

2.2 MODEL

Two basic 0.442-scale models (Fig. 2) using the same forebody were tested. Forebody ordinates are given in Fig. 2c. The FF (fixed fin) configuration has four fins on a cylindrical afterbody and is shown in Fig. 2a. The ISRE (inflatable stabilizer retarder with extender) configuration has eight fins on a flared afterbody and is shown in Fig. 2b. A second set of fins for each model had a large single slot in each fin (denoted by s following the basic configuration code). For some runs, small wedges (W1 or W2) were attached to each fin, causing the model to autorotate. Table 1 lists the configurations tested.

9

The model was made of aluminum alloy and was anodized to harden the surface. It was statically and dynamically balanced about the spin axis. The model was built at AEDC to fit the existing VKF Magnus-force test mechanism. A photograph of the ISRE model mounted in the wind tunnel is shown in Fig. 3.

2.3 TEST MECHANISM

Basically, the Magnus-force test mechanism is a sting-mounted, four-component, internal balance surrounded by a shell which is supported by ball bearings that allow the model to spin freely about its longitudinal axis (Fig. 4). A two-stage, air-driven turbine is mounted inside the model mounting shell at a fixed axial position near the forward end of the sting. The turbine is used to spin the model to some desired speed and then is disengaged with an air-operated sliding clutch to allow the model to spin freely on the ball bearings. It is estimated that the turbine will produce a starting torque of 50 in.-lb and develop a torque of approximately 100 in.-lb while spinning. The mechanism is designed to operate under normal-force loads up to 500 lb, axial-force loads of 125 lbs, and for a maximum spin rate of approximately 25,000 rpm; however, a spin rate of approximately 4,000 rpm was adequate for the present test. An air-operated brake is also incorporated to stop the model or restrict the spin rate.

2.4 INSTRUMENTATION AND PRECISION

Tunnel 4T stilling chamber pressure was measured with a mercury column Ideal manometer. The precision of this manometer is estimated to be ±0.1 percent of the measured pressure for the pressure range used in this test. The stilling chamber temperature was measured with a Chromel®-Alumel® thermocouple to a precision of ±2.2°R, based on the thermocouple wire manufacturer's specification.

The roll position and rate are measured by the tachometer system (Fig. 4) which is internal to the mechanism and is composed of a small light reflection transducer mounted close to a segmented ring of 30 bright and 30 dark strips. Light from an infrared emitting diode impinges on the segmented ring and reflects back to a phototransistor. The resulting pulses are counted electronically to give roll angle and roll rate. The tachometer system could measure the roll angle with a precision of ±3 deg.

The VKF moment-type, strain-gage balance (Fig. 5) was specially designed for Magnus type tests. Small outrigger side beams of the balance, with semiconductor strain gages, were used to obtain the sensitivity required to measure small side loads while maintaining adequate balance stiffness for the larger pitch loads. When a yawing moment is imposed on the balance, secondary bending moments are induced in the side beams. Thus, the outrigger beams act as mechanical amplifiers, and a normal-force to side-force ratio of 20 is possible for a 500-lb normal-force loading.

The balance was calibrated at PWT prior to the test. Static loads in each plane were applied to the balance to simulate the range of loads and center-of-pressure locations anticipated during the test. The following uncertainties represent the bands of 95 percent of the measurement residuals, based on differences between the applied loads and the corresonding values calculated from the balance calibration equations included in the final data reduction. The range of check loads and the measurement uncertainties follow.

Component	Balance Design Loads	Range of Check Loads	Measurement Uncertainty
Normal force, lb	500	400	0.12
Pitching moment,* in.-lb	2,500	915	0.52
Side force, lb	50	30	0.09
Yawing moment,* in.-lb	250	138	0.18

*About balance center

The transfer distances from the balance center to the model moment reference location were 6.84 in. for the FF configurations, 7.90 in. for the ISRE configurations along the longitudinal axis, zero inches along the vertical axis, and were measured with an estimated precision of ±0.005 in.

3.0 PROCEDURE

3.1 TEST CONDITIONS

The test Mach number was varied from 0.4 to 1.3 while the stagnation conditions were kept nearly constant at a pressure of 1,200 psfa and a temperature of 560°R. The resulting free-stream conditions are as follows:

M_∞	T_∞, °R	p_∞, lb/ft²	q_∞, lb/ft²	V_∞, ft/sec	Re_d x 10⁻⁶
0.4	545	1,075	120.4	457	0.54
0.8	496	787	352.7	873	0.89
0.9	482	709	402.2	968	0.94
1.0	467	634	443.8	1,058	0.97
1.1	451	562	476.0	1,144	0.99
1.2	435	495	498.8	1,226	1.00
1.3	419	433	512.4	1,303	1.00

A test summary, showing all configurations tested and the variables for each, is presented in Table 1.

3.2 TEST PROCEDURE

For the symmetrical model configurations (no wedges on the fins) the model was spun with the turbine. Upon reaching about 4,000 rpm, the turbine air pressure was cut off and the clutch disengaged allowing the model to spin freely and the spin rate to decay toward zero. The roll angle and roll rate were continuously recorded from which the roll damping was calculated. At the same time, four-component (C_N, C_m, C_Y, and C_n) force data were taken.

For the unsymmetrical model configurations (wedges W1 or W2 attached to fins) the model brake was applied at first to keep the model from spinning. The brake was released, and the model was allowed to spin up close to steady-state roll rate. As before, roll rate and four-component data were taken. The model was stopped so the clutch could be engaged, and the model was spun by the turbine to about 2,000 rpm above steady-state roll rate (roll direction was always positive). The clutch was disengaged and the turbine air cut off, permitting the model to spin down freely to near steady-state speed as data were taken. Sometimes, at high angles of attack (>20 deg), the model would not start spinning, while at other times it would oscillate in roll for a while before starting to spin.

The data-taking time was preset to various intervals (from 6 to 30 sec), and 500 data points were taken during this time unless terminated manually, which was occasionally done to avoid an excess of data points near steady-state speed. An excess of data points near steady-state speeds causes the curve fit to be unduly weighted at this end of the data. Most of the data were computed, tabulated, and plotted online so that the quality of data could be continuously monitored.

3.3 DATA REDUCTION

The four-component balance data were reduced to coefficients (C_N, C_m, C_Y, and C_n) by the standard force program used for static force tests. Corrections were made for balance interactions and for sting deflections. Moments are transferred to the moment reference points shown in Fig. 2.

The roll angle versus time data were reduced to roll-damping coefficients as follows. The one-degree-of-freedom roll equation for a model and bearing system can be written as

$$I_x p - L_p p - L_o = 0 \qquad (1)$$

where

$$L_p = L_{p_a} + L_{p_v}$$

$$L_o = L_{o_a} + L_{o_v}$$

The solution of the above equation, assuming constant coefficients, with the boundary condition, $p = p_i$ at $t = 0$, is

$$p = \frac{d\phi}{dt} = \left(p_i + \frac{L_o}{L_p} \right) e^{[L_p t/I_x]} - \left(\frac{L_o}{L_p} \right) \qquad (2)$$

Integrating Eq. (2) with the boundary condition, $\phi = \phi_i$ at $t = 0$, gives

$$\phi = \left[\frac{I_x p_i}{L_p} + \frac{I_x L_o}{L_p^2} \right] \left[e^{(L_p t/I_x)} - 1 \right] - \left(\frac{L_o}{L_p} \right) t + \phi_i \qquad (3)$$

Equation (3) was curve fitted to 500 samples of (ϕ, t) data using a least squares, differential correction technique to determine L_o and L_p. Bearing tares obtained under vacuum conditions were determined before and after the test. L_{o_v} was insignificant; hence, the following tare values were used to reduce the data:

$$L_{o_v} = 0$$

$$L_{p_v} = -0.0003 \; \frac{\text{ft-lb-sec}}{\text{radian}}$$

Coefficients were calculated as follows:

$$C_{\ell_p} = L_{p_a} (2V_\infty/q \; Ad^2)$$

$$C_{\ell_o} = L_{o_a}/q \; Ad$$

$$(pd/2V_\infty)_s = -C_{\ell_o}/C_{\ell_p}$$

In some cases, the data were found to be nonlinear with p; hence, the assumption of constant coefficients (L_p and L_o) is not valid. For this condition the total rolling moment, L, was calculated directly from Eq. (1).

$$L = L_o + L_p \; p = I_x \dot{p}$$

The roll rate versus time data is differentiated to obtain $\dot{p}$ as a function of time. This method gives an L_o (where $p = 0$) and a p_{ss} (where $\dot{p} = 0$) and variation of L with p which may or may not be linear (L_p is a function of p). Bearing tares are removed and the resulting total aerodynamic rolling moment converted to coefficient form is

$$C_\ell = \frac{I_x \dot{p} - L_{p_v} p}{q_\infty \; Ad}$$

3.4 DATA UNCERTAINTY

An evaluation of the influence of random measurement errors is presented in this section to provide a partial measure of the uncertainty of the final test results presented in this report. Although evaluation of the systematic measurement error (bias) is not included, it should be noted that the instrumentation precision values (given in Section 2.3) used in this evaluation represent a total uncertainty combination of both systematic and two-sigma random error contributions.

3.4.1 Test Conditions

Uncertainties in the basic tunnel parameters p_o and T_o (see Section 2.3) and the two-sigma deviation in Mach number determined from test section flow calibrations were used to estimate uncertainties in the other free-stream properties, using the Taylor series method of error propagation.

M_∞	Uncertainty (±), percent						
	M_∞	p_o	T_o	p_∞	q_∞	Re_d	V_∞
0.4	0.58	0.1	0.39	0.161	1.039	0.713	0.595
0.8	0.32			0.273	0.399	0.539	0.345
0.9	0.34			0.347	0.362	0.534	0.352
1.0	0.40			0.477	0.348	0.531	0.387
1.1	0.55			0.757	0.364	0.529	0.484
1.2	0.77			1.209	0.349	0.526	0.629
1.3	1.44			2.018	0.282	0.541	0.874

3.4.2 Test Data

The data are presented in the body-axis system. Pitching and yawing moments are referenced to a point 45.850 percent of the model length from the model nose for the FF configurations and 43.216 percent of the model length from the model nose for the ISRE configurations.

The balance uncertainties listed in Section 2.3 were combined with uncertainties in the tunnel parameters, using the Taylor series method of error propagation, to estimate the uncertainty of the aerodynamic coefficients, and these are presented below.

Coefficient Precision, Uncertainty (±)

Configu-ration	M_∞	a	C_N	C_m	C_Y	C_n	C_l	$(pd/2V_\infty)_x$
F1	0.4	0	0.0081	0.0138	0.0061	0 0091	0 001	0.0004
	0.4	25	0.0423	0 0440	0.0139	0.0325	↓	↓
	0.8	0	0 0028	0 0047	0 0021	0.0031		0.0002
	0.8	25	0.0162	0.0172	0.0030	0.0064		
	0.9	0	0.0024	0.0041	0 0018	0.0027		
	0.9	25	0.0147	0.0157	0.0027	0 0058		
	1.0	0	0.0022	0.0037	0.0016	0.0025		
	1.0	25	0.0141	0.0150	0.006	0.0055		
	1 1	0	0.0020	0.0035	0.0015	0.0023		
	1.1	25	0.0147	0.0156	0.0026	0.0056		
	1.2	0	0.0020	0.0033	0.0015	0.0022		
	1.2	25	0.0141	0.0150	0.0024	0 0054		
	1.3	0	0.0019	0.0032	0.0014	0.0021		
	1.3	25	0.0115	0.0125	0.0021	0.0045	↓	↓
ISRE	0.4	0	0.0081	0.0154	0.0061	0.0104	0.003	0 0004
	0.4	25	0.0526	0.1031	0.0139	0 0329	↓	↓
	0.8	0	0.0028	0 0052	0.0021	0.0036		0.0002
	0.8	25	0.0201	0.0398	0 0029	0.0054		
	0.9	0	0.0024	0.0046	0.0018	0.0031		
	0.9	25	0.0183	0.0362	0.0026	0.048		
	1.0	0	0.0022	0.0042	0 0016	0.0028		
	1.0	25	0.0175	0.0348	0.0024	0 0045		
	1.1	0	0 0020	0.0039	0.0015	0.0026		
	1.1	25	0.0183	0.0363	0.0024	0.0045		
	1.2	0	0.0020	0.0037	0.0015	0.0025		
	1.2	25	0.0176	0.0348	0.0023	0.0043		
	1.3	0	0.0019	0.0036	0.0014	0.0025		
	1.3	25	0.0143	0.0284	0.0020	0.0038	↓	↓

Derivative Coefficient Precision, Uncertainty (±)

Configu-ration	M_∞	C_{N_α}, deg^{-1}	C_{m_α}, deg^{-1}	$C_{Y_{p_\alpha}}$, rad^{-2}	$C_{n_{p_\alpha}}$, rad^{-2}	$C_{Y_{p_\alpha}}$	$C_{n_{p_\alpha}}$	$(x_{cp}/d)_N$
F1	0.4	0.0035	0.0032	0.0025	0 0022	0.14	0.34	0.15
	0.8	0.0017	0.0017	0.0012	0.0018	0 04	0.10	0.10
	0 9	0.0017	0.0019	0.0011	0.0018	↓	↓	↓
	1.0	0 0017	0.0021	0.0010	0.0018			
	1.1	0.0017	0.0019	0.0009	0.0018			
	1 2	0.0016	0.0016	0.0009	0.0018			
	1.3	0.0015	0.0012	0.009	0.0017	↓	↓	↓
ISRE	0.4	0.0042	0.0070	0.0025	0.0032	0.14	0.34	0.15
	0.8	0.0028	0.0068	0.0011	0.0018	0.04	0.10	0.10
	0.9	0.0028	0.0071	0.0008	0.0026	↓	↓	↓
	1.0	0.0027	0.0070	0.0010	0 0035			
	1.1	0.0028	0.0071	0.0012	0.0069			
	1.2	0.0028	0.0072	0.0012	0.0069			
	1.3	0.0028	0.0074	0.0012	0.0069	↓	↓	↓

15

The uncertainty in model angle of attack (a), as determined from tunnel sector calibrations and consideration of the possible errors in model deflection calculations, is estimated to be 0.042 deg.

4.0 RESULTS AND DISCUSSION

4.1 EFFECT OF SPIN RATE

The Magnus coefficients, C_Y and C_n, are plotted versus $pd/2V_\infty$ for various angles of attack for all conditions tested in Figs. 6 through 17. The lines are second- or third-order polynominal least squares curve fits to the data points (usually 500). The symbol at the end is for identification. For angles of attack of 10 deg and less, the Magnus coefficients are small and variable in direction. There was a tendency for some of the data, especially for the ISRE configurations at $M_\infty = 1.1$ to 1.3, to have a positive C_Y and a negative C_n for the positive $pd/2V_\infty$, differing from the majority of the data. At angles of attack above about 15 deg, the Magnus coefficients increased markedly and nearly always had a negative C_Y and positive C_n for the positive $pd/2V_\infty$. These high-a Magnus coefficients were larger at the lower Mach numbers and were quite nonlinear at $M_\infty = 0.4$.

Typical rolling-moment coefficient data obtained from the spin acceleration are plotted versus $pd/2V_\infty$ in Fig. 18a. Only every fifth point was plotted to avoid excessive clutter. The lines go through every point. Most of these data on the two configurations are linear. The steady-state spin-rate parameter, $(pd/2V_\infty)_s$, is the intersection with the horizonal axis; the roll-damping coefficient, $C\ell_p$, is the slope; and the static rolling-moment coefficient, $C\ell_o$, is the intersection with the vertical axis (after a slight extrapolation). About 95 percent of the data were sufficiently linear to be adequately represented by the parameters, $C\ell_p$ and $C\ell_o$, which are discussed later in the report. Most of the nonlinear data are plotted in Fig. 18b through e. The nonlinear data were primarily confined to high angles of attack. Nonlinearities were also more prevalent at the lower Mach numbers. The steady-state spin rate is quite well defined even for the nonlinear cases, but $C\ell_p$ depends on $pd/2V_\infty$. The static rolling-moment coefficient, $C\ell_o$, is indeterminate since roll rates near zero were not measured. However, the fixed-fin configurations with wedges would often refuse to start spinning when released at high a (> 20 deg) at all Mach numbers, indicating zero $C\ell_o$ for certain roll positions. Once started with the turbine, they would continue to spin without assistance.

4.2 EFFECT OF ANGLE OF ATTACK

It was found that spinning had no significant effect on C_N and C_m within the spin-rate range of test. These coefficients are plotted in Figs. 19 and 20 as functions of a.

The Magnus derivative coefficients, C_{Y_p} and C_{n_p} are plotted in Figs. 21 and 22. These are the slopes of the C_Y and C_n versus $pd/2V_\infty$ for values of $pd/2V_\infty$ between 0 and 0.04. The derivative coefficients, C_{Y_p} and C_{n_p}, are very nonlinear with respect to α, usually remaining very small up to about $\alpha = 10$ deg and then increasing rather rapidly further illustrating the observations made in Section 4.1.

In general, the roll-damping parameters, C_{ℓ_o}, C_{ℓ_p} and $(pd/2V_\infty)_s$ are only weak functions of α (Figs. 23 and 24); however, one notable exception is the $(pd/2V_\infty)_s$ at $M_\infty = 0.4$ (Fig. 24). These are nonlinear cases as were discussed in Section 4.1. Since the ISRE configurations have almost twice the total fin area at considerably more radial distance, C_{ℓ_o} and C_{ℓ_p} are much higher than for the FF configurations as expected. Steady-state spin-rate parameter, $(pd/2V_\infty)_s$, however is slightly higher for the FF configurations.

4.3 EFFECT OF MACH NUMBER

The longitudinal stability of the two basic configurations versus M_∞ is shown in Fig. 25 in terms of C_{N_α} and C_{m_α}. The same data are shown in terms of $(X_{cp}/d)_N$ in Fig. 26. These data agree well with the static data of Ref. 1. The large flare and greater total fin area of the ISRE configurations lead to greater stability. The slots in the tail have only a minor effect.

The Magnus-force characteristics are shown in terms of $C_{Y_{p_\alpha}}$ and $C_{n_{p_\alpha}}$ versus M_∞ in Fig. 27. As was pointed out earlier, the derivative data are for a range of $pd/2V_\infty$ between 0 and 0.04, and in addition, for an α range of ± 2 deg. Within these limits, the Magnus forces are very small and variable in direction. Under these conditions, center-of-pressure data $(X_{cp}/d)_Y$ are very erratic and virtually meaningless, hence they are not presented. The effect of the fin slots is generally small, although a measurable effect is shown for the ISRE fins at $M_\infty = 1.2$ and 1.3.

The roll-damping parameters, C_{ℓ_o}, C_{ℓ_p} and $(pd/2V_\infty)_s$ are plotted versus M_∞ in Fig. 28. The steady-state spin-rate parameter, $(pd/2V_\infty)_s$, decreases with Mach number especially at $\alpha = 20$ deg. This can be explained by the plot of C_{ℓ_o} which shows a decreasing trend with Mach number, while the plot of C_{ℓ_p} shows an increasing trend (larger negative value) with Mach number. In general, the slots in the fins have only a very small effect; however, there is a noticeable reduction in the damping coefficient, C_{ℓ_p}, at $\alpha = 10$ and 20 deg, being more pronounced for the FF configuration.

5.0 CONCLUDING REMARKS

An investigation was made in a transonic wind tunnel to measure the Magnus and roll-damping characteristics of a bomb shape, which is a candidate for replacement of

the MK-82 Snakeye. The Mach numbers ranged from 0.4 to 1.3 and the Reynolds numbers, based on model diameter, were from 0.54×10^6 to 1.0×10^6. Two basic fin configurations, the fixed fin (FF) and the inflatable stabilizer retarder with extender (ISRE), were tested with and without wedge-shaped tabs and slots. The angle of attack ranged from -2 to 26 deg. The general observations given below apply to both fin configurations.

1. The Magnus coefficients, C_Y and C_n, for angles of attack of 10 deg and less were small and variable in direction.

2. Above about 15-deg angle of attack the Magnus coefficients increased markedly and nearly always had a negative C_Y and a positive C_n for the positive $pd/2V_\infty$. These high-α Magnus coefficients were larger at the lower Mach numbers and were nonlinear at $M_\infty = 0.4$.

3. Spin rate had no significant effect on C_N and C_m.

4. Significant nonlinear roll-damping effects were found at $M_\infty = 0.4$ and high angles of attack. For nearly all other conditions, the data were linear.

5. The ISRE configuration, because of its large fin area and span, produced over twice the damping and static rolling moment as the FF configuration.

6. The effects of the fin slots on Magnus coefficients and roll damping were, in general, very small.

7. The fin wedges produced the desired rolling moment but had only very small effects on roll damping and Magnus coefficients.

REFERENCES

1. Anderson, C. F. and Carleton, W. E. "Static and Dynamic Stability Characteristics of the Fixed-Fin and Inflatable Stabilizer Retarder Configurations of the MK-82 Store at Transonic Speeds." AEDC-TR-75-149, AFATL-TR-75-141, November 1975.

2. Test Facilities Handbook (Tenth Edition). "Propulsion Wind Tunnel Facility, Vol. 4." Arnold Engineering Development Center, May 1974.

60°

0.500 DIAM

AIRSTREAM SURFACE

0.375

0.375
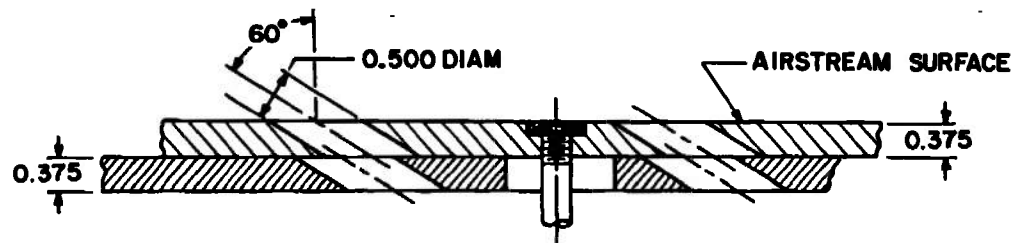
TYPICAL PERFORATED WALL CROSS SECTION

SOLID AREAS

PERFORATED WALLS (10% MAXIMUM OPEN AREA)

FLOW
EXPANSION
REGION

STA.
0.0

STA.
36.0

STA.
81.0

STA.
150.0
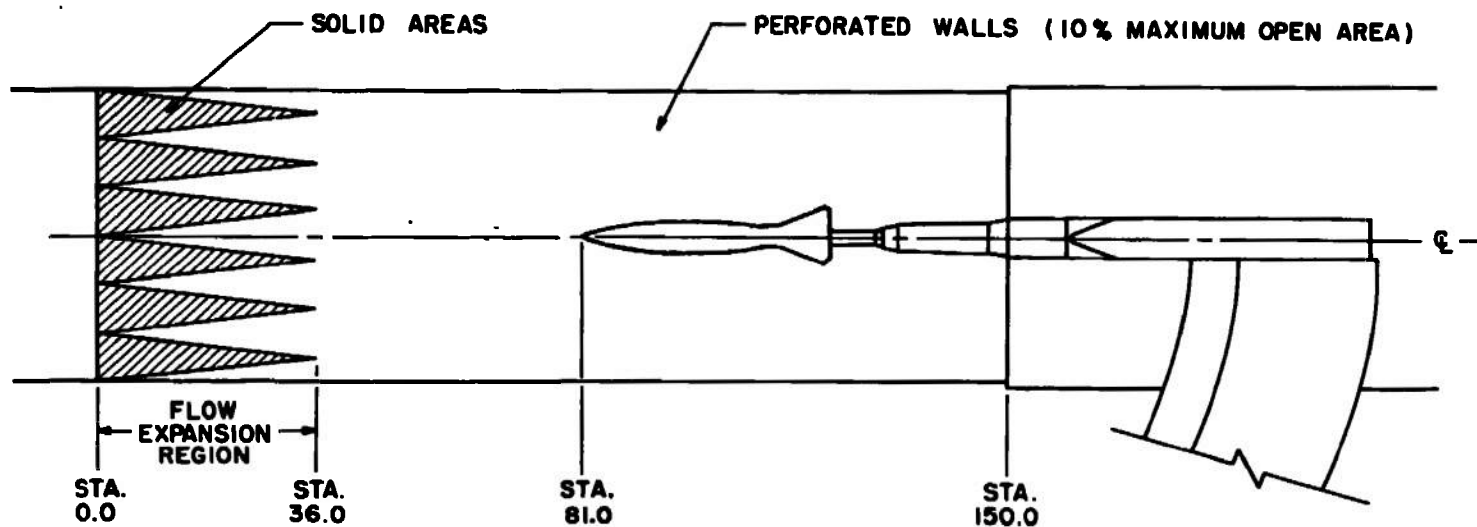
Figure 1. Schematic of test section with model and balance installed.

19

AEDC-TR-75-163

0.320 (Typ)

0.806°

1.145°

45°

0.214°

5.933

Fin Details

0.125

0.065 (Typ)

1.387

30° (Typ)

6° (Typ)

*These dimensions apply to slotted fins only.

Flush with Top of Fin

Flush with Aft Edge of Fin

1.322 Nominal

Part No.
W1 15°
W2 25°

Wedge Details

40.052

18.364

4.750 Diam

12.914

3.881 Diam

See Fig. 1c for Contour

Dimensions in Inches

3.881 Diam

Moment Reference Point

15.600

5.605

5.933

Weight Ring
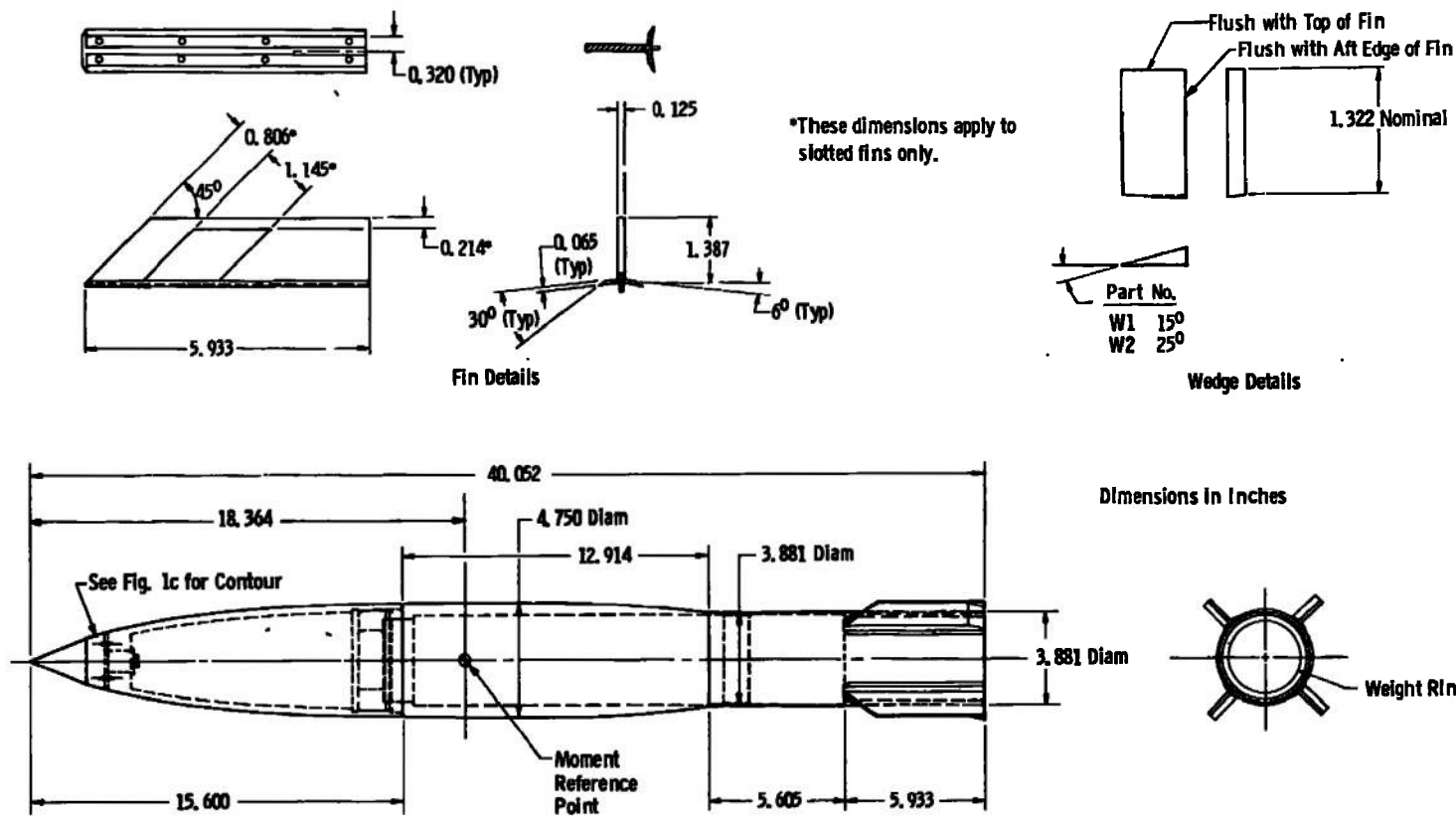
a. Fixed-fin model (configuration FFW2)
Figure 2. Model details.

Fin Details

*These dimensions apply to slotted fins only.

Wedge Details

Part No.	
W1	15°
W2	25°

Dimensions In Inches

b. Inflatable stabilizer model (configuration ISREW2)
Figure 2. Continued.
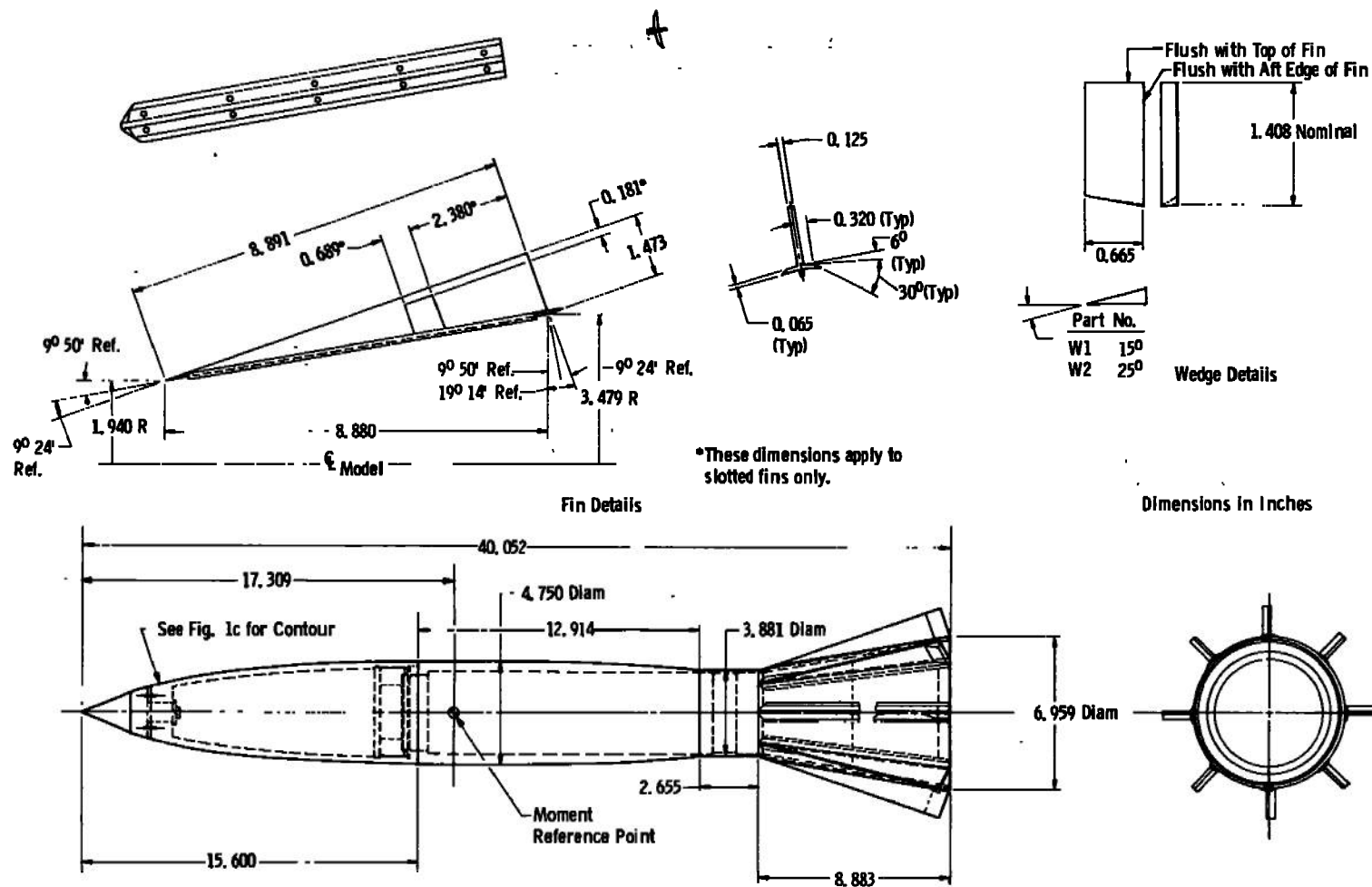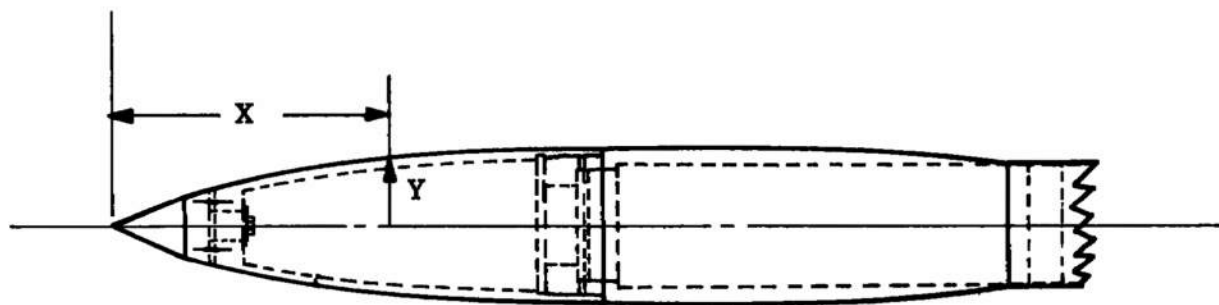
X	Y
0	0
2.3560	1.0218
2.4273	1.0429
3.1493	1.2372
3.3345	1.2813
3.7858	1.3813
4.2370	1.4754
5.1443	1.6350
6.0468	1.7680
6.9540	1.8813
7.8565	1.9798
8.7638	2.0675
9.6663	2.1463
10.5735	2.2169
11.4760	2.2783
12.3833	2.3282
13.2858	2.3622
14.1930	2.3750
15.6000	2.3750
20.0735	2.3750
20.9760	2.3693
21.8833	2.3529
22.7858	2.3258
23.6930	2.2886
24.5955	2.2420
25.4980	2.1862
26.4053	2.1218
27.3078	2.0494
28.2150	1.9694
28.5143	1.9404

c. Model forebody ordinates
Figure 2. Concluded.

22
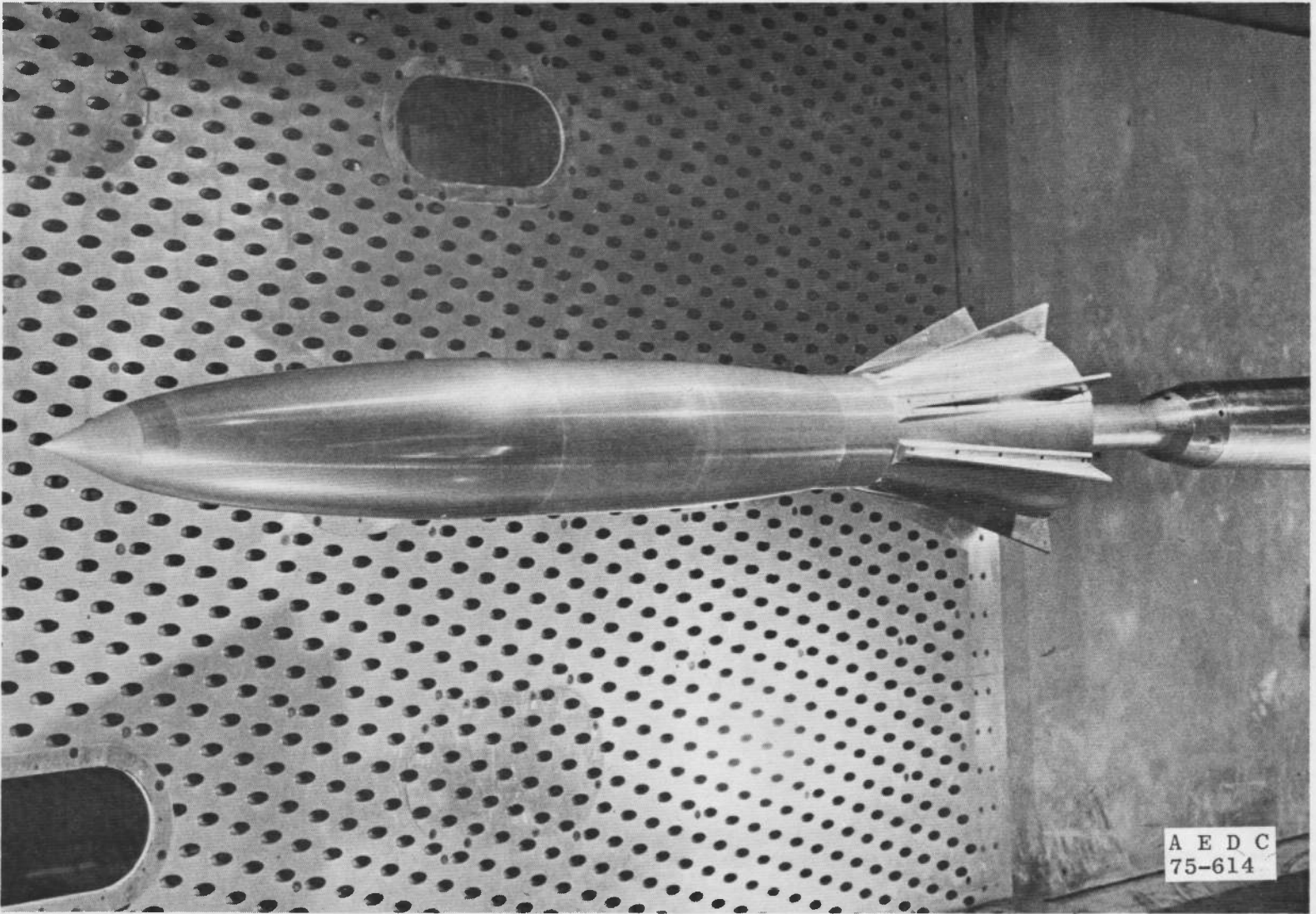
Figure 3. Photograph of the inflatable stabilizer model in the wind tunnel.

Brake

Tachometer

Clutch

Balance
Water Jacket

Turbine Typical
Model

Sting

Tachometer Ring

Balance Model Support Can
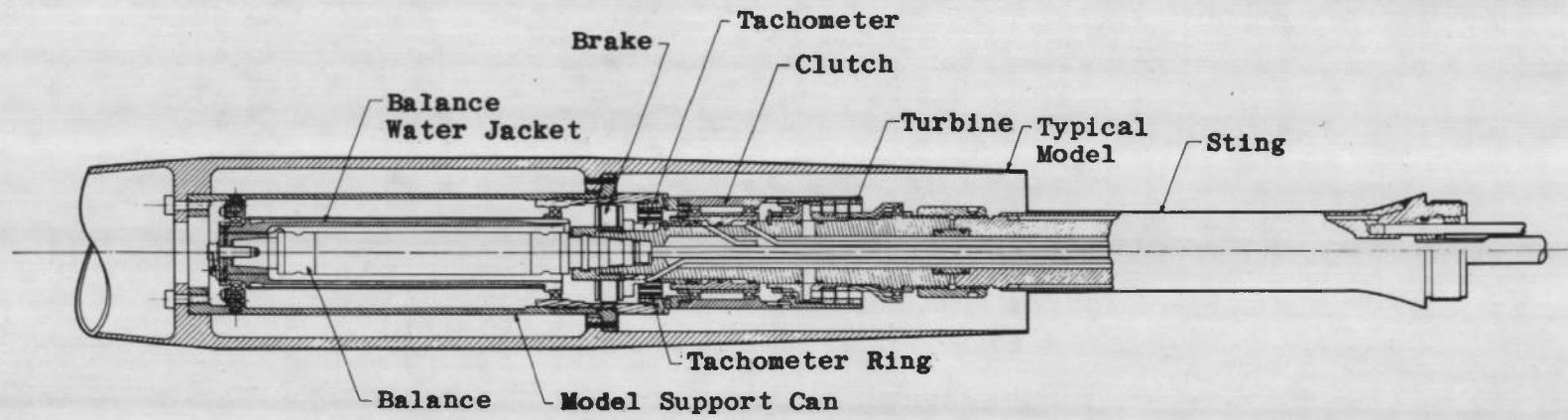
Figure 4. Magnus-force test mechanism.
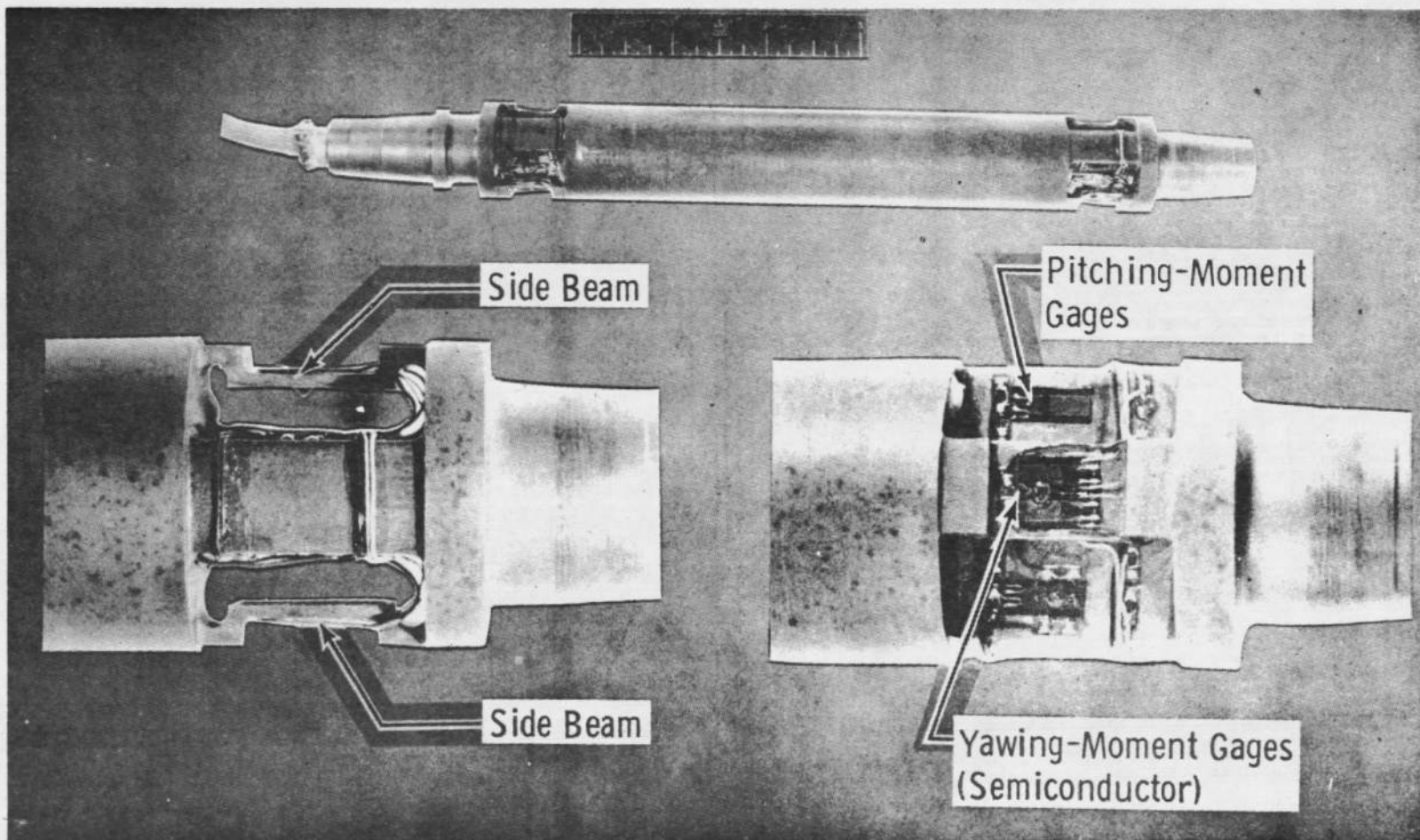
Figure 5. Balance details.
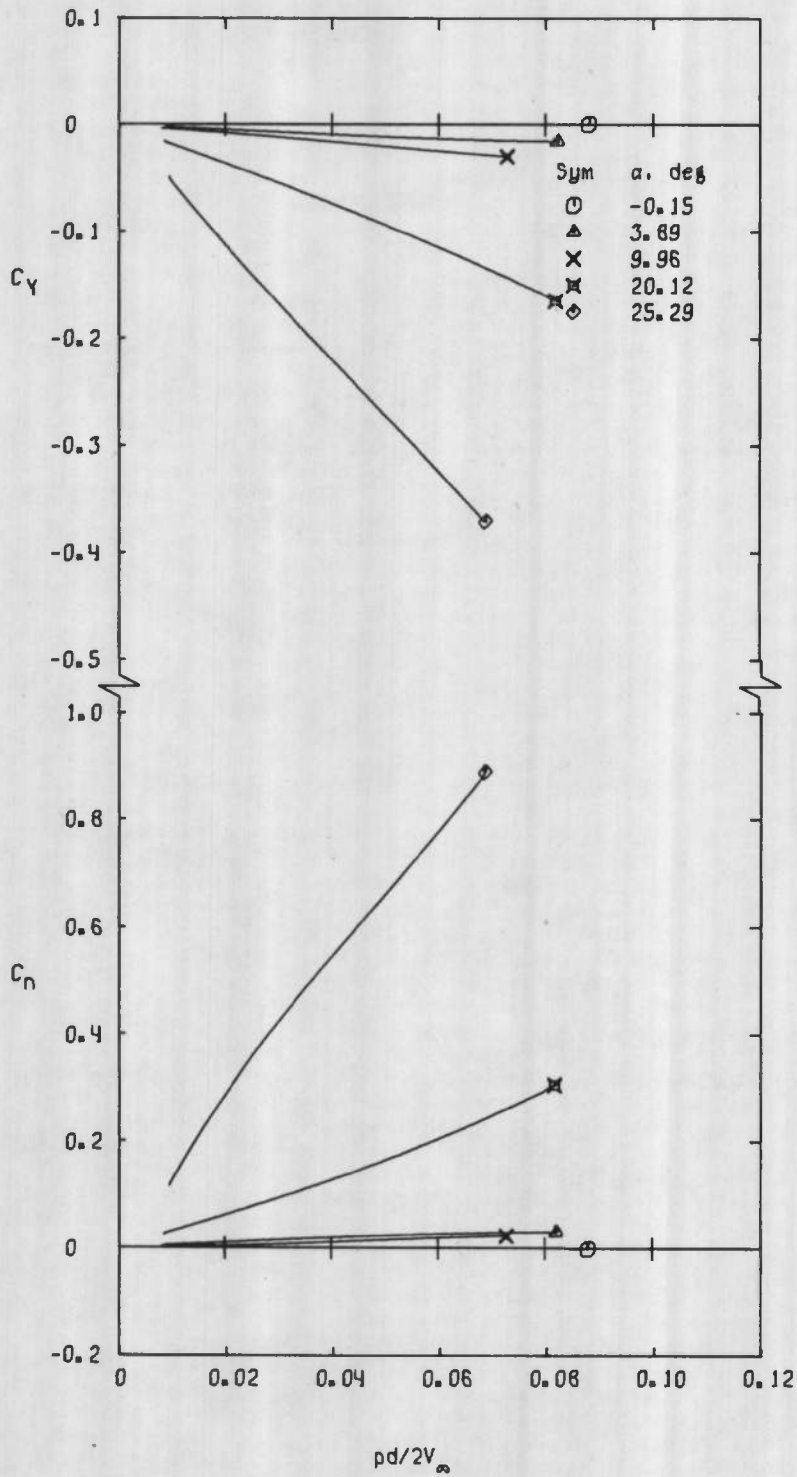
a. $M_\infty = 0.8$

Figure 6. Variation of C_Y and C_n with pd/2V for configuration FF.

26
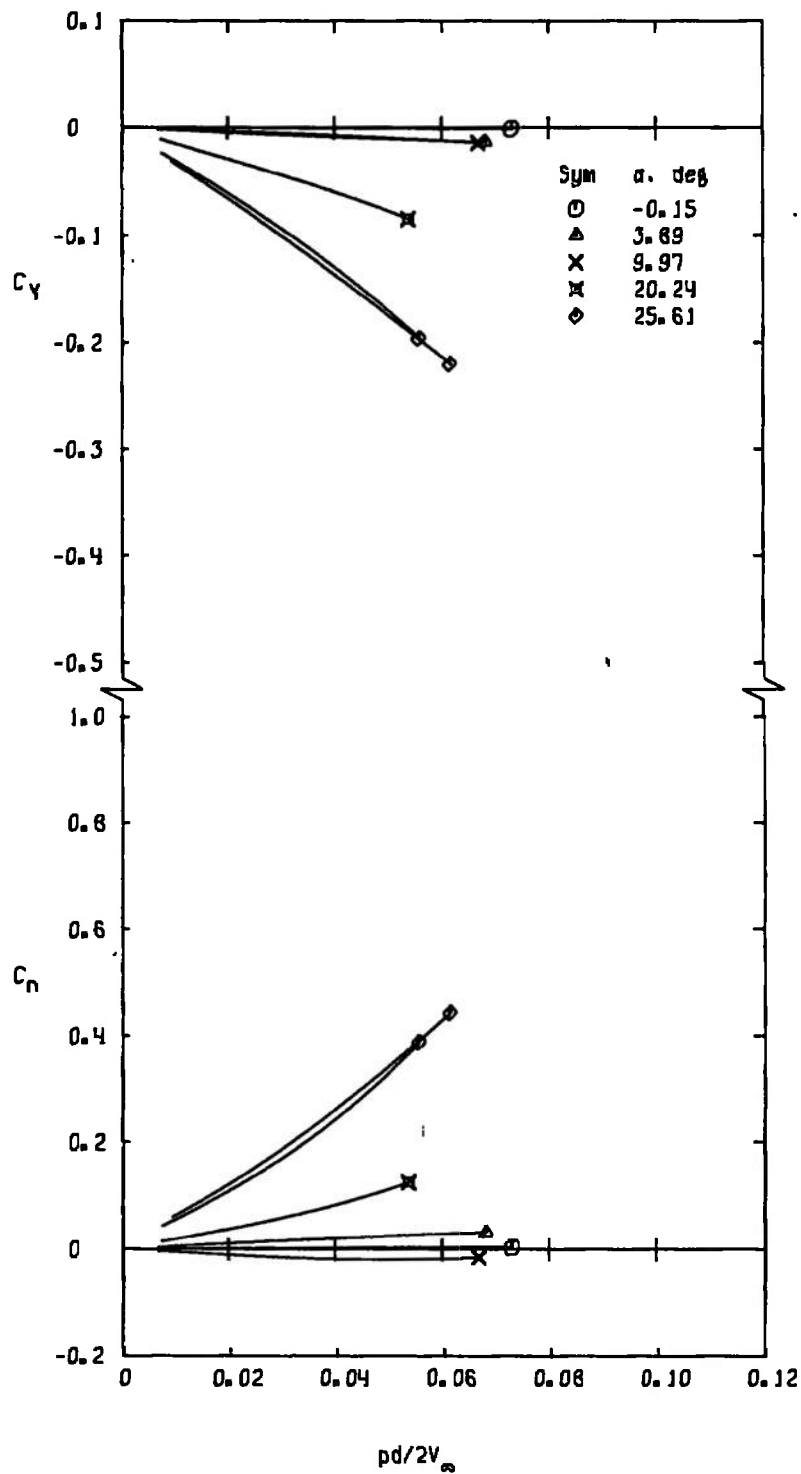
b. $M_\infty = 1.0$
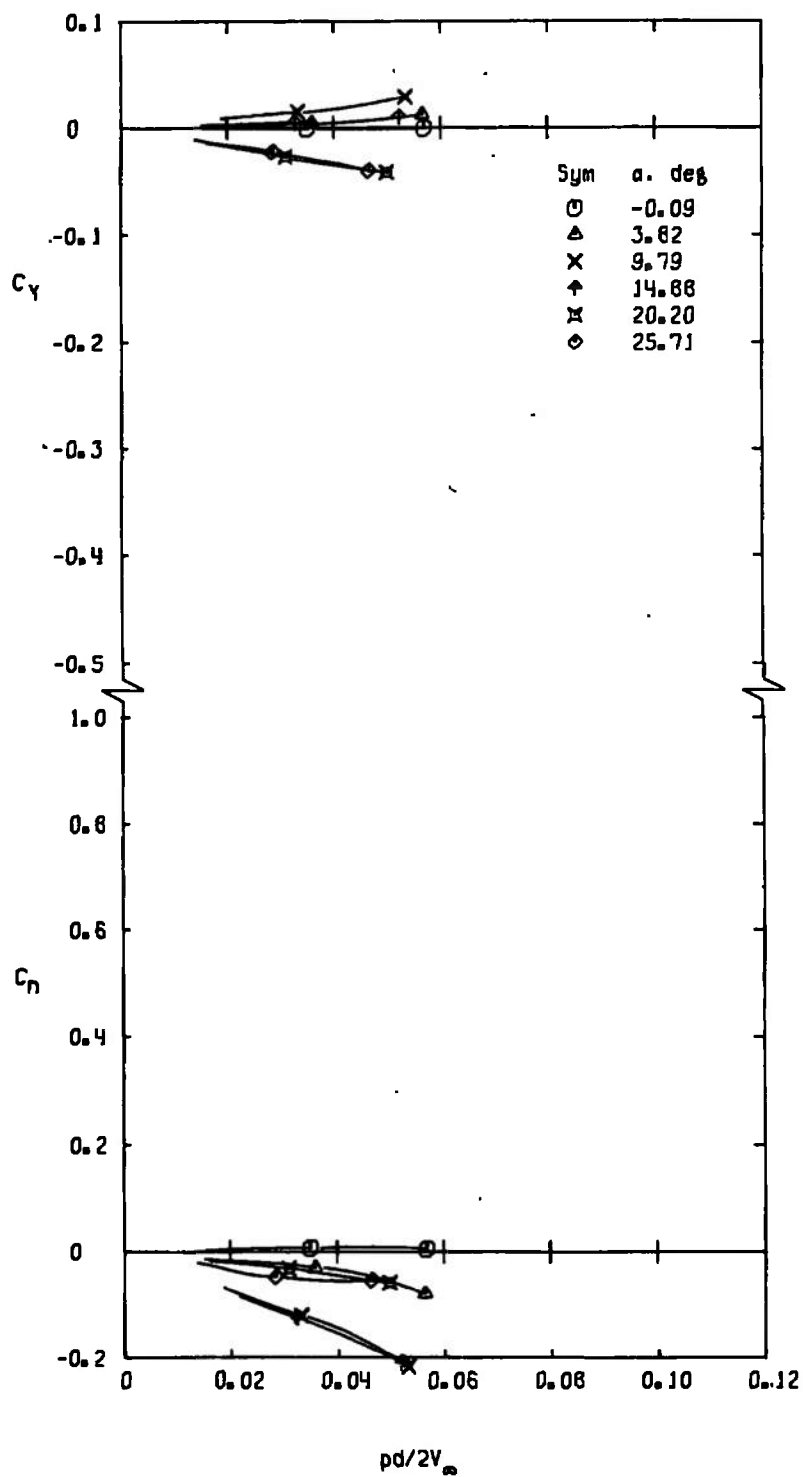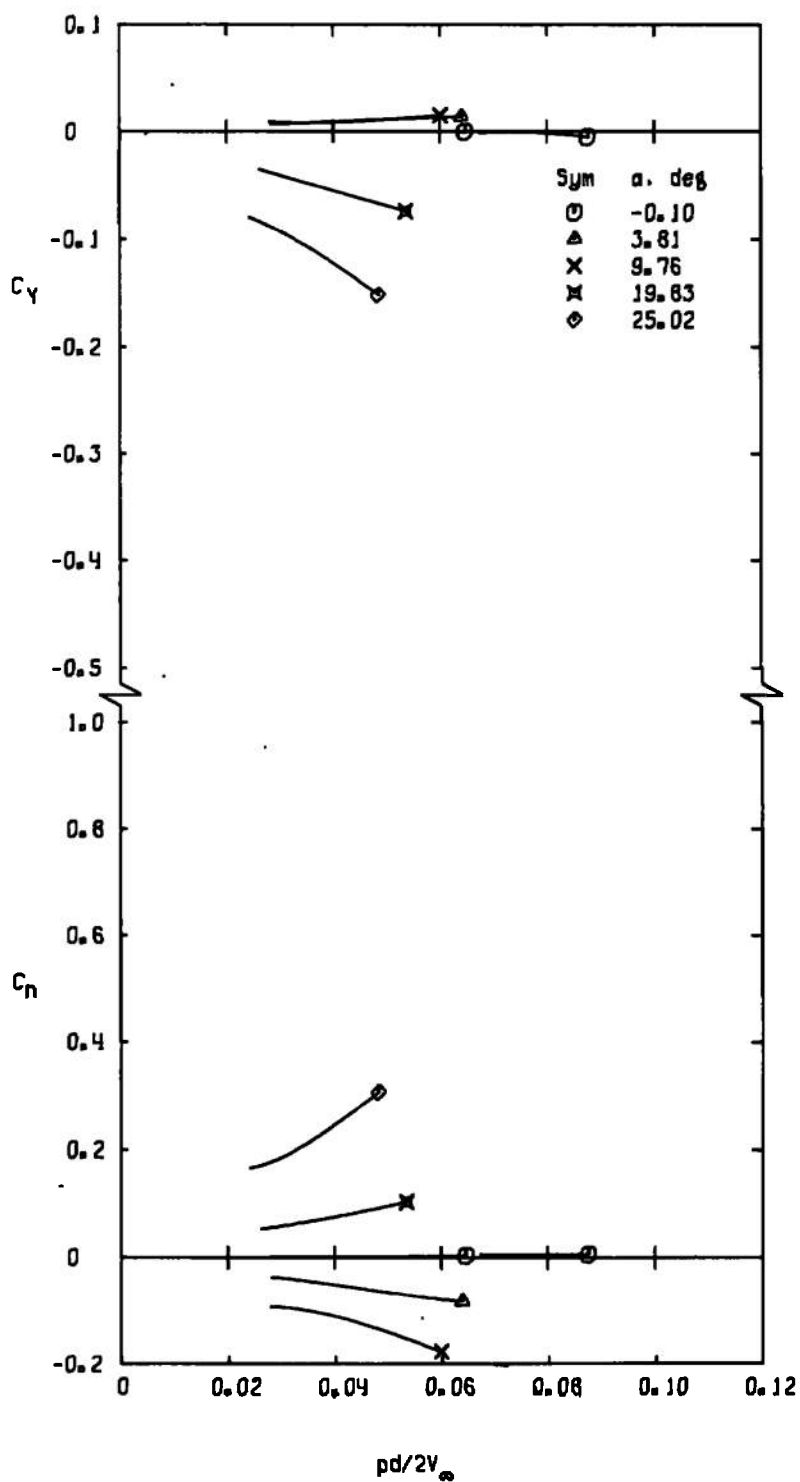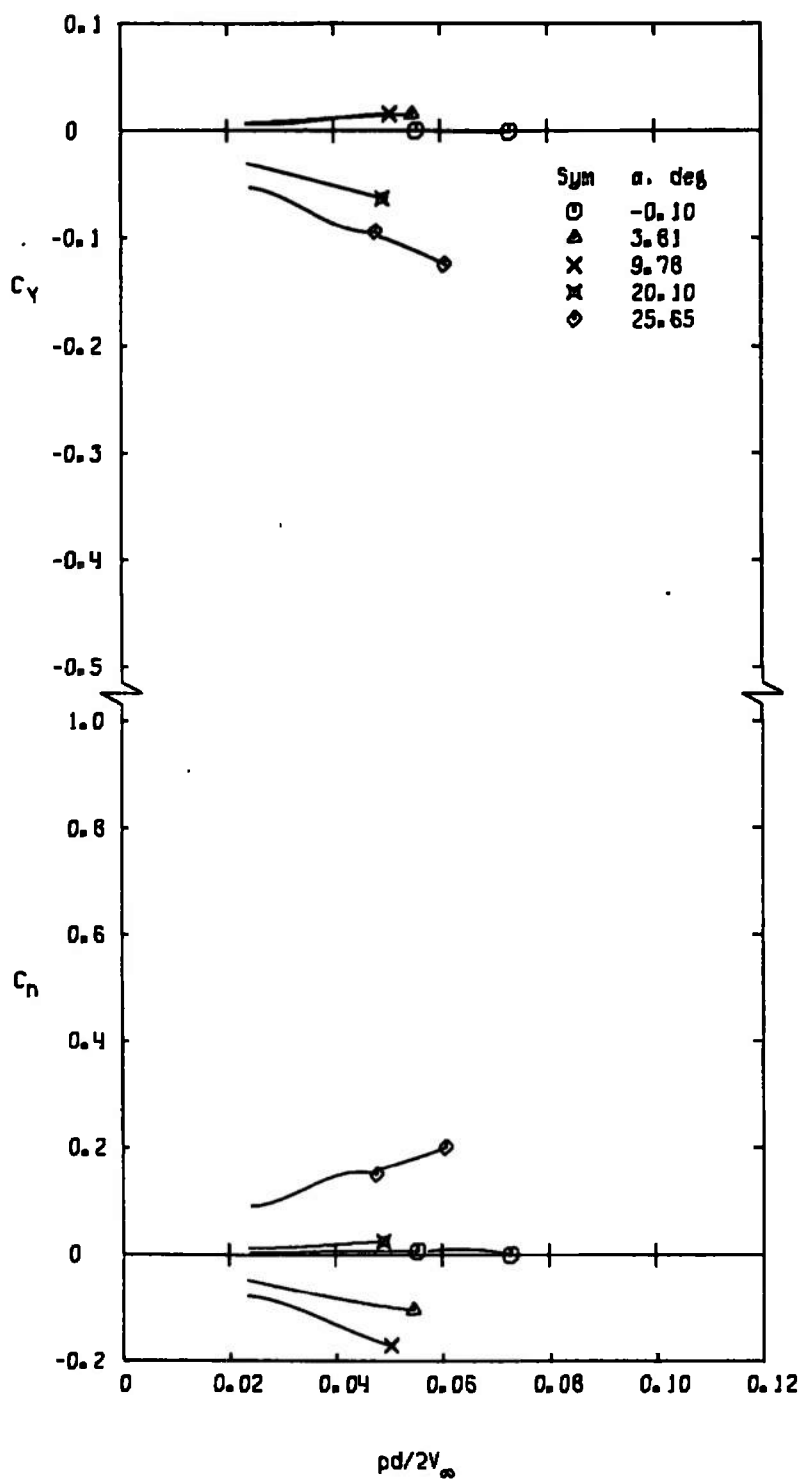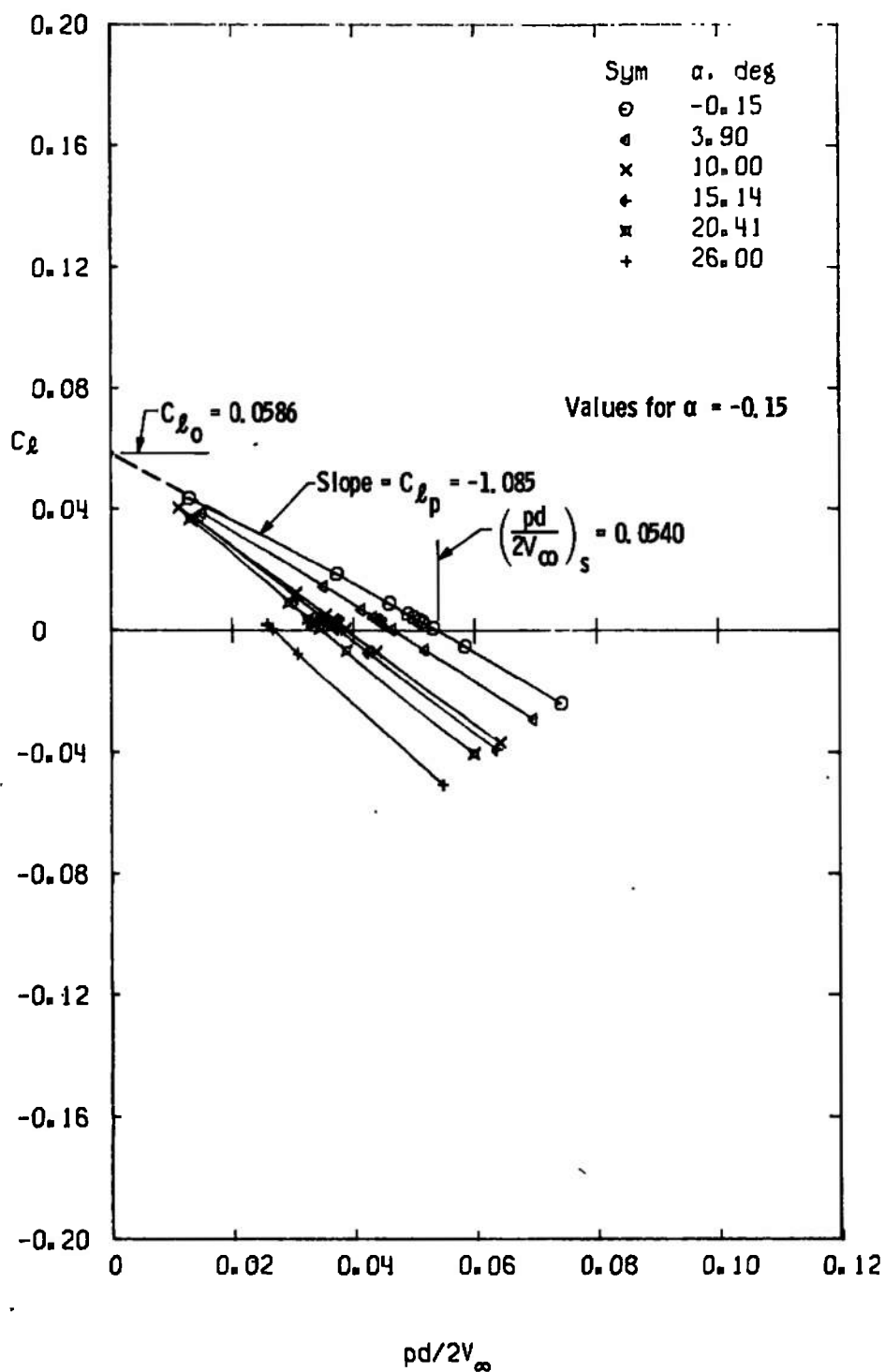Figure 6. Continued.
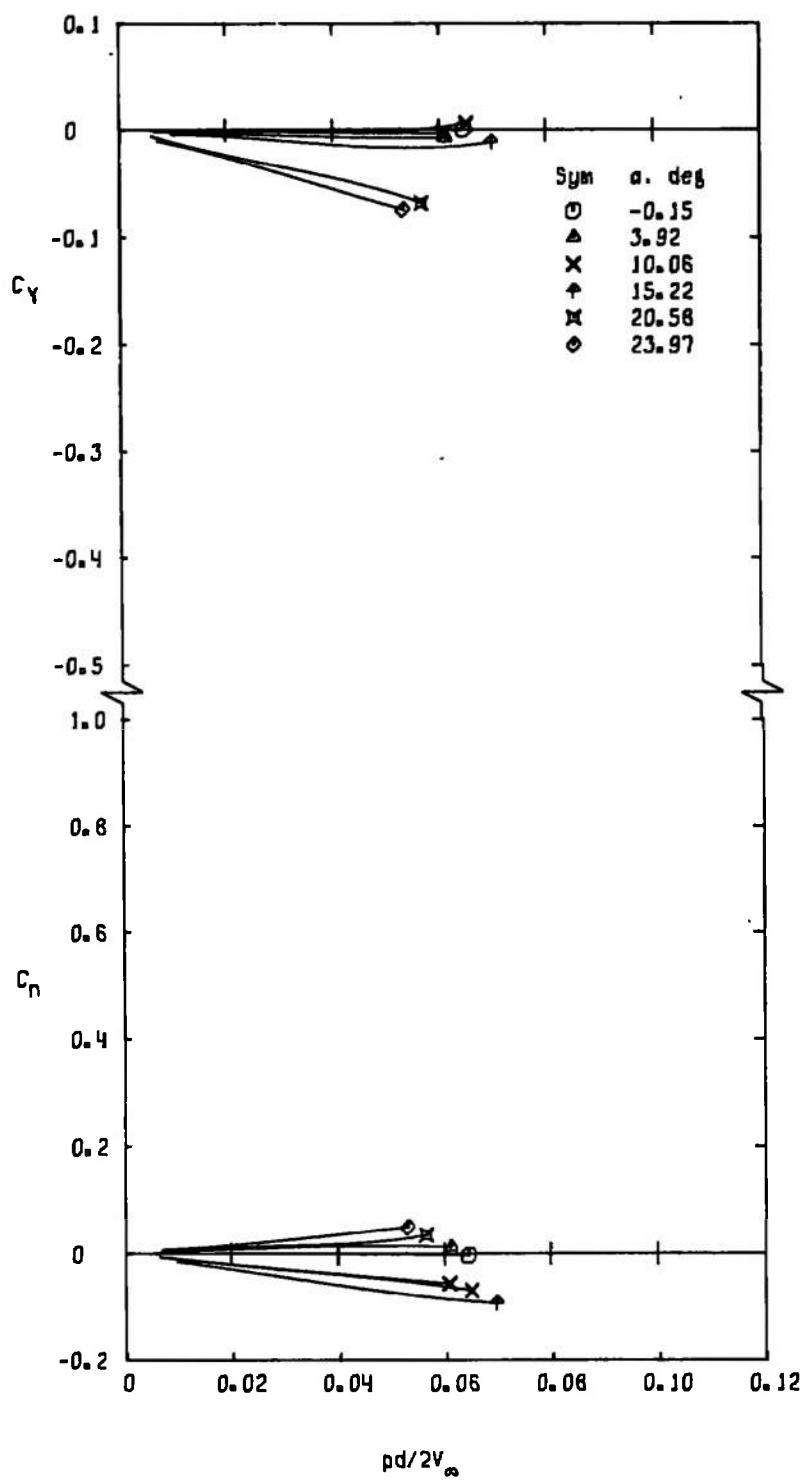
c. $M_\infty = 1.2$
Figure 6. Concluded.
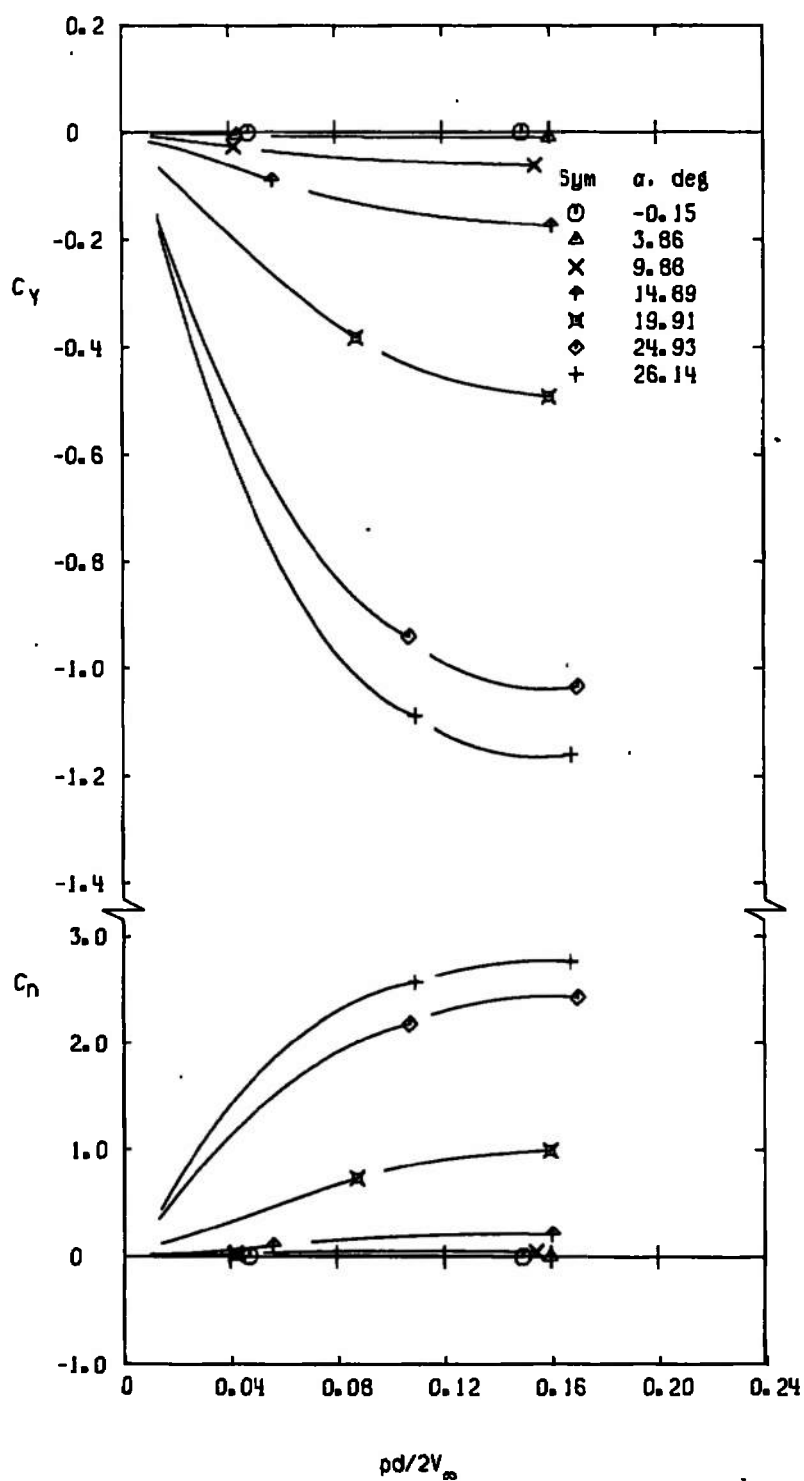
a. $M_\infty = 0.4$

Figure 7. Variation of C_Y and C_n with $pd/2V_\infty$ for configuration FFW1.
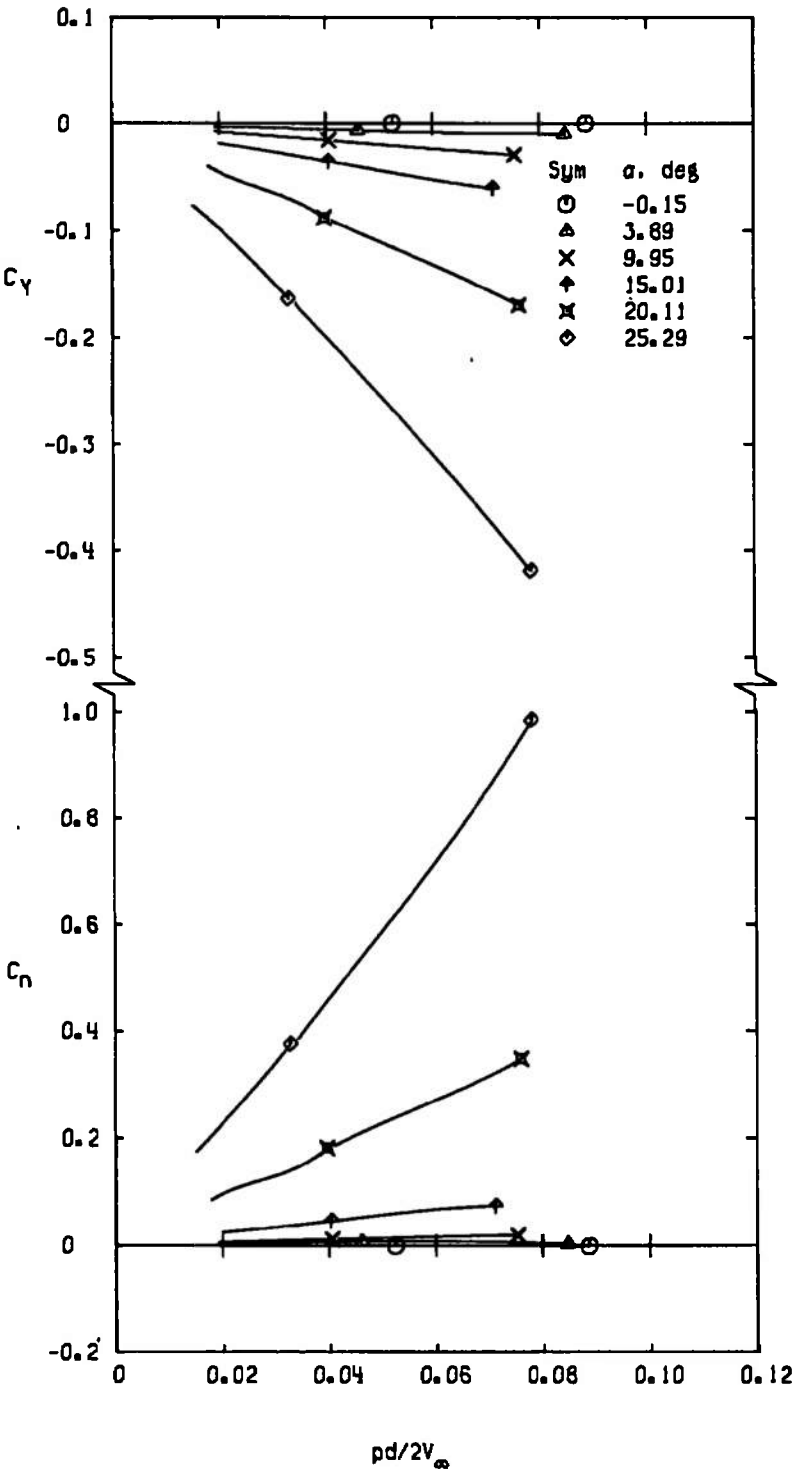
b. $M_\infty = 0.8$
Figure 7. Continued.
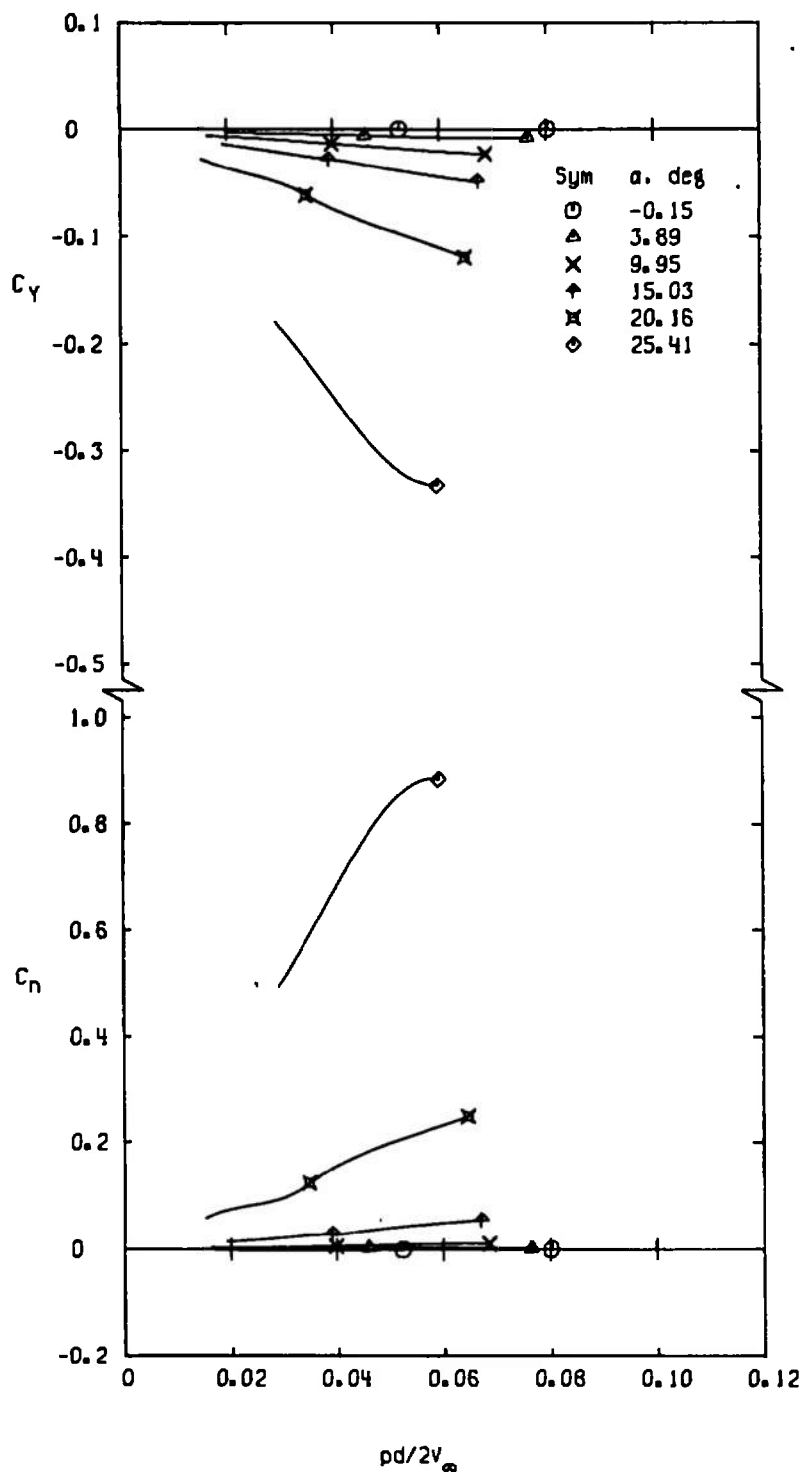
c. $M_\infty = 0.9$
Figure 7. Continued.
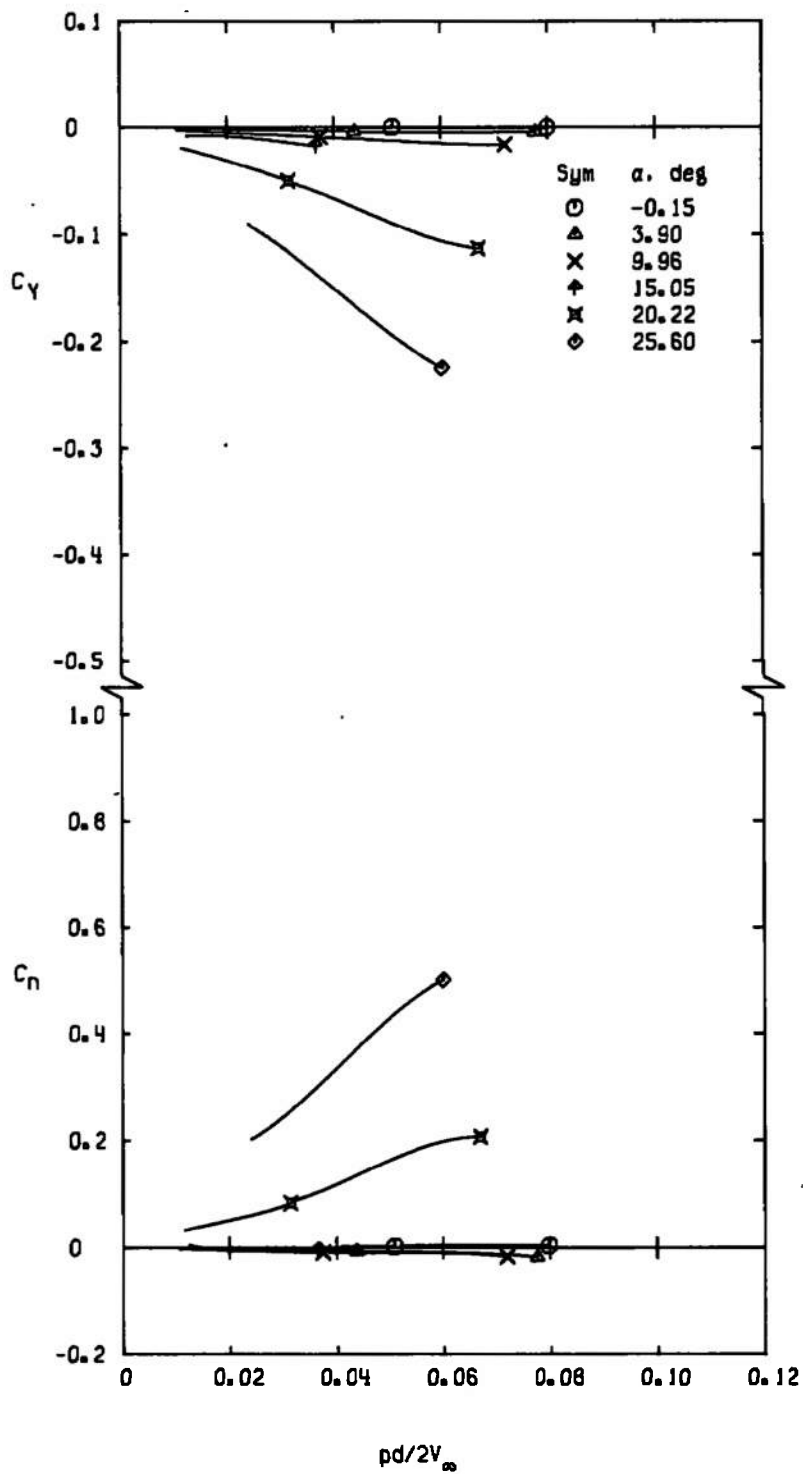
d. $M_\infty = 1.0$
Figure 7. Continued.
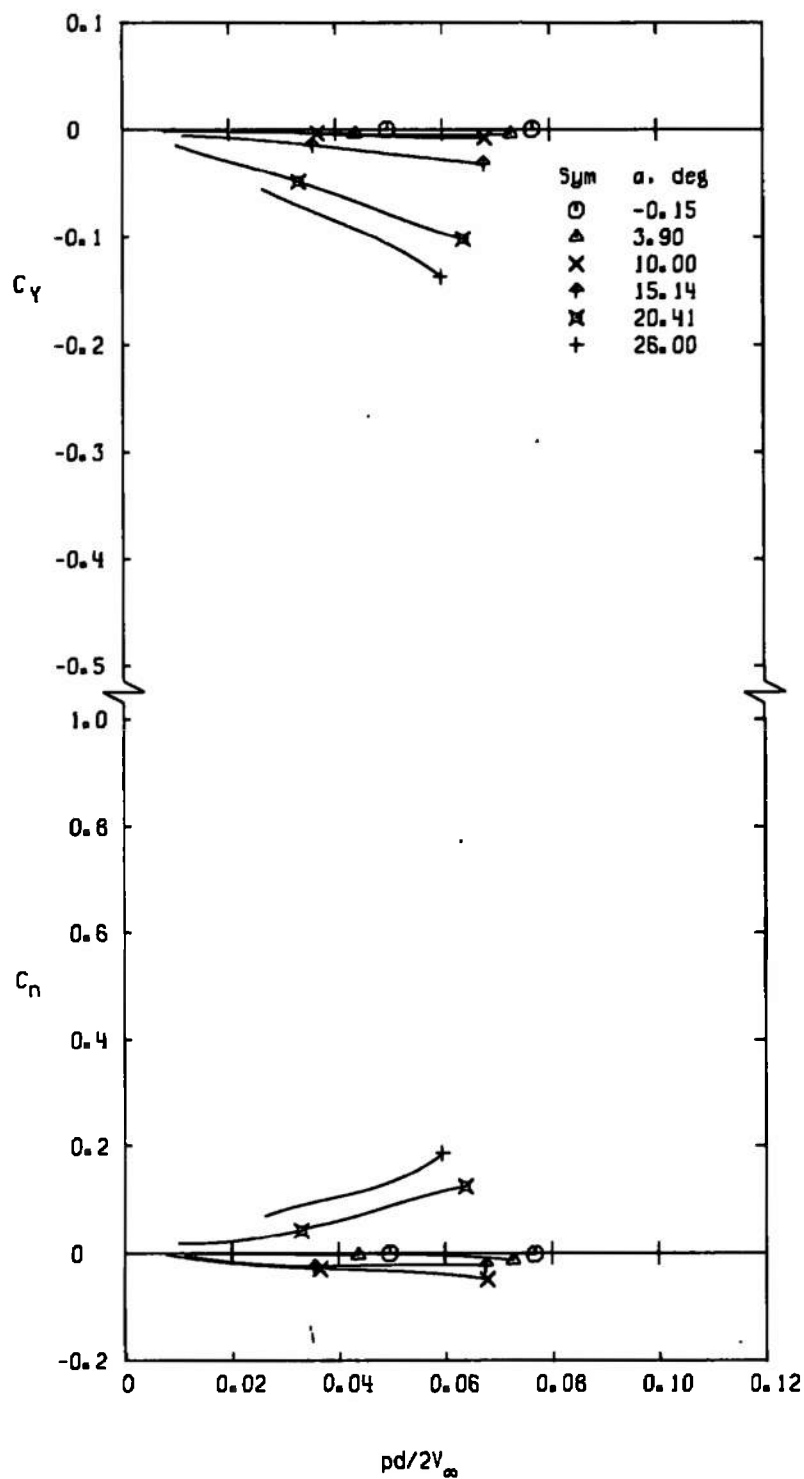
e. $M_\infty = 1.1$

Figure 7. Continued.

33
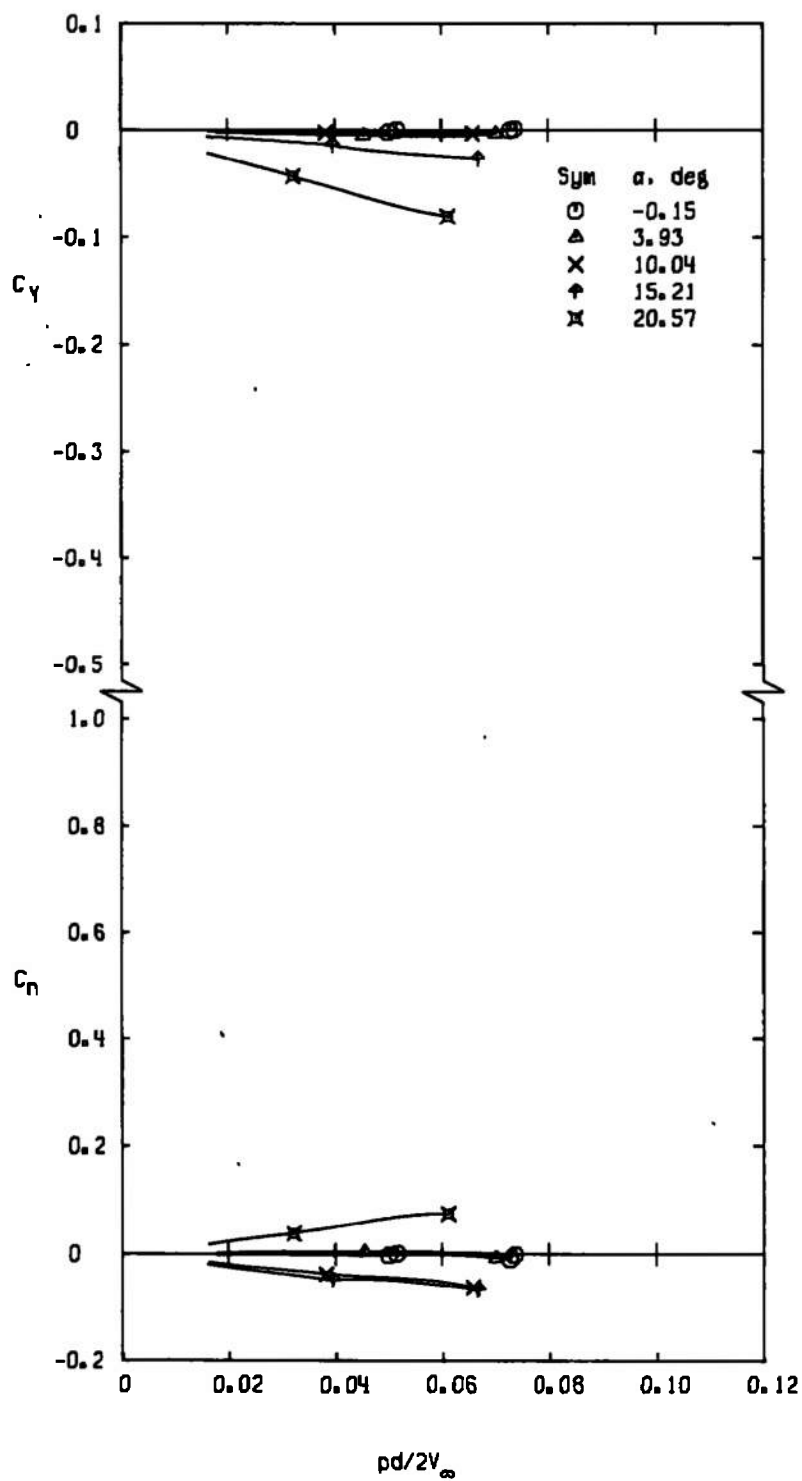
f. $M_\infty = 1.2$
Figure 7. Continued.
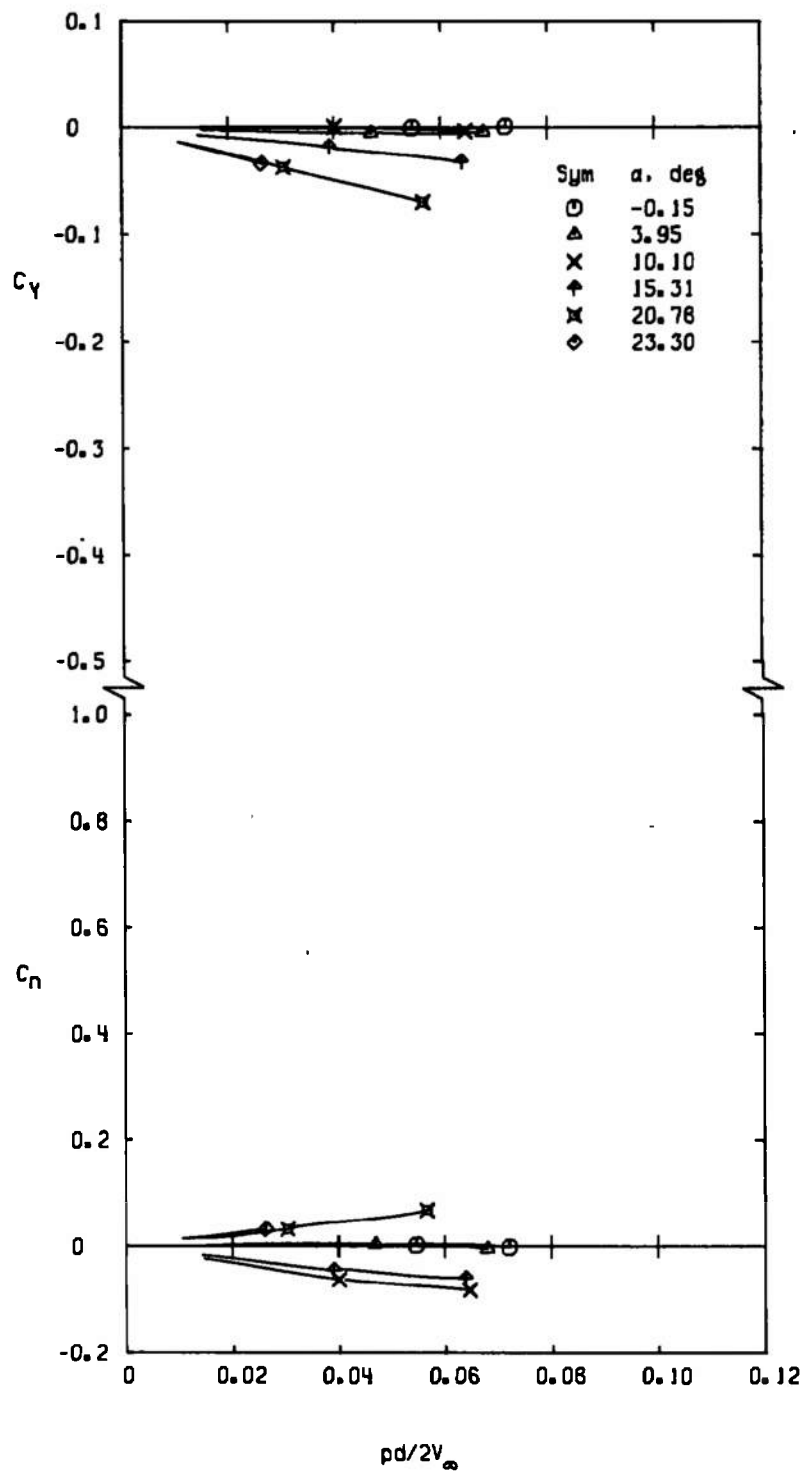
g. $M_\infty = 1.3$

Figure 7. Concluded.
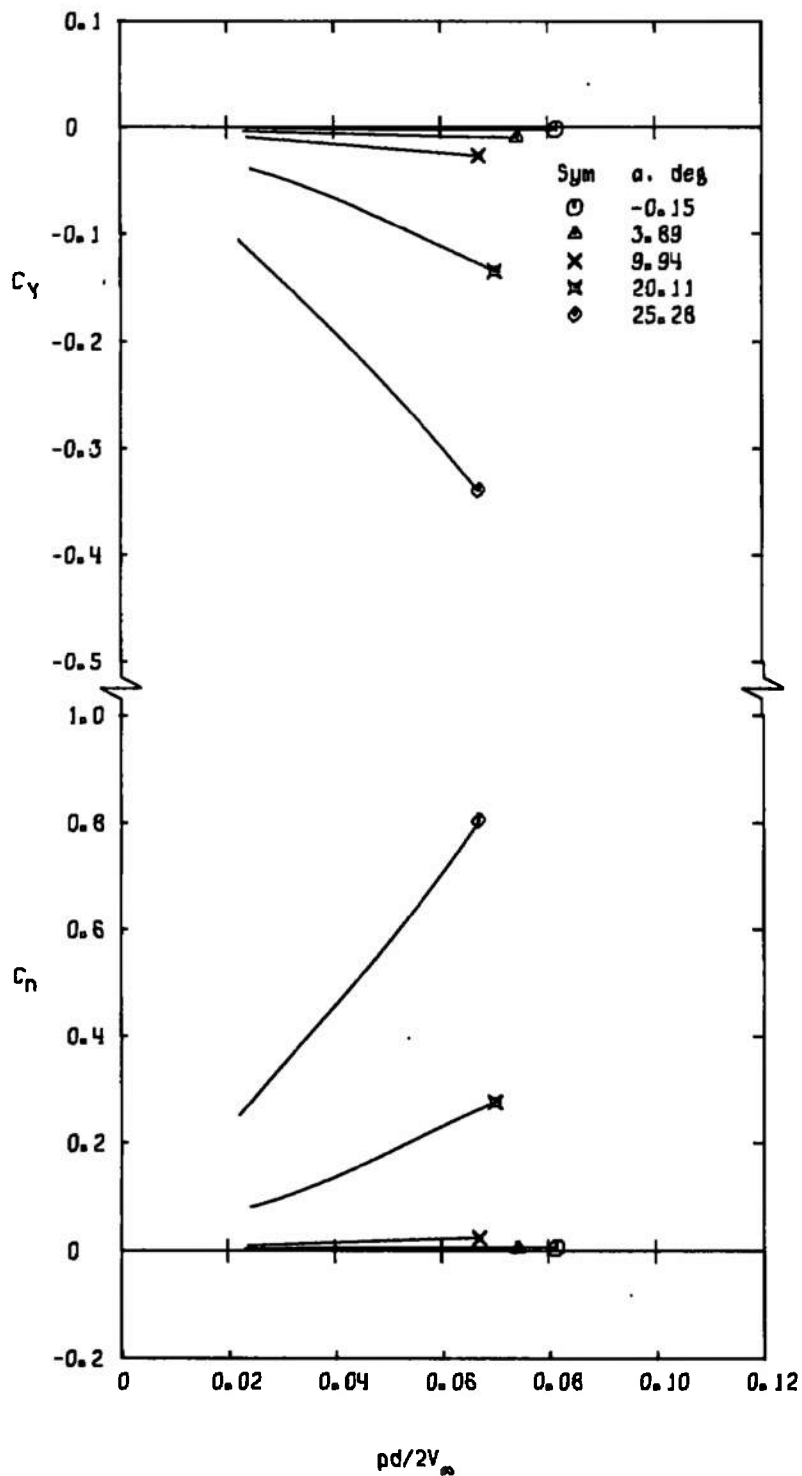
a. $M_\infty = 0.8$

Figure 8. Variation of C_Y and C_n with $pd/2V_\infty$ for configuration FFW2.
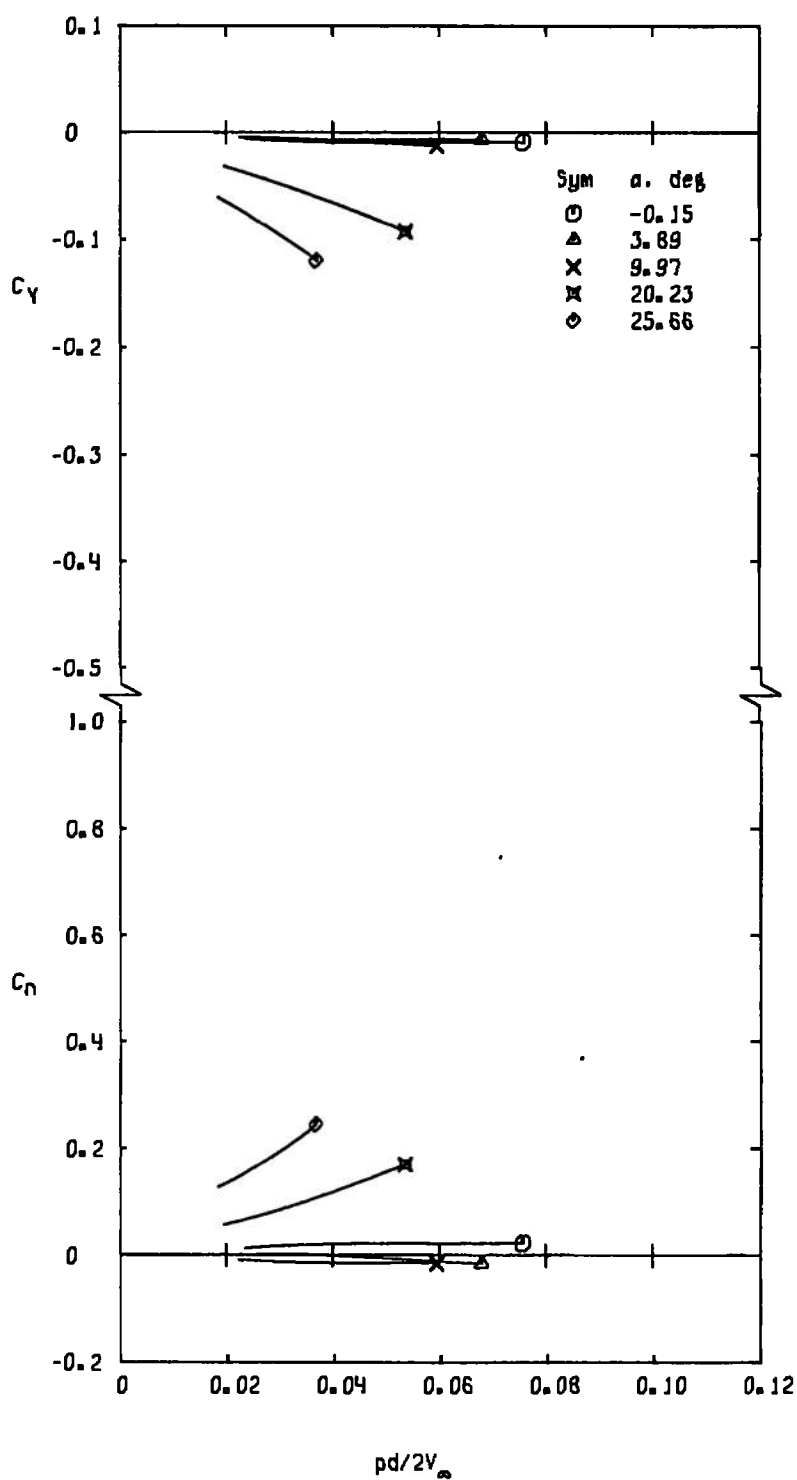
b. $M_\infty = 1.0$
Figure 8. Continued.
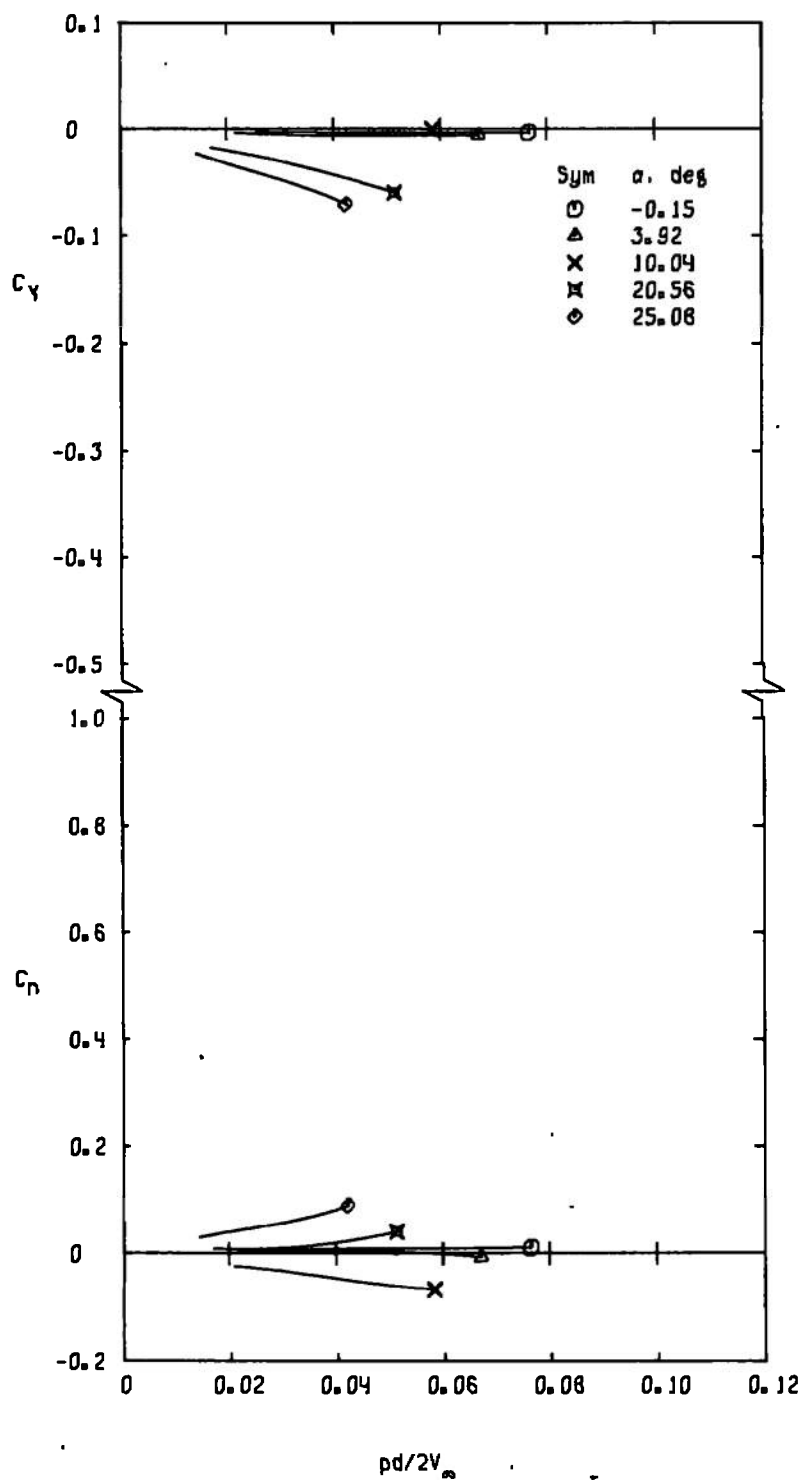
c. $M_\infty = 1.2$

Figure 8. Concluded.
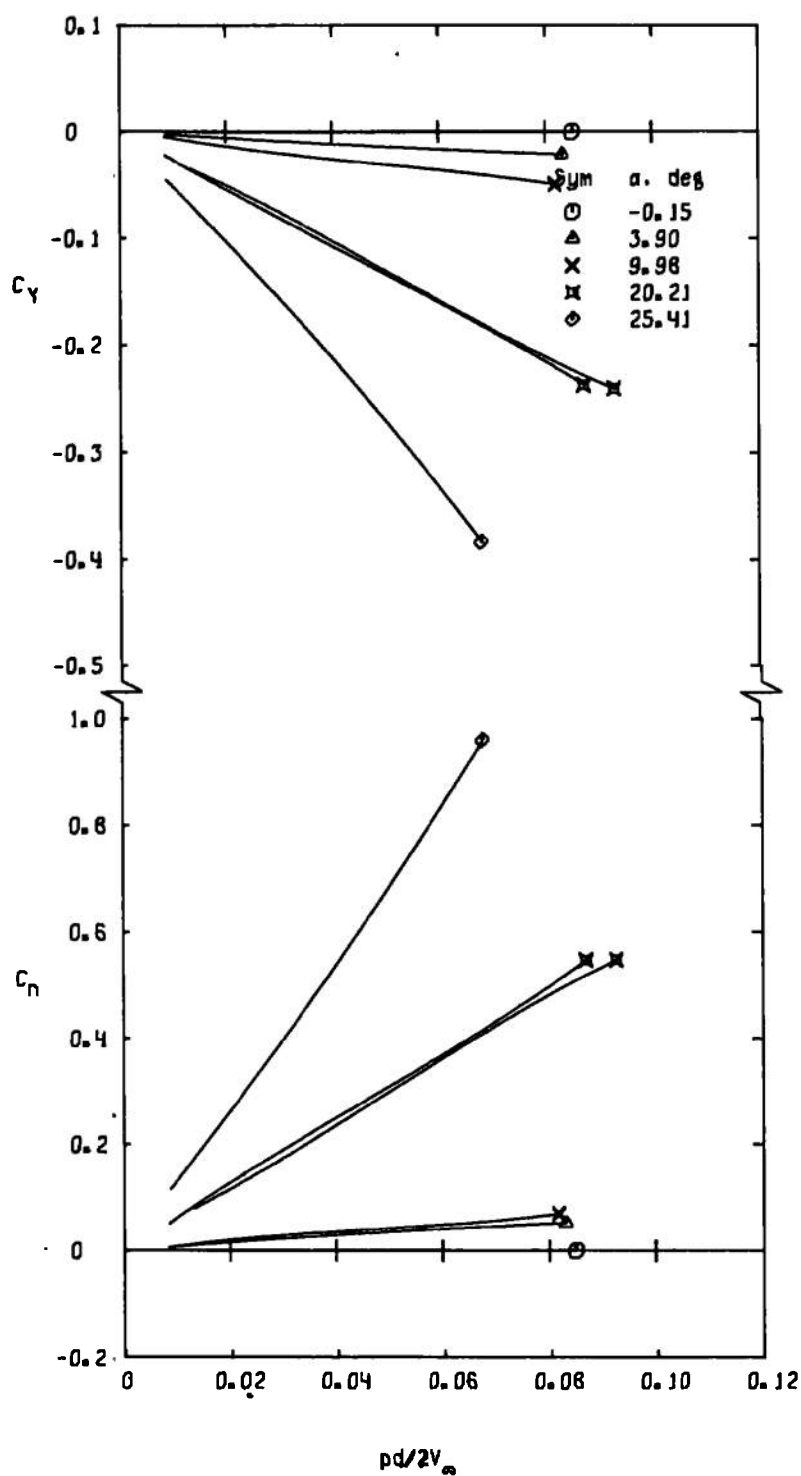
a. $M_\infty = 0.8$

Figure 9. Variation of C_Y and C_n with $pd/2V_\infty$ for configuration FFS.
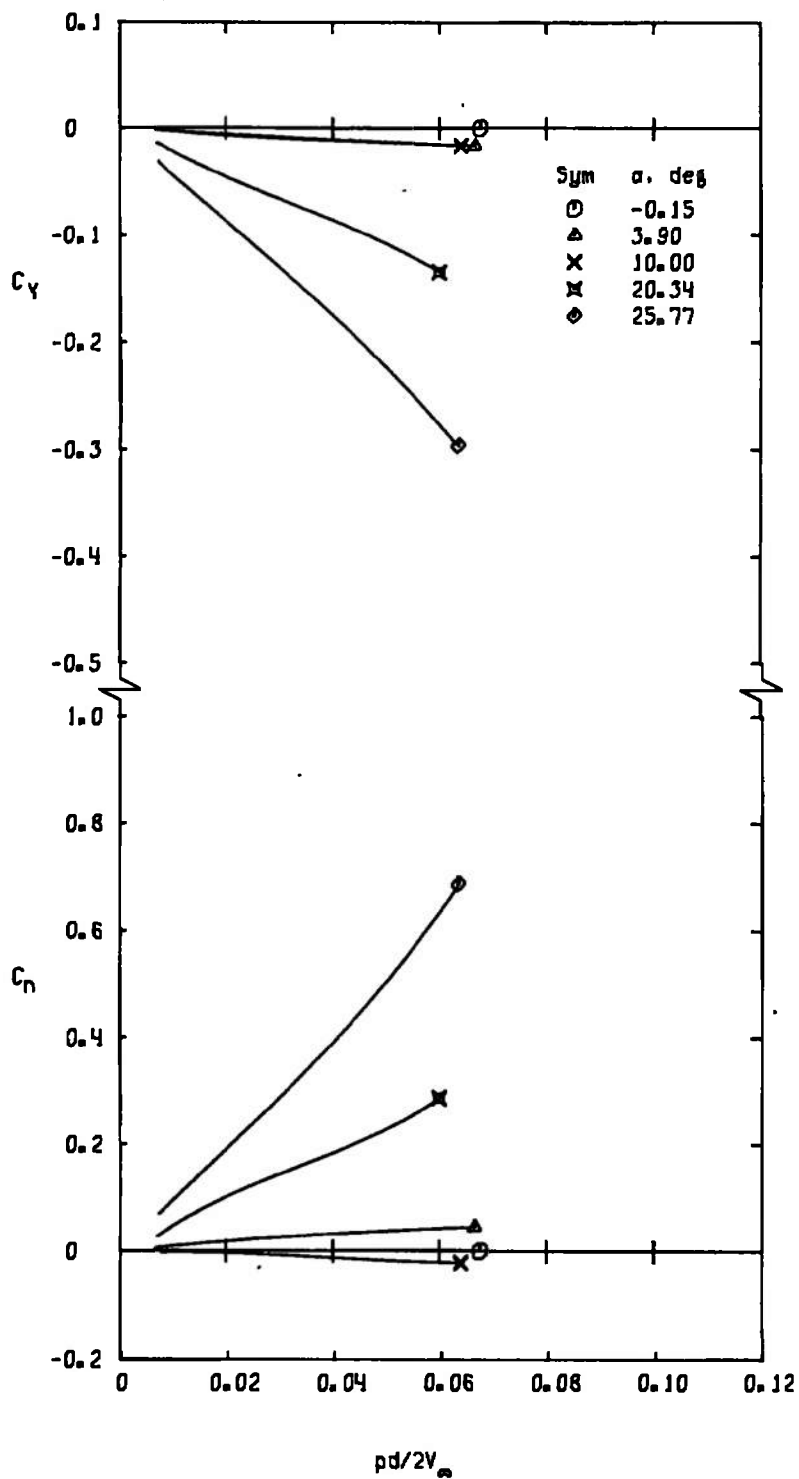
b. $M_\infty = 1.0$
Figure 9. Continued.
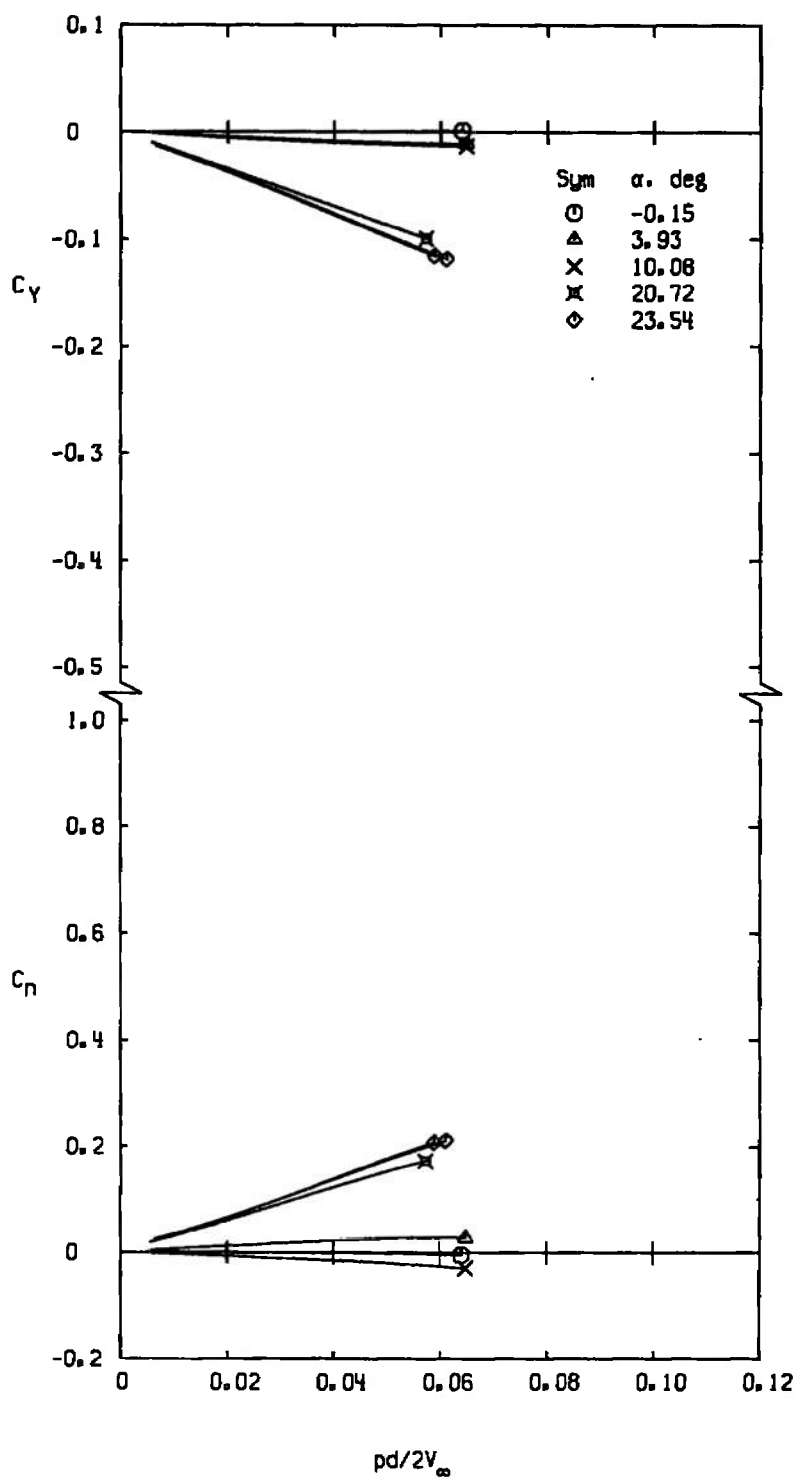
c. $M_\infty = 1.2$

Figure 9. Concluded.
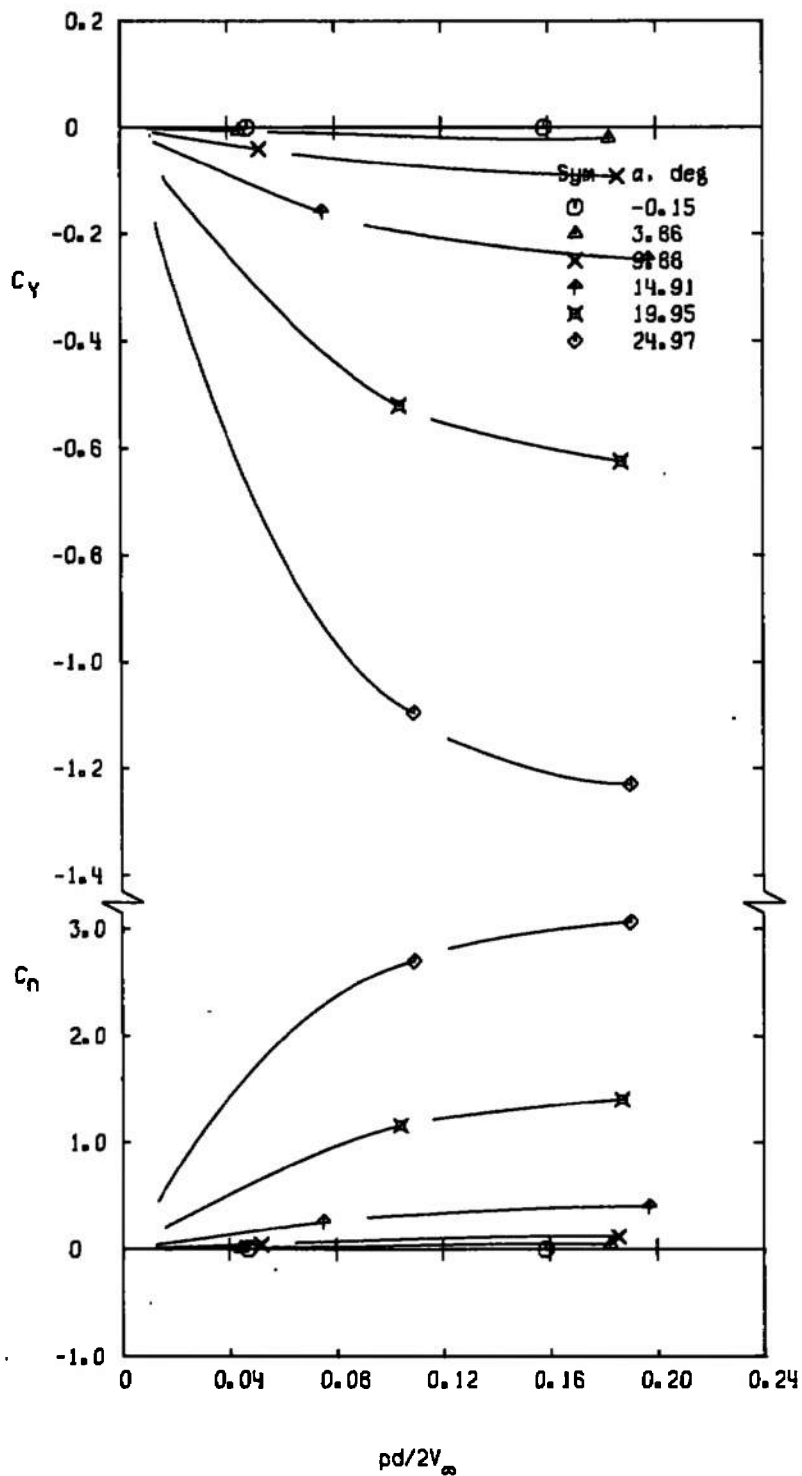
a. $M_\infty = 0.4$

Figure 10. Variation of C_Y and C_n with $pd/2V_\infty$ for configuration FFSW1.
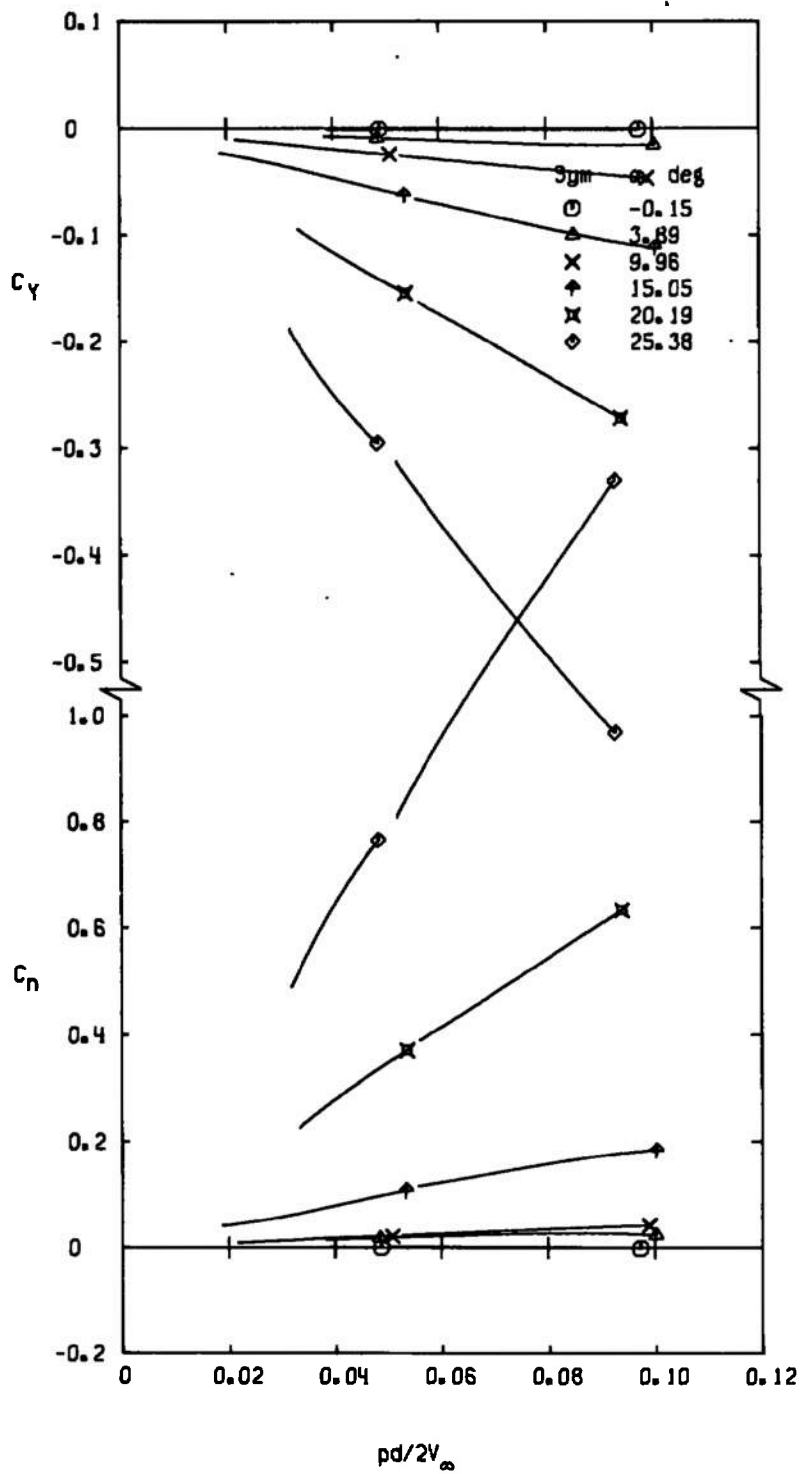
b. $M_\infty = 0.8$
Figure 10. Continued.
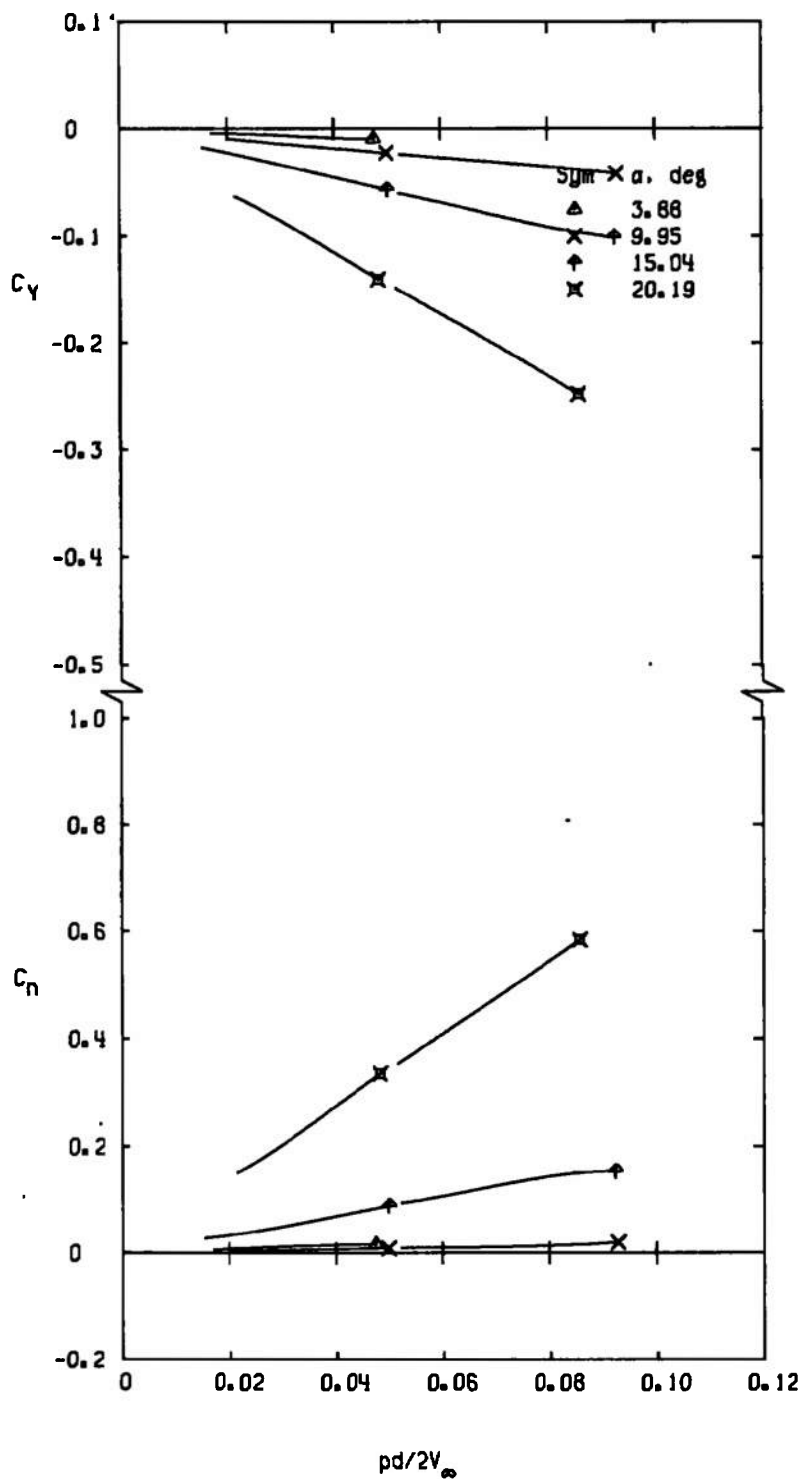
c. $M_\infty = 0.9$
Figure 10. Continued.
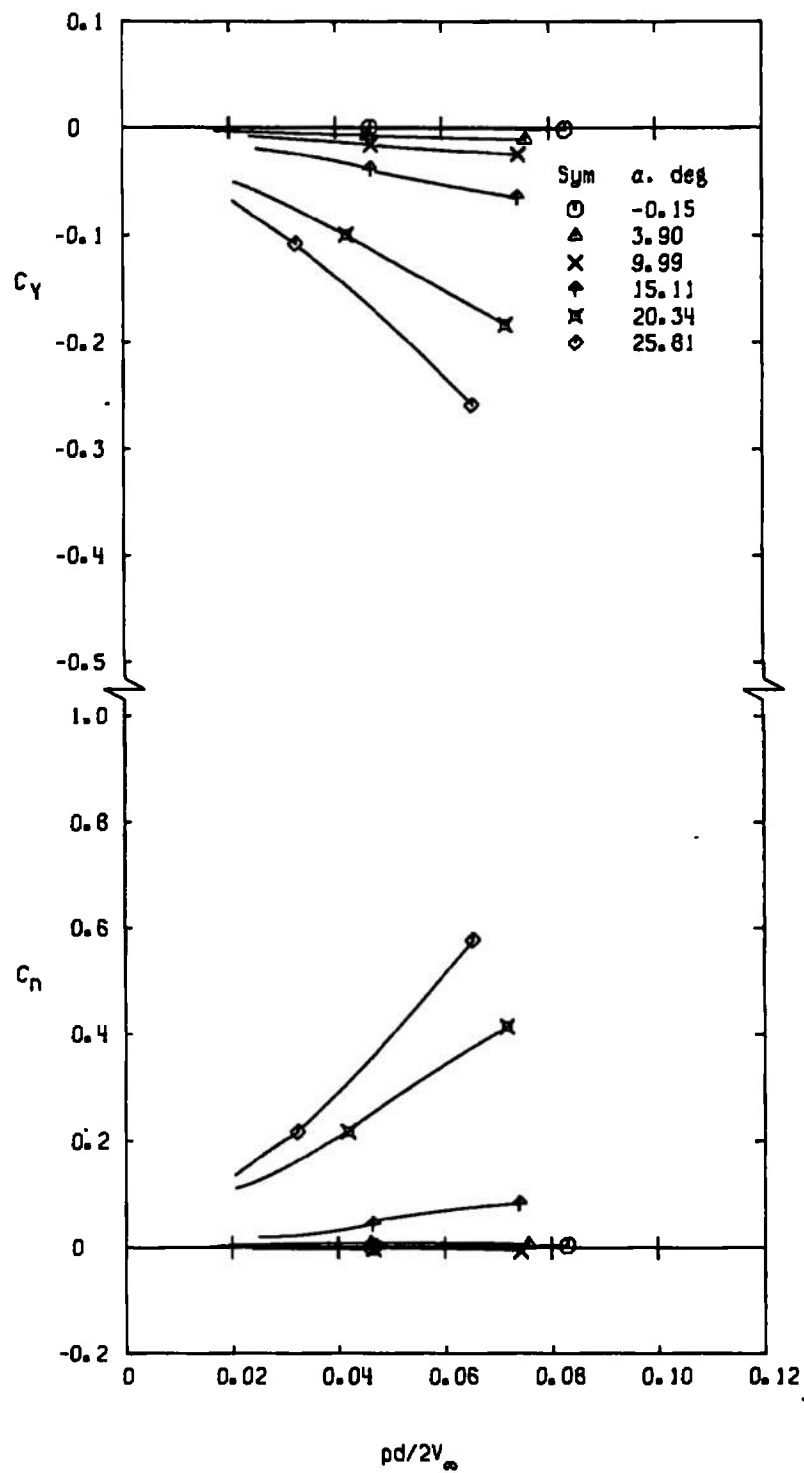
d. $M_\infty = 1.0$
Figure 10. Continued.
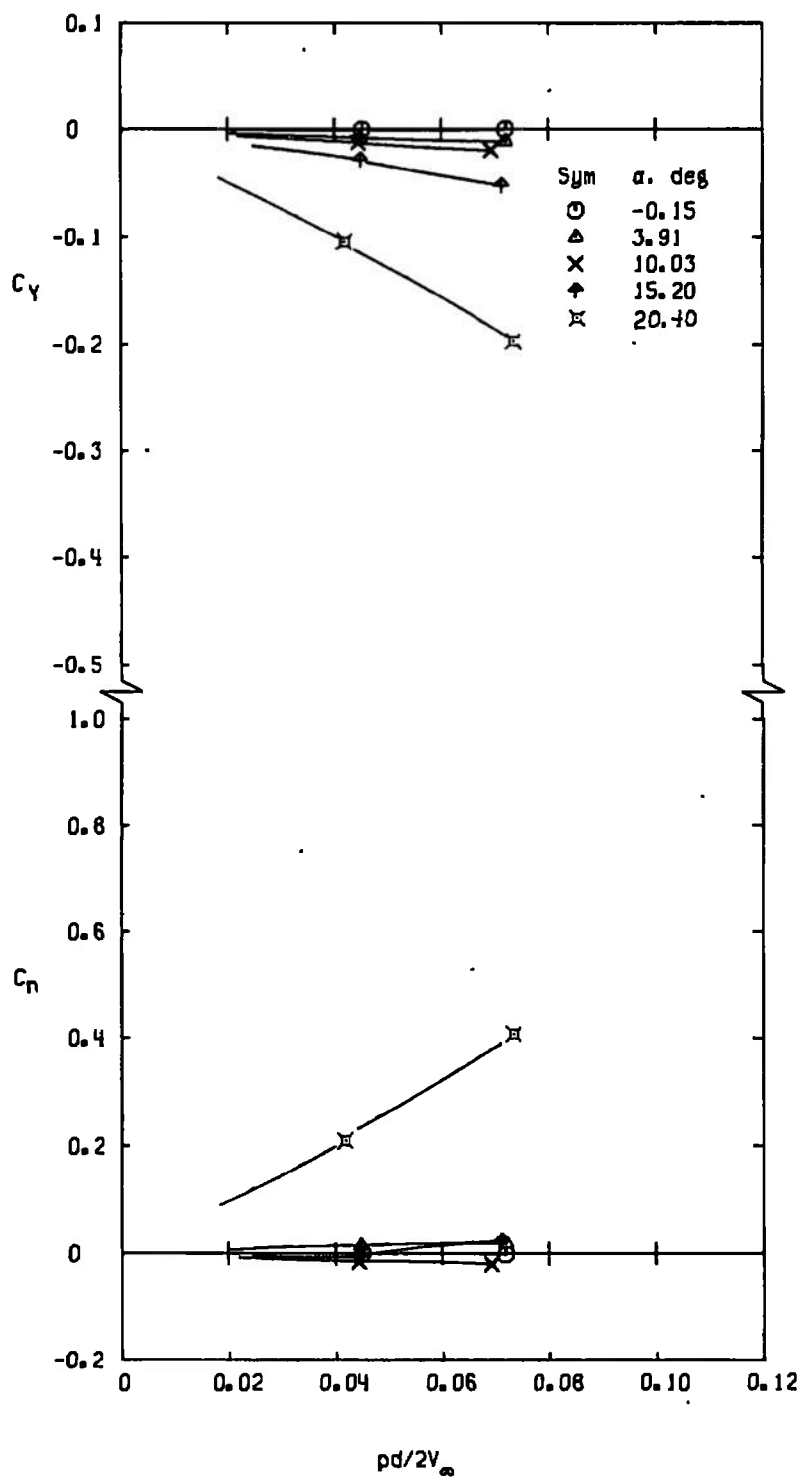
e. $M_\infty = 1.1$
Figure 10. Continued.

46
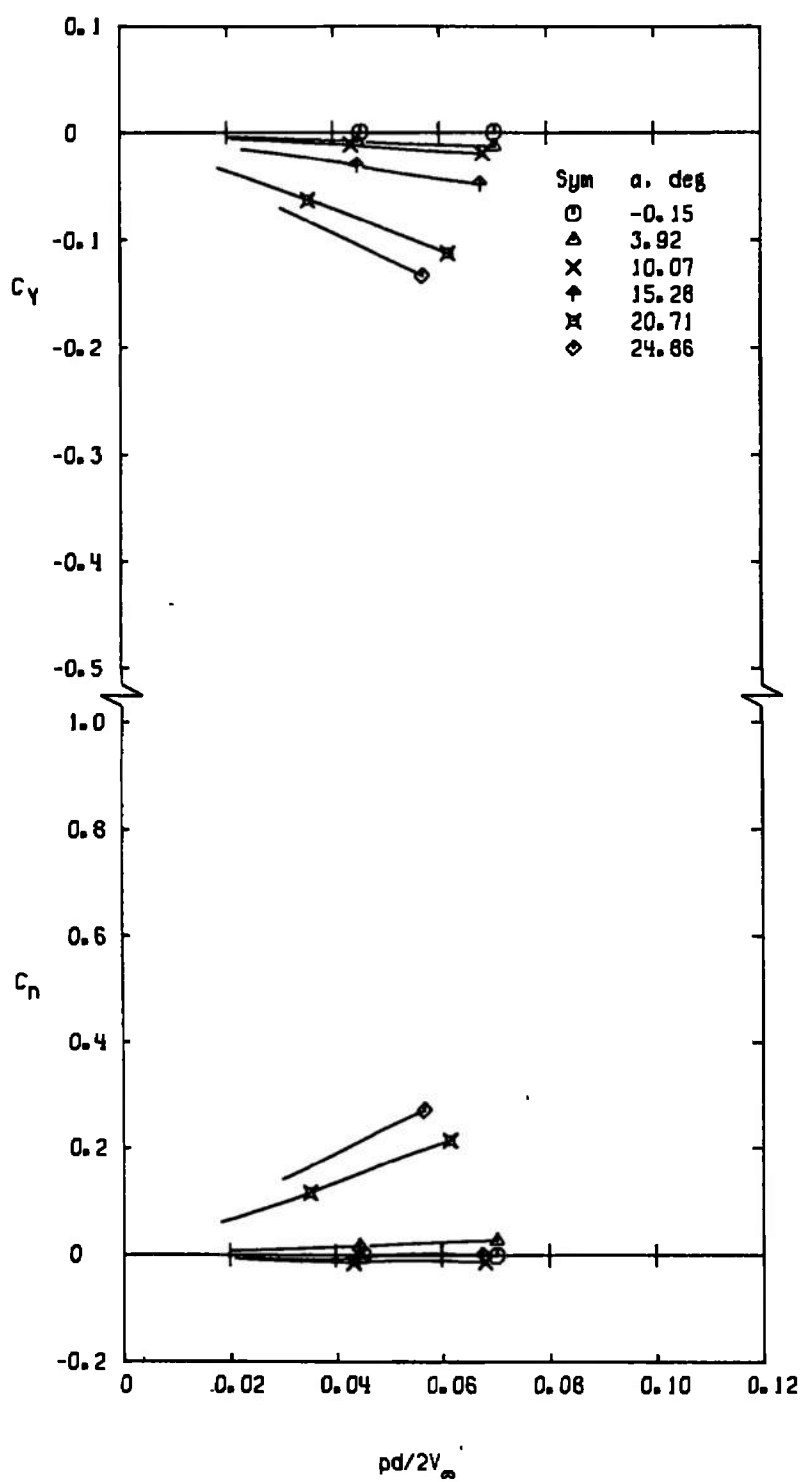
f. $M_\infty = 1.2$
Figure 10. Continued.
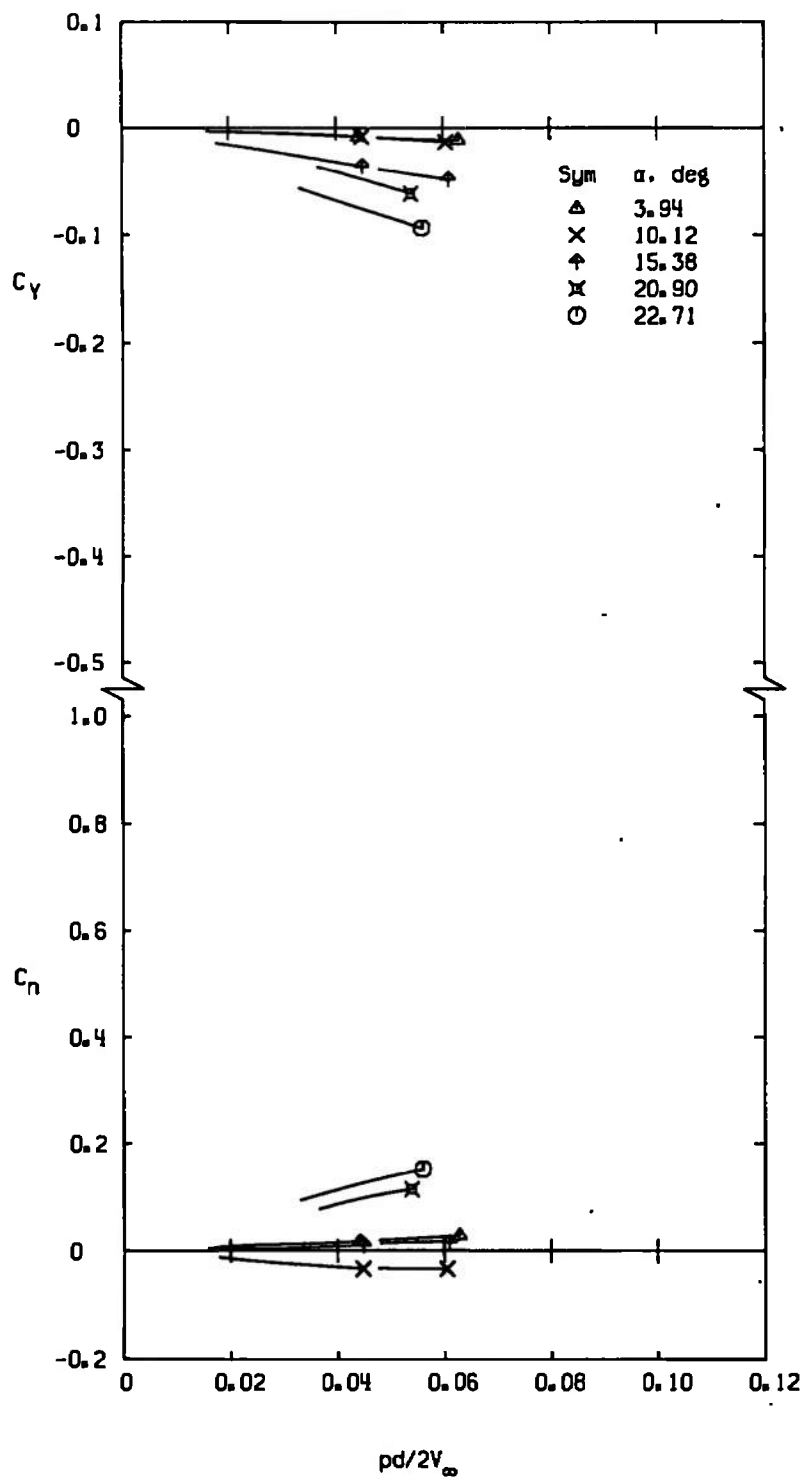
g. $M_\infty = 1.3$
Figure 10. Concluded.
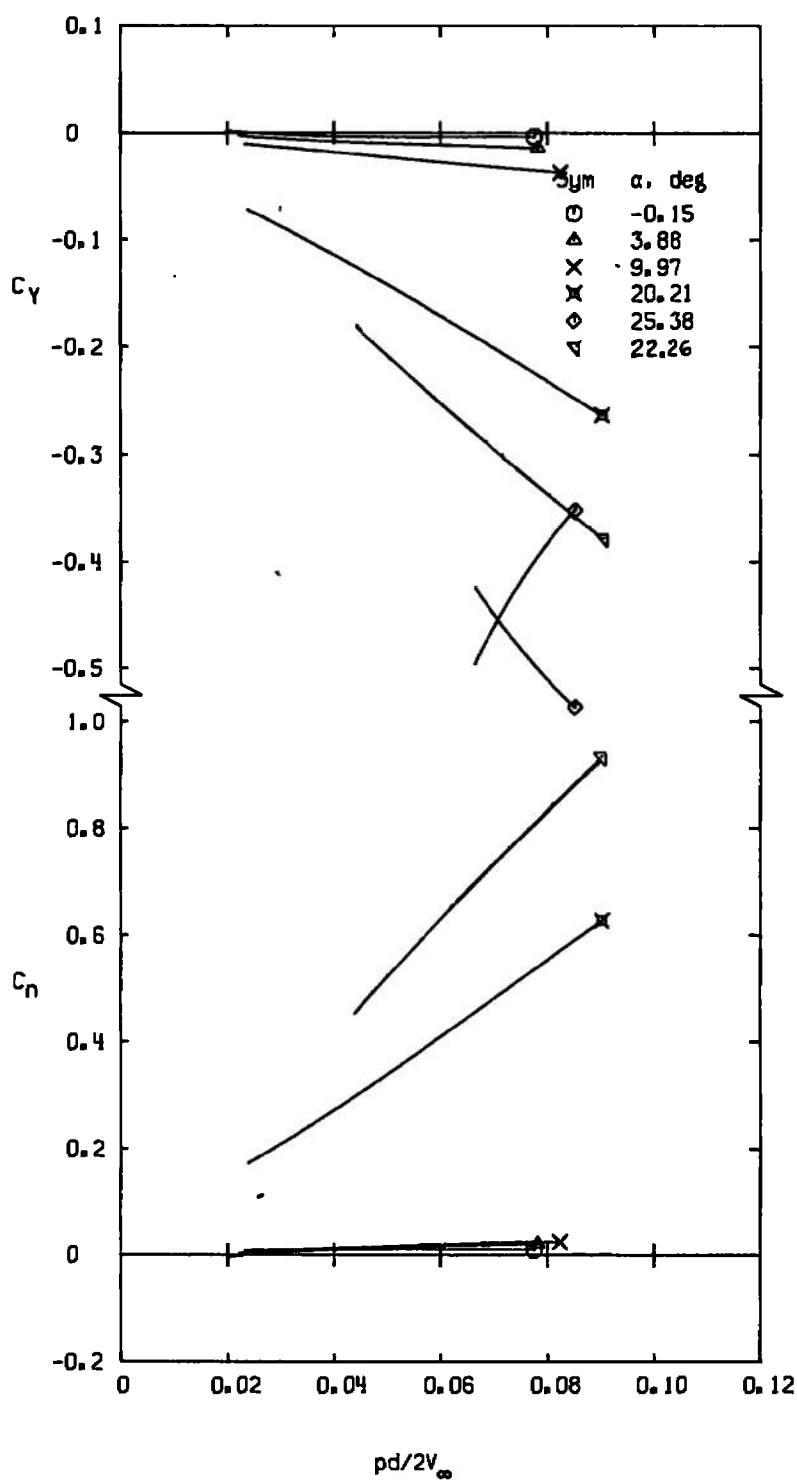
a. $M_\infty = 0.8$

Figure 11. Variation of C_Y with C_n with $pd/2V_\infty$ for configuration FFSW2.
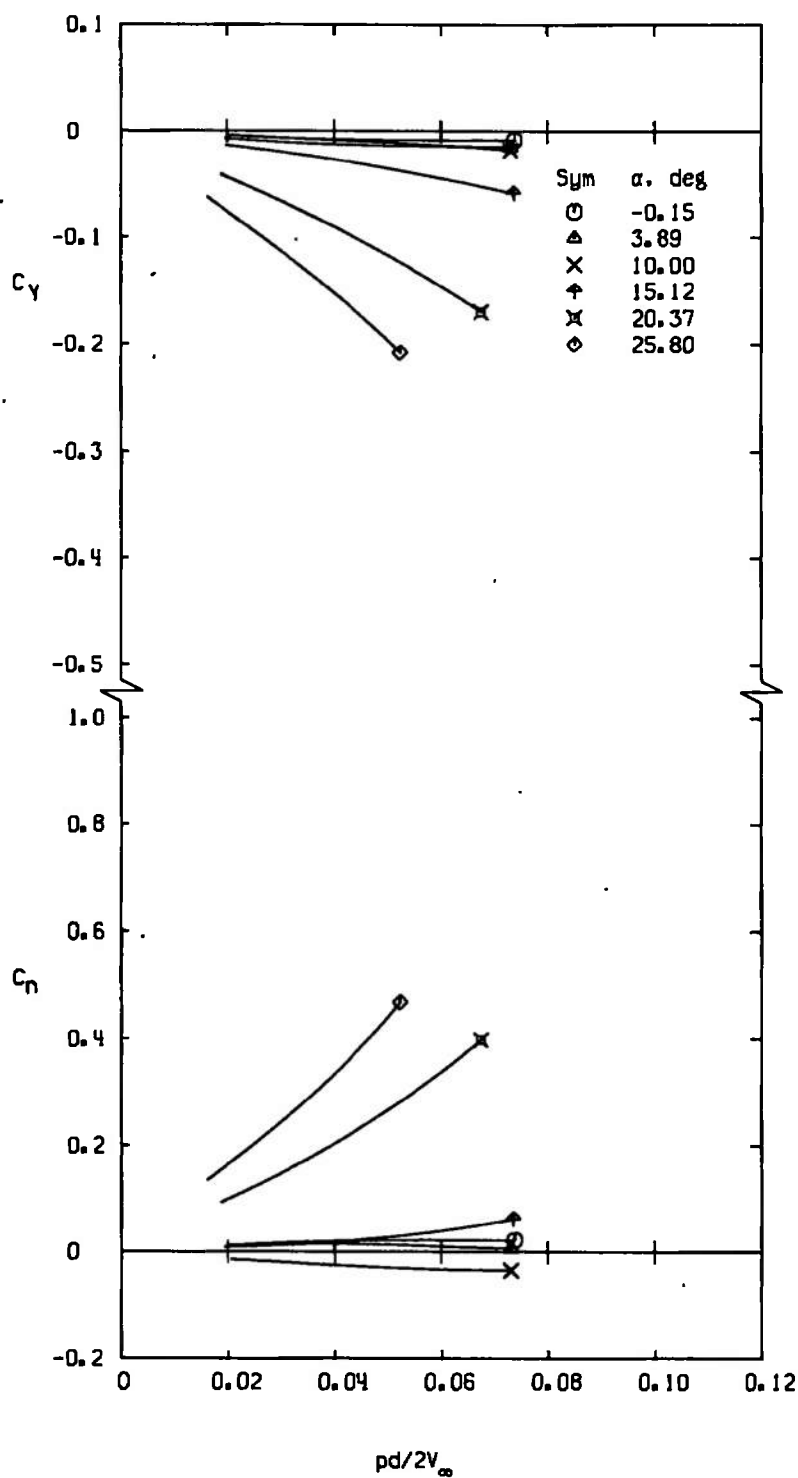
b. $M_\infty = 1.0$
Figure 11. Continued.
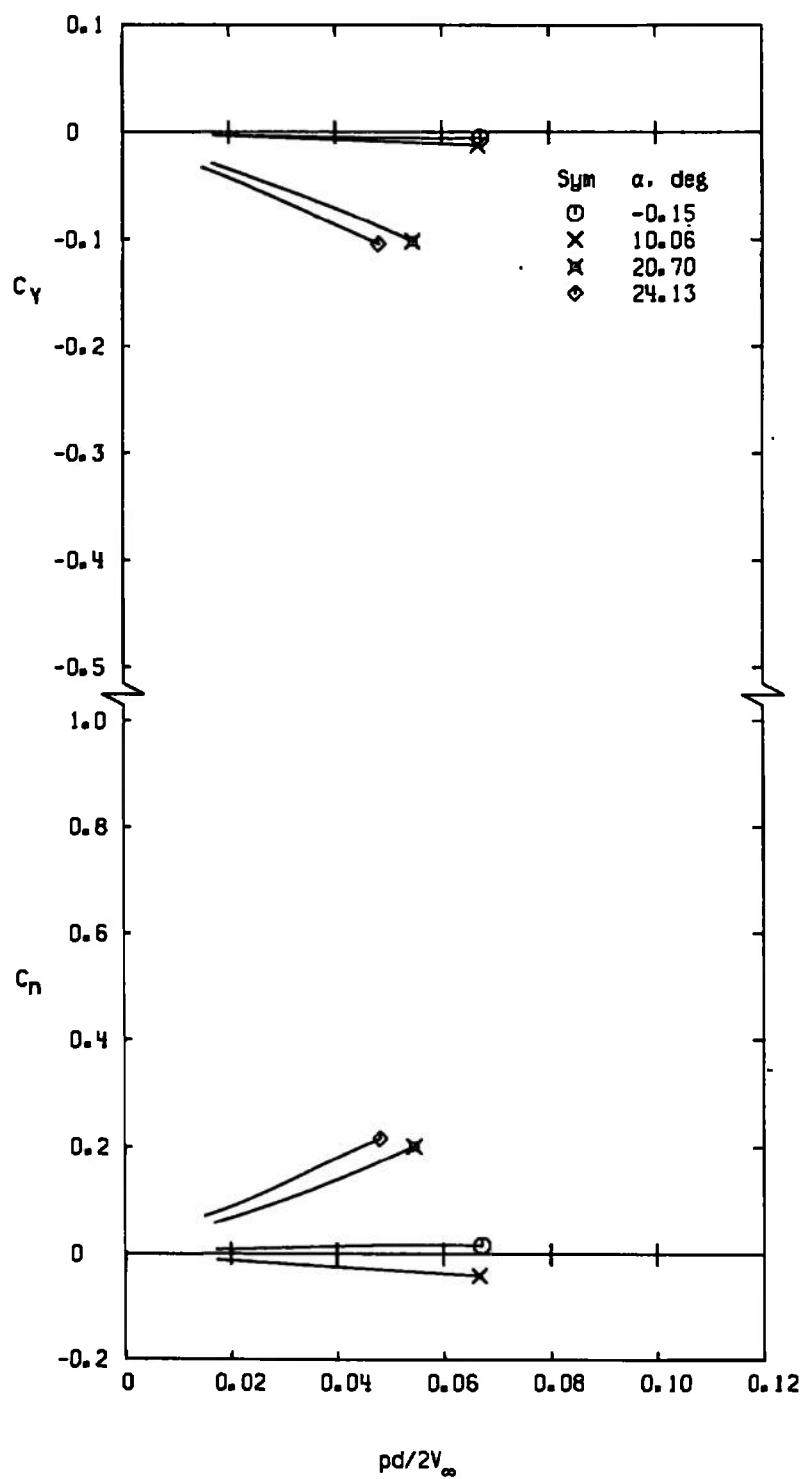
c. $M_\infty = 1.2$
Figure 11. Concluded.
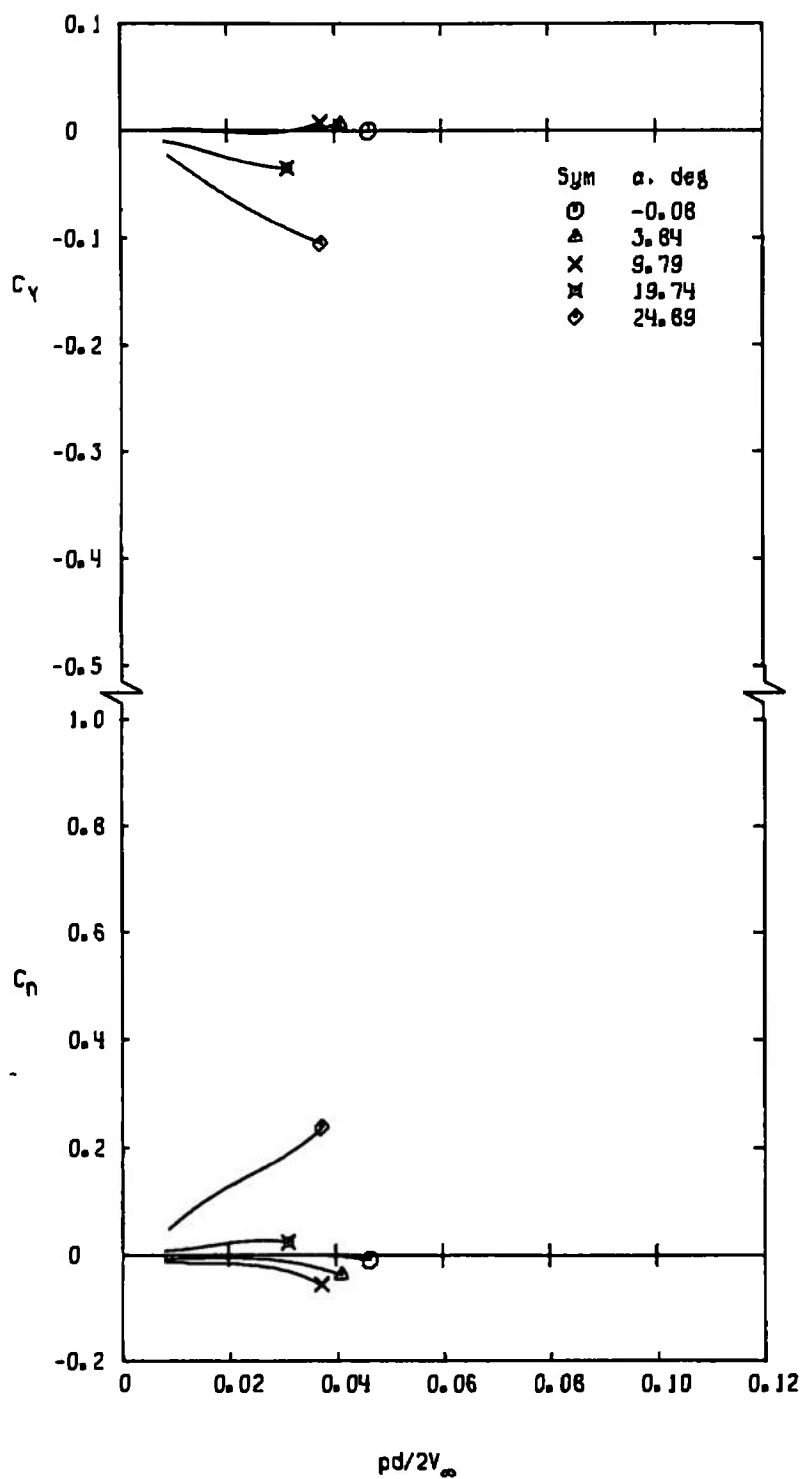
a. $M_\infty = 0.8$

Figure 12. Variation of C_Y and C_n with $pd/2V_\infty$ for configuration ISRE.
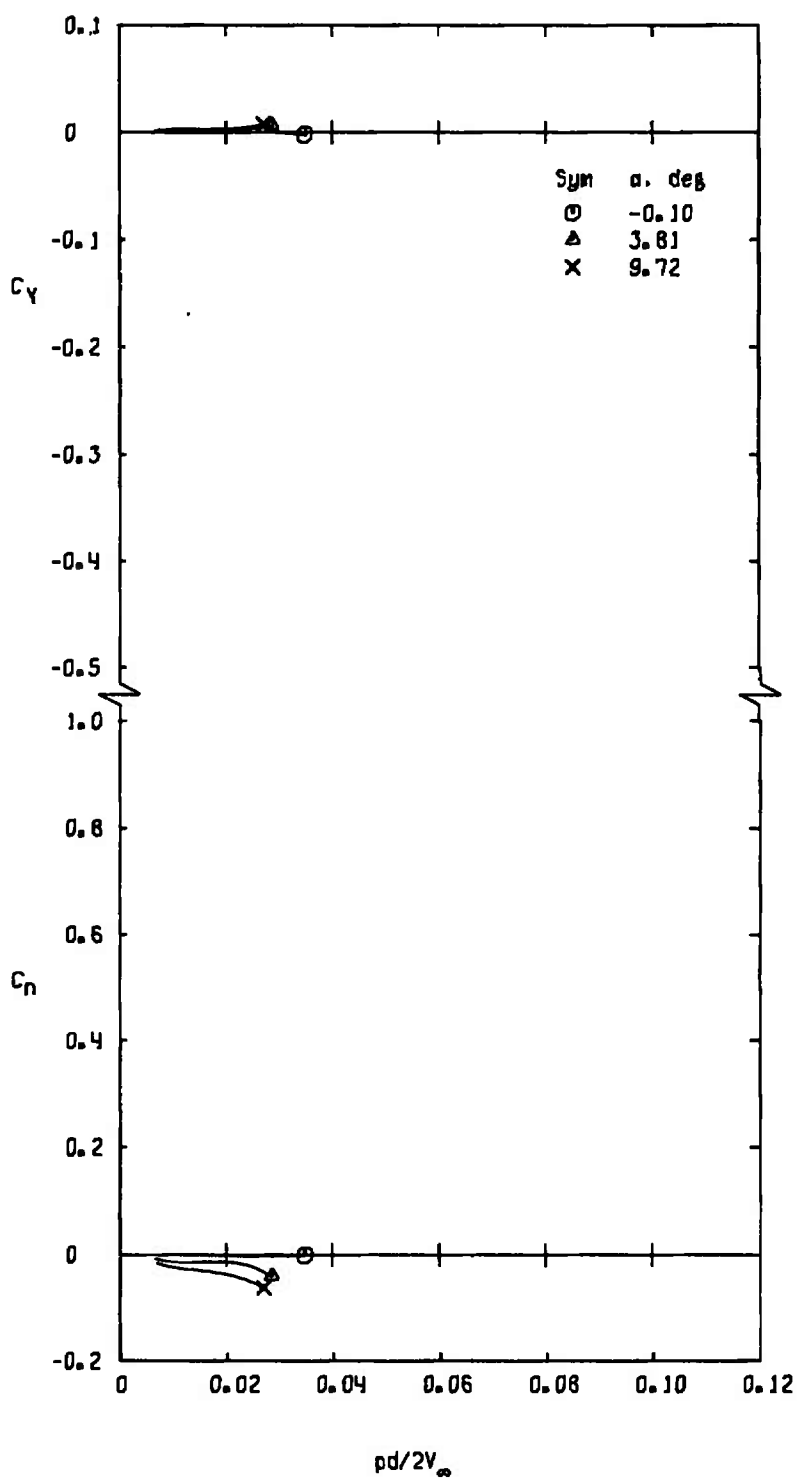
b. $M_\infty = 1.0$
Figure 12. Continued.

53
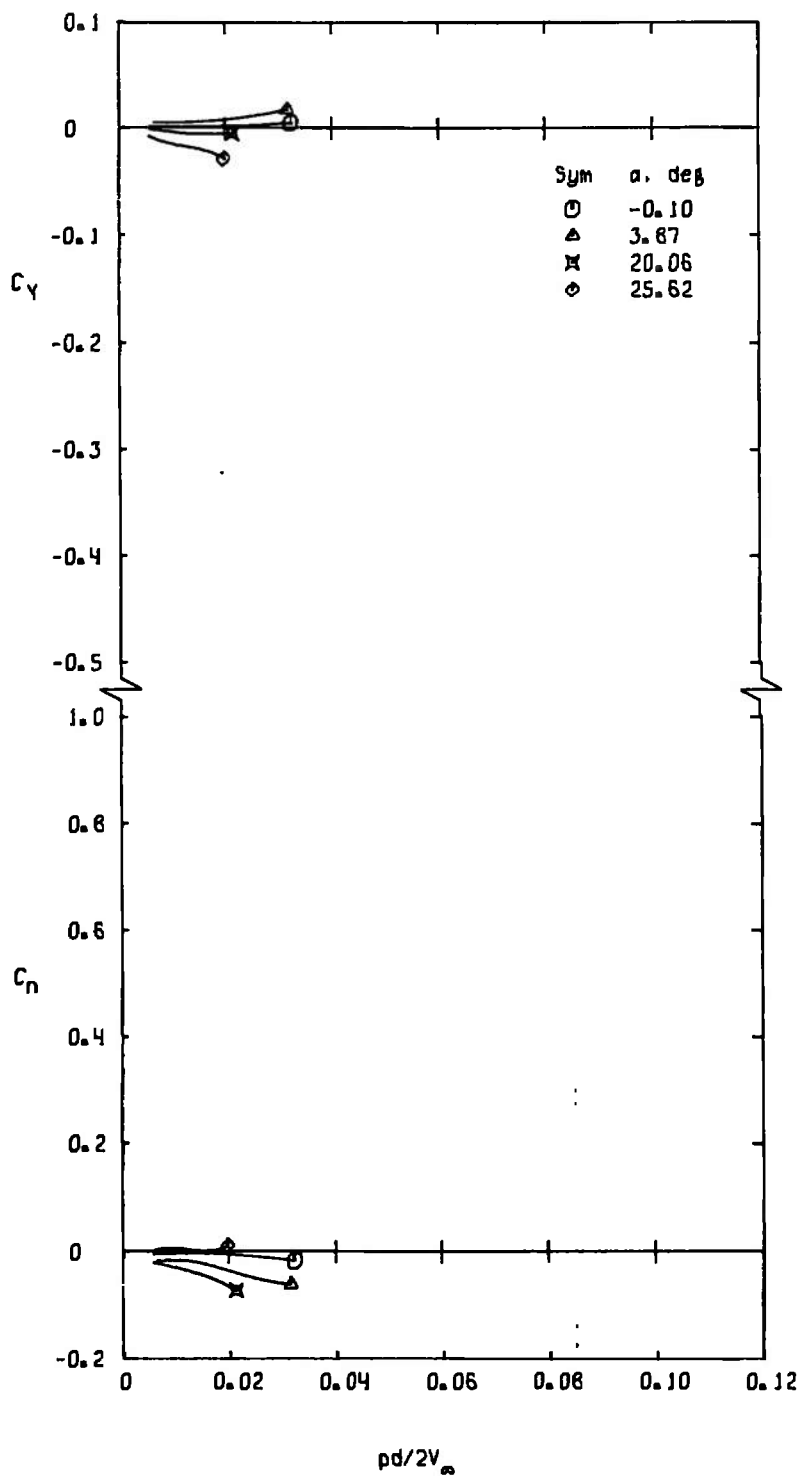
c. $M_\infty = 1.2$
Figure 12. Concluded.
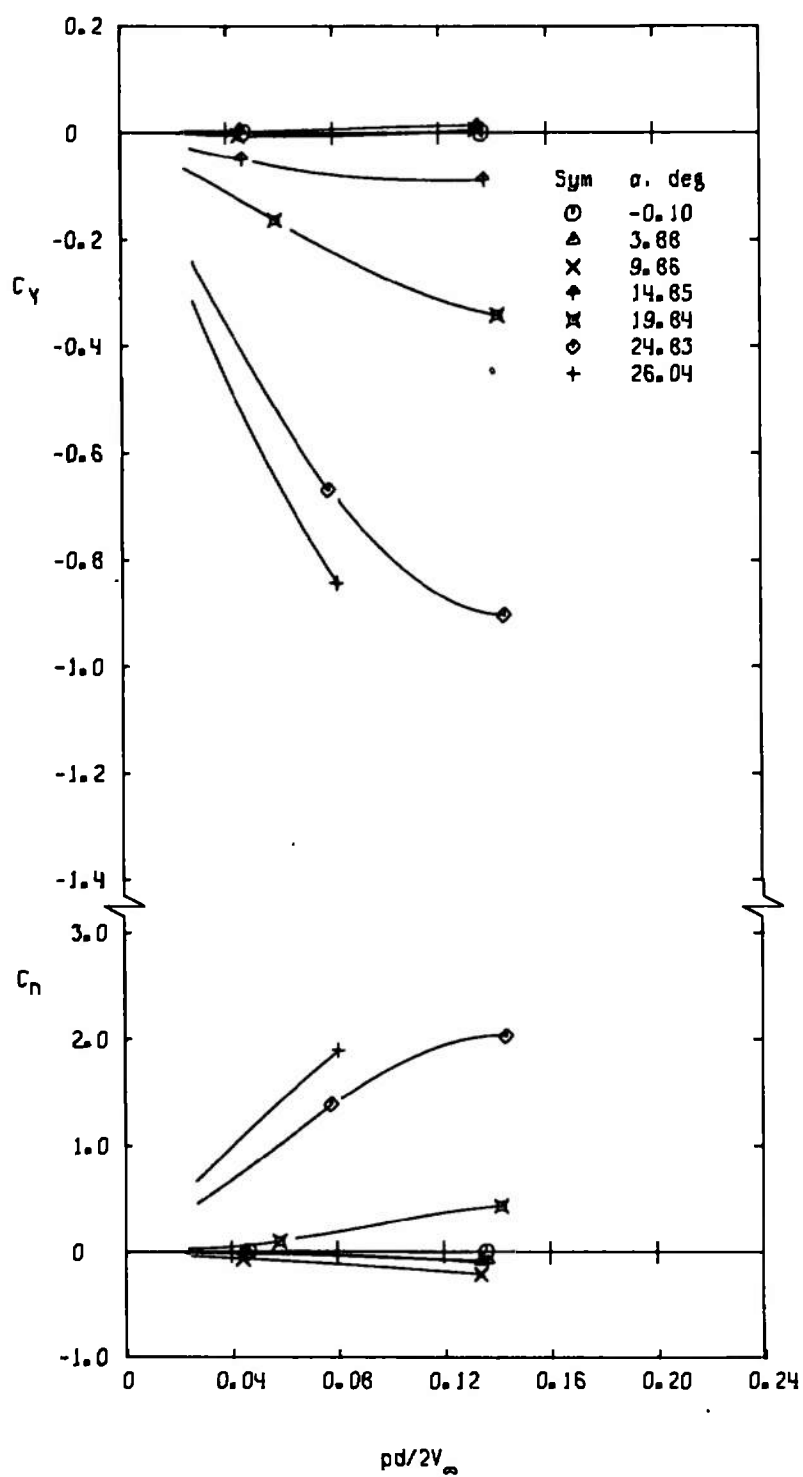
a. $M_\infty = 0.4$

Figure 13. Variation of C_Y and C_n with $pd/2V_\infty$ for configuration ISREW1.
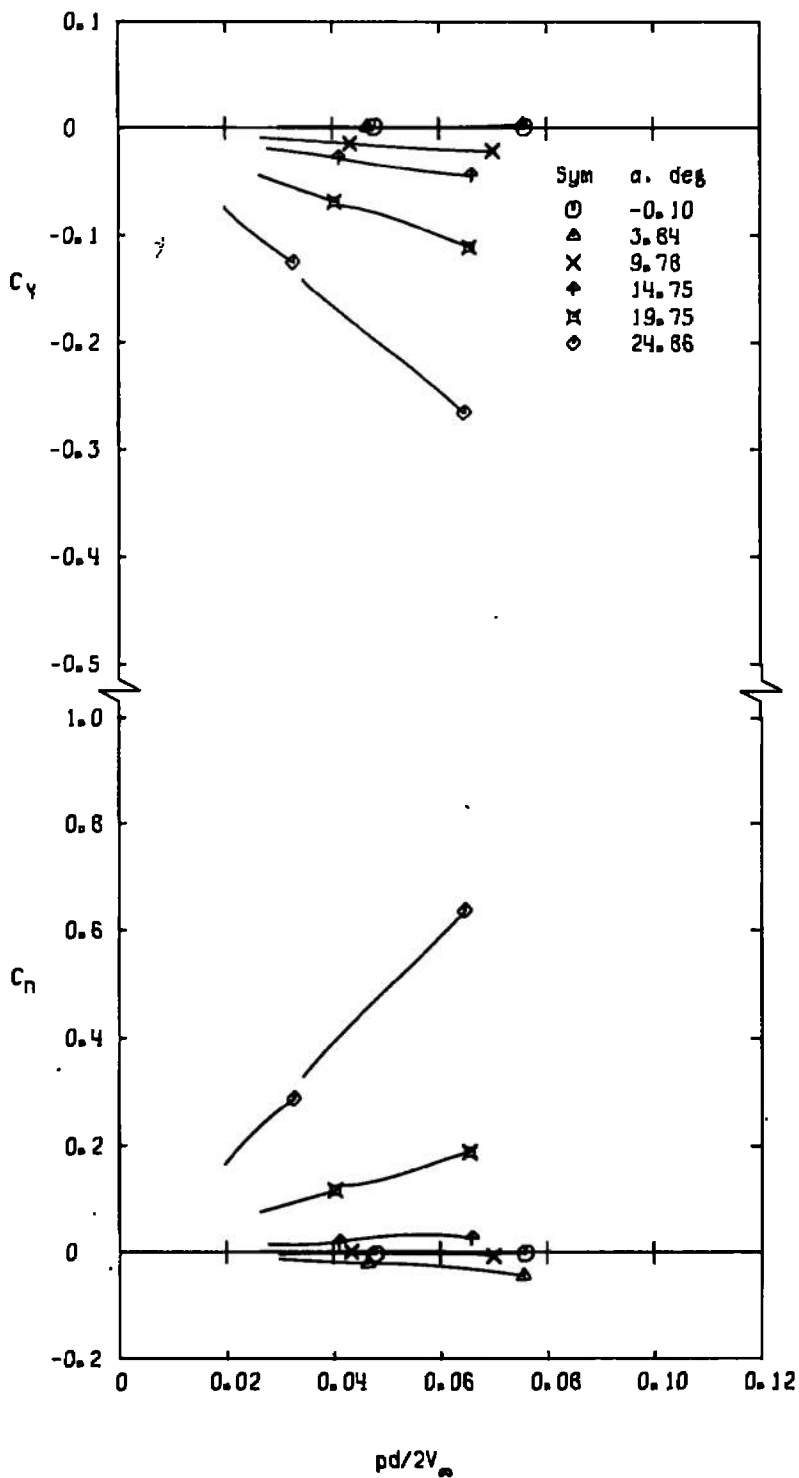
b. $M_\infty = 0.8$

Figure 13. Continued.
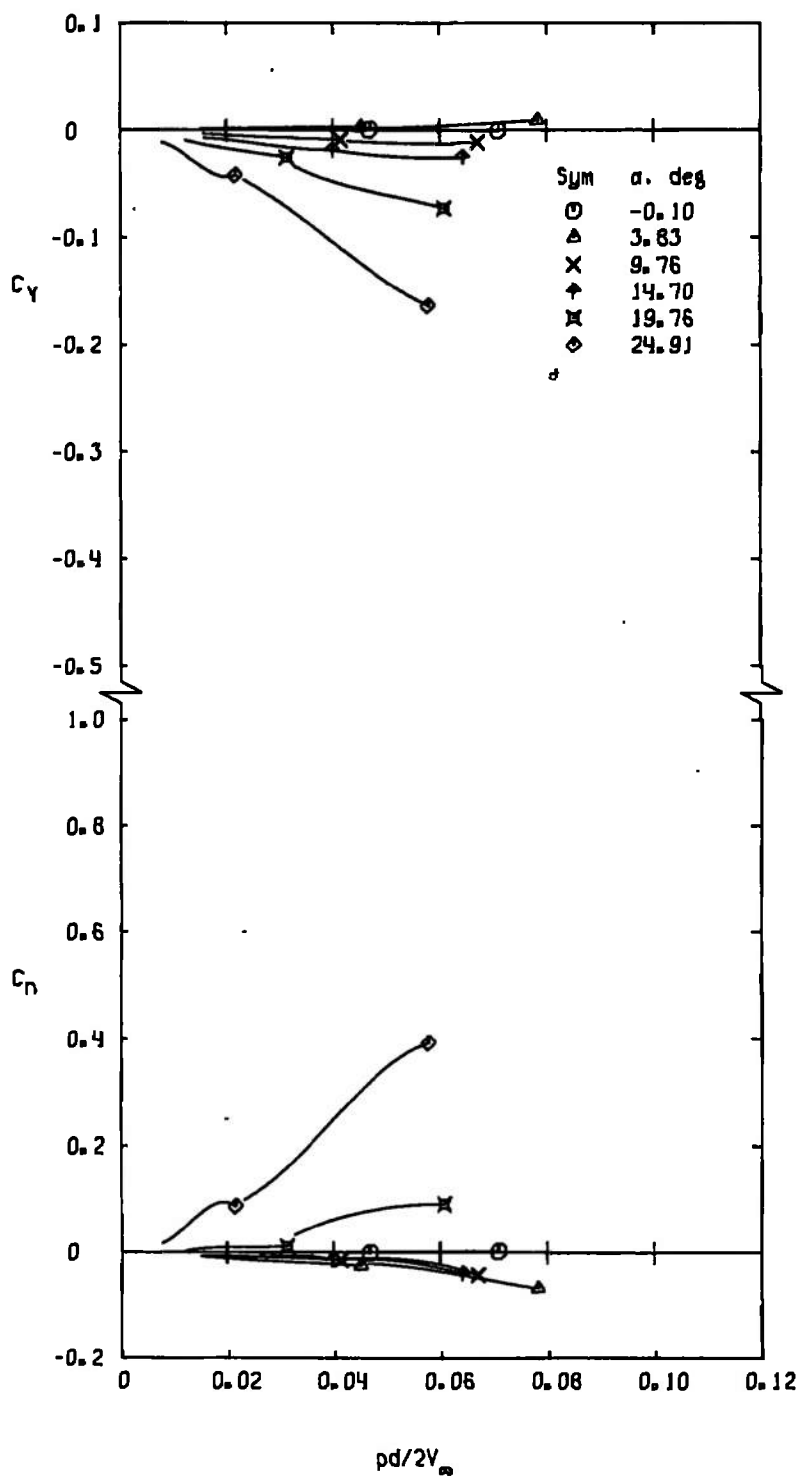
c. $M_\infty = 0.9$
Figure 13. Continued.
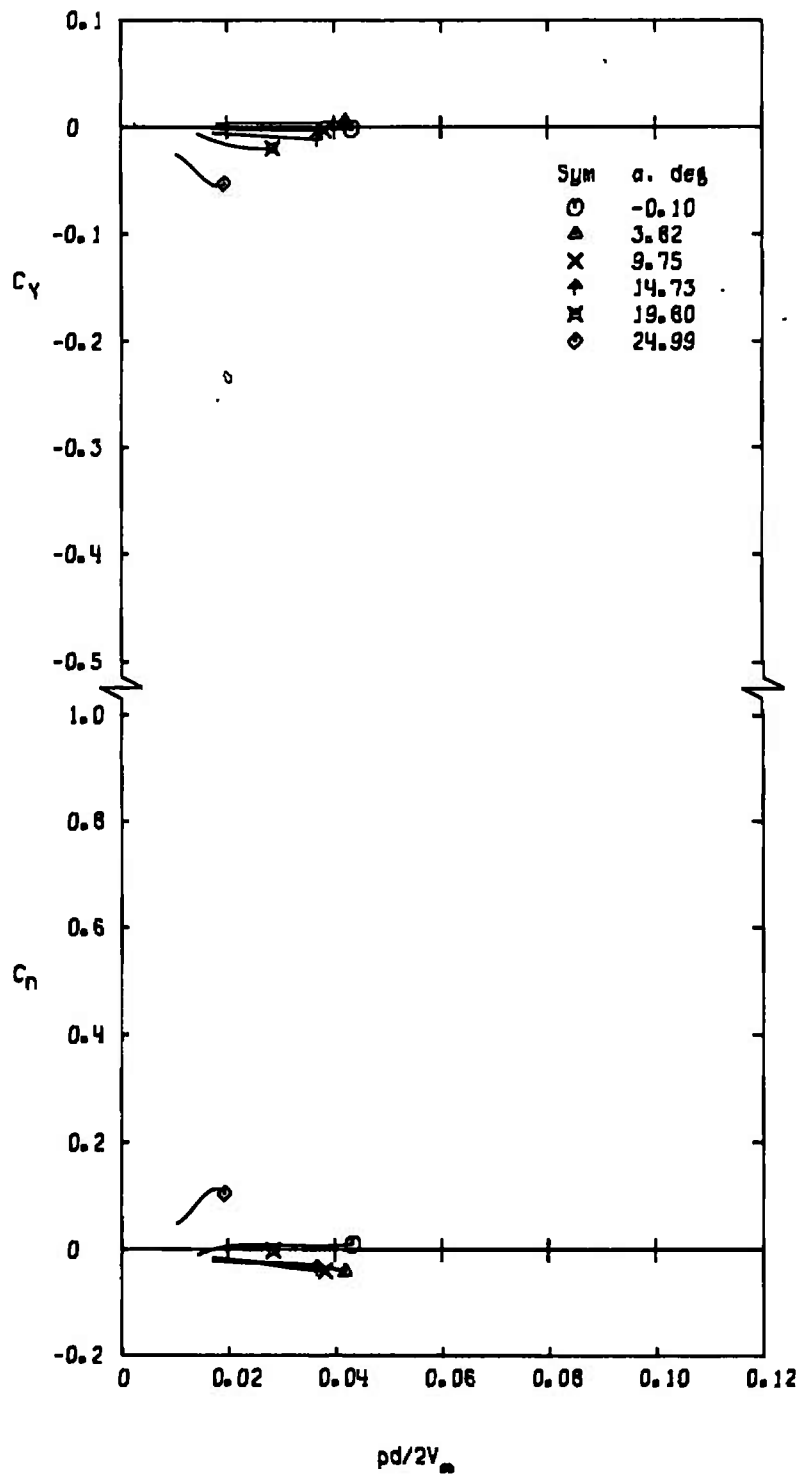
d. $M_\infty = 1.0$
Figure 13. Continued.
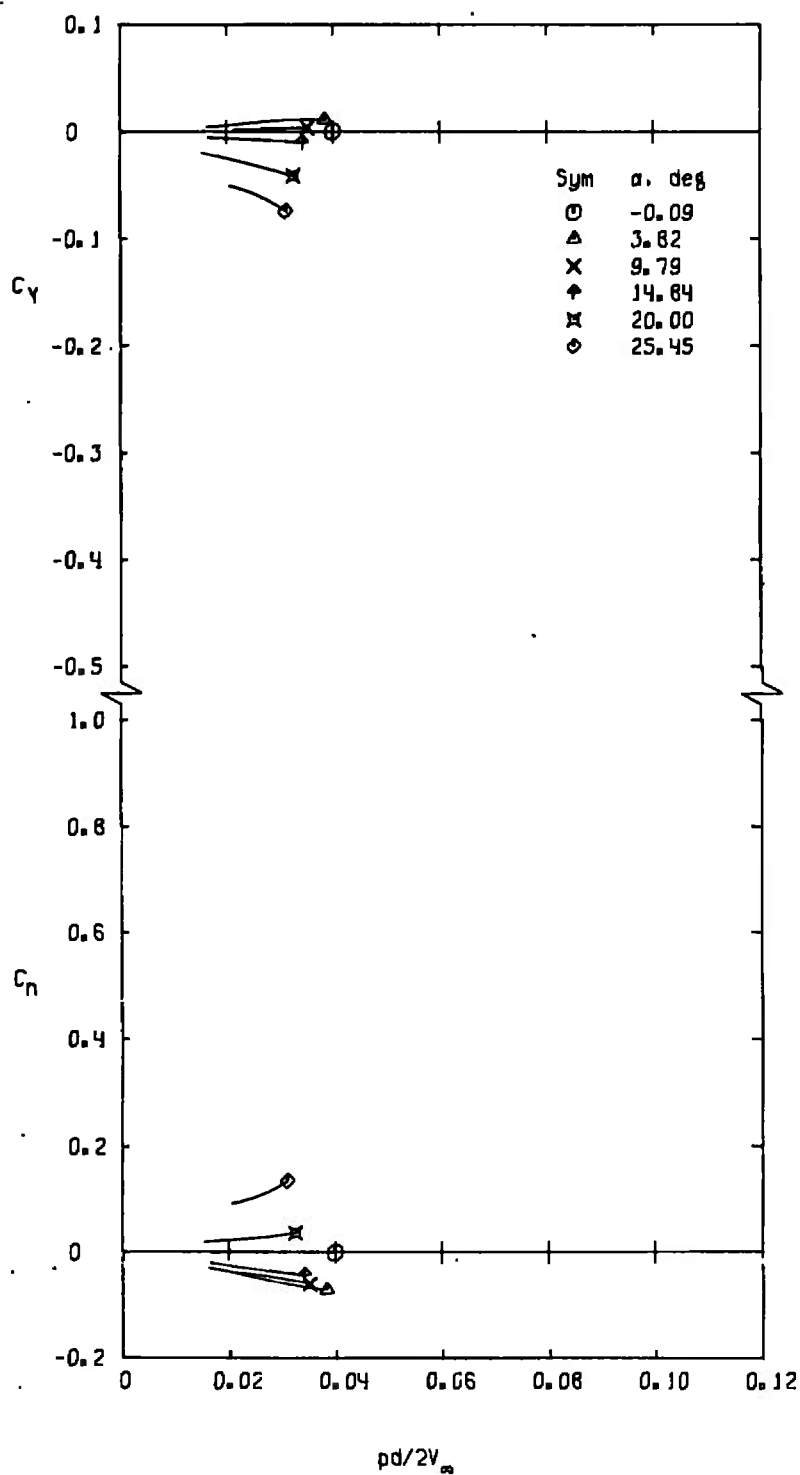
e. $M_\infty = 1.1$
Figure 13. Continued.
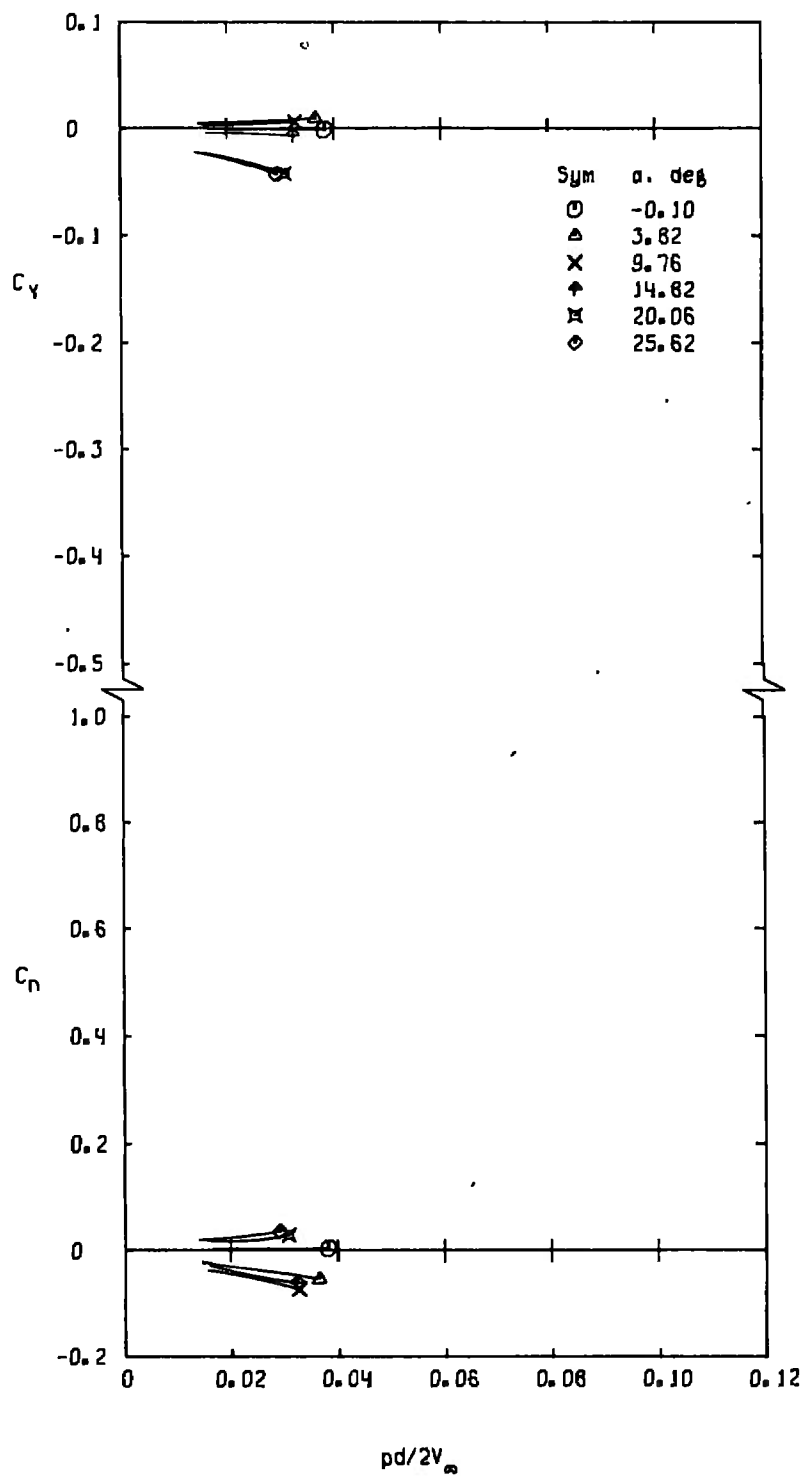
f. $M_\infty = 1.2$
Figure 13. Continued.
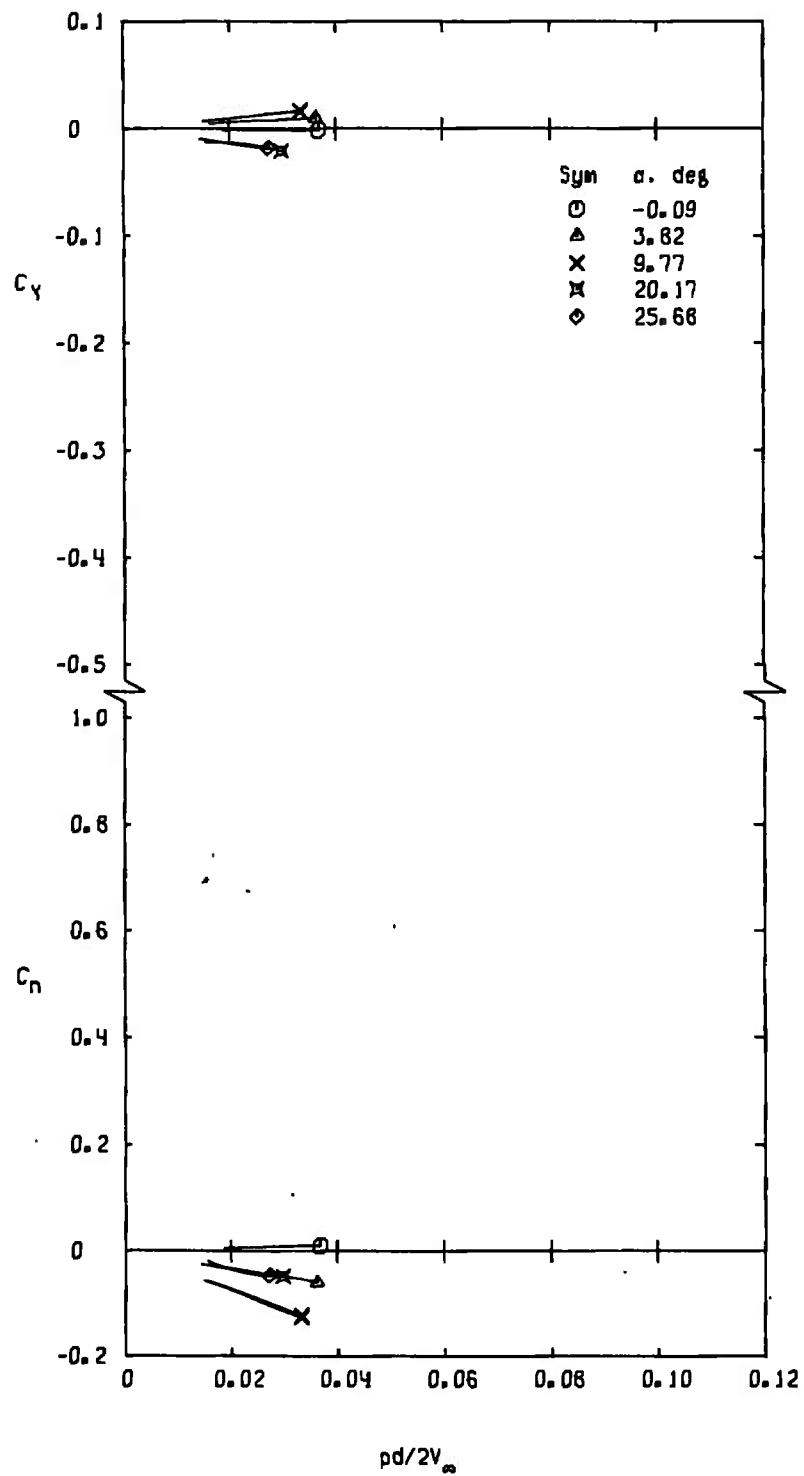
g. $M_\infty = 1.3$

Figure 13. Concluded.
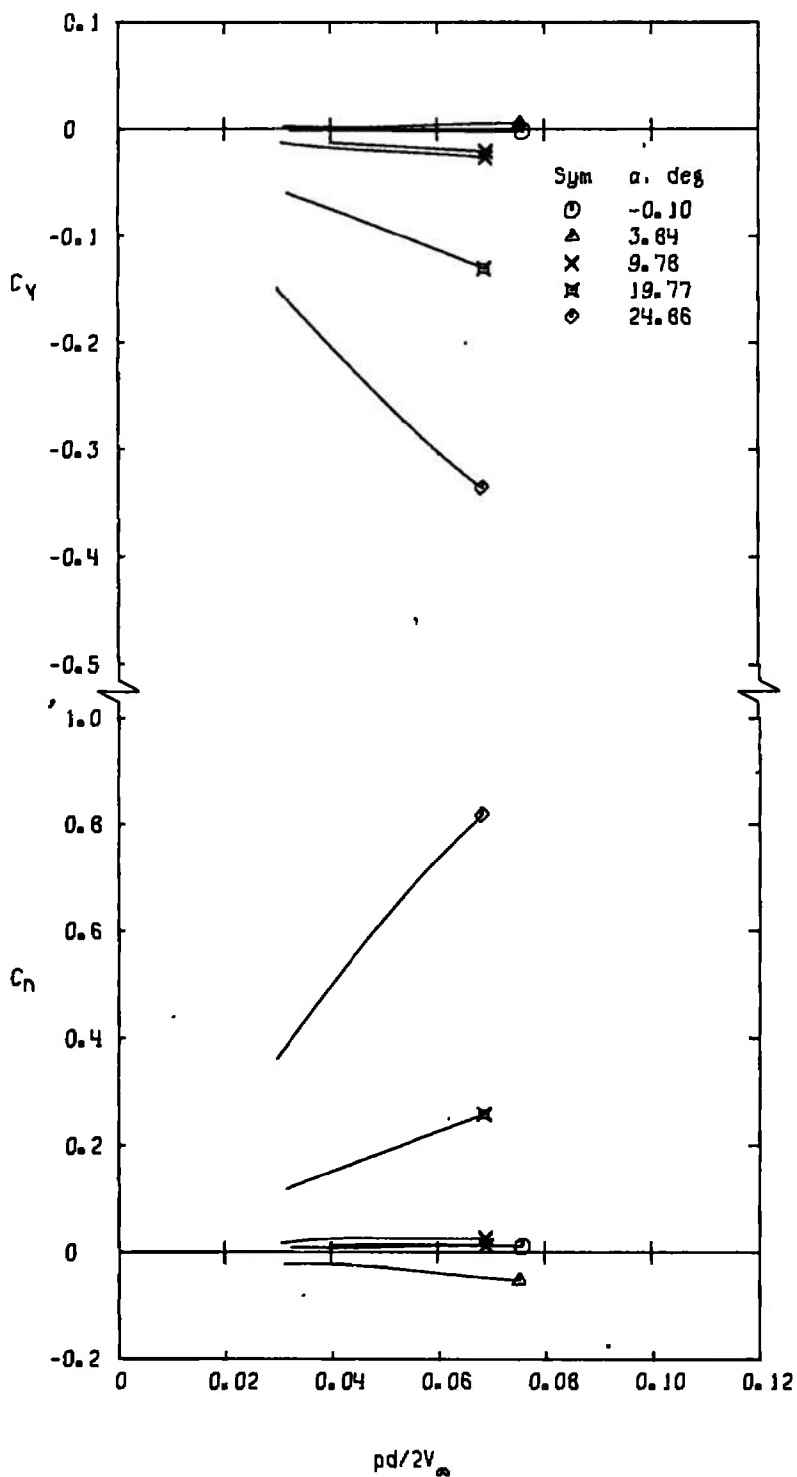
a. $M_\infty = 0.8$
Figure 14. Variation of C_Y and C_n with $pd/2V_\infty$ for configuration ISREW2.
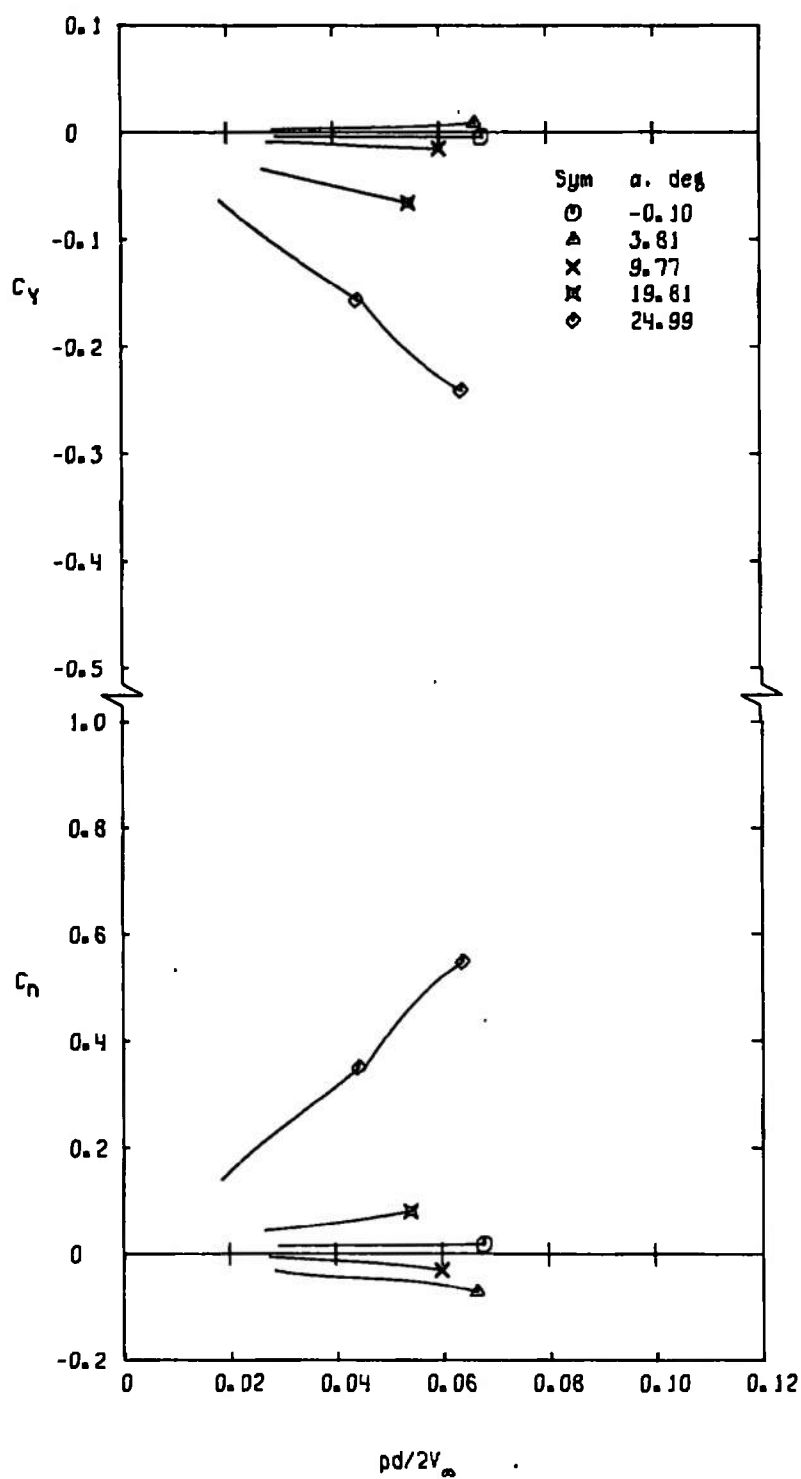
b. $M_\infty = 1.0$
Figure 14. Continued.
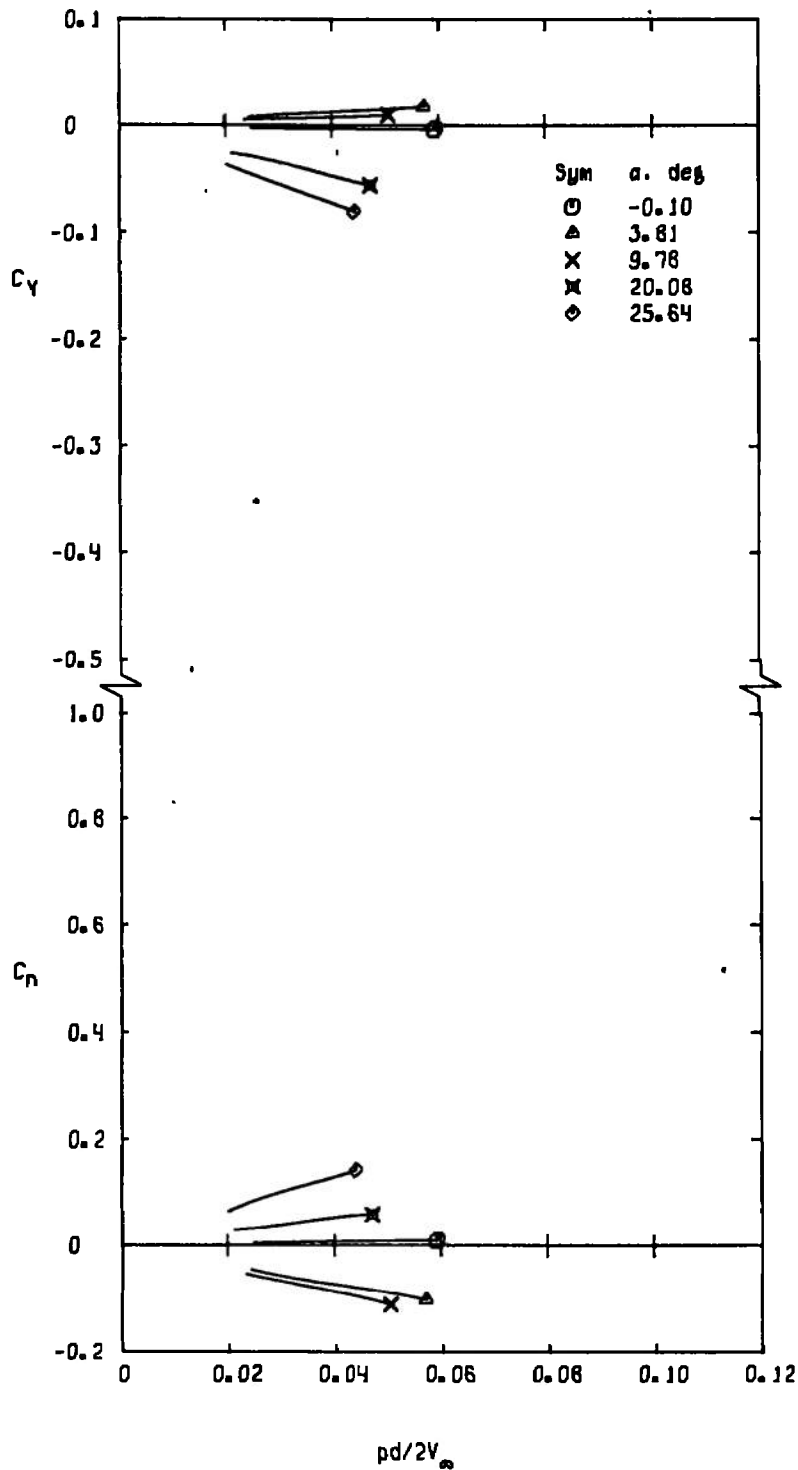
c. $M_\infty = 1.2$

Figure 14. Concluded.
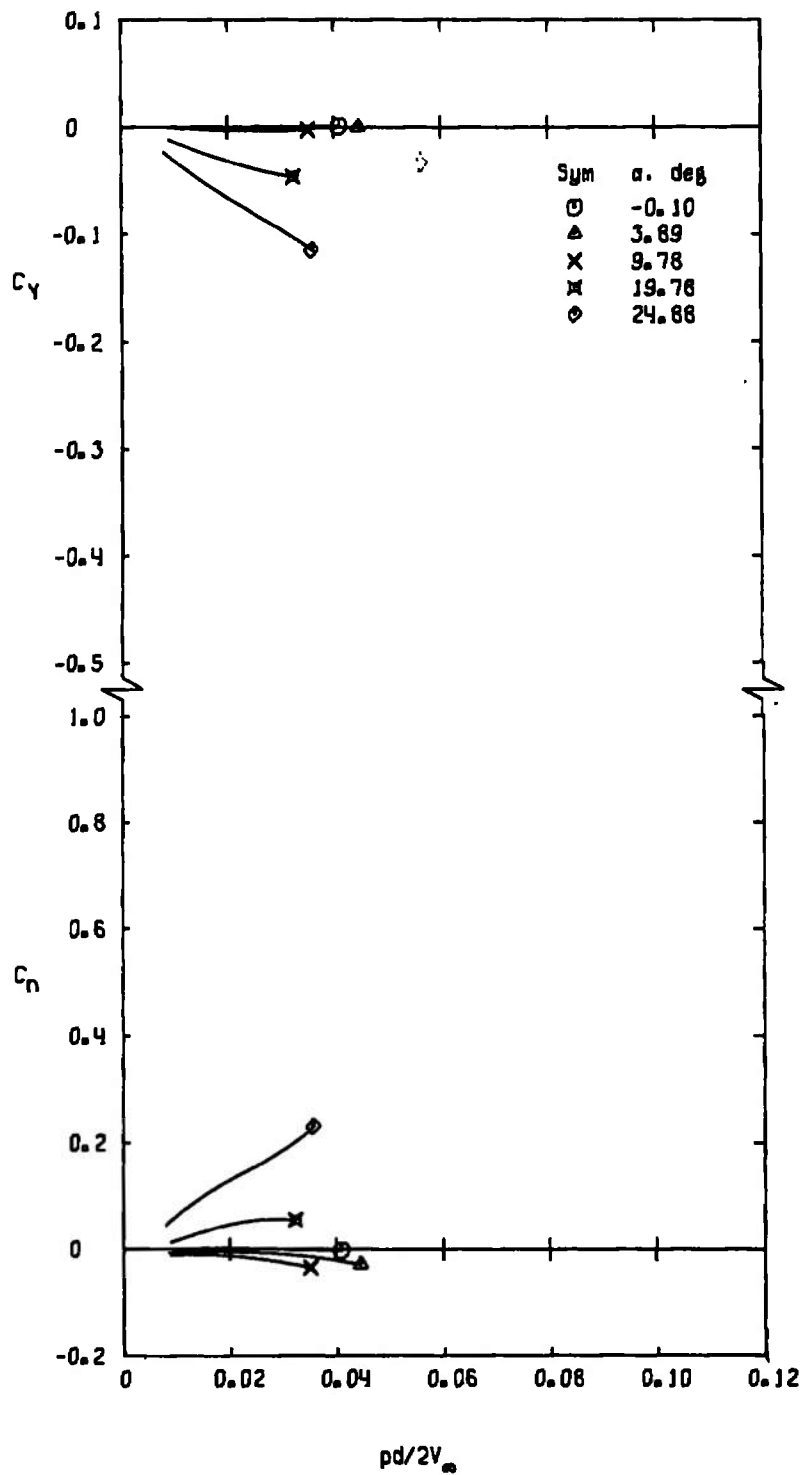
a. $M_\infty = 0.8$

Figure 15. Variation of C_Y and C_n with $pd/2V_\infty$ for configuration ISRES.
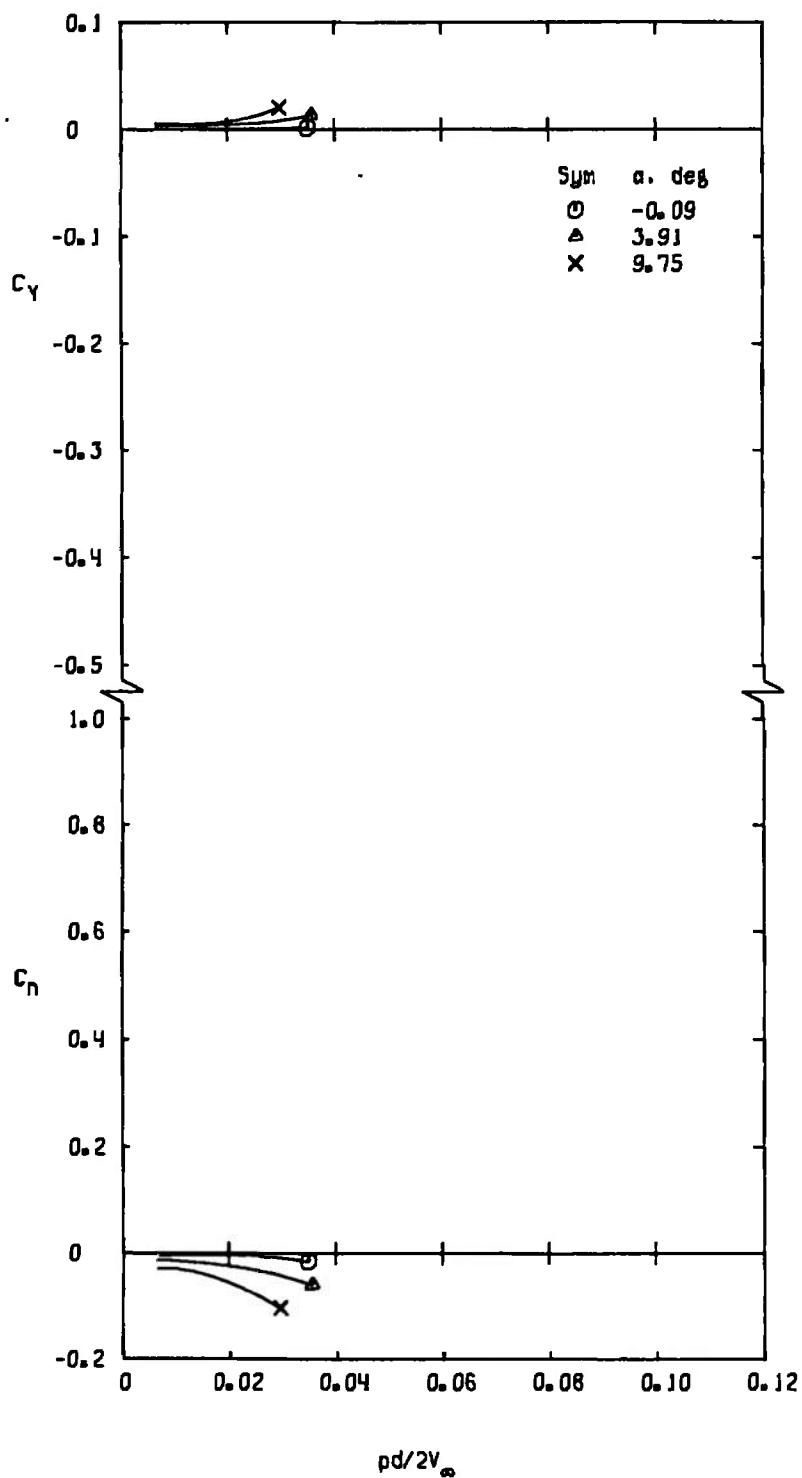
b. $M_\infty = 1.0$

Figure 15. Continued.
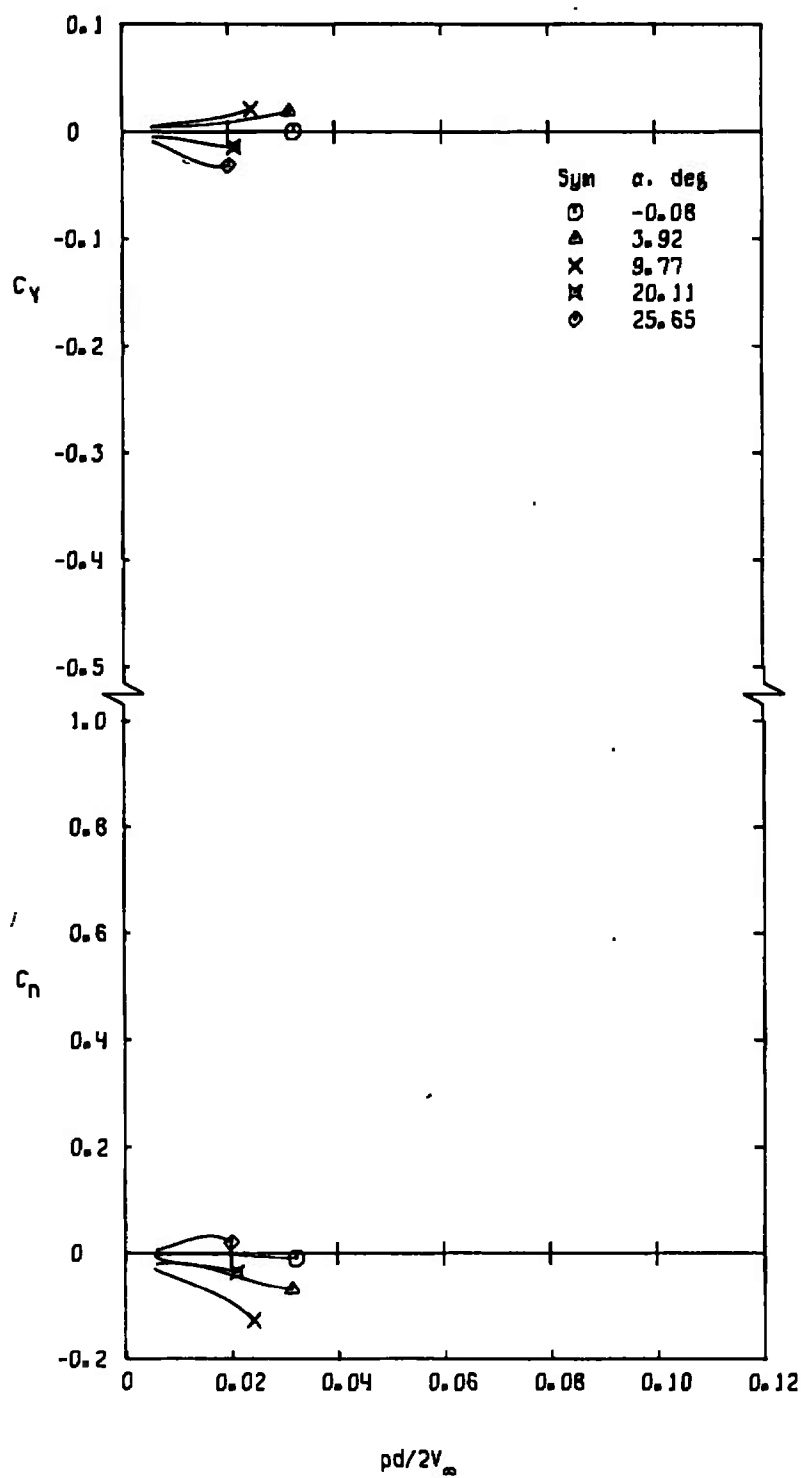
c. $M_\infty = 1.2$
Figure 15. Concluded.
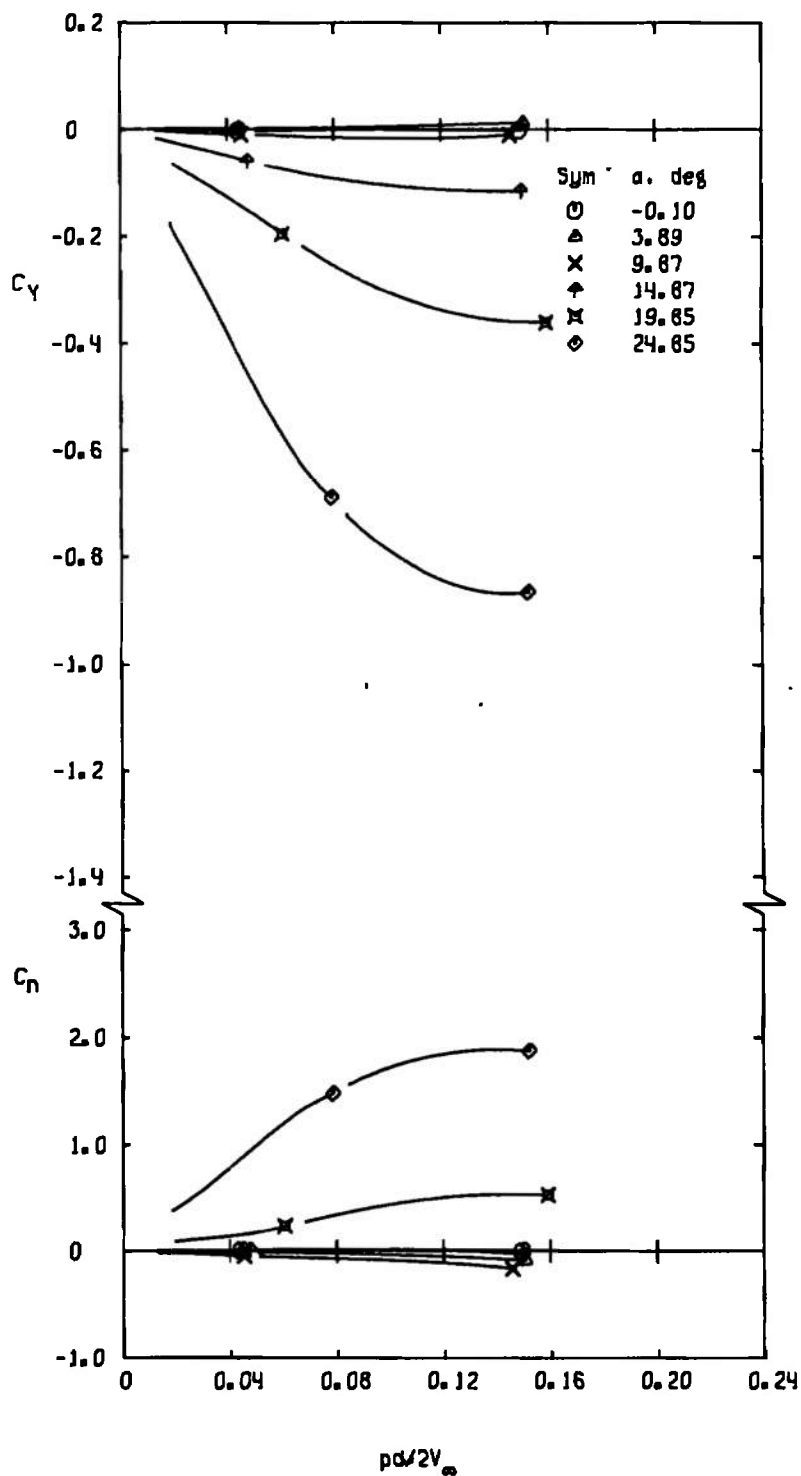
pd/2V∞

a. M∞ = 0.4

Figure 16. Variation of C_Y and C_n with pd/2V∞ for configuration ISRESW1.
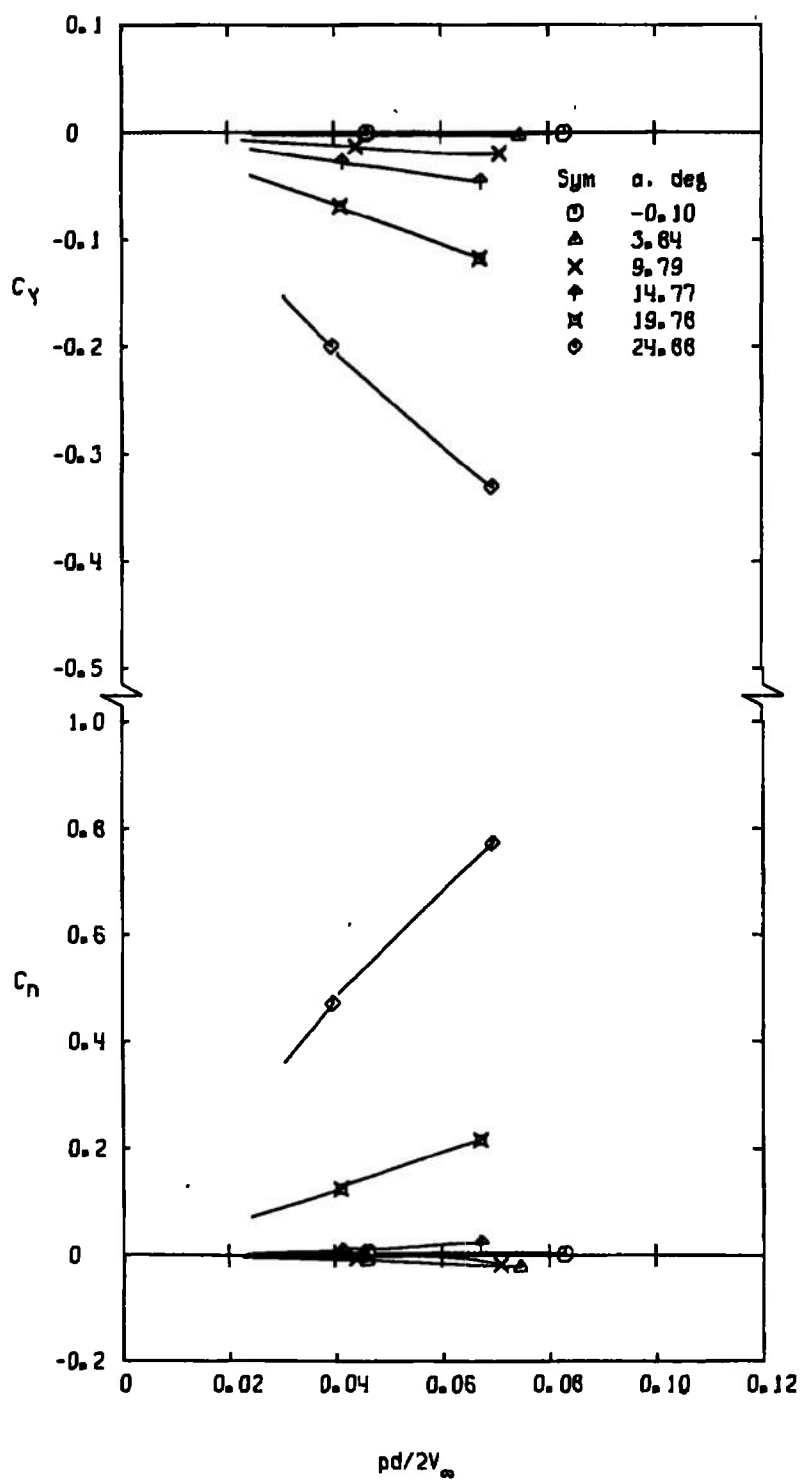
b. $M_\infty = 0.8$
Figure 16. Continued.
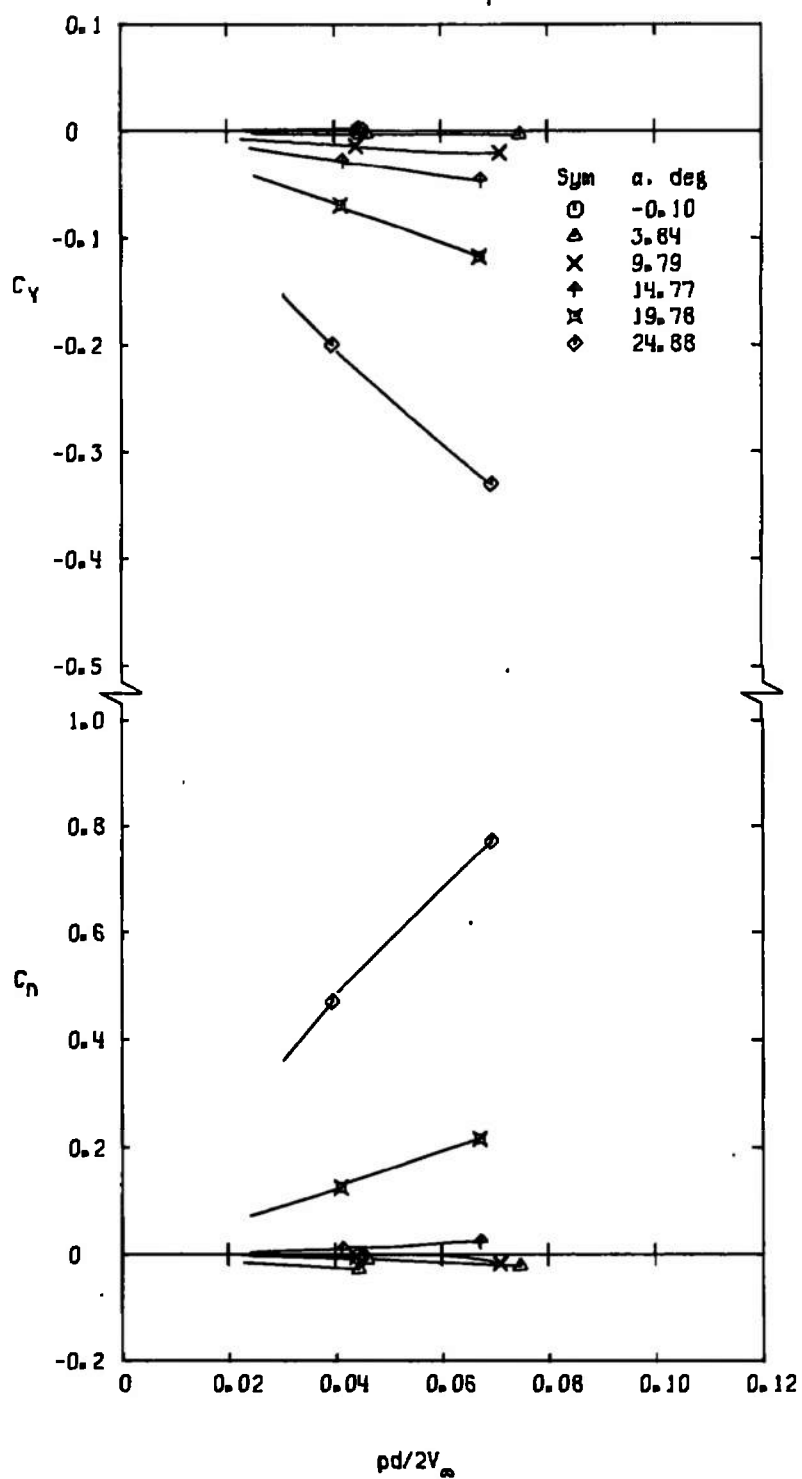
c. $M_\infty = 0.9$

Figure 16. Continued.
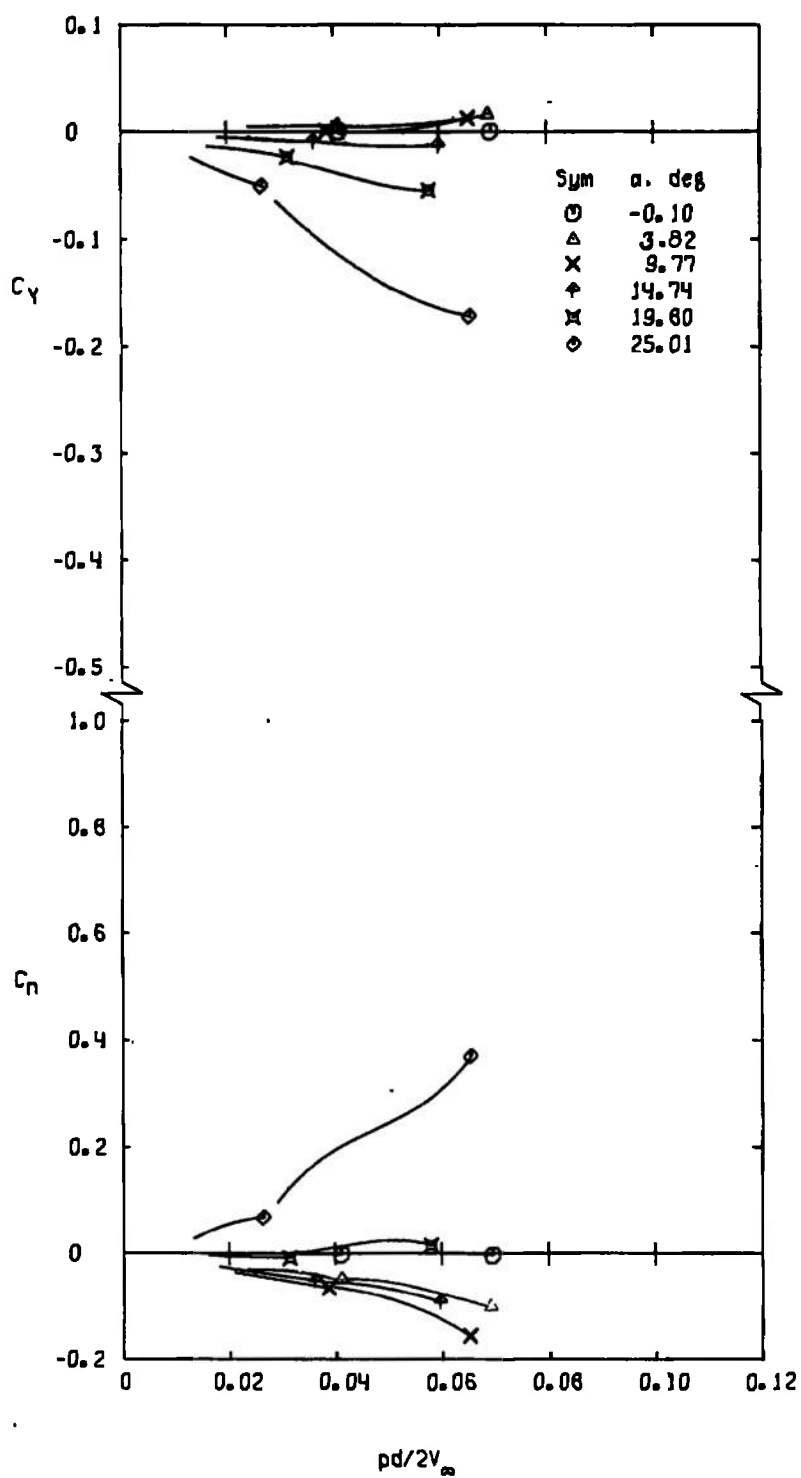
d. $M_\infty = 1.0$
Figure 16. Continued.
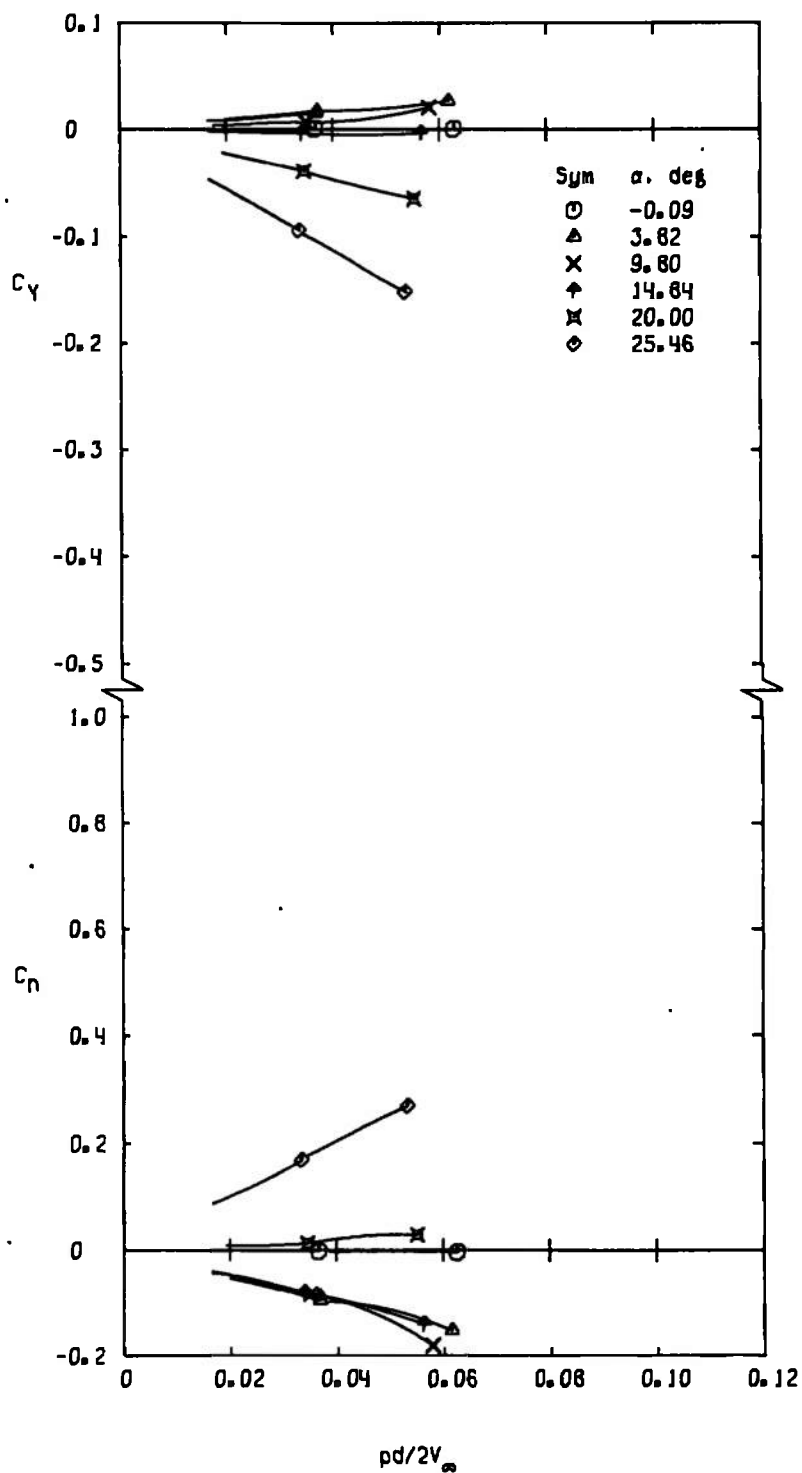
e. $M_\infty = 1.1$
Figure 16. Continued.
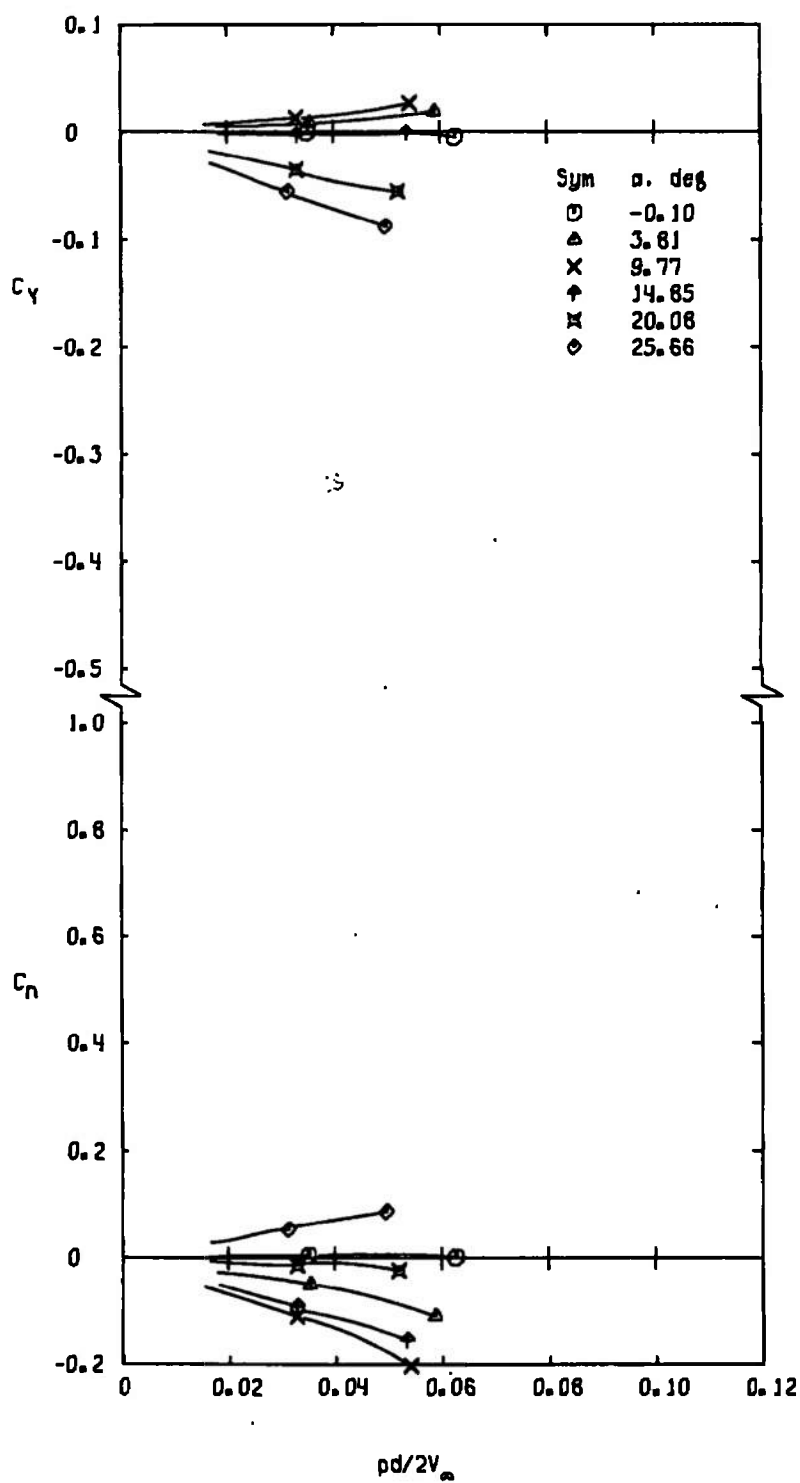
f. $M_\infty = 1.2$
Figure 16. Continued.

g. $M_\infty = 1.3$

Figure 16. Concluded.
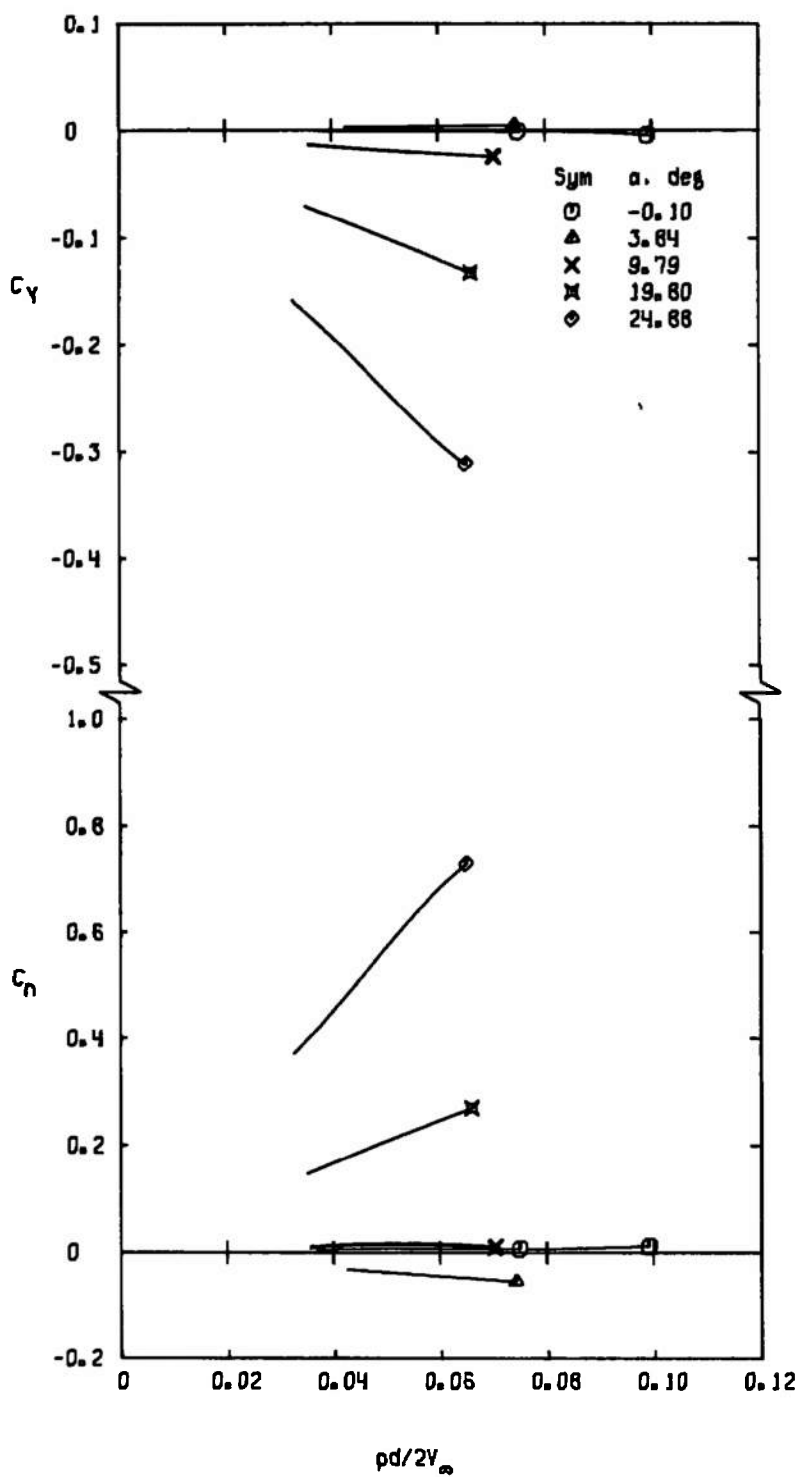
a. $M_\infty = 0.8$

Figure 17. Variation of C_Y and C_n with $pd/2V_\infty$ for configuration ISRESW2.

75

pd/2V$_\infty$

b. M$_\infty$ = 1.0
Figure 17. Continued.

c. $M_\infty = 1.2$

Figure 17. Concluded.

a. Configuration FFW1, $M_\infty = 1.1$
Figure 18. Variation of C_ℓ with $pd/2V_\infty$.
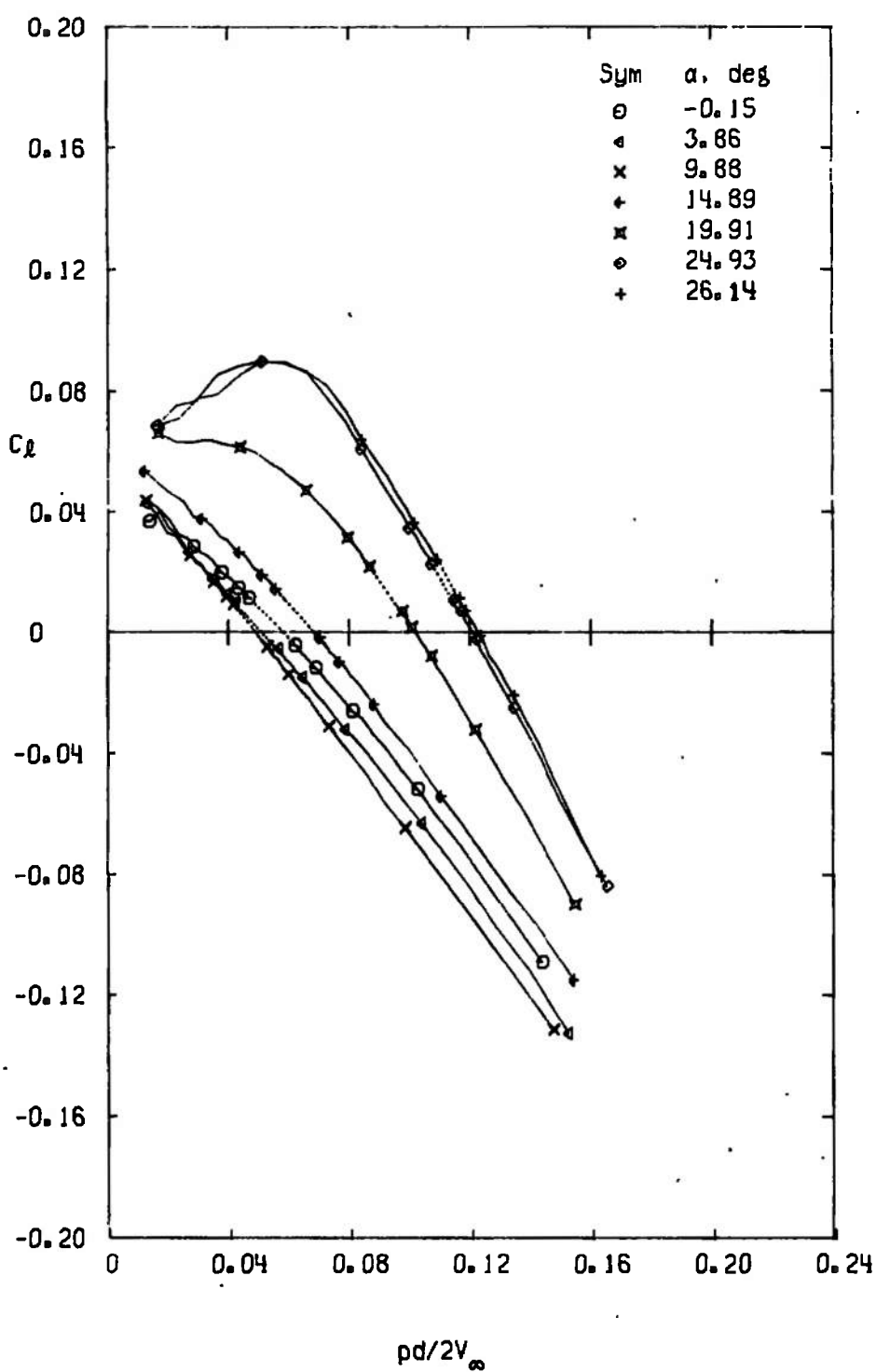
b. Configuration FFW1, $M_\infty = 0.4$
Figure 18. Continued.
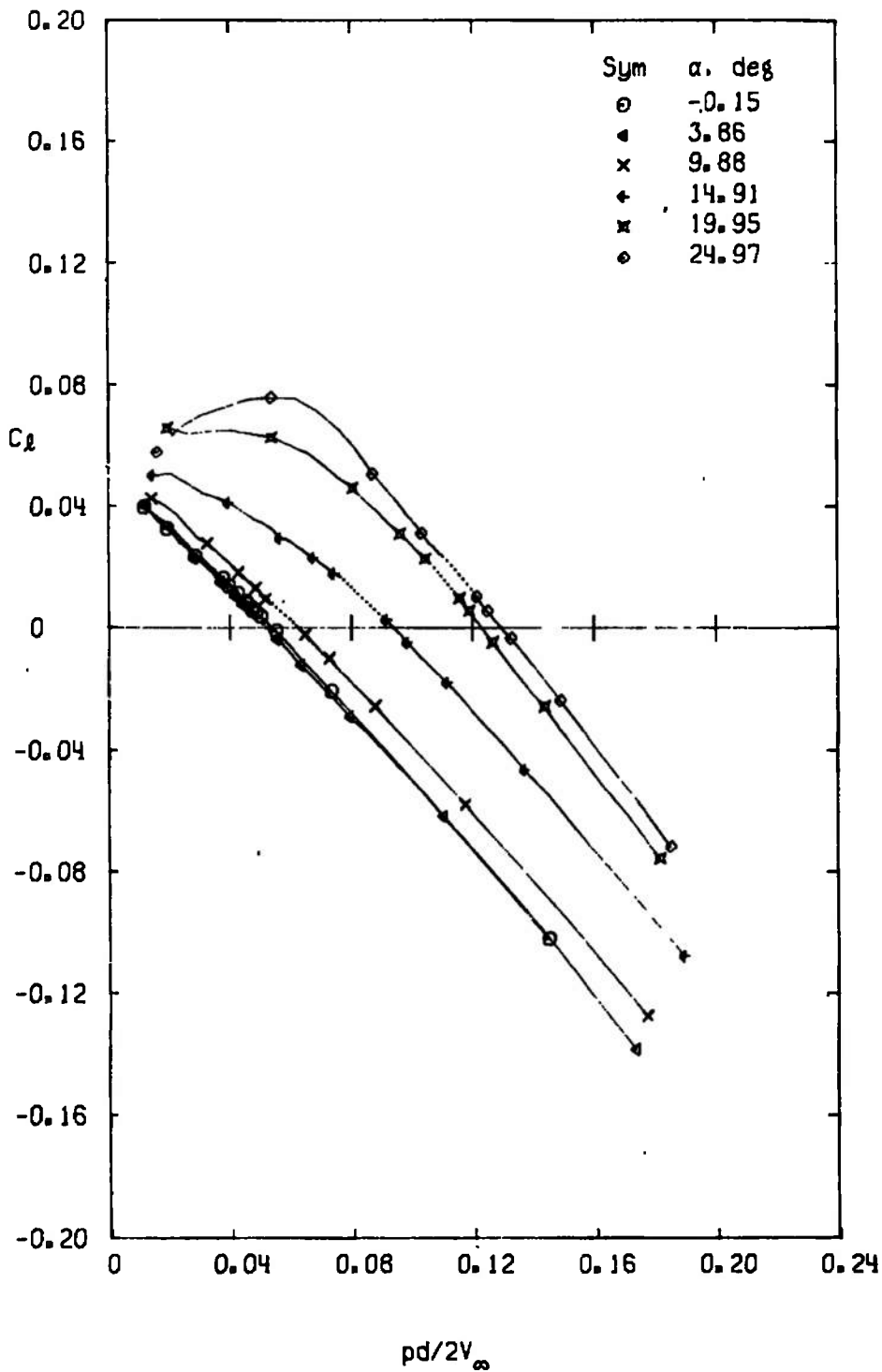
c. Configuration FFSW1, $M_\infty = 0.4$
Figure 18. Continued.
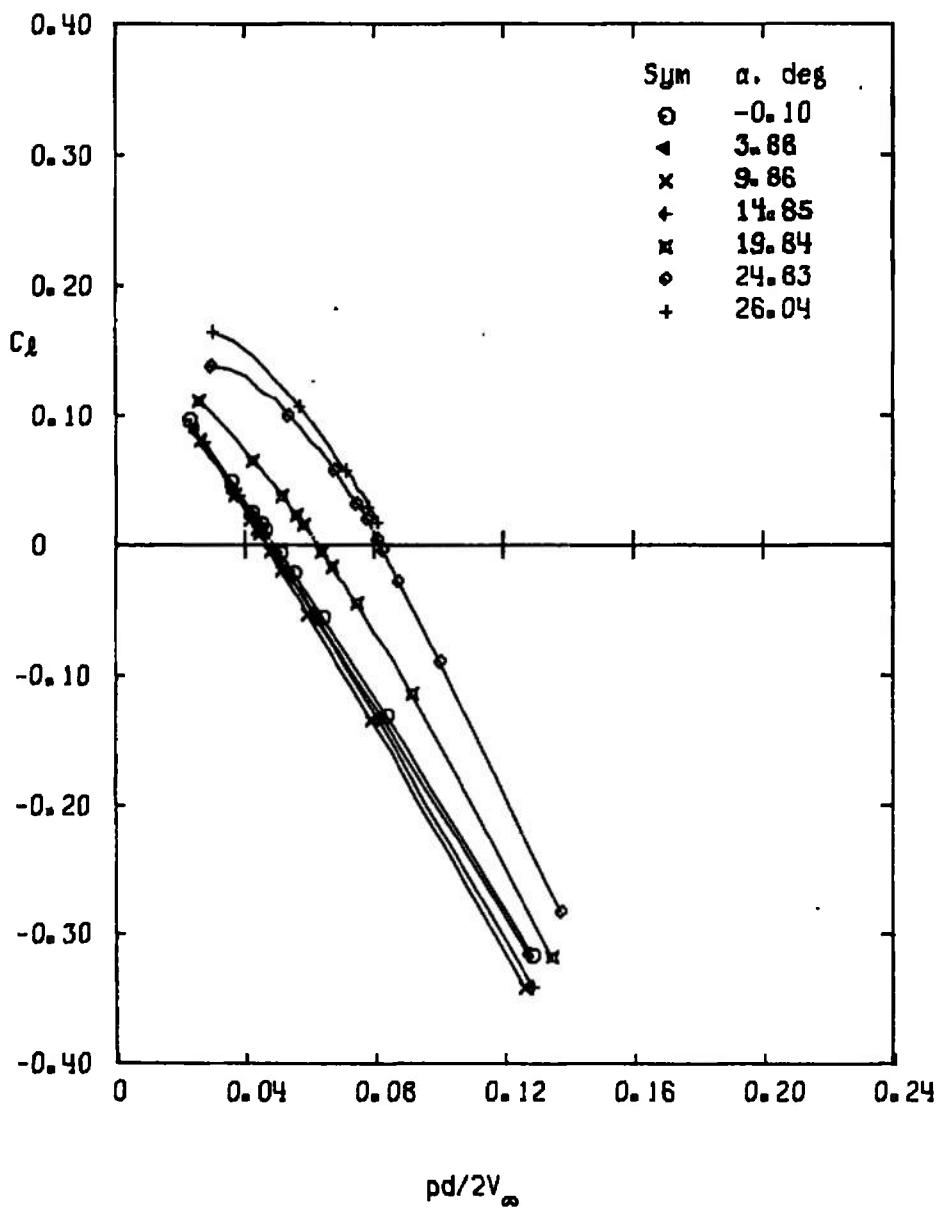
d. Configuration ISREW1, $M_\infty = 0.4$
Figure 18. Continued.
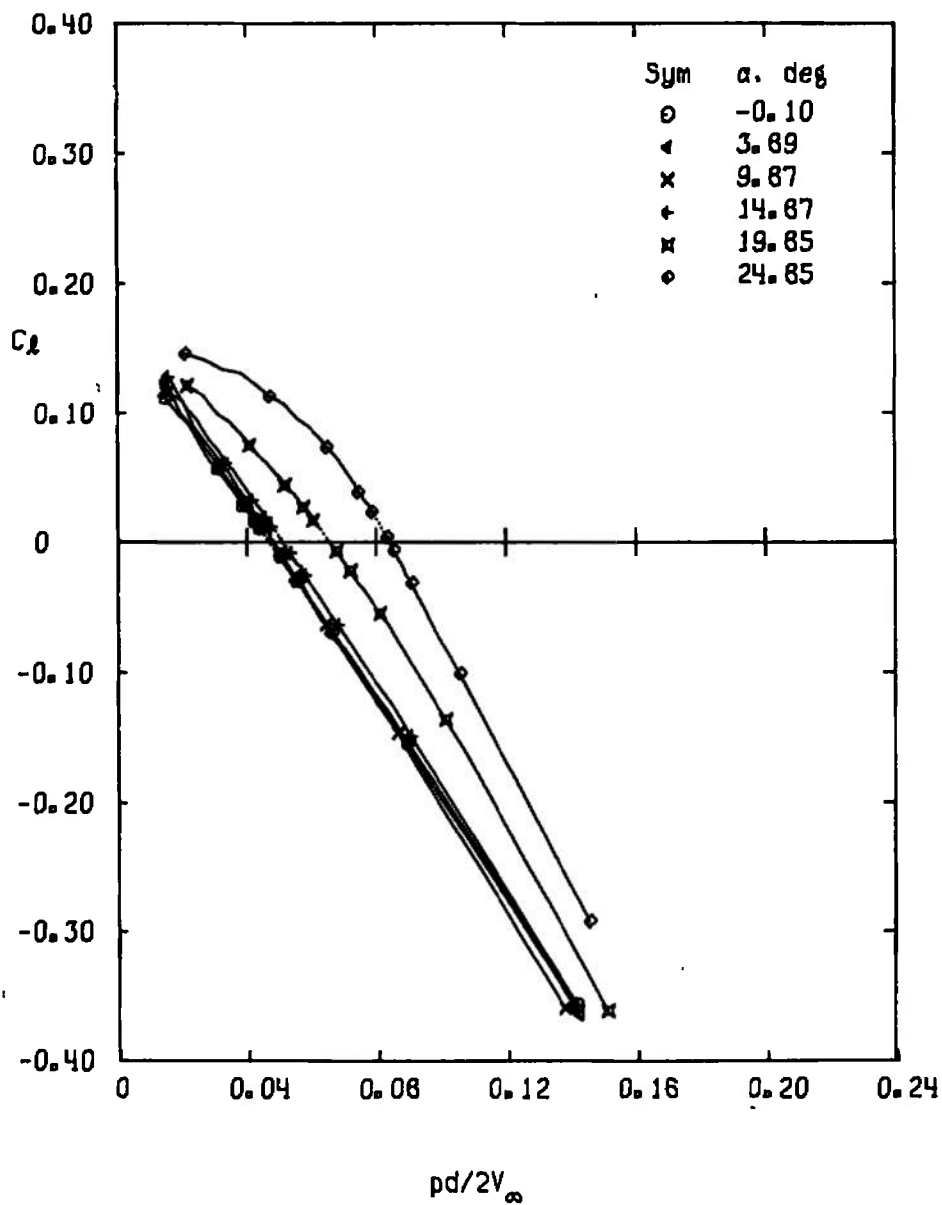
e. Configuration ISRESW1, $M_\infty = 0.4$
Figure 18. Concluded.
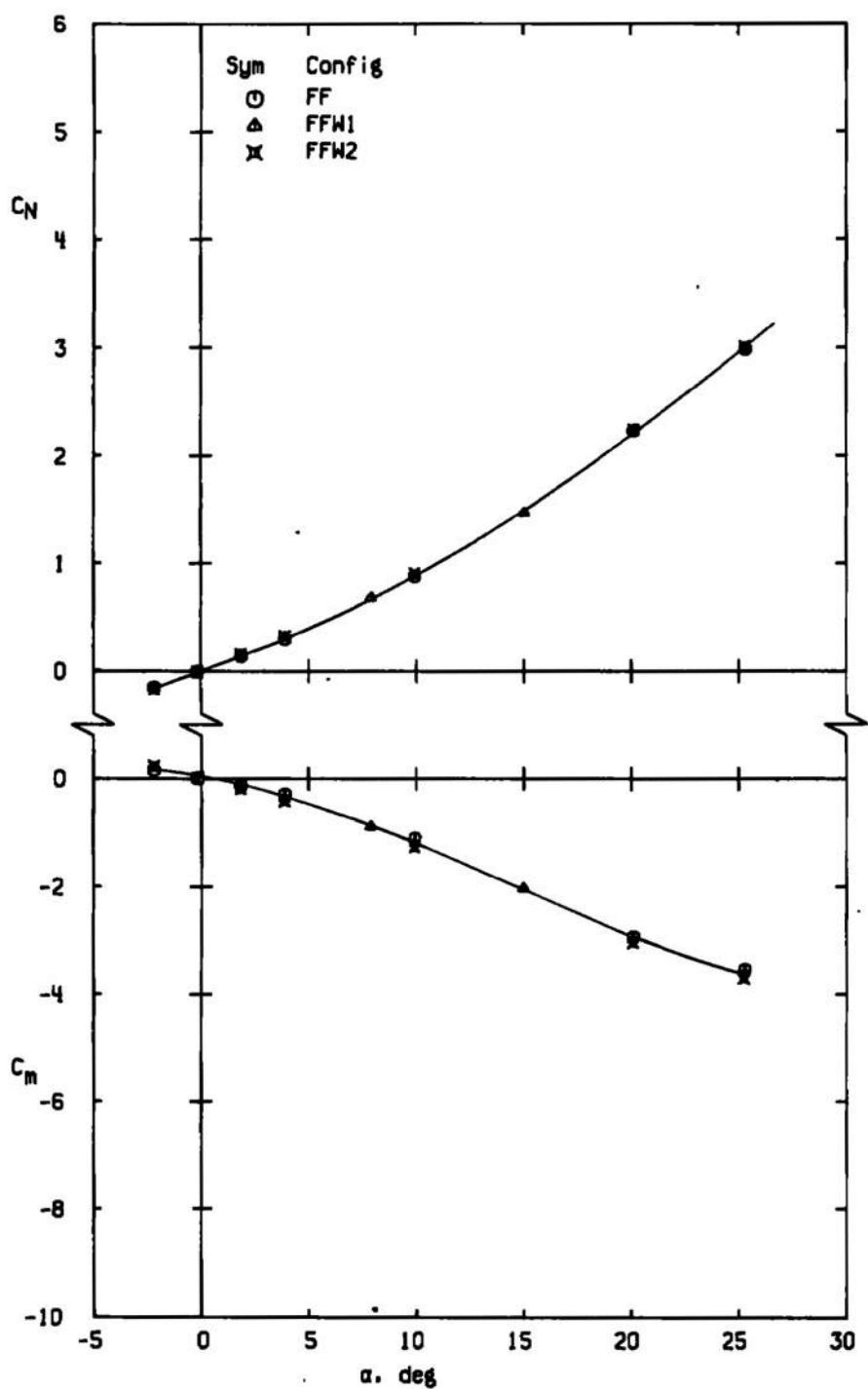
a. Configurations FF, $M_\infty = 0.8$

Figure 19. Variation of C_N and C_m with angle of attack showing effect of fin wedges.
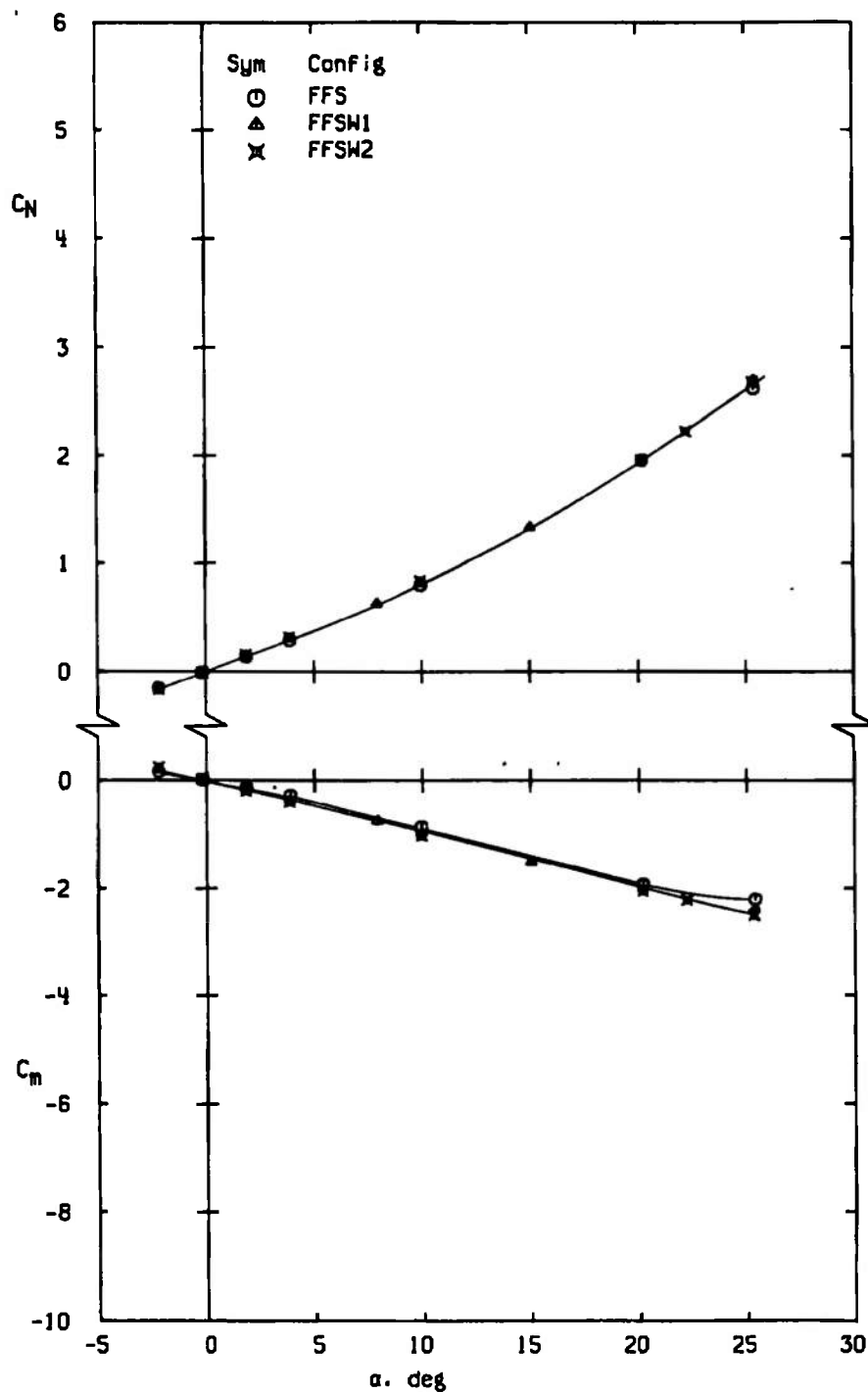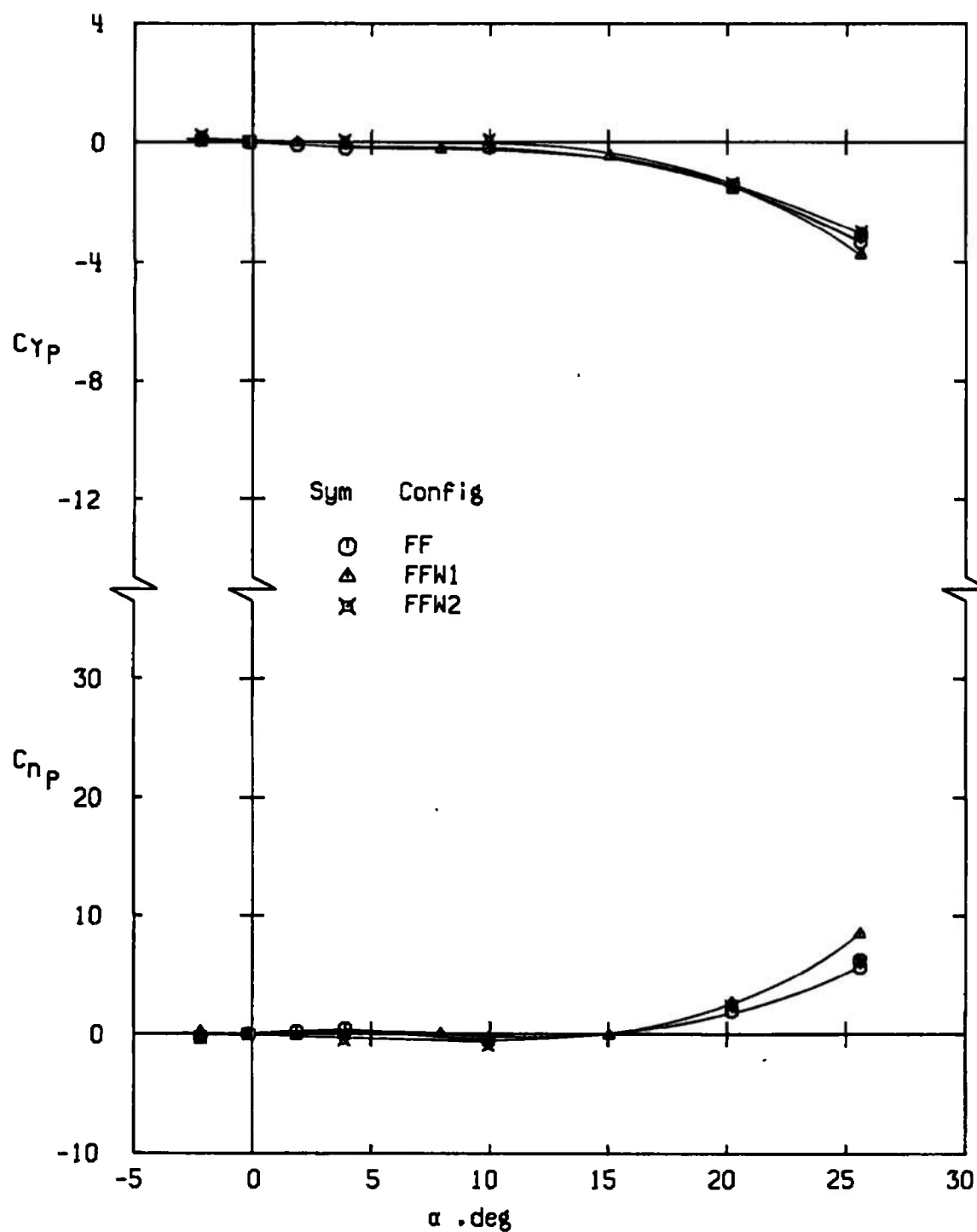
b. Configurations FFS, $M_\infty = 0.8$
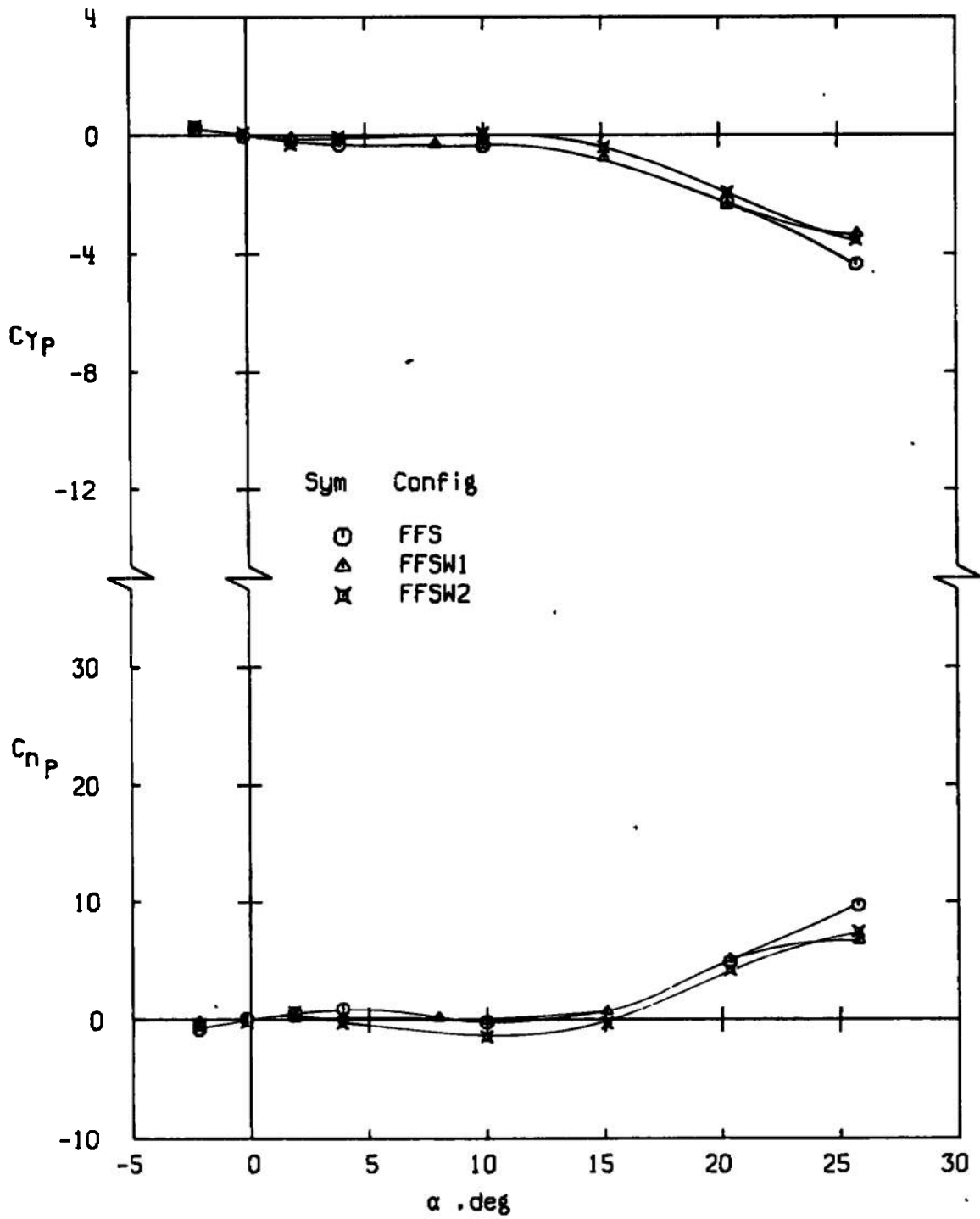Figure 19. Continued.
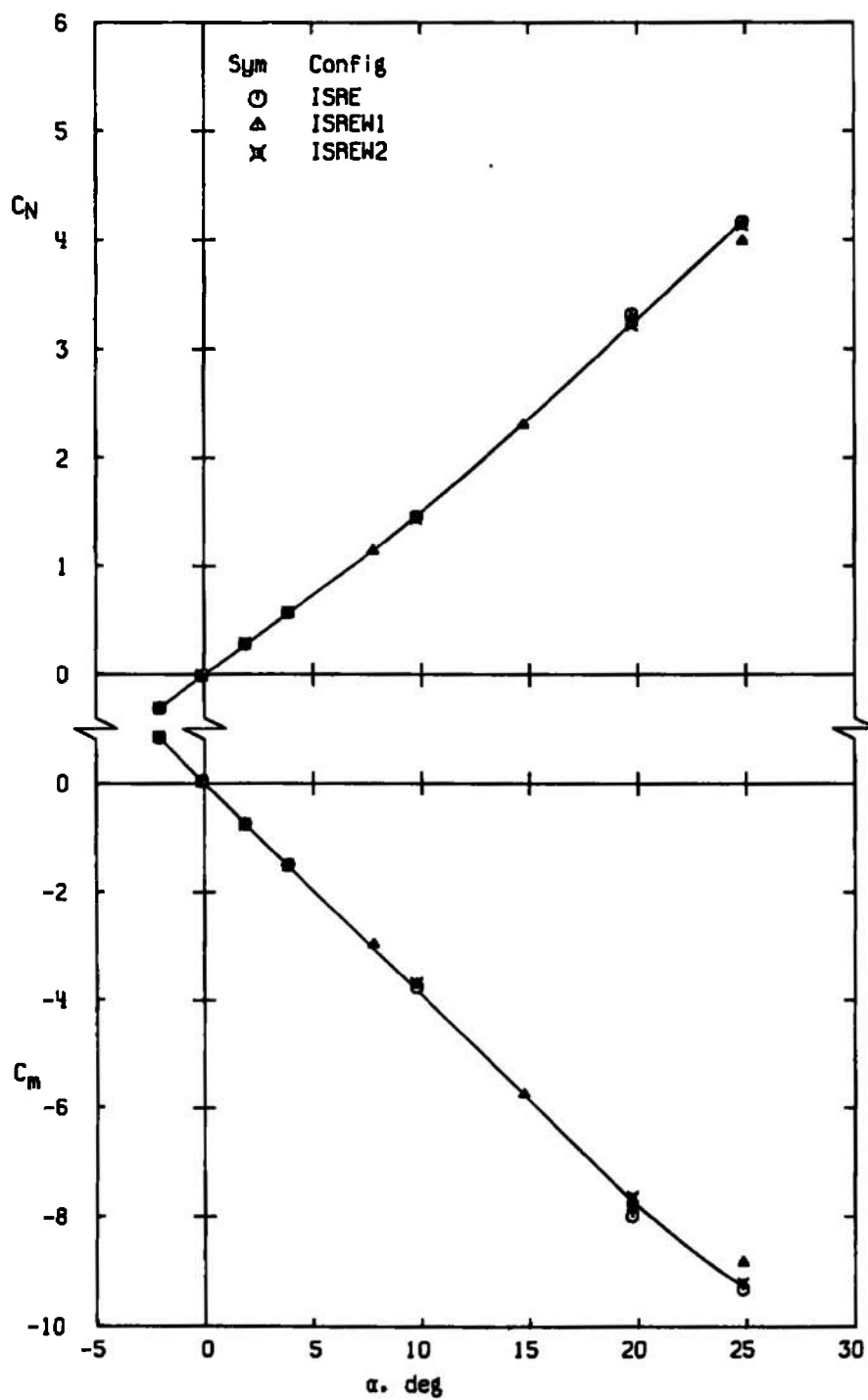
c. Configurations ISRE, $M_\infty = 0.8$
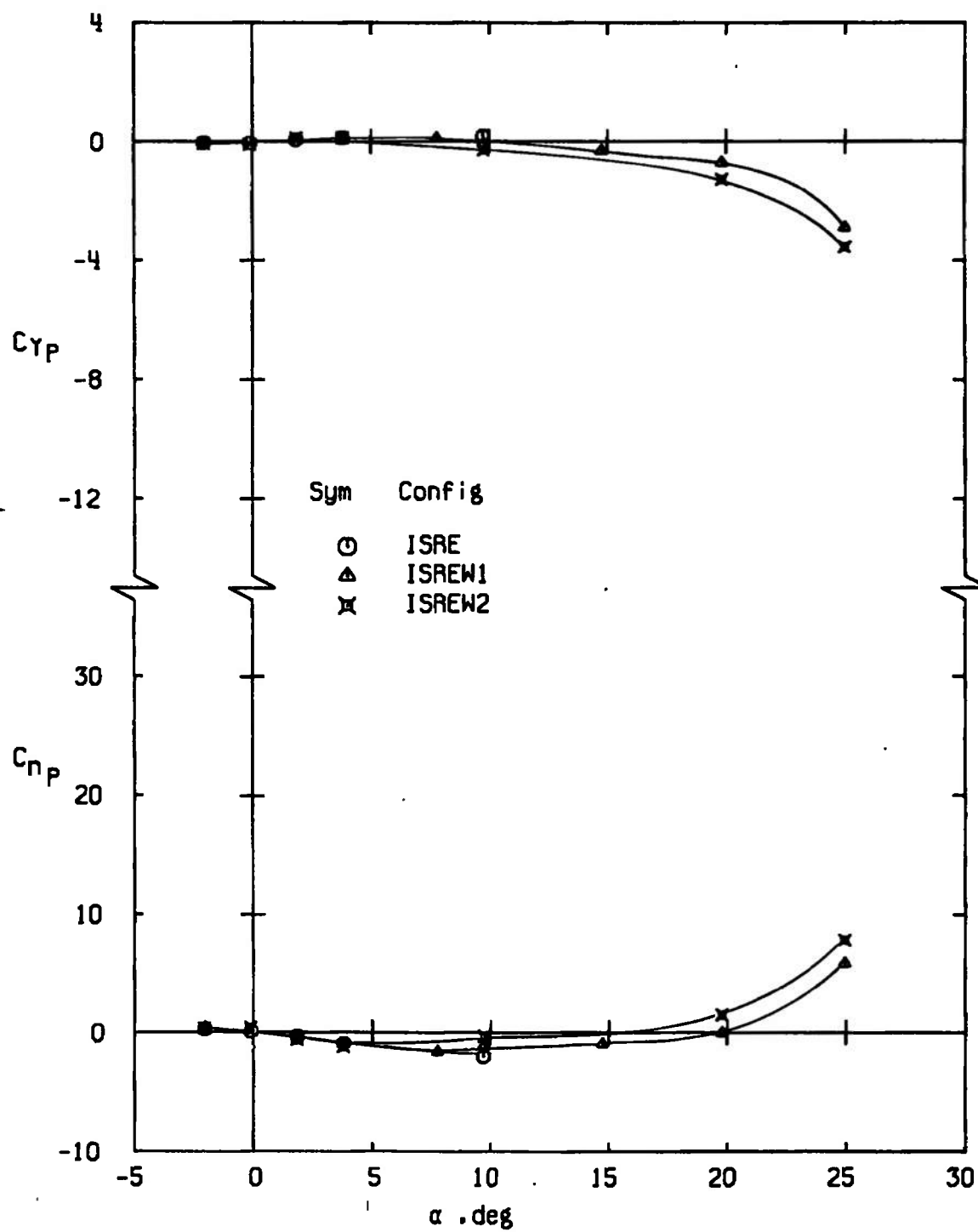Figure 19. Continued.
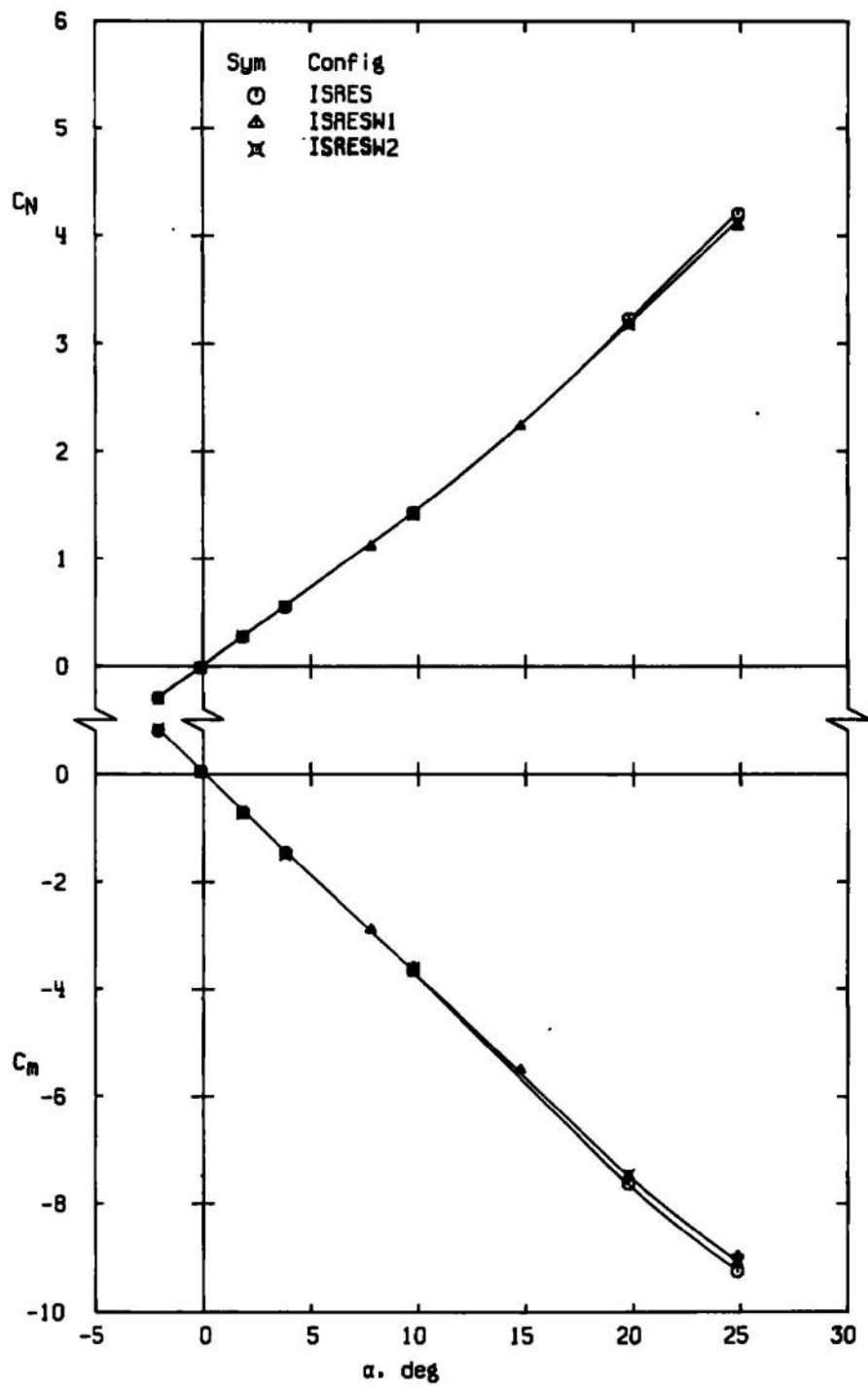
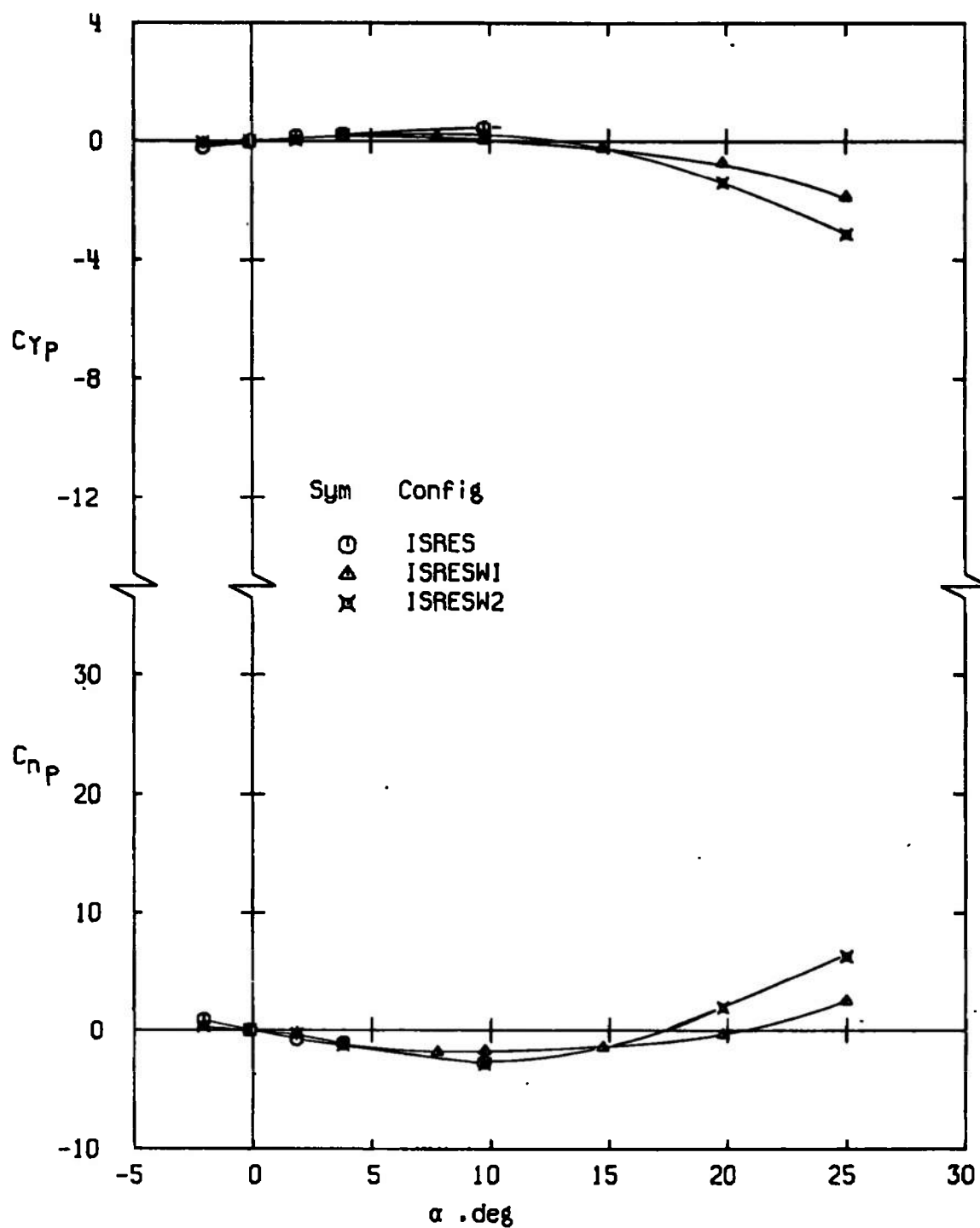d. Configurations ISRES, $M_\infty = 0.8$
Figure 19. Continued.
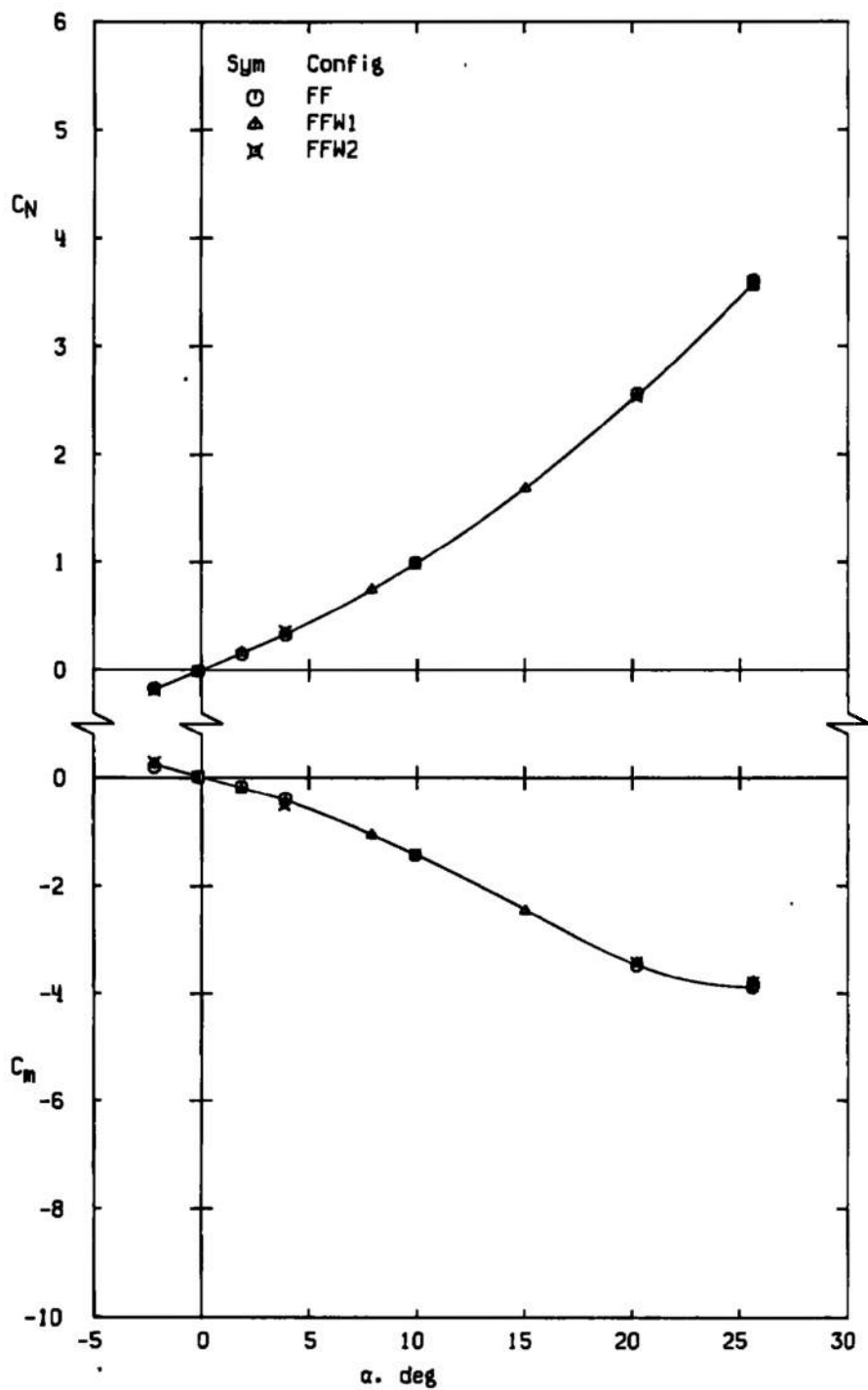
e. Configurations FF, $M_\infty = 1.0$
Figure 19. Continued.
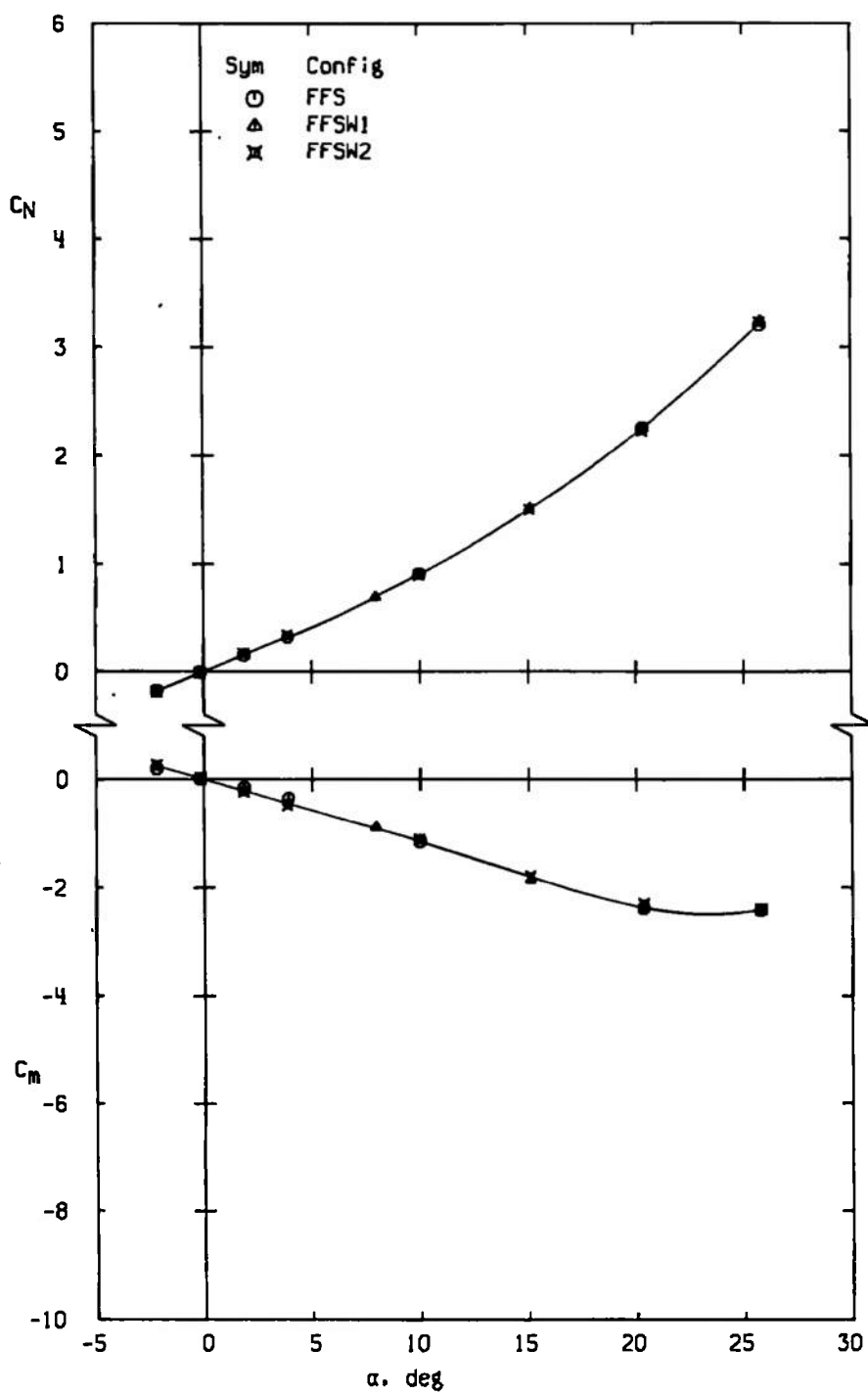
f. Configurations FFS, $M_\infty = 1.0$
Figure 19. Continued.
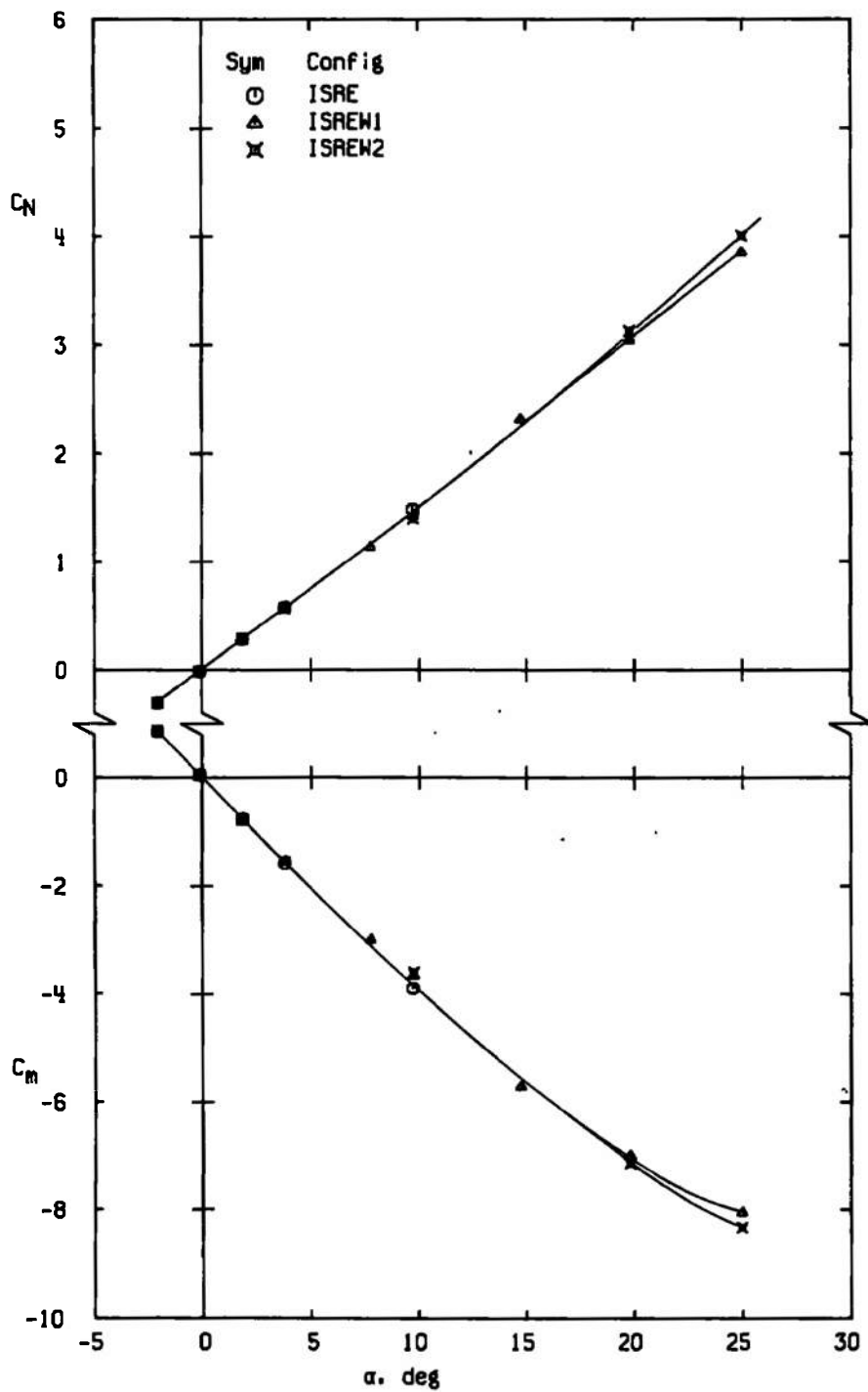
g. Configurations ISRE, $M_\infty = 1.0$
Figure 19. Continued.
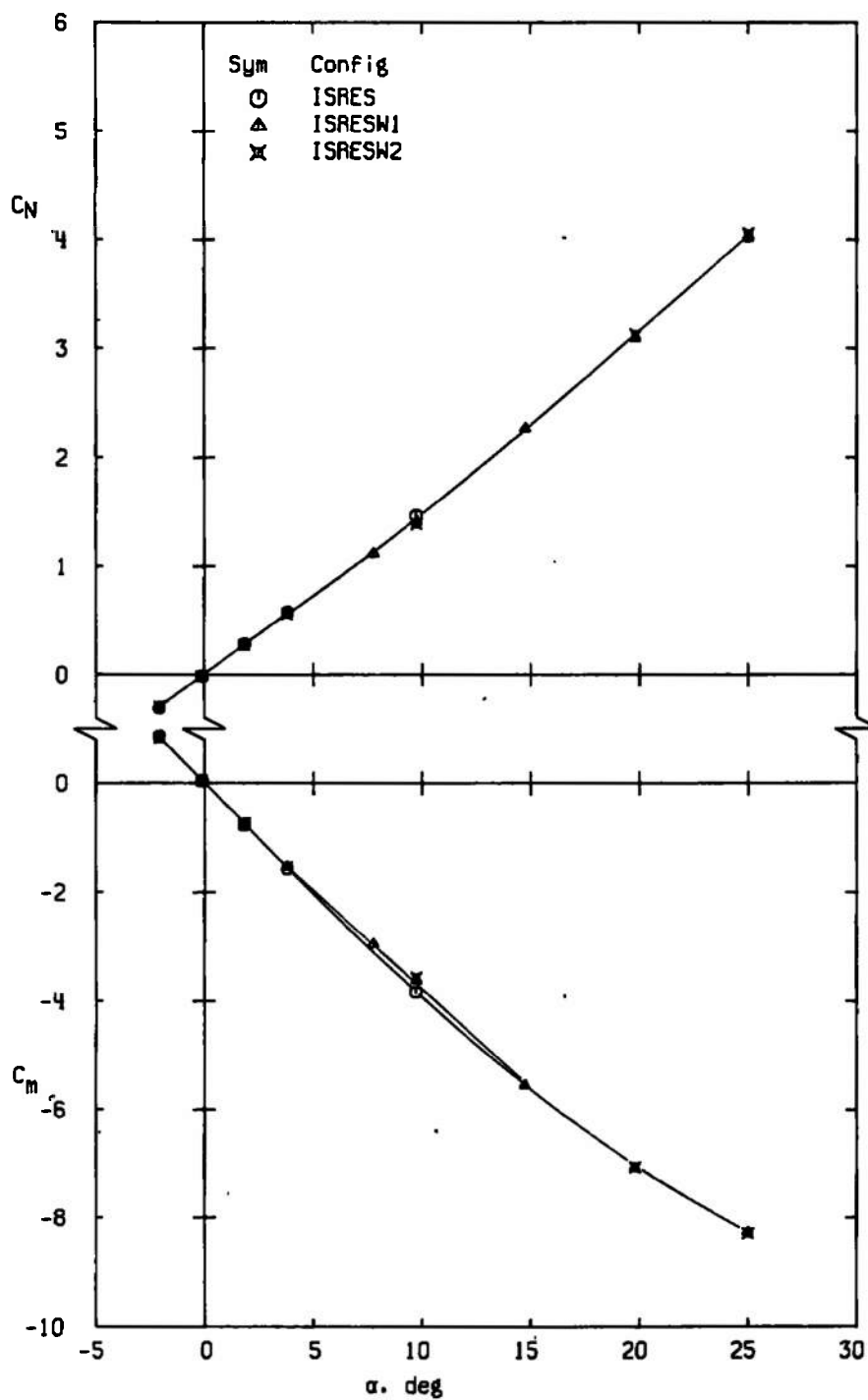
h. Configurations ISRES, $M_\infty = 1.0$
Figure 19. Continued.
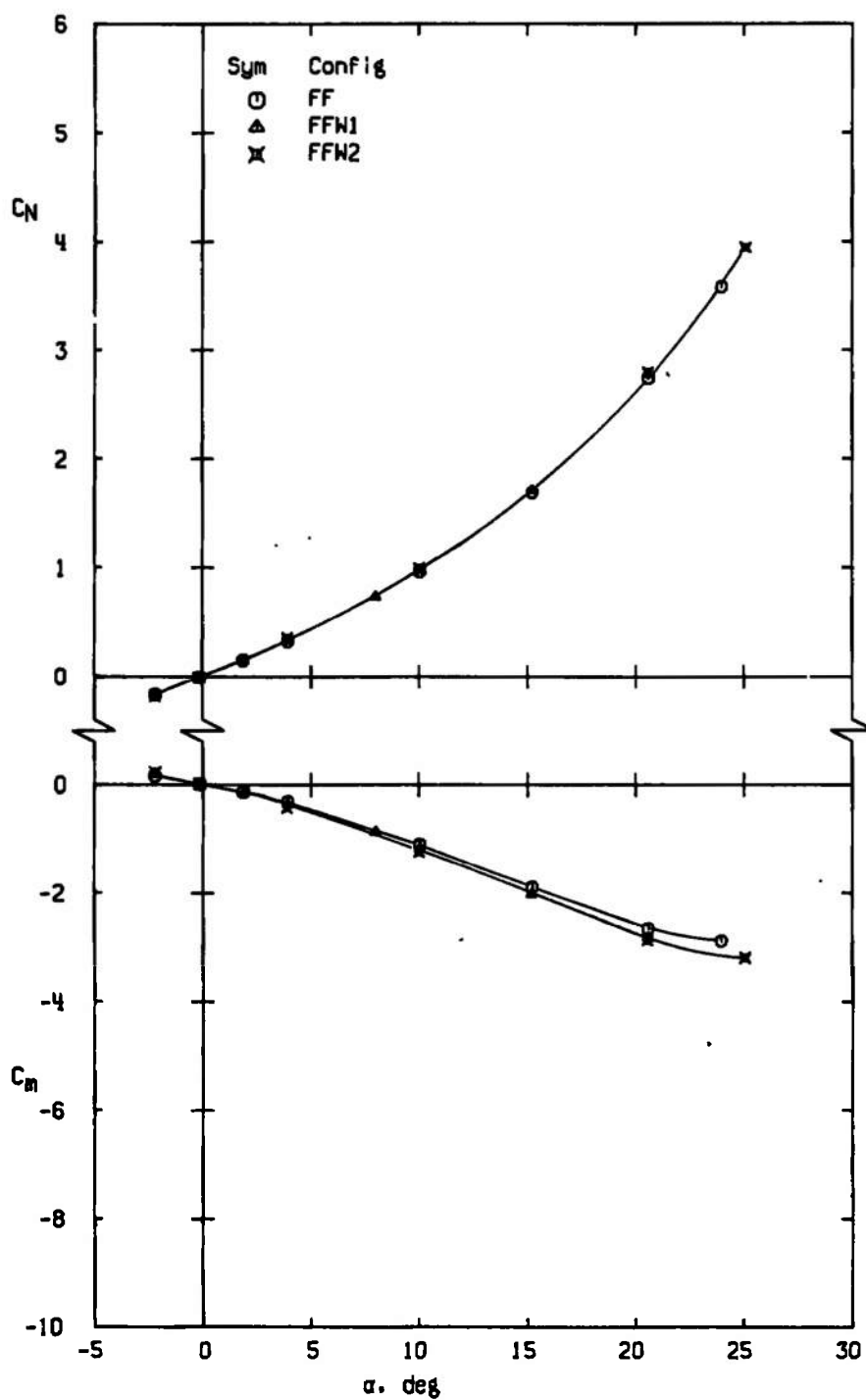
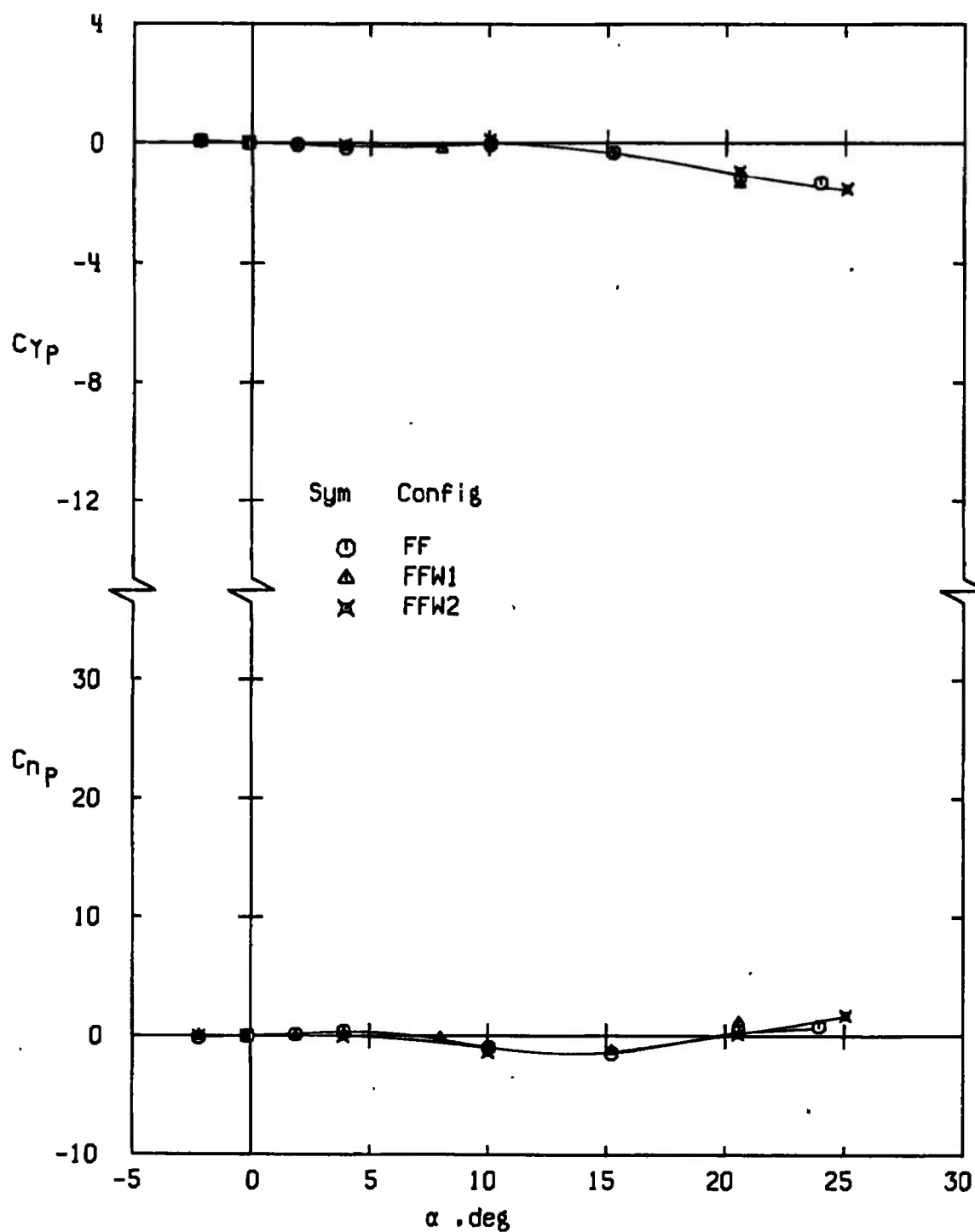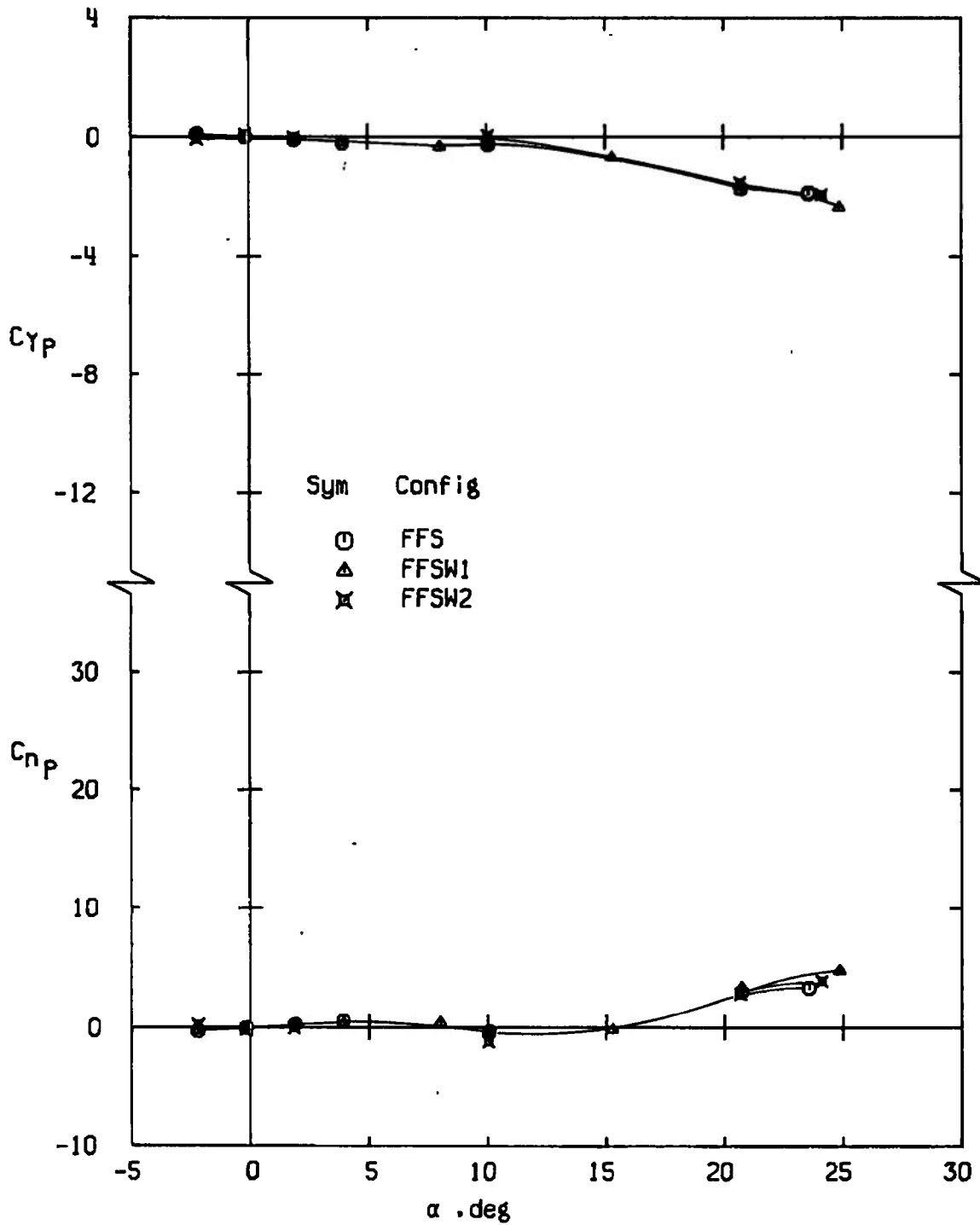i. Configurations FF, $M_\infty = 1.2$
Figure 19. Continued.

91
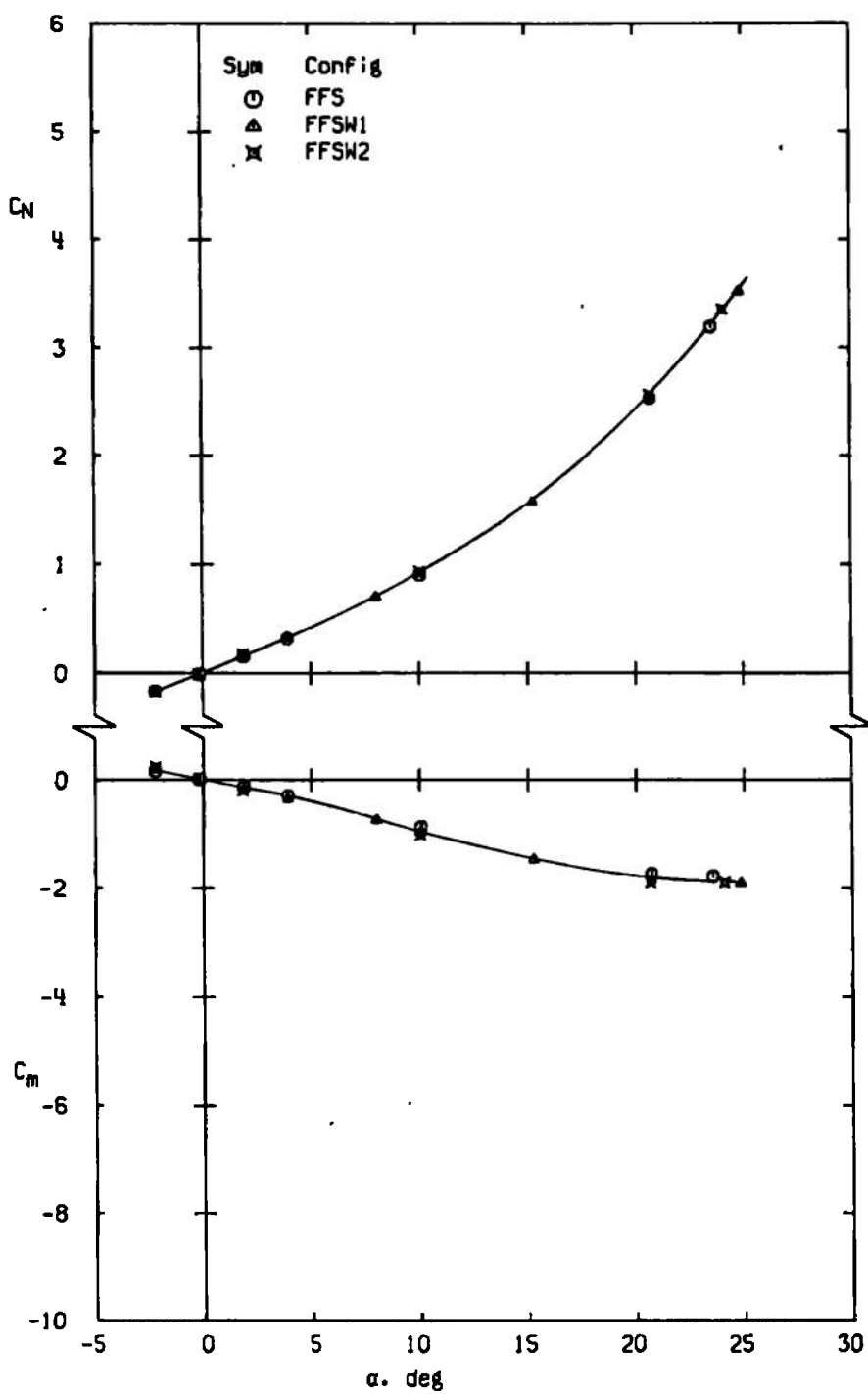
j. Configurations FFS, $M_\infty = 1.2$
Figure 19. Continued.
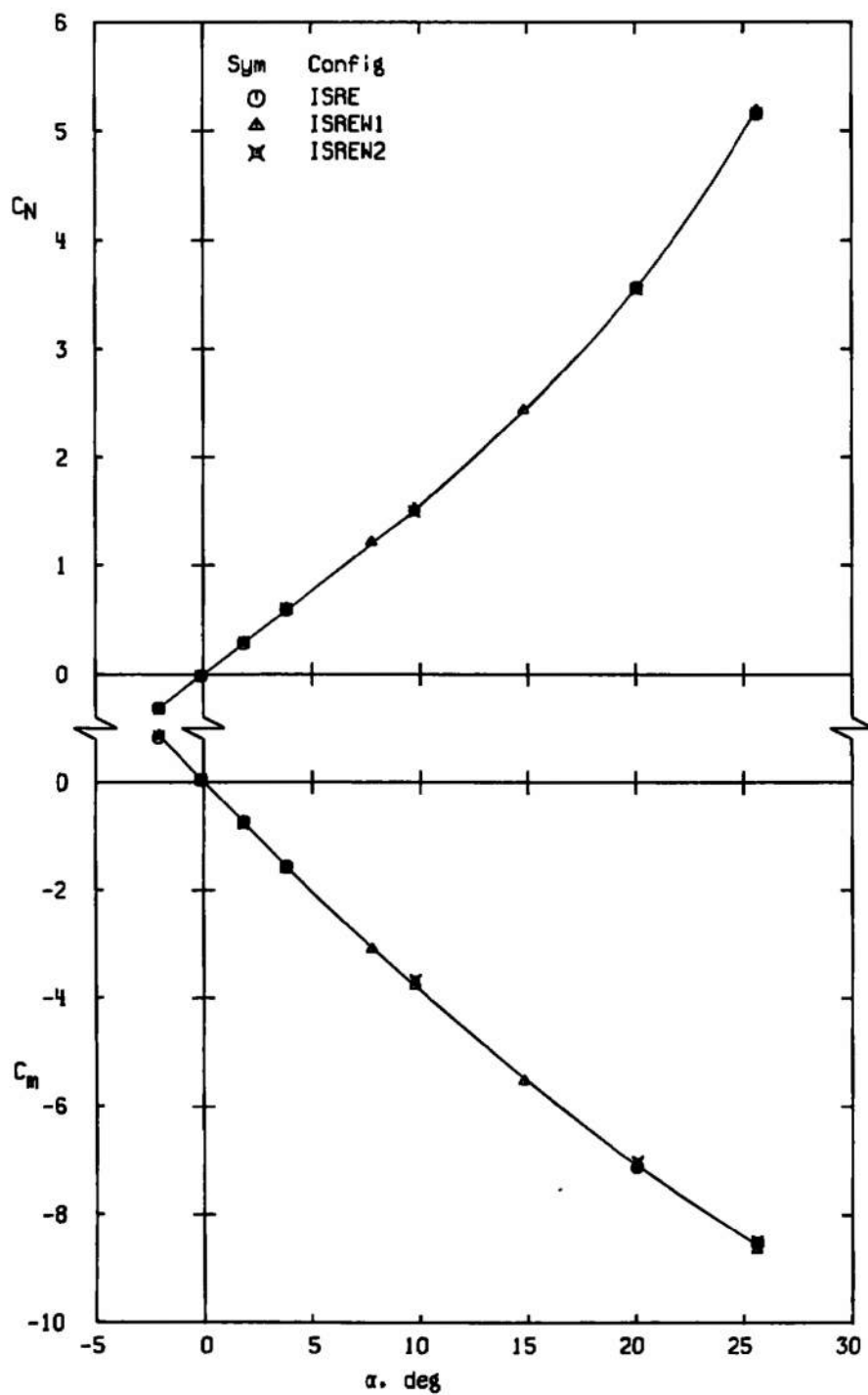
k. Configurations ISRE, $M_\infty = 1.2$
Figure 19. Continued.
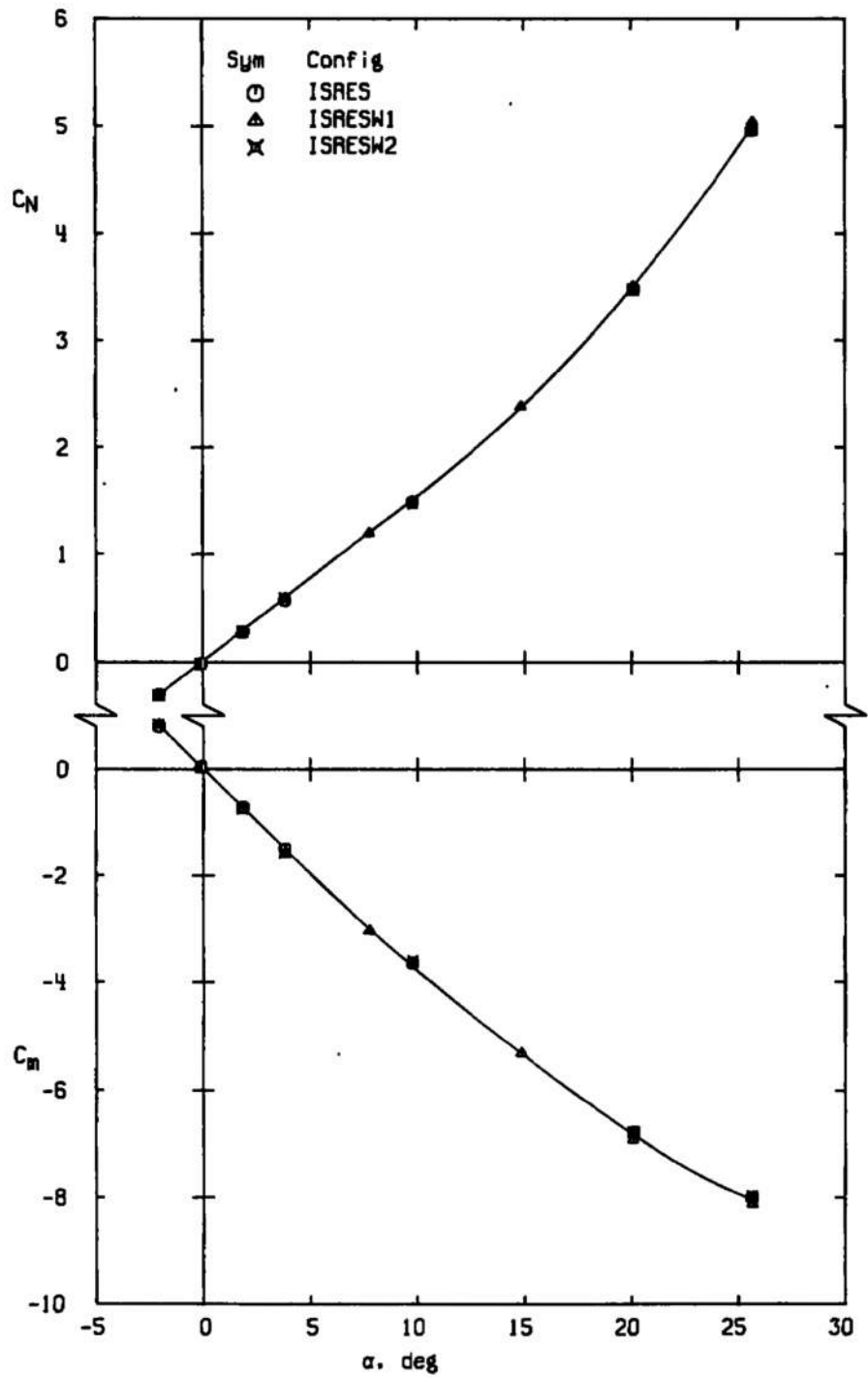
I. Configurations ISRES, M_∞ = 1.2
Figure 19. Concluded.
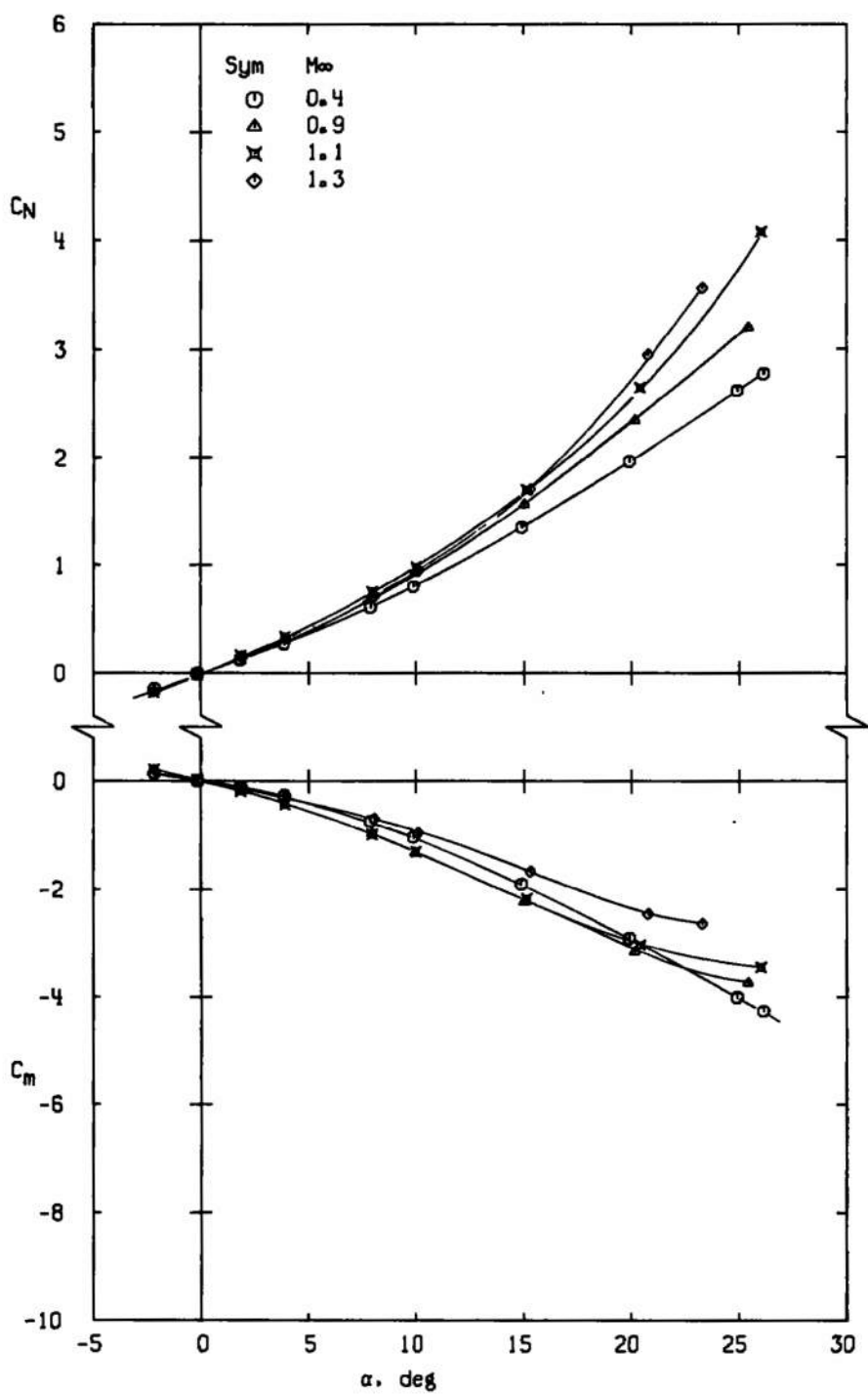
a. Configuration FFW1
Figure 20. Variation of C_N and C_m with angle of attack showing effect of Mach number.
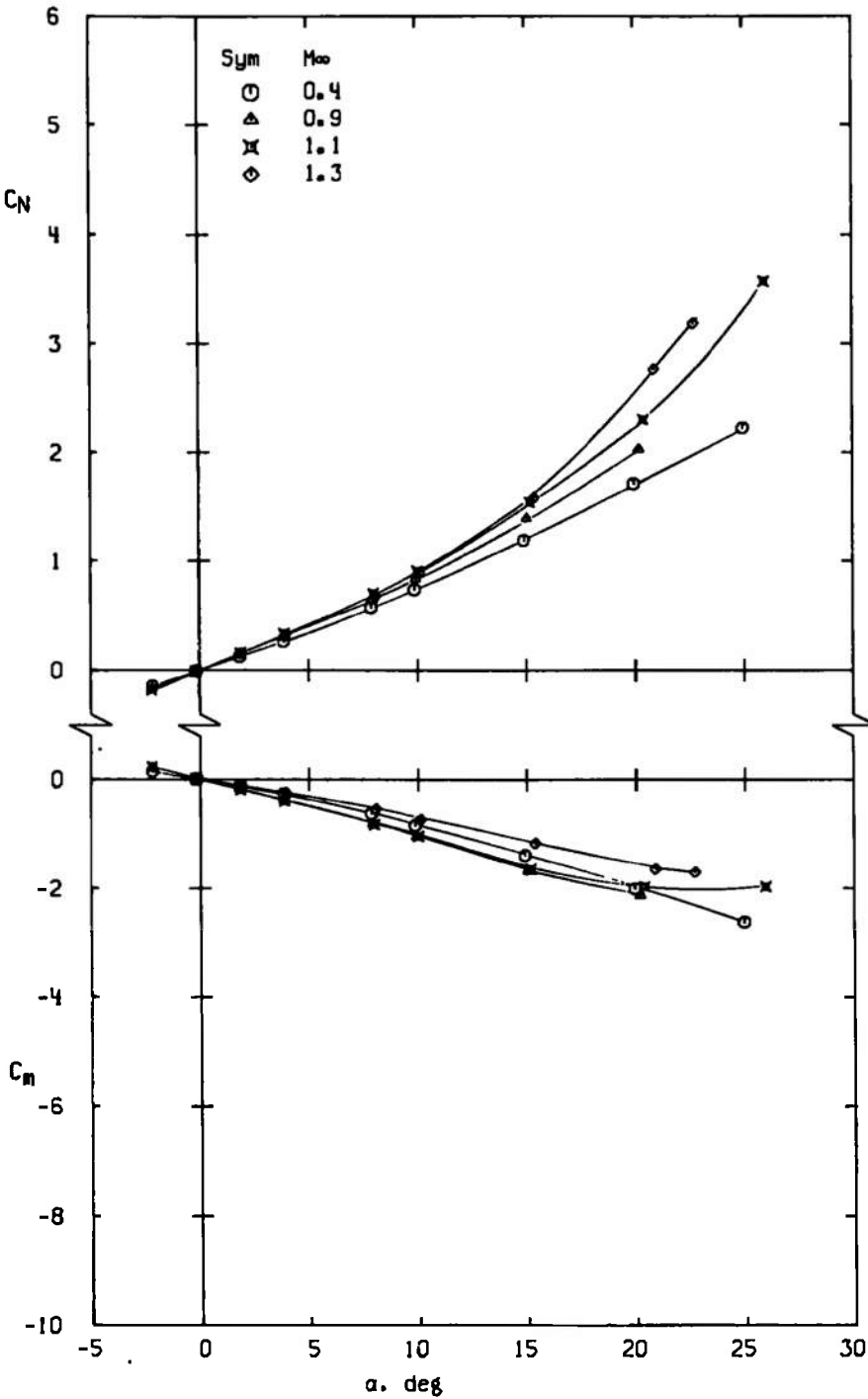
b. Configuration FFSW1
Figure 20. Continued.
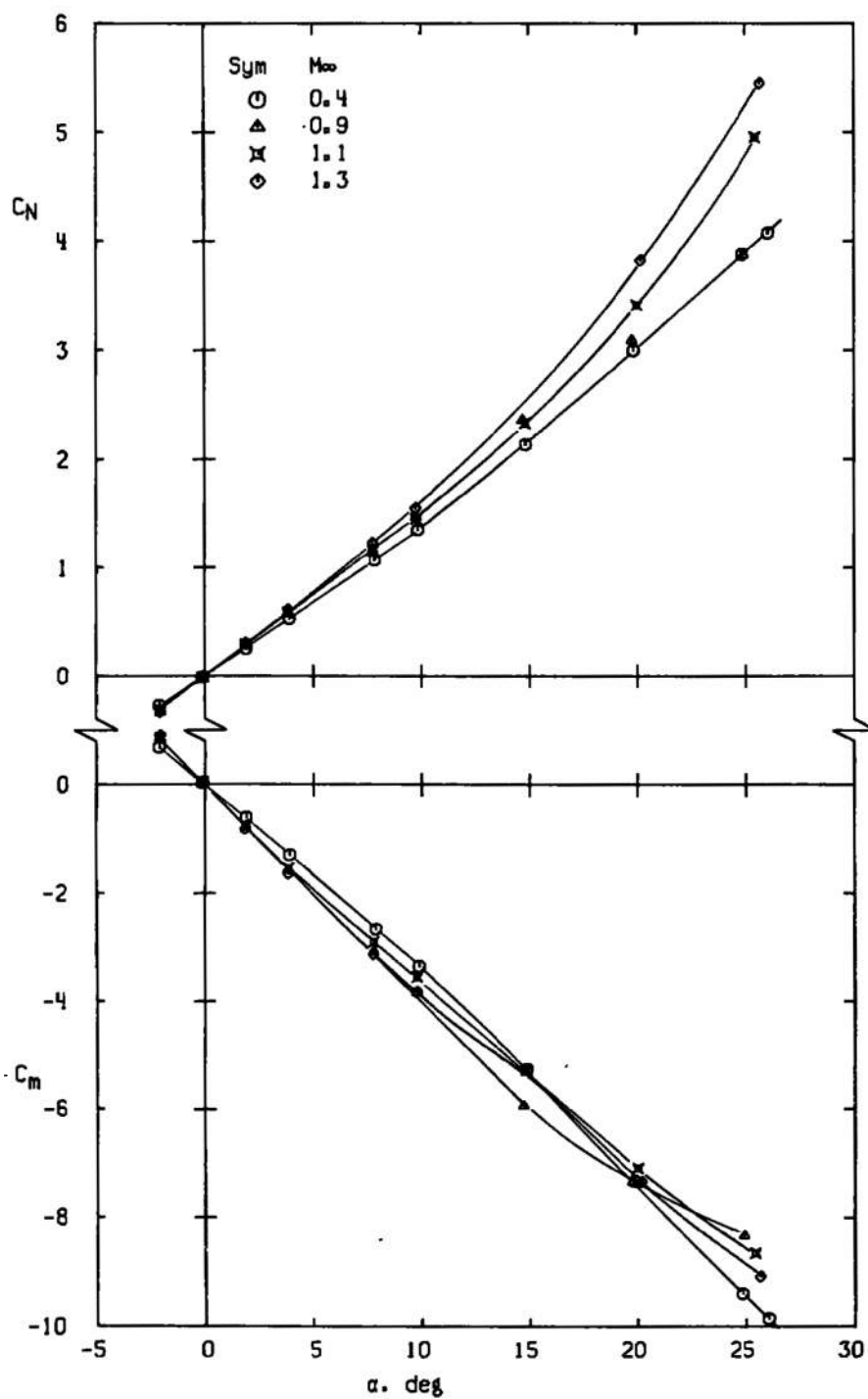
c. Configuration ISREW1
Figure 20. Continued.
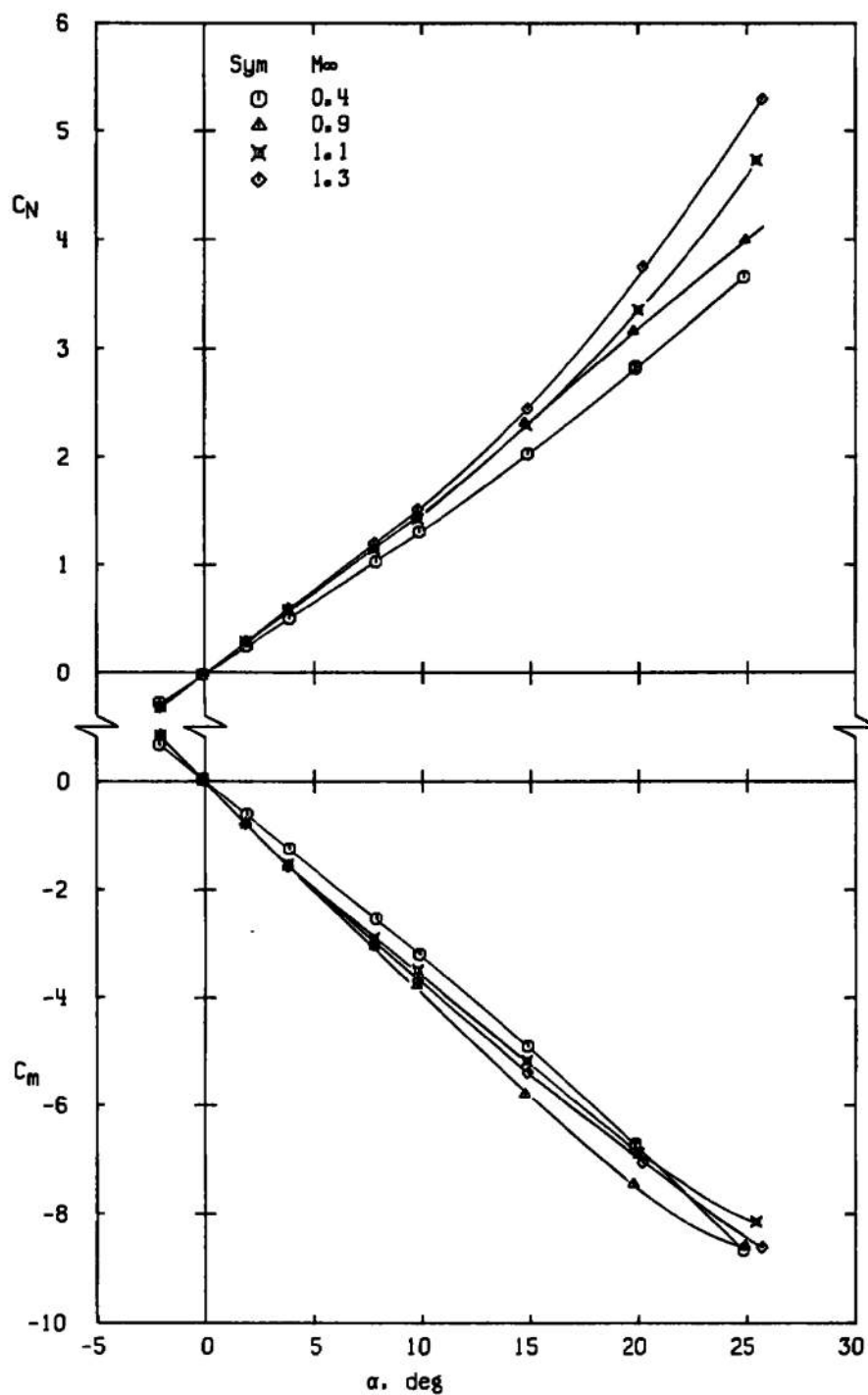
d. Configuration ISRESW1
Figure 20. Concluded.
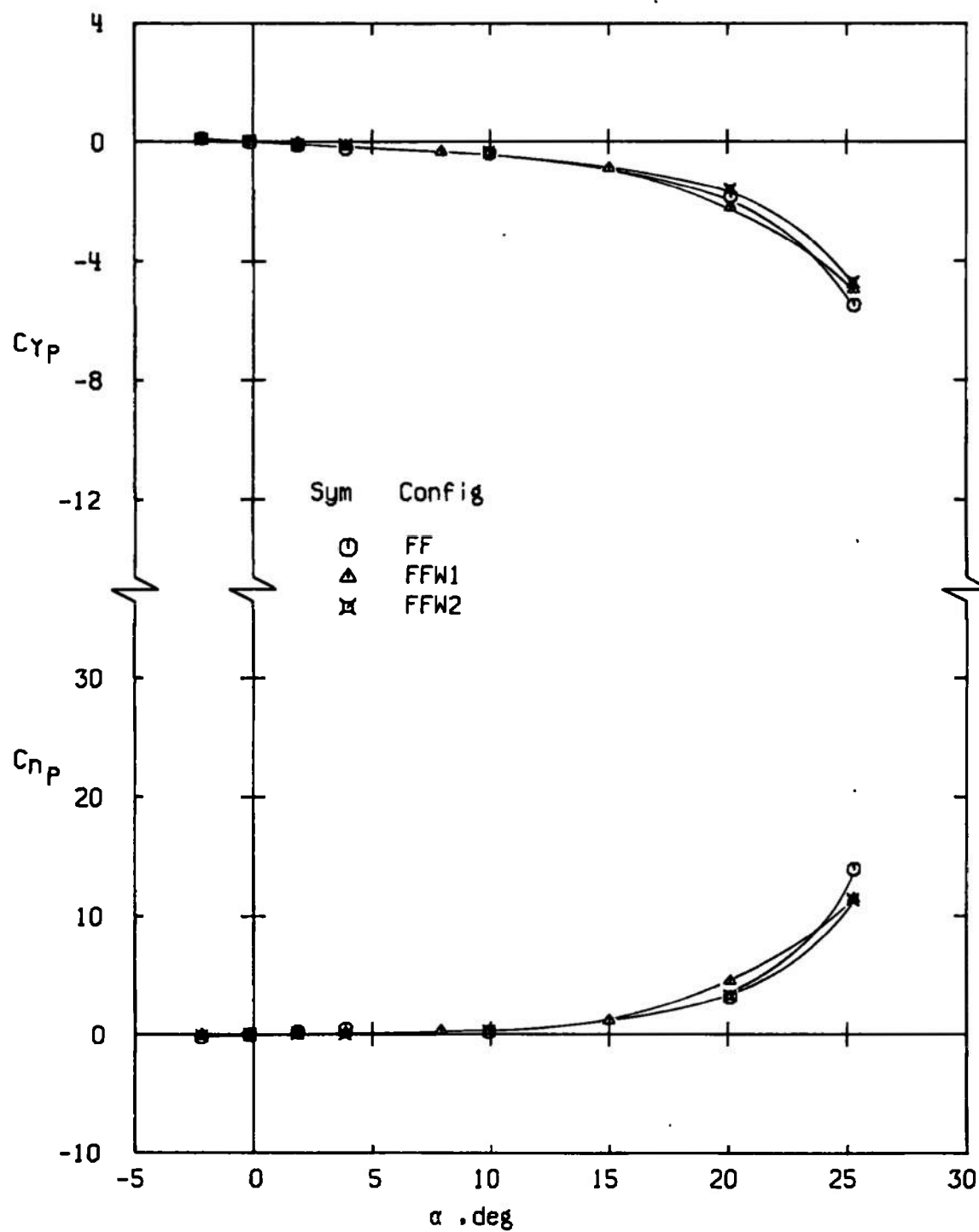
a. Configurations FF, $M_\infty = 0.8$

Figure 21. Variation of C_{Y_p} and C_{n_p} with angle of attack showing effect of fin wedges.
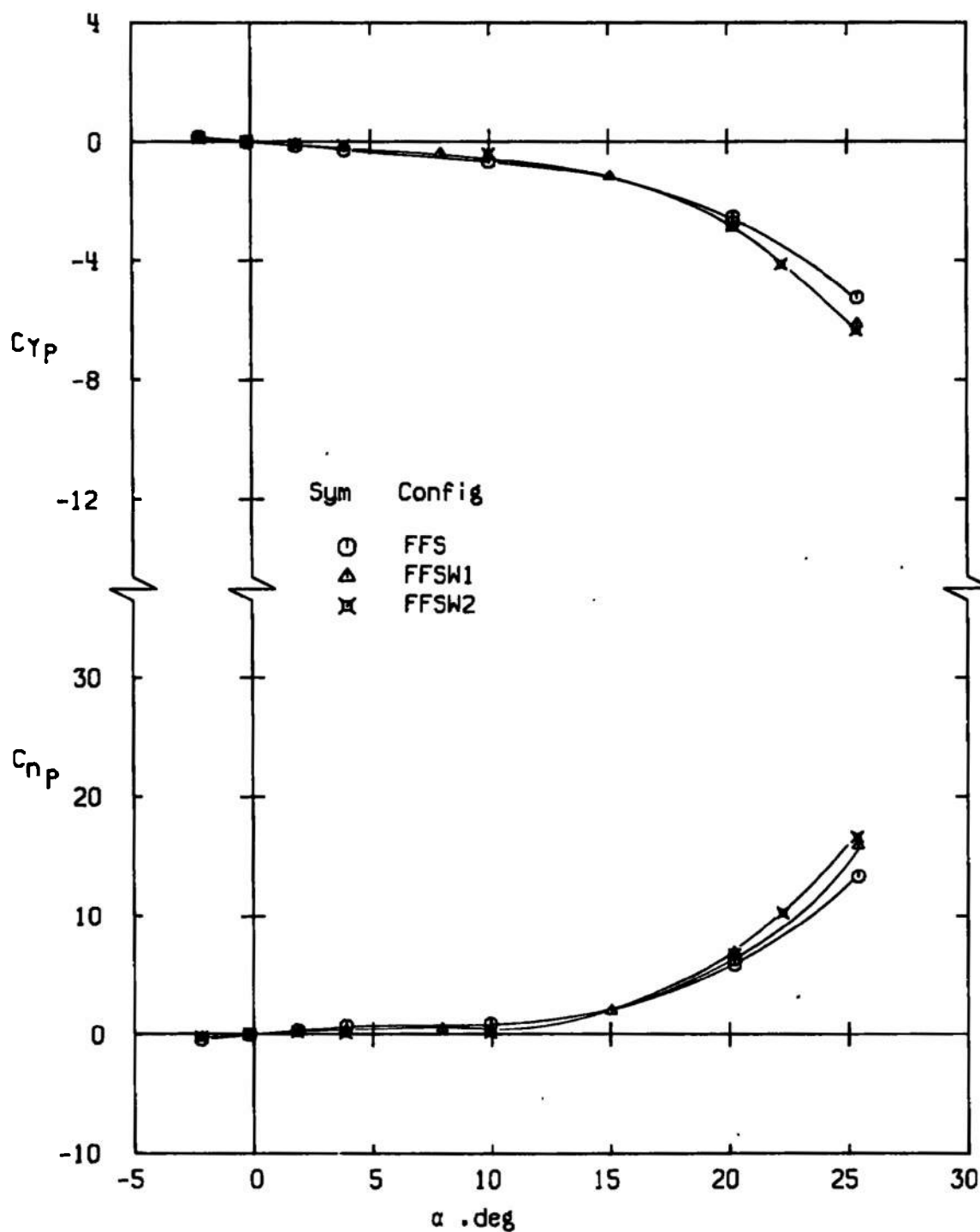
b. Configurations FFS, $M_\infty = 0.8$
Figure 21. Continued.
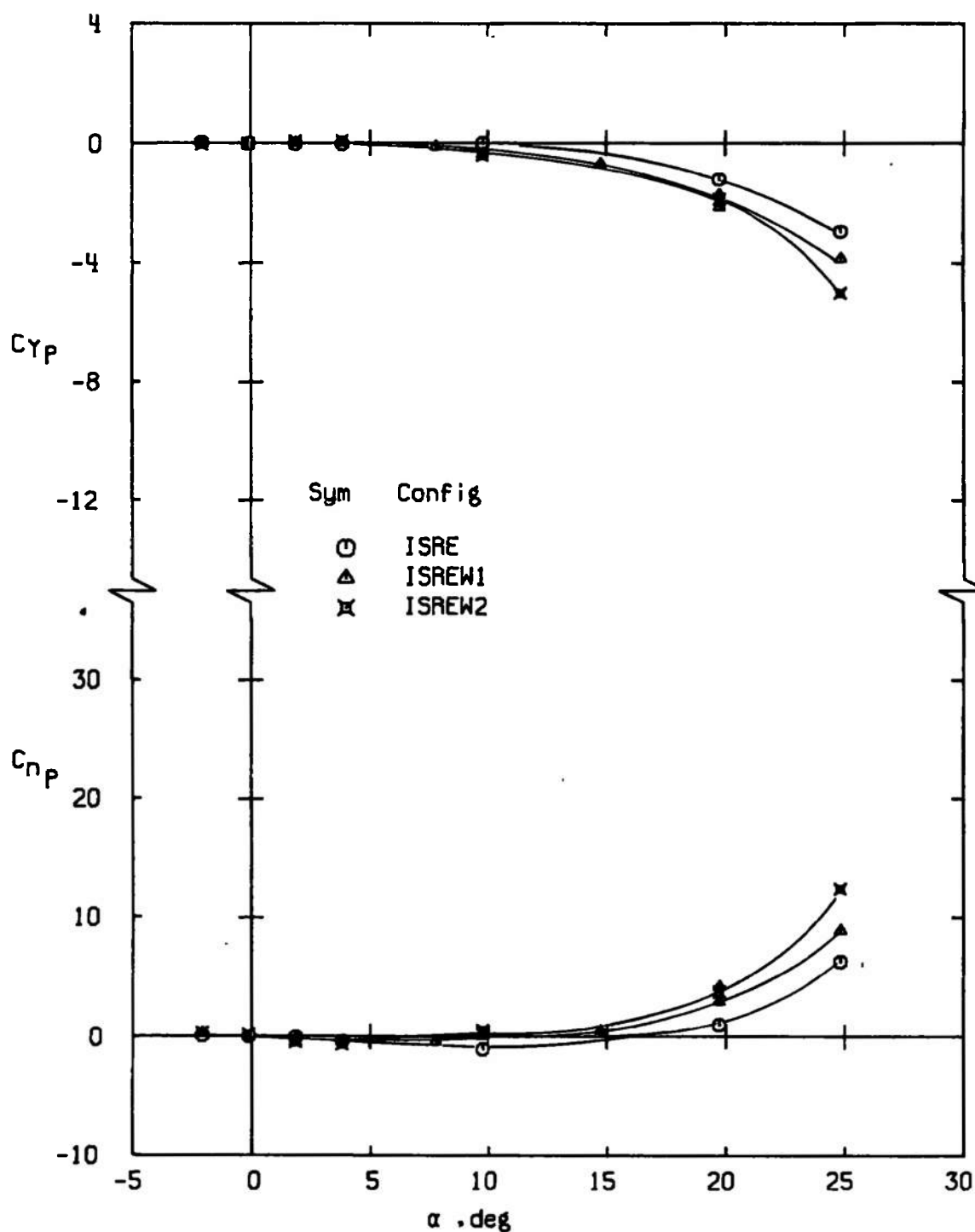
c. Configurations ISRE, $M_\infty = 0.8$
Figure 21. Continued.
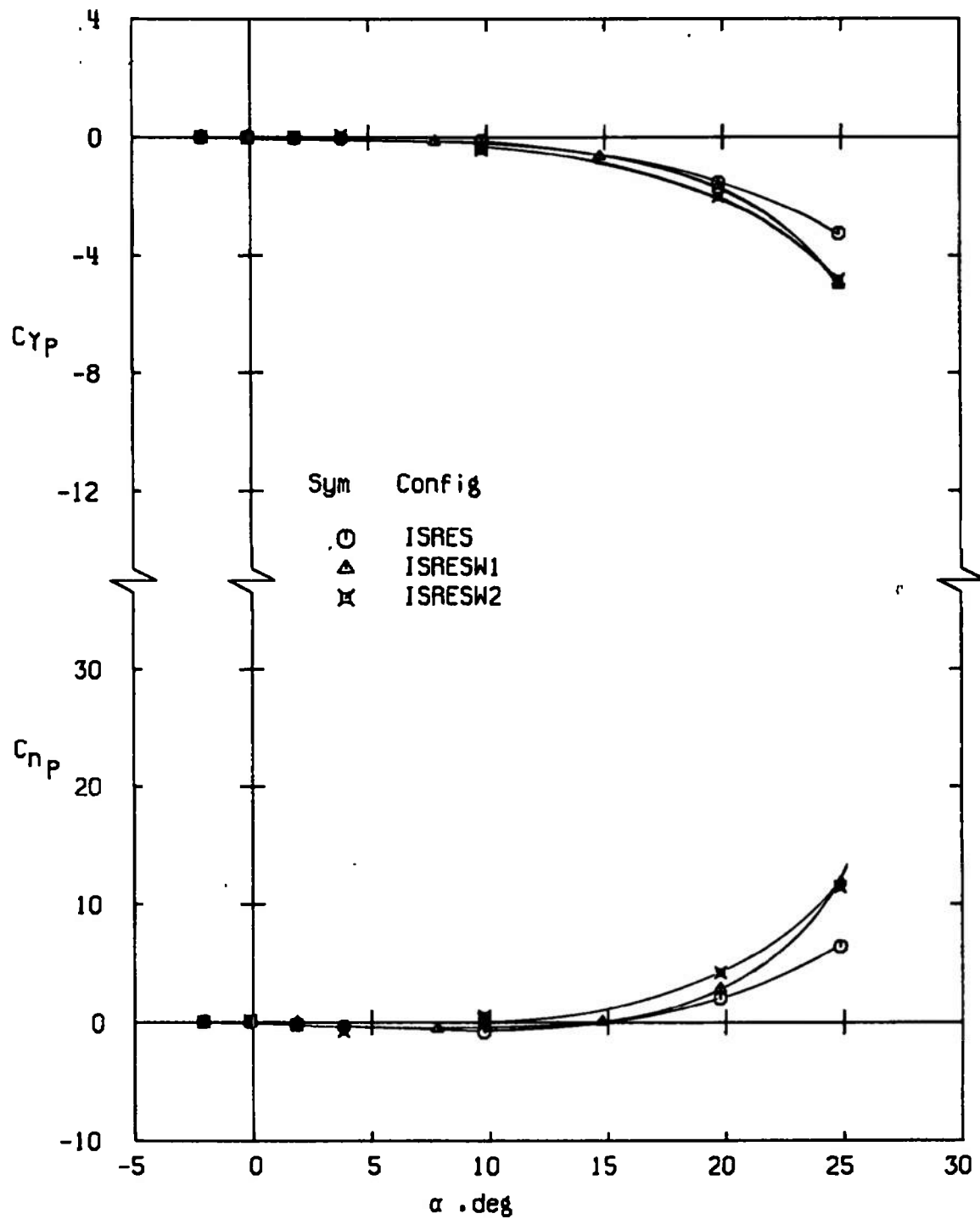
d. Configurations ISRES, $M_\infty = 0.8$
Figure 21. Continued.

e. Configurations FF, $M_\infty = 1.0$
Figure 21. Continued.

f. Configurations FFS, $M_\infty = 1.0$
Figure 21. Continued.

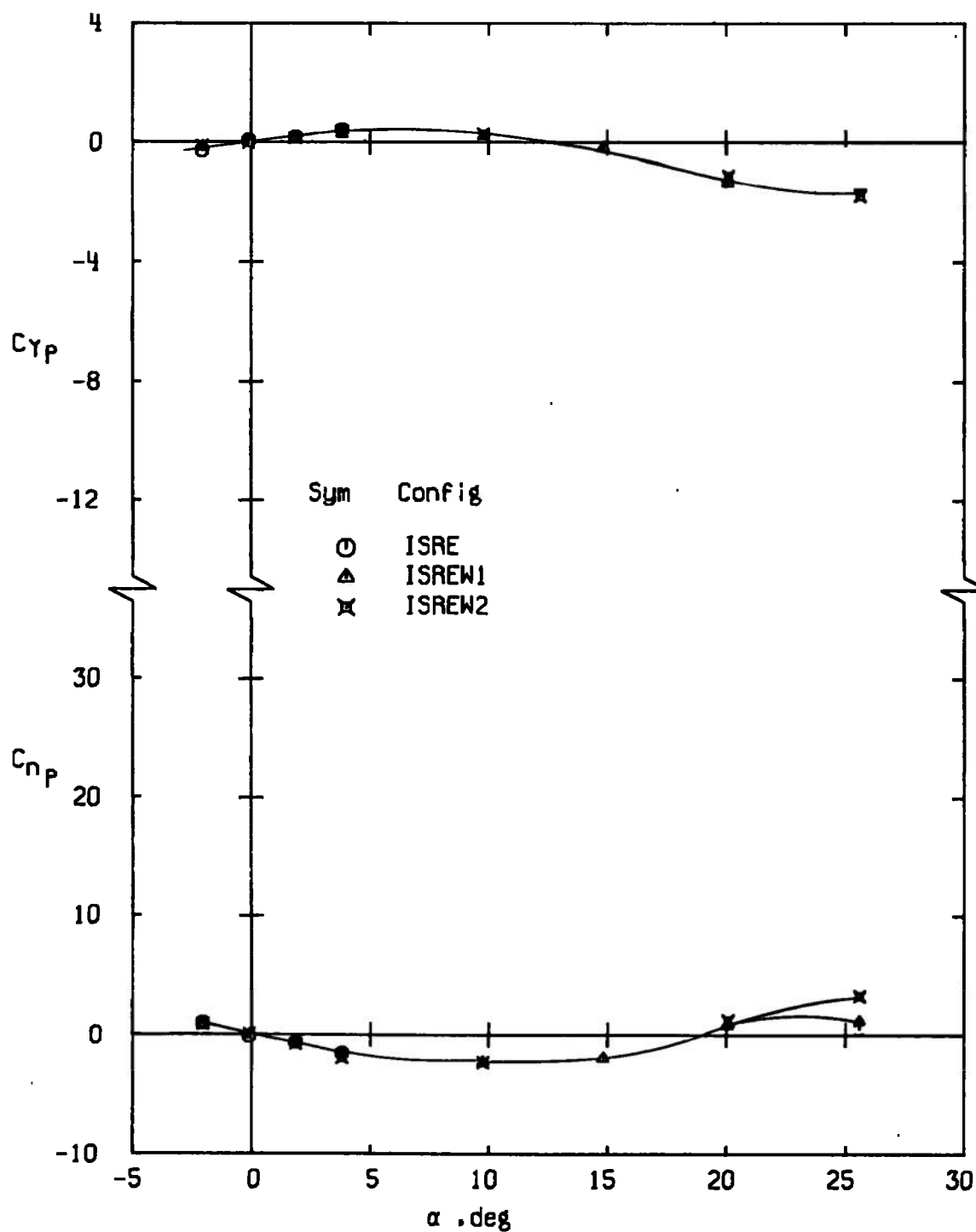g. Configurations ISRE, $M_\infty = 1.0$
Figure 21. Continued.

h. Configurations ISRES, $M_\infty = 1.0$
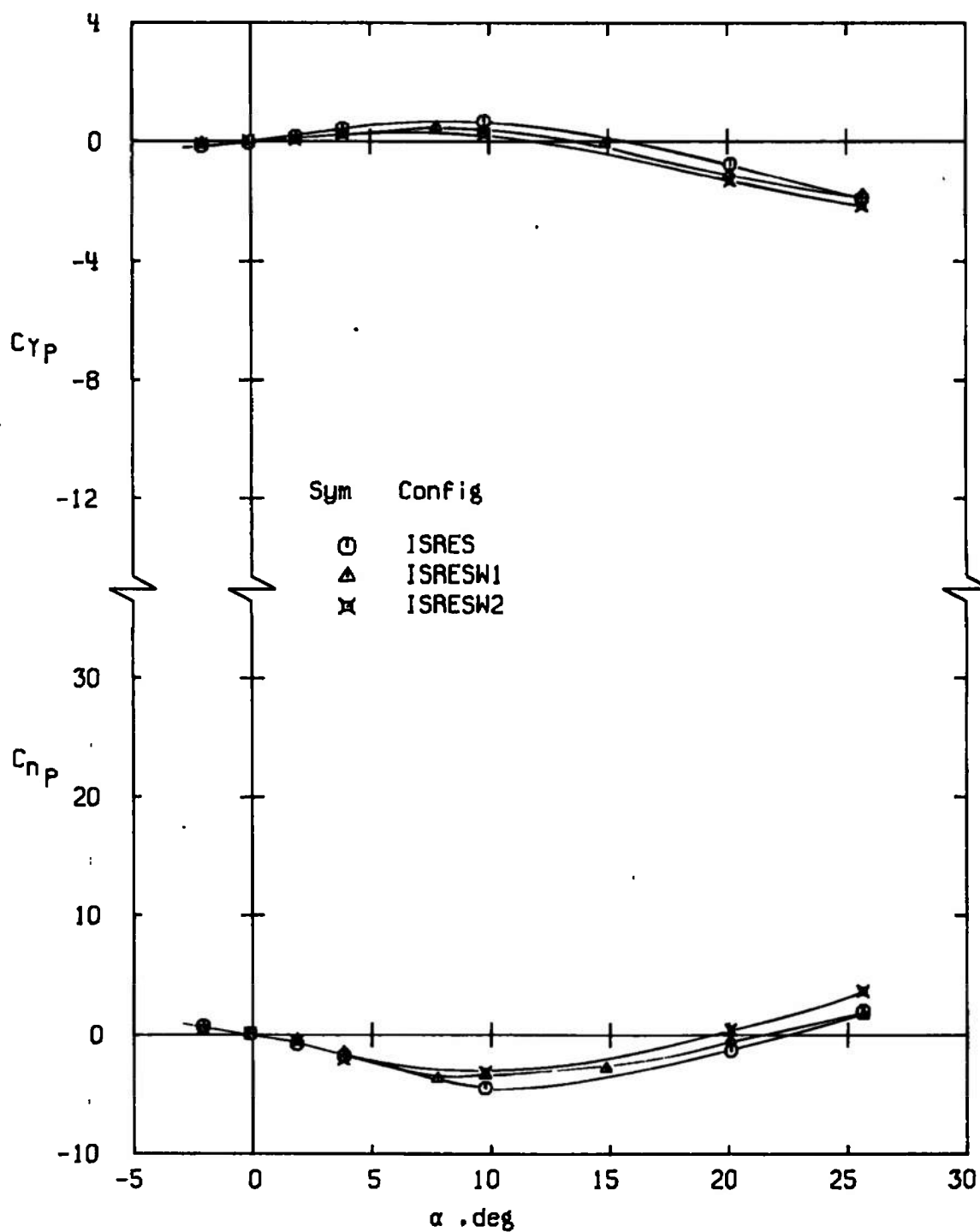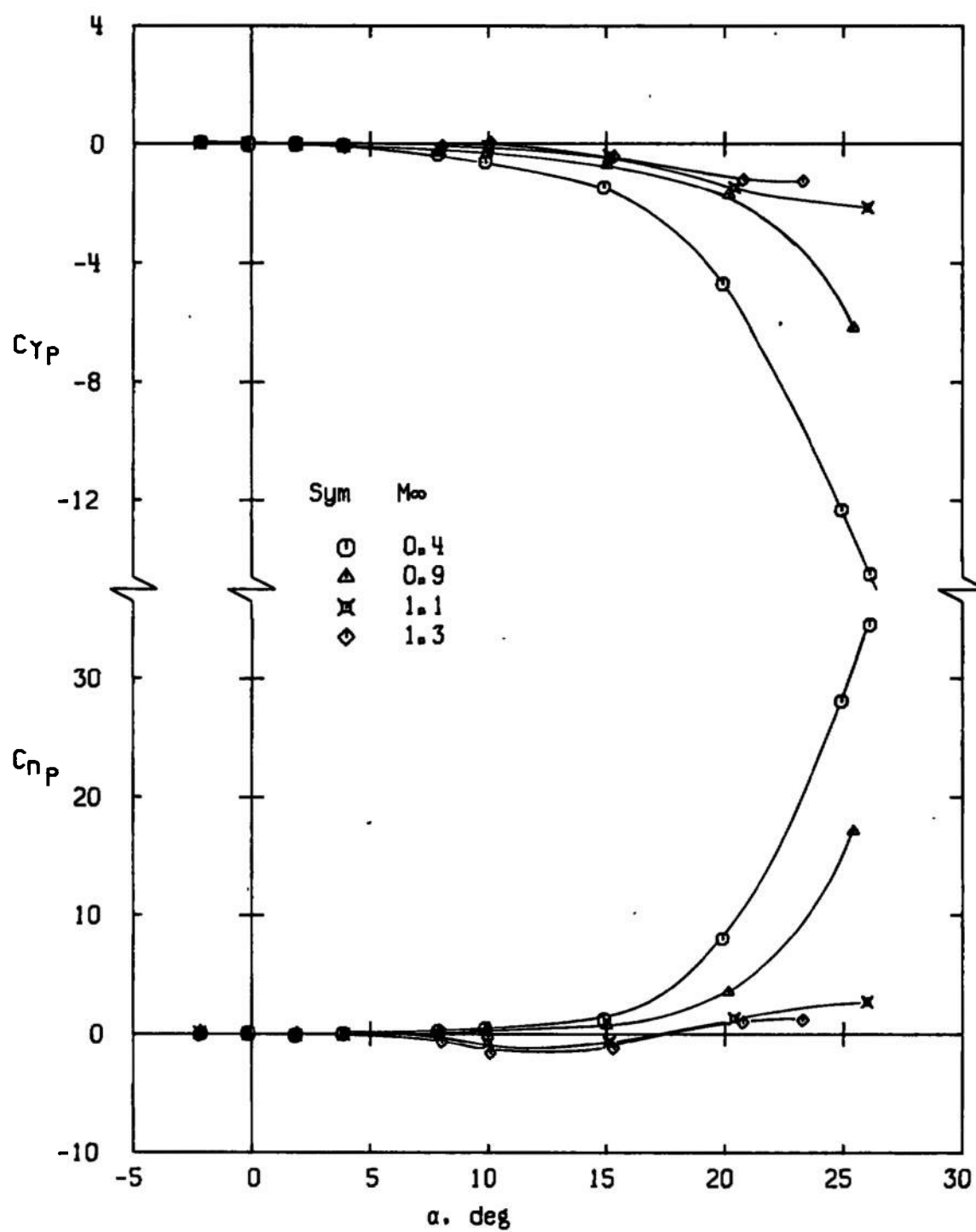Figure 21. Continued.

i. Configurations FF, $M_\infty = 1.2$
Figure 21. Continued.

j. Configurations FFS, $M_\infty = 1.2$
Figure 21. Continued.

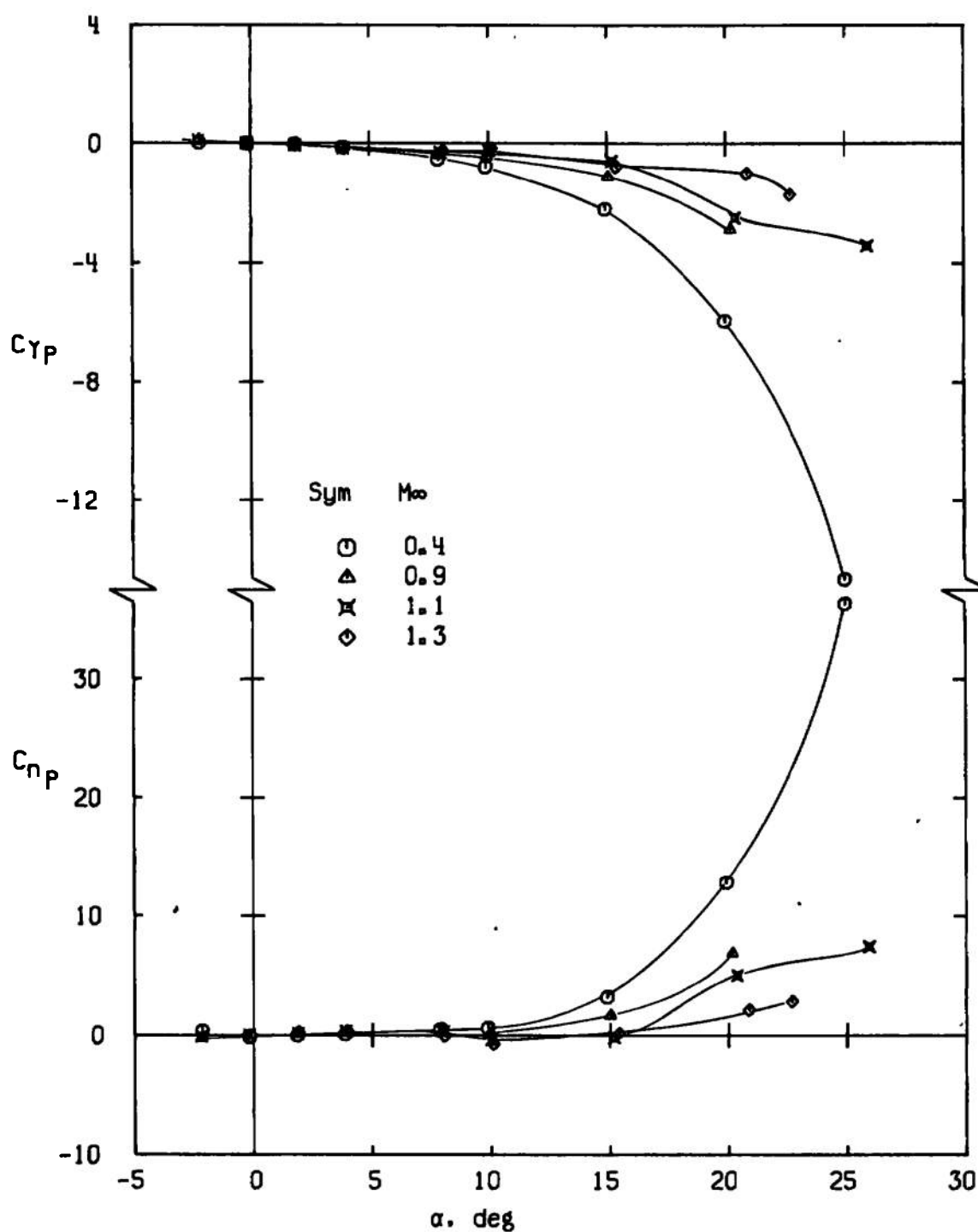k. Configurations ISRES, M_∞ = 1.2
Figure 21. Continued.

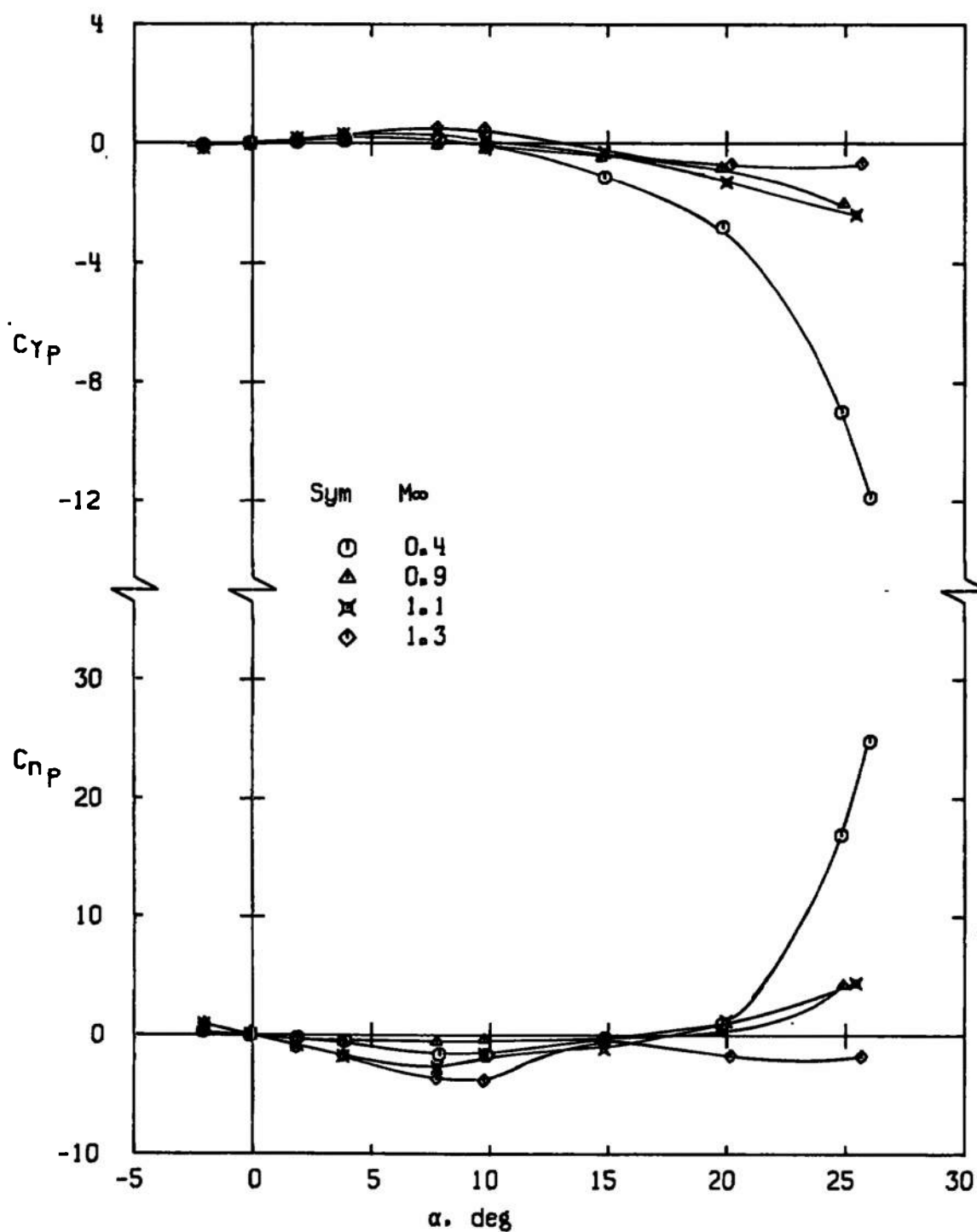I. Configurations ISRES, $M_\infty = 1.2$
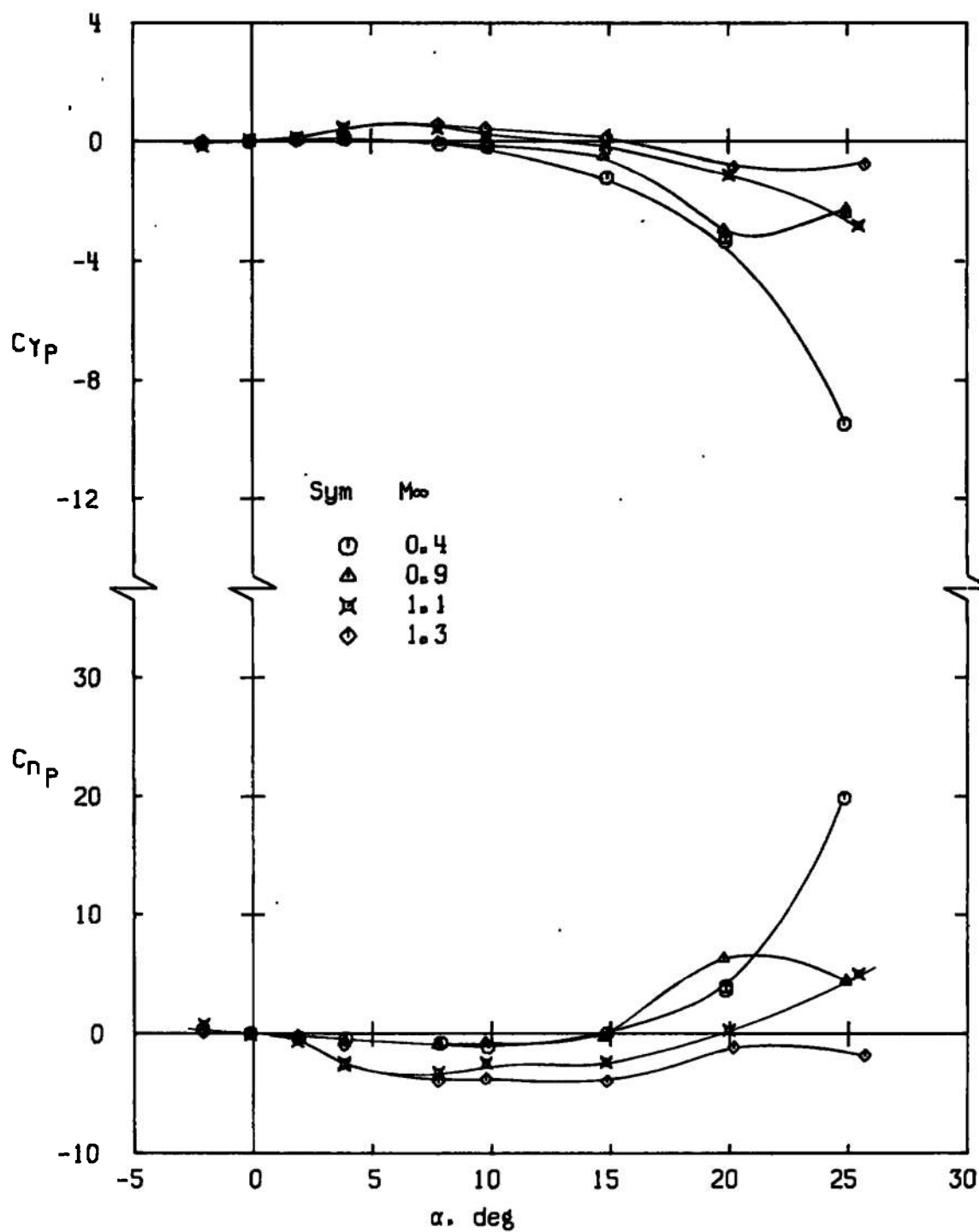Figure 21. Concluded.

a. Configuration FFW1
Figure 22. Variation of C_{Y_p} and C_{n_p} with angle of attack showing effect of Mach number.
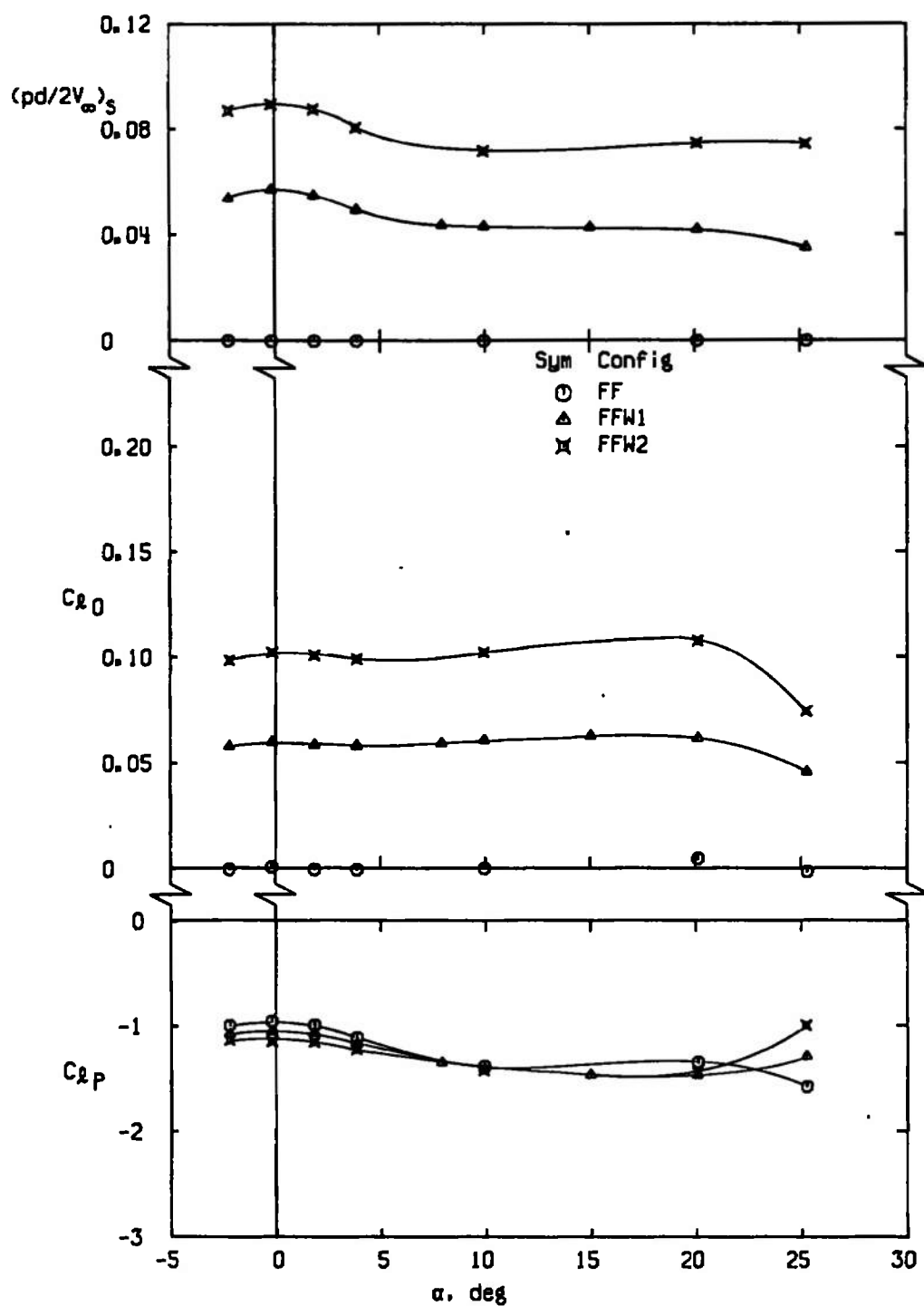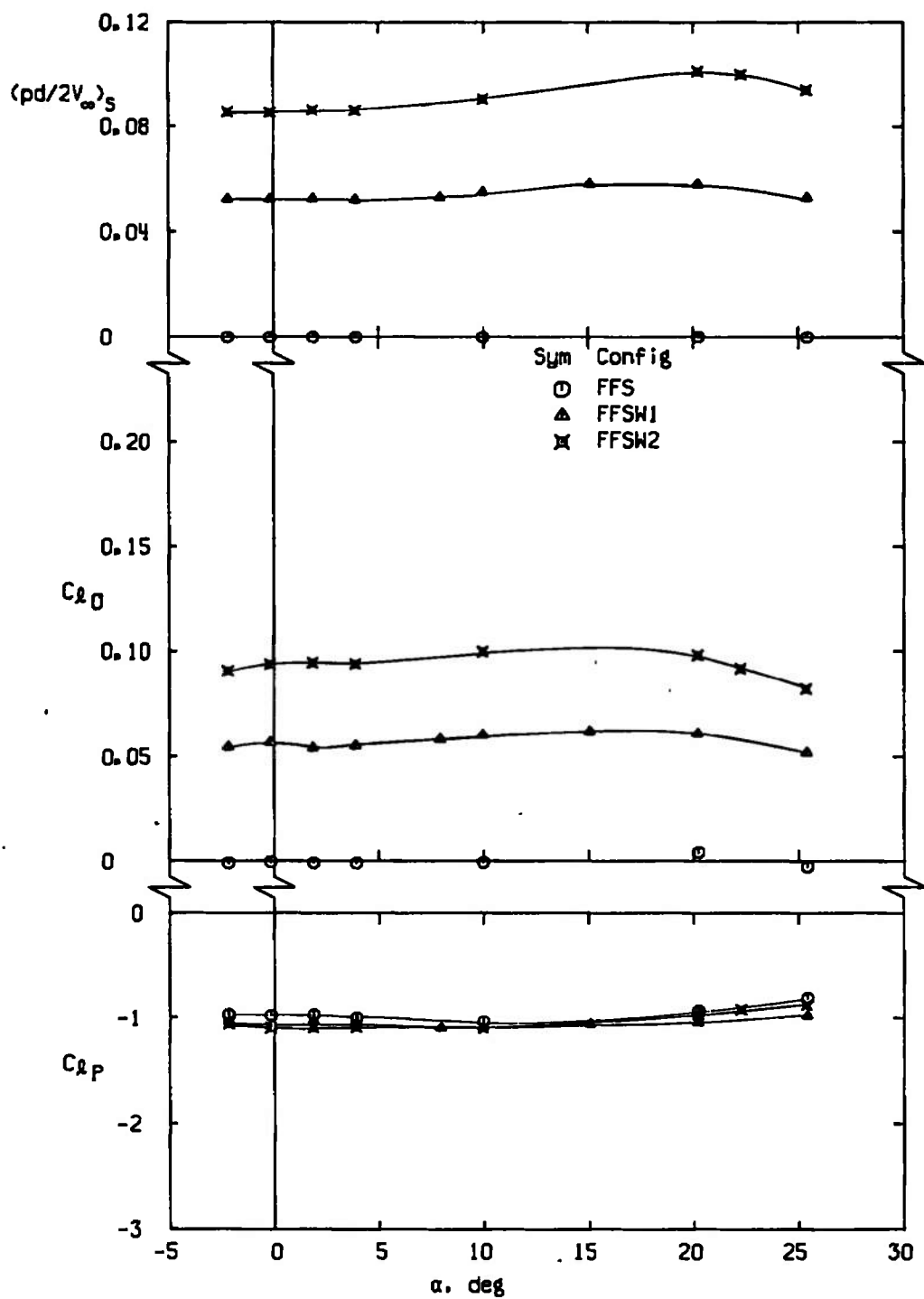
b. Configuration FFSW1
Figure 22. Continued.
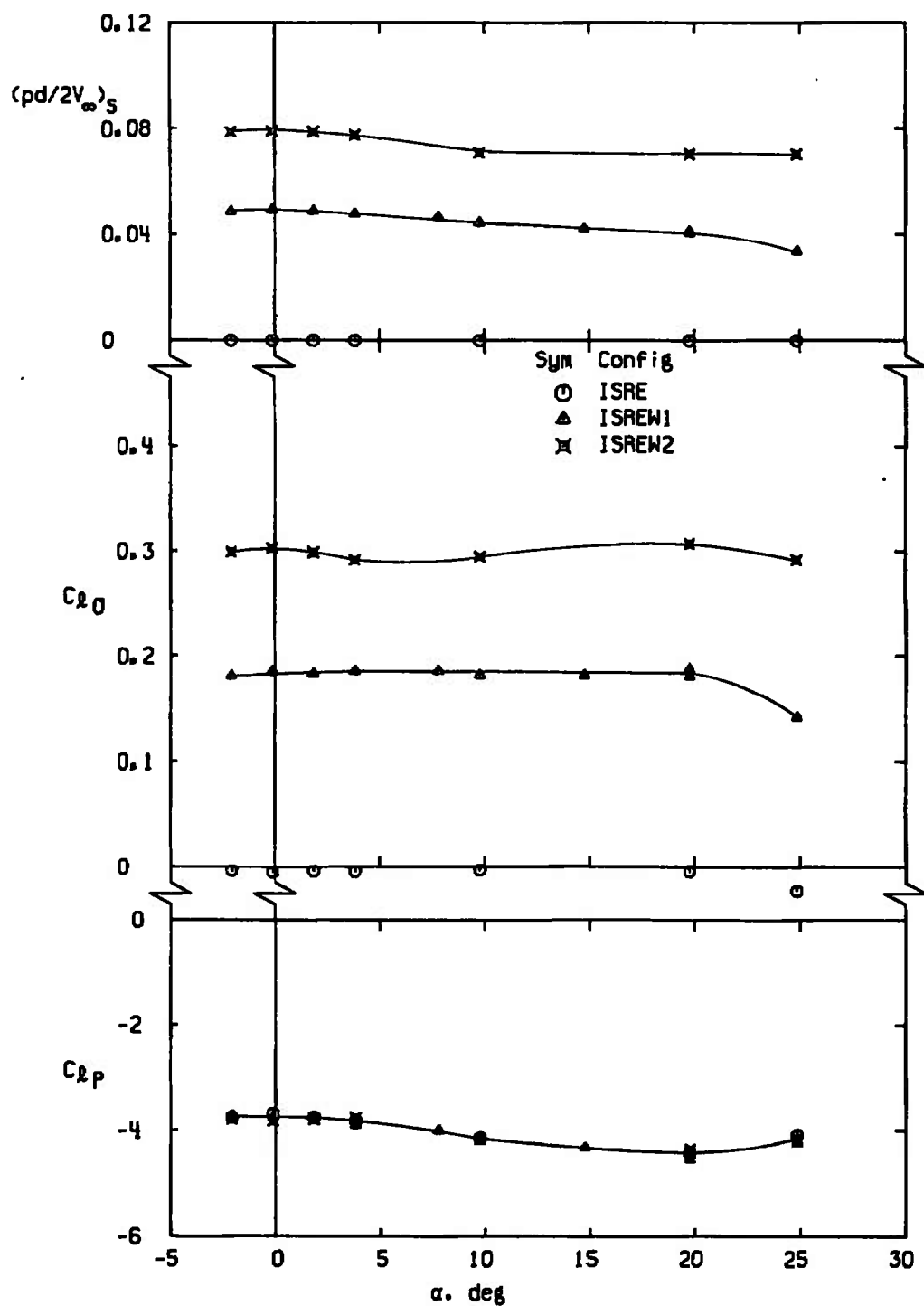
c. Configuration ISREW1
Figure 22. Continued.

d. Configuration ISRESW1
Figure 22. Concluded.

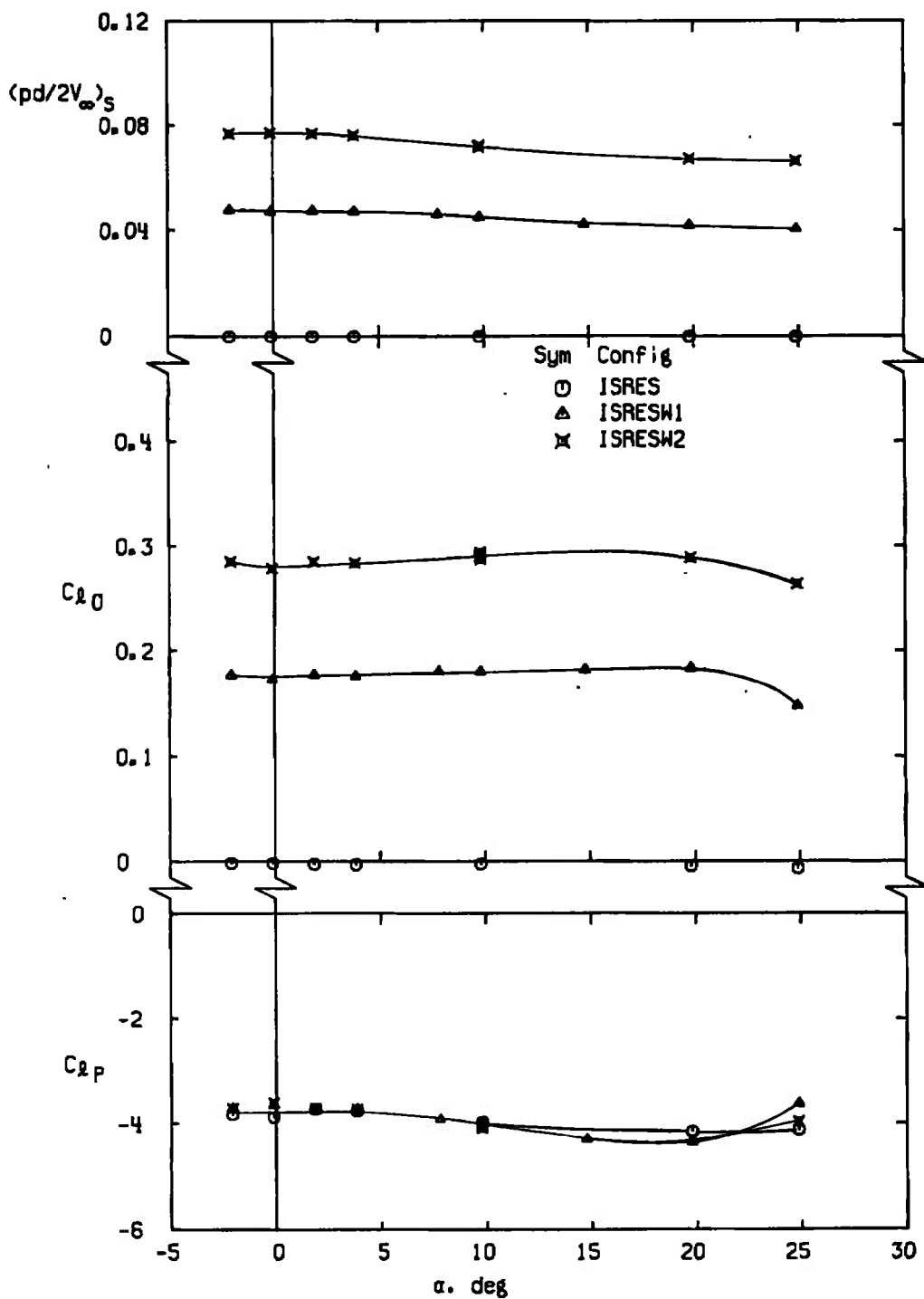a. Configurations FF, $M_\infty = 0.8$

Figure 23. Variation of $(pd/2V_\infty)_s$, C_{ℓ_0} and C_{ℓ_p} with angle of attack showing effect of fin wedges.
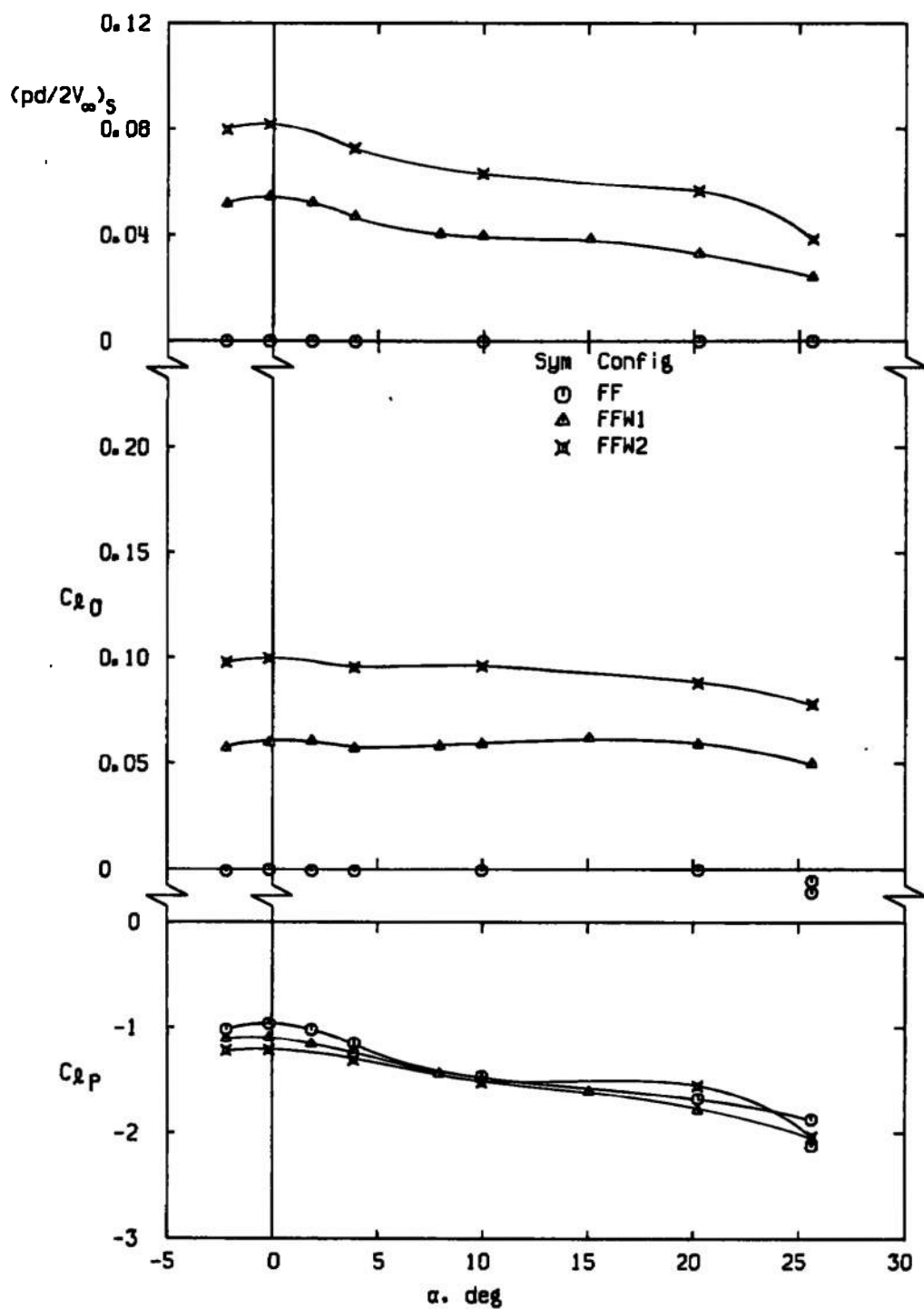
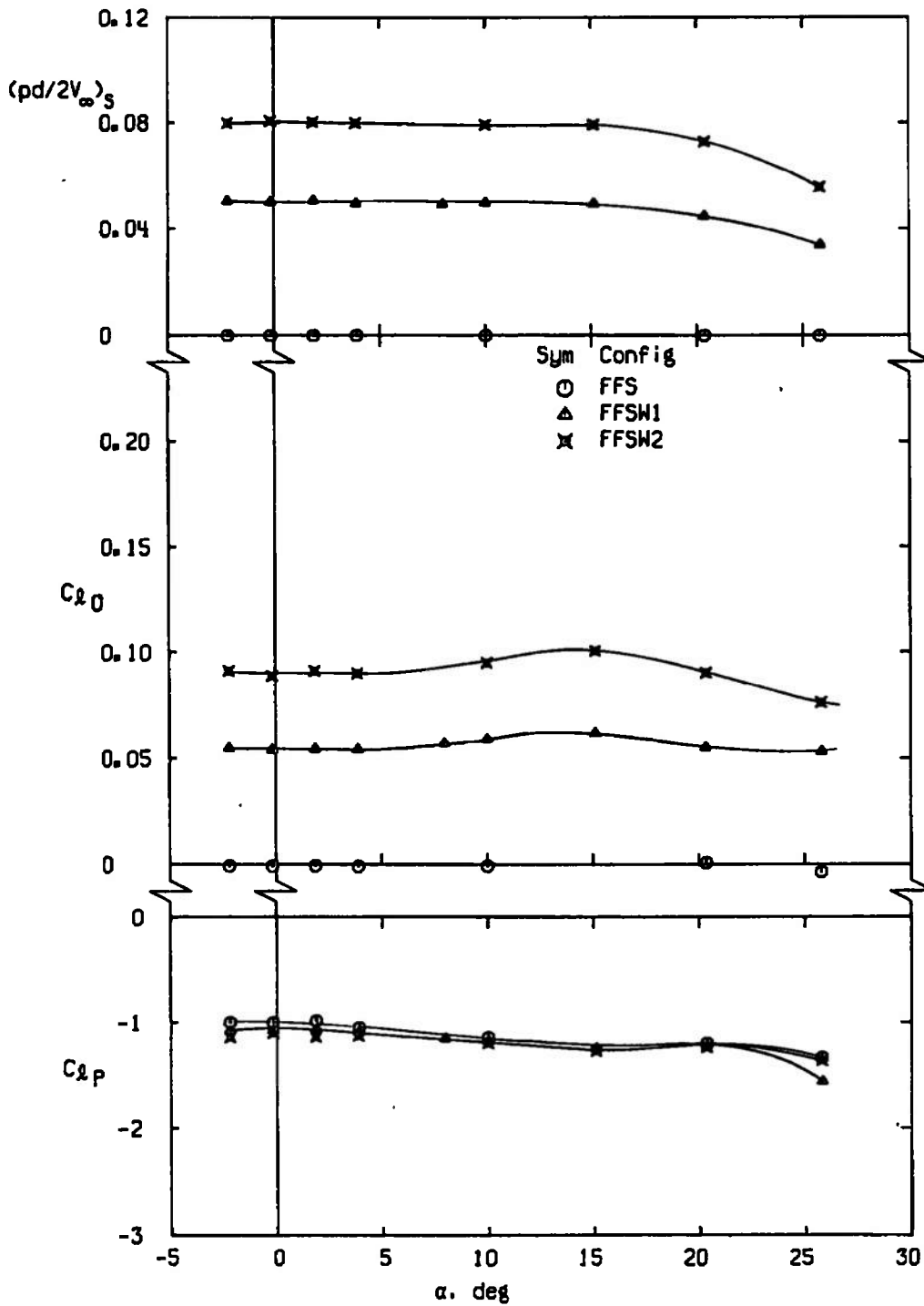b. Configurations FFS, $M_\infty = 0.8$
Figure 23. Continued.

c. Configurations ISRE, $M_\infty = 0.8$
Figure 23. Continued.

d. Configurations ISRES, $M_\infty = 0.8$
Figure 23. Continued.

e. Configurations FF, $M_\infty = 1.0$
Figure 23. Continued.

f. Configurations FFS, $M_\infty = 1.0$
Figure 23. Continued.

g. Configurations ISRE, $M_\infty = 1.0$
Figure 23. Continued.

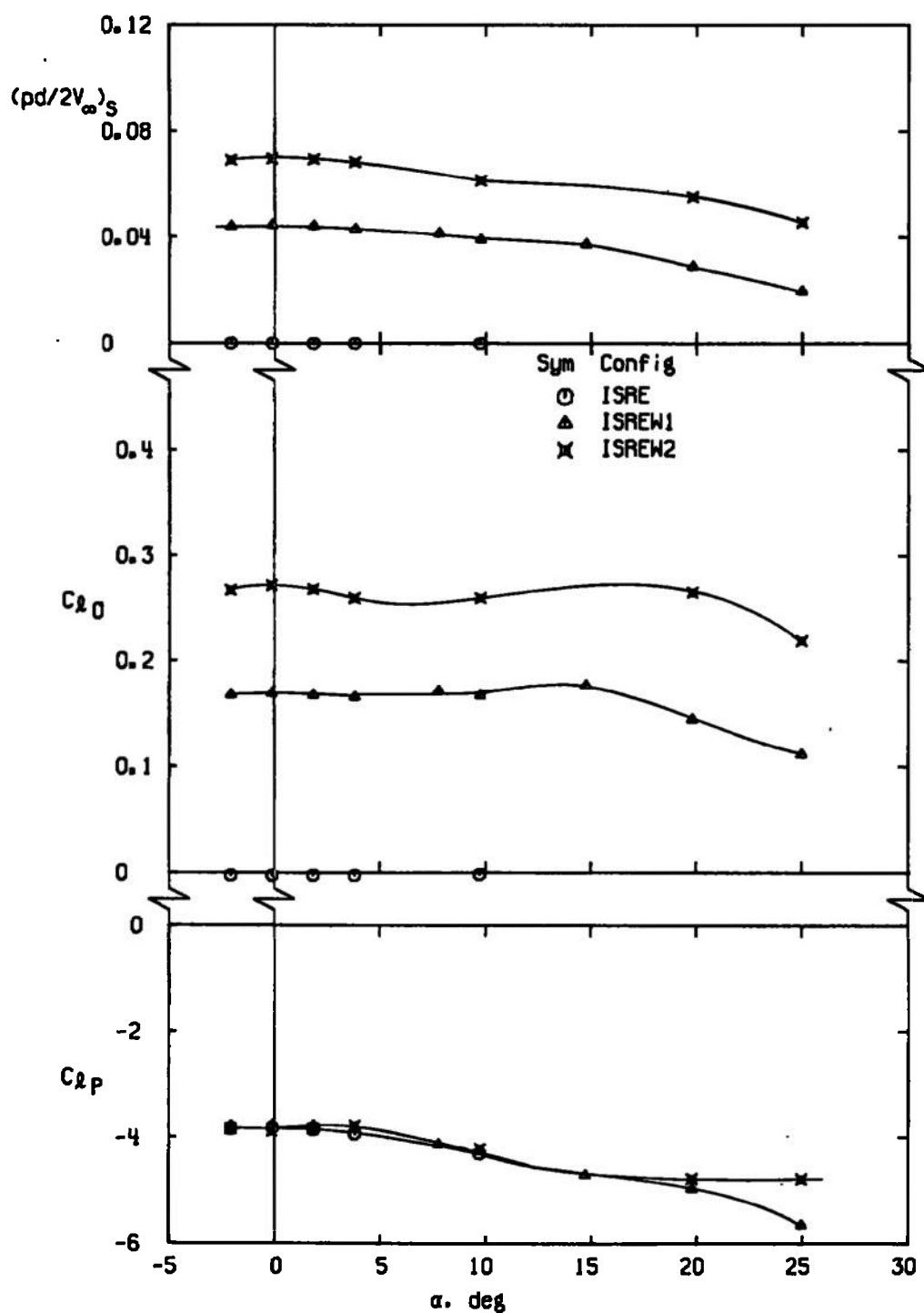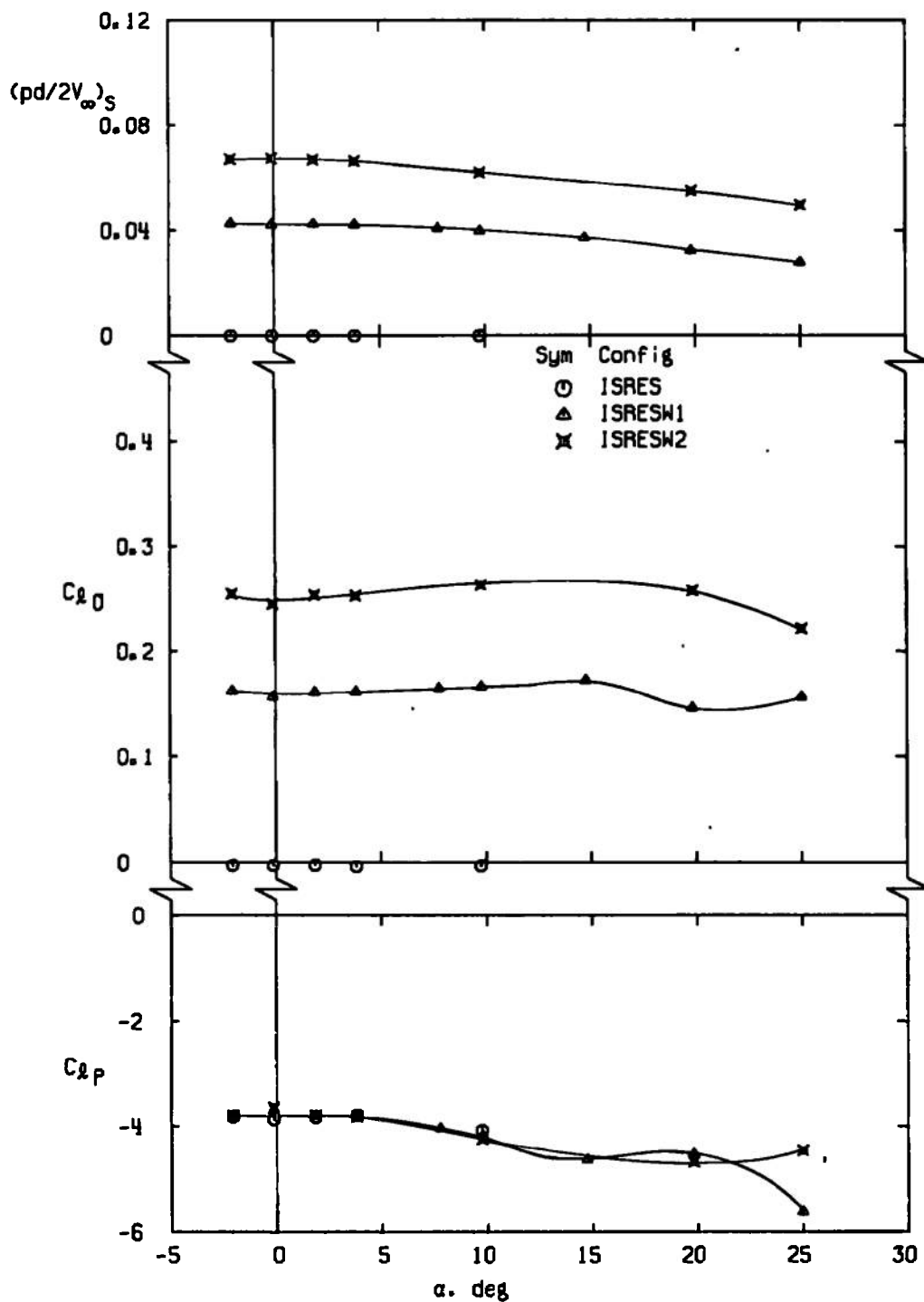h. Configurations ISRES, $M_\infty \approx 1.0$
Figure 23. Continued.

122

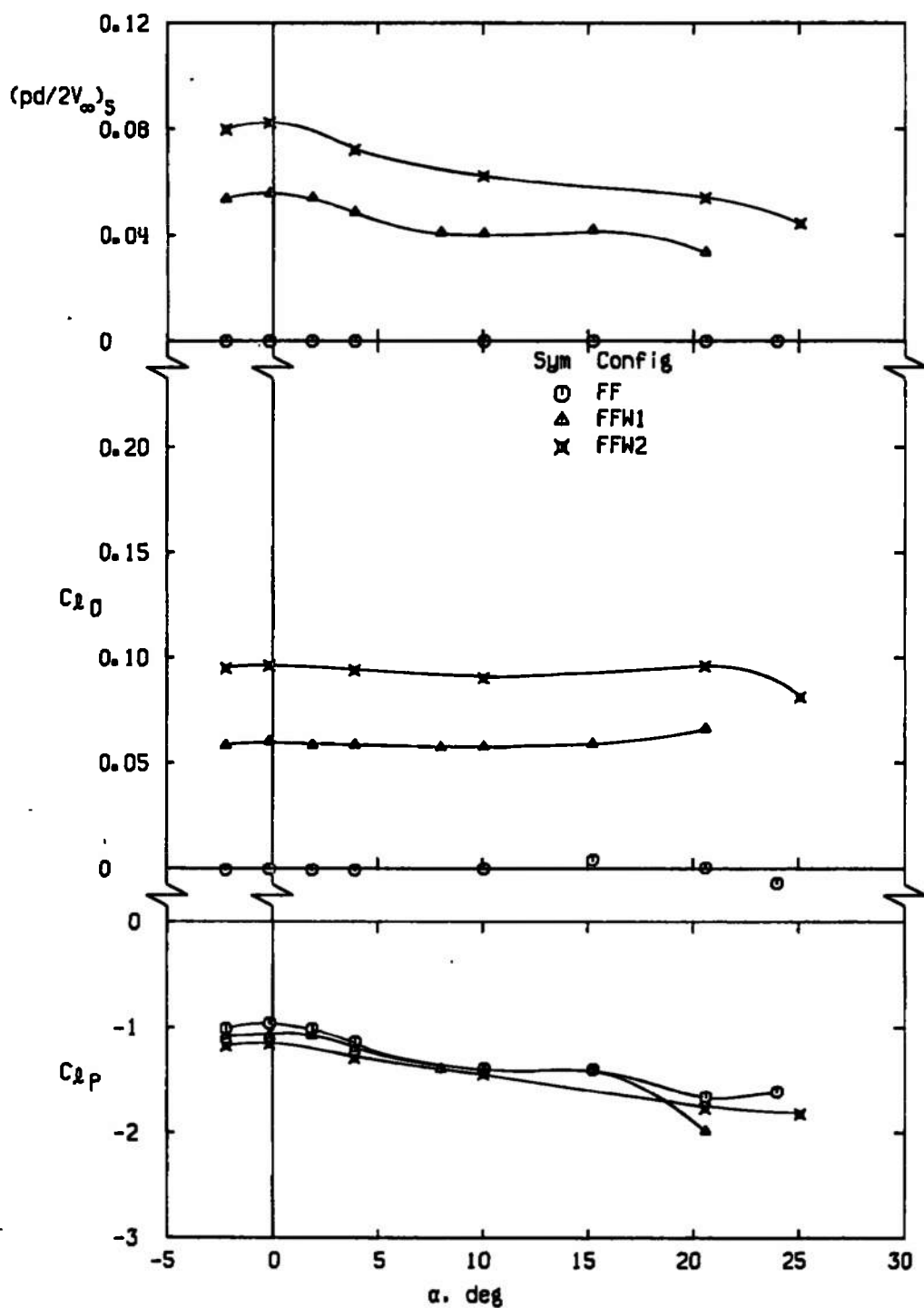i. Configurations FF, $M_\infty = 1.2$
Figure 23. Continued.

j. Configurations FFS, $M_\infty = 1.2$
Figure 23. Continued.

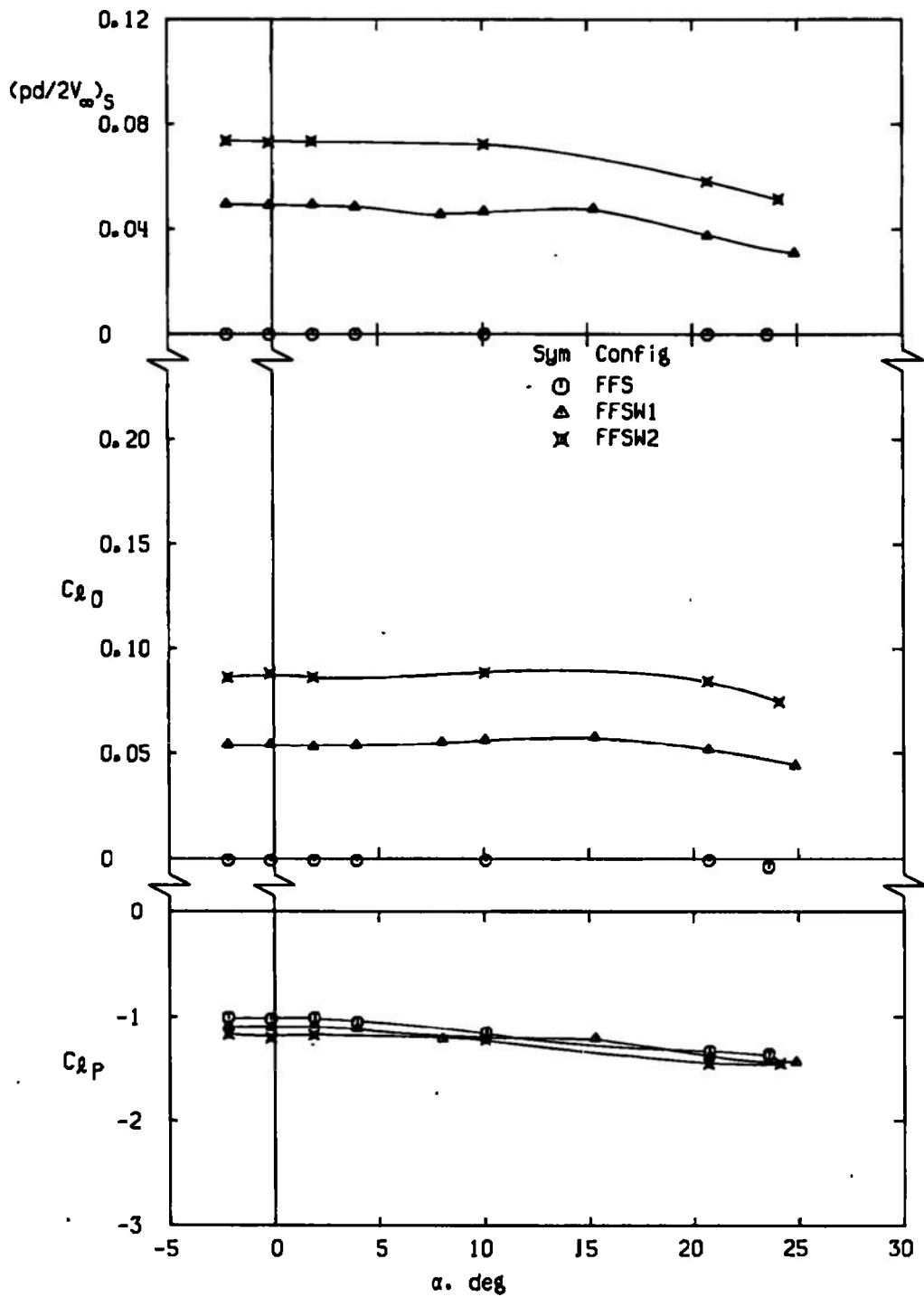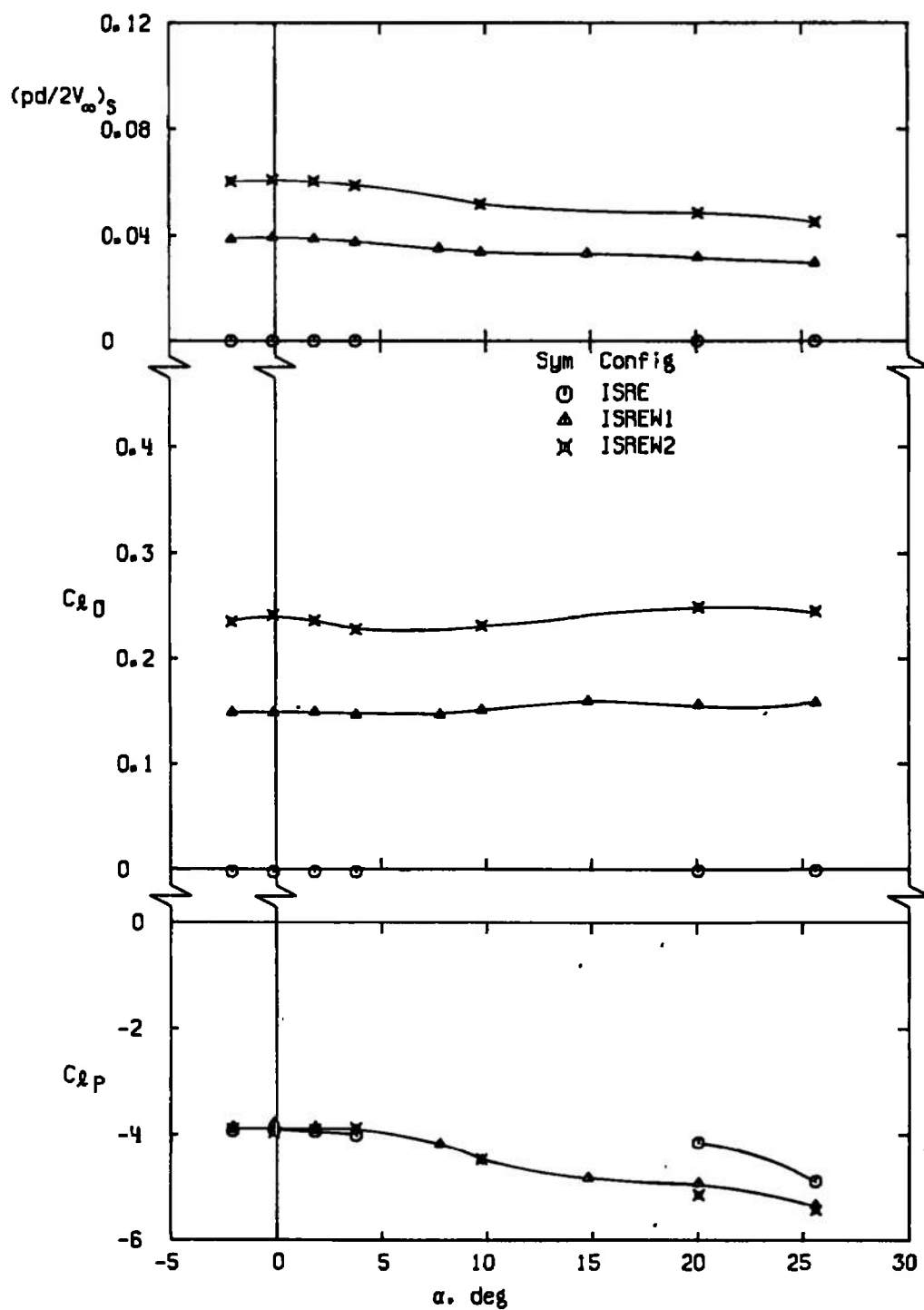k. Configurations ISRE, $M_\infty = 1.2$
Figure 23. Continued.
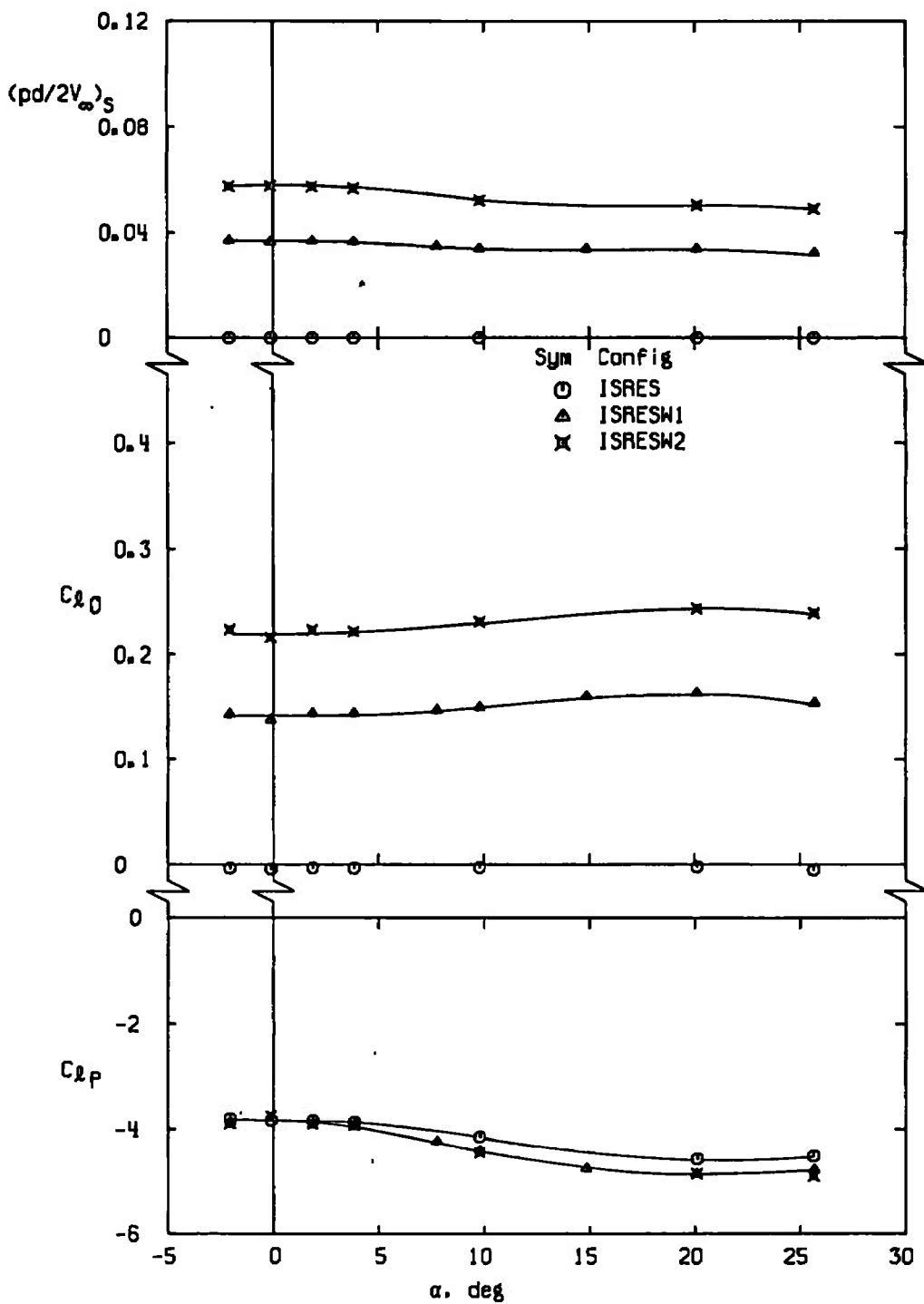
I. Configurations ISRES, M_∞ = 1.2
Figure 23. Concluded.
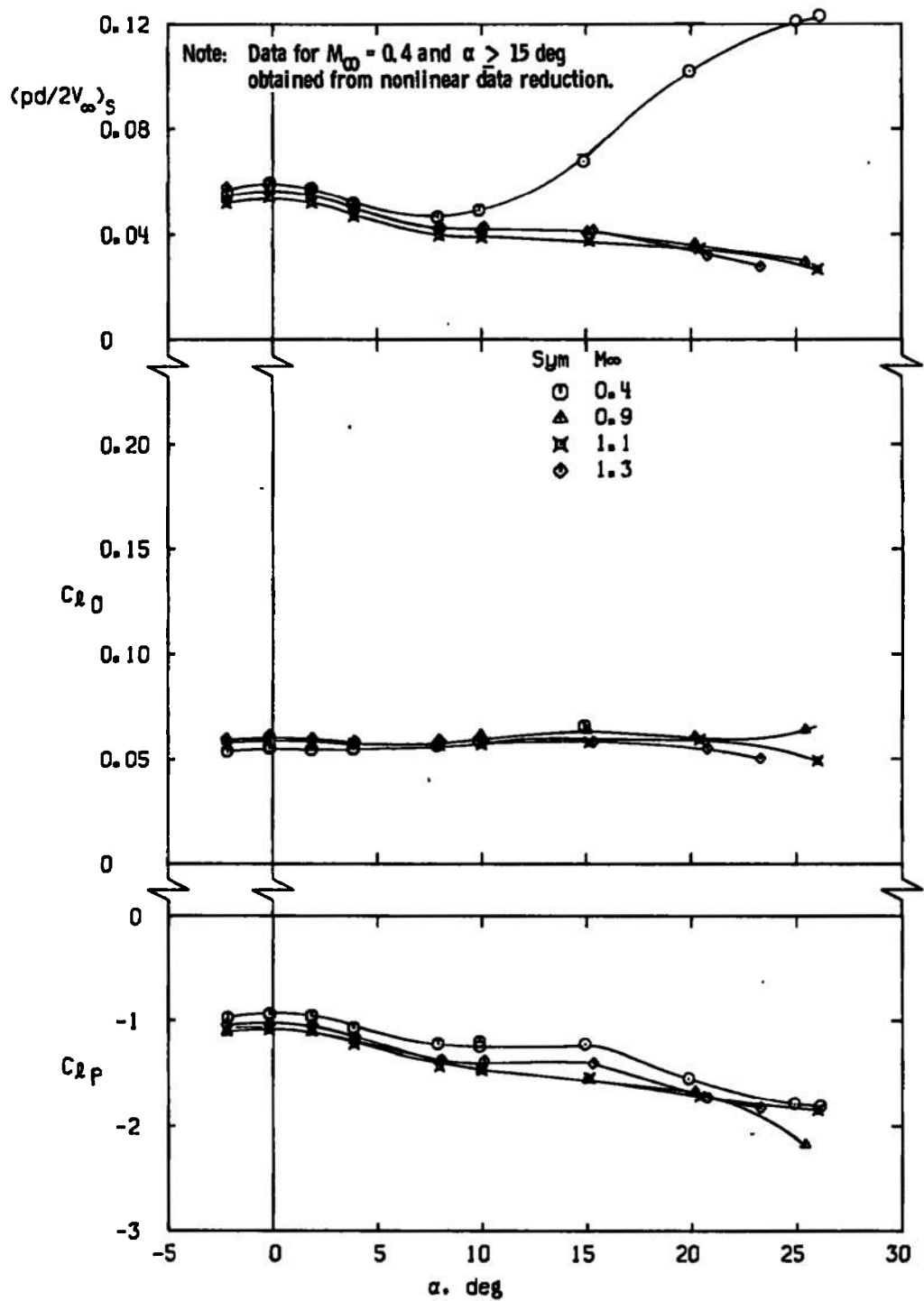
a. Configuration FFW1
Figure 24. Variation of $(pd/2V_\infty)_s$, C_{ℓ_0} and C_{ℓ_p} with angle of attack showing effect of Mach number.
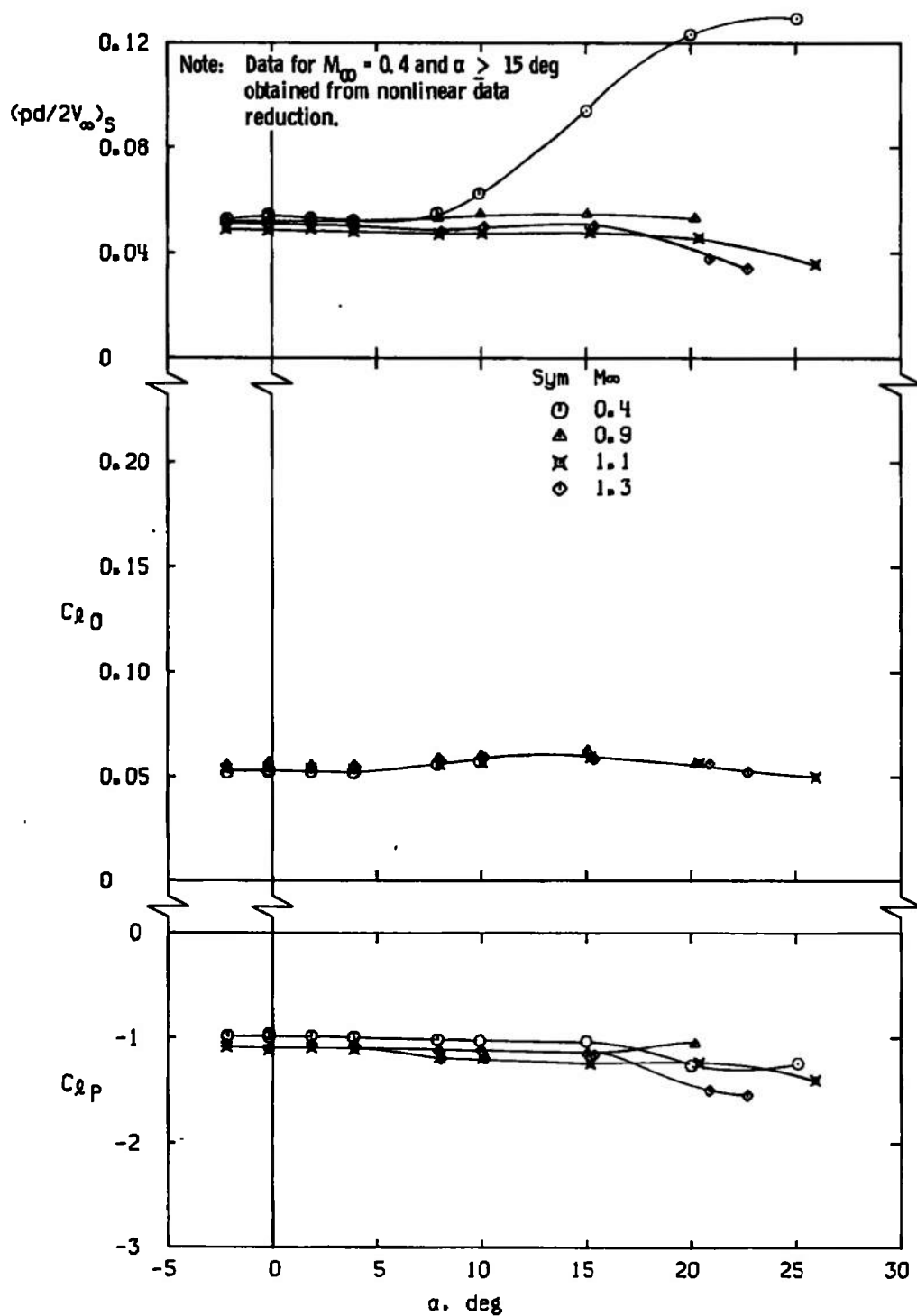
b. Configuration FFSW1
Figure 24. Continued.
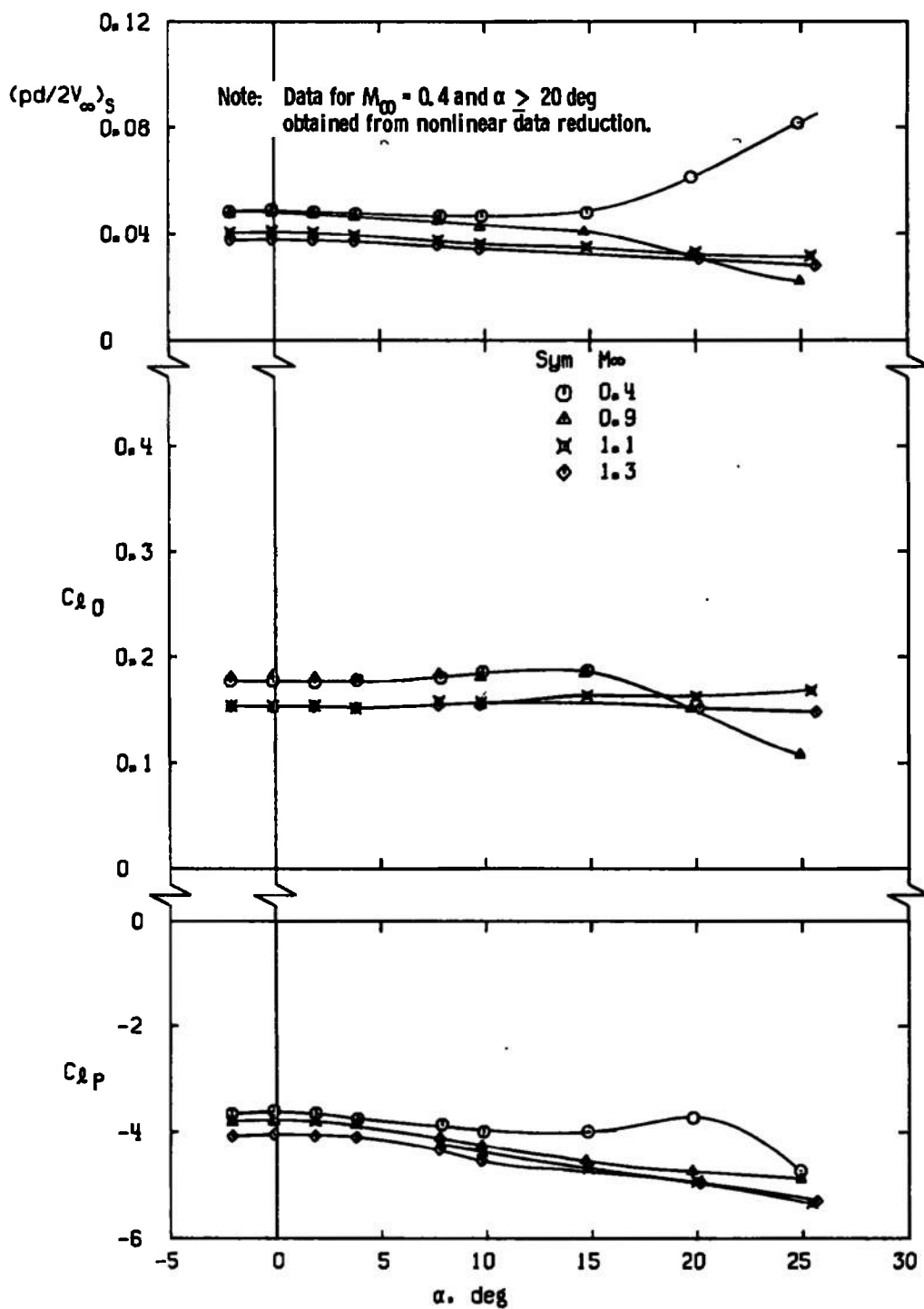
c. Configuration ISREW1
Figure 24. Continued.
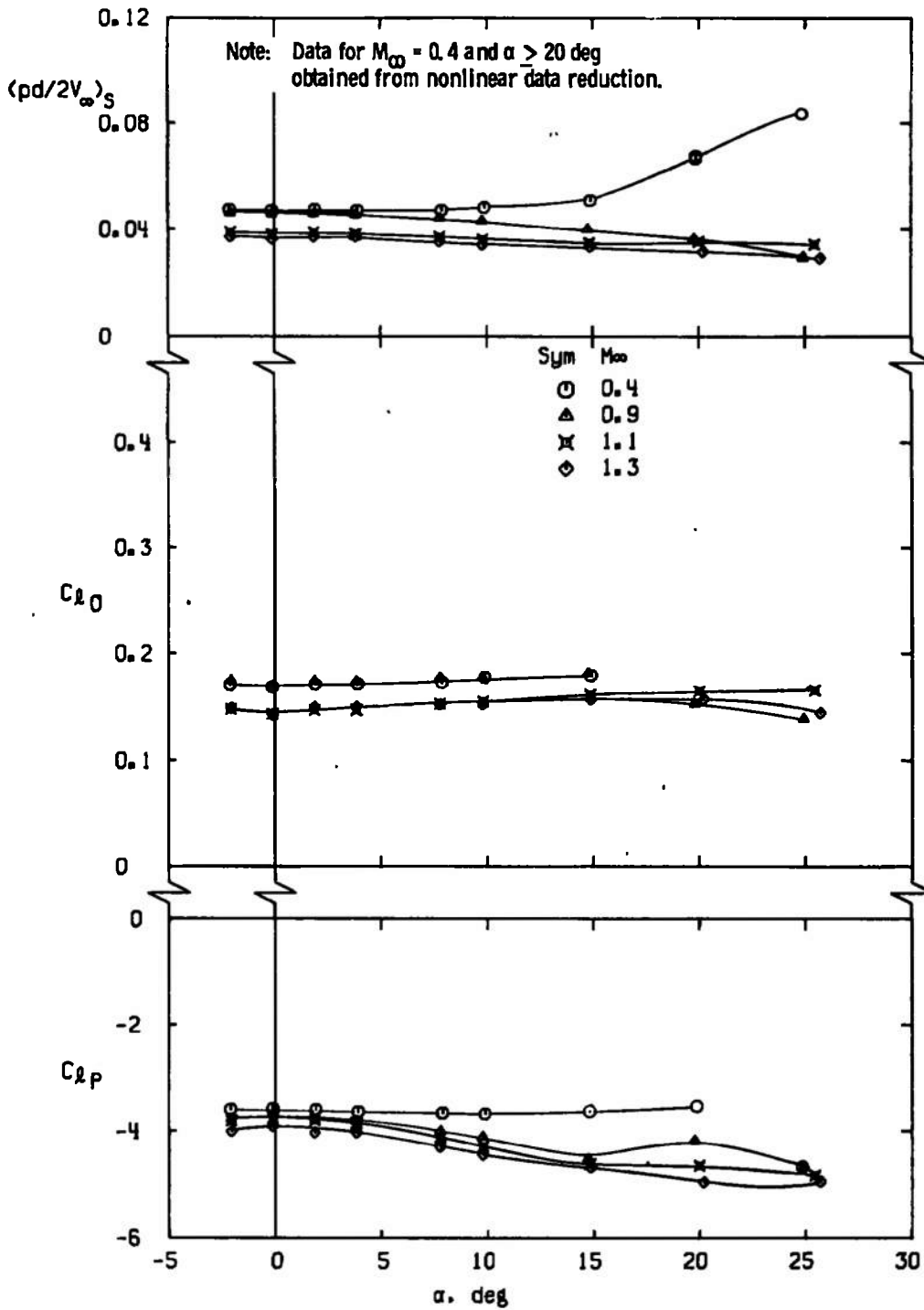
d. Configuration ISRESW1
Figure 24. Concluded.
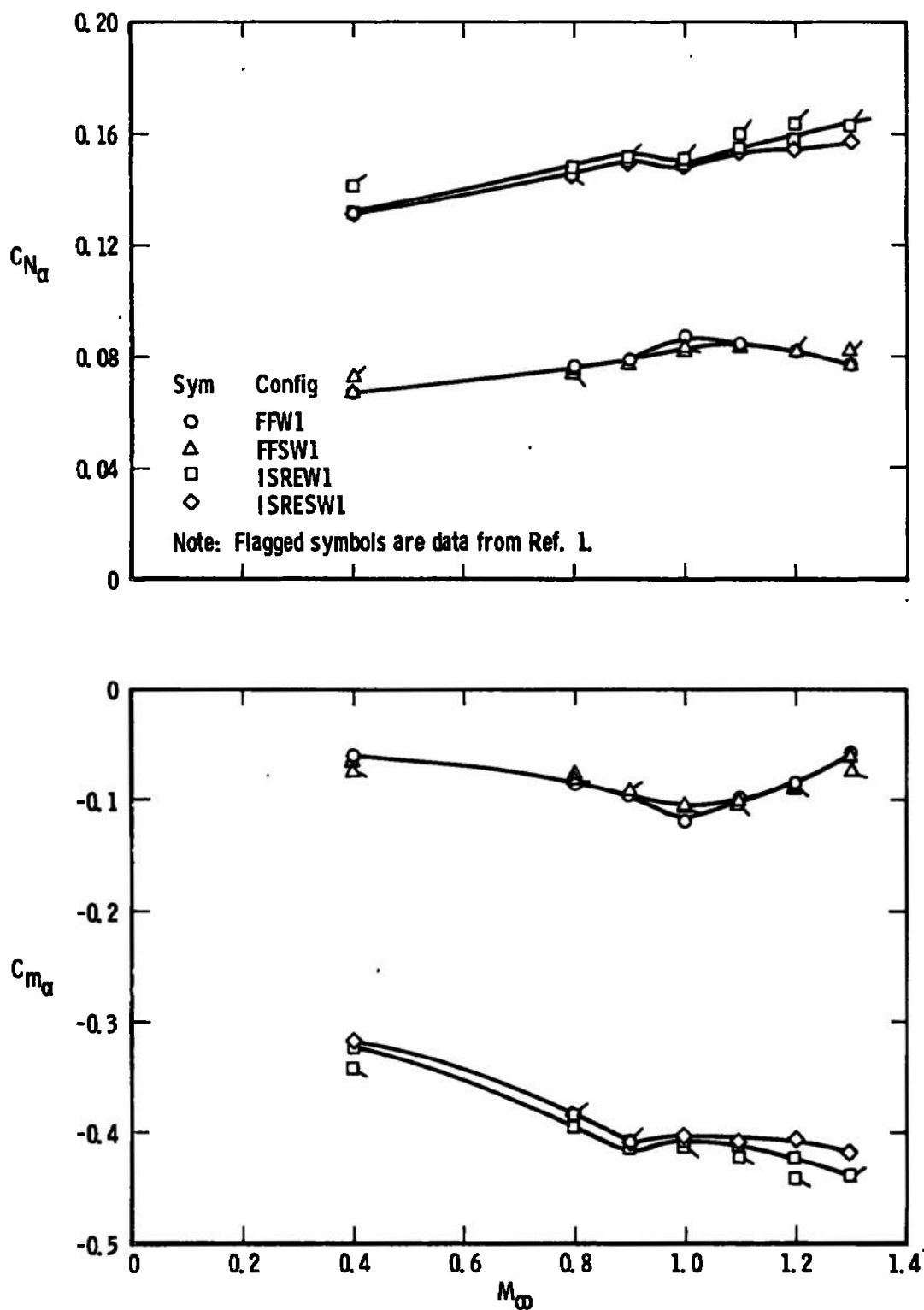
Figure 25. Variation of C_{N_α} and C_{m_α} with Mach number, $a = 0$.
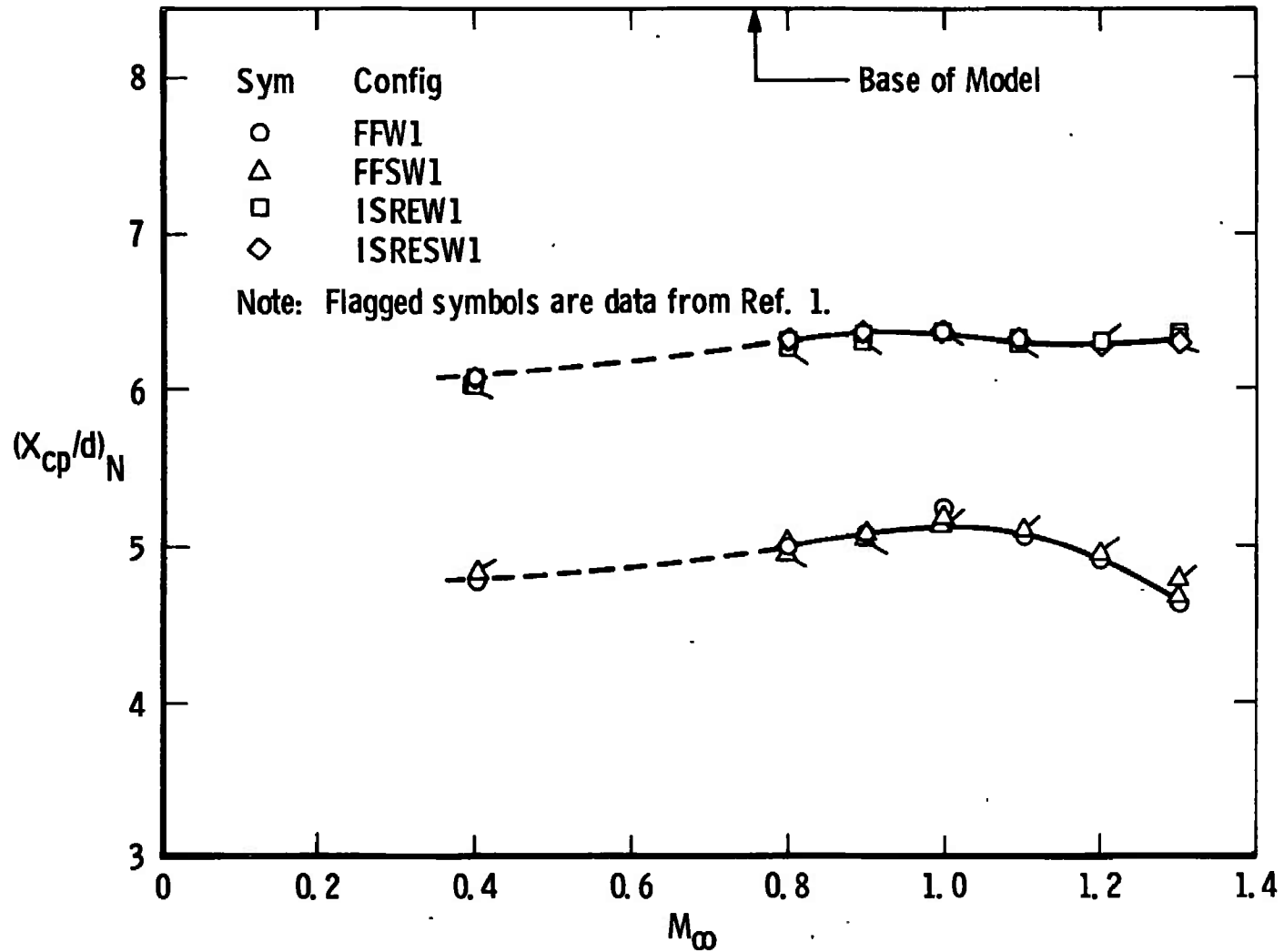
Figure 26. Variation of longitudinal center of pressure, $(x_{cp}/d)_N$, with Mach number, $\alpha = 0$.
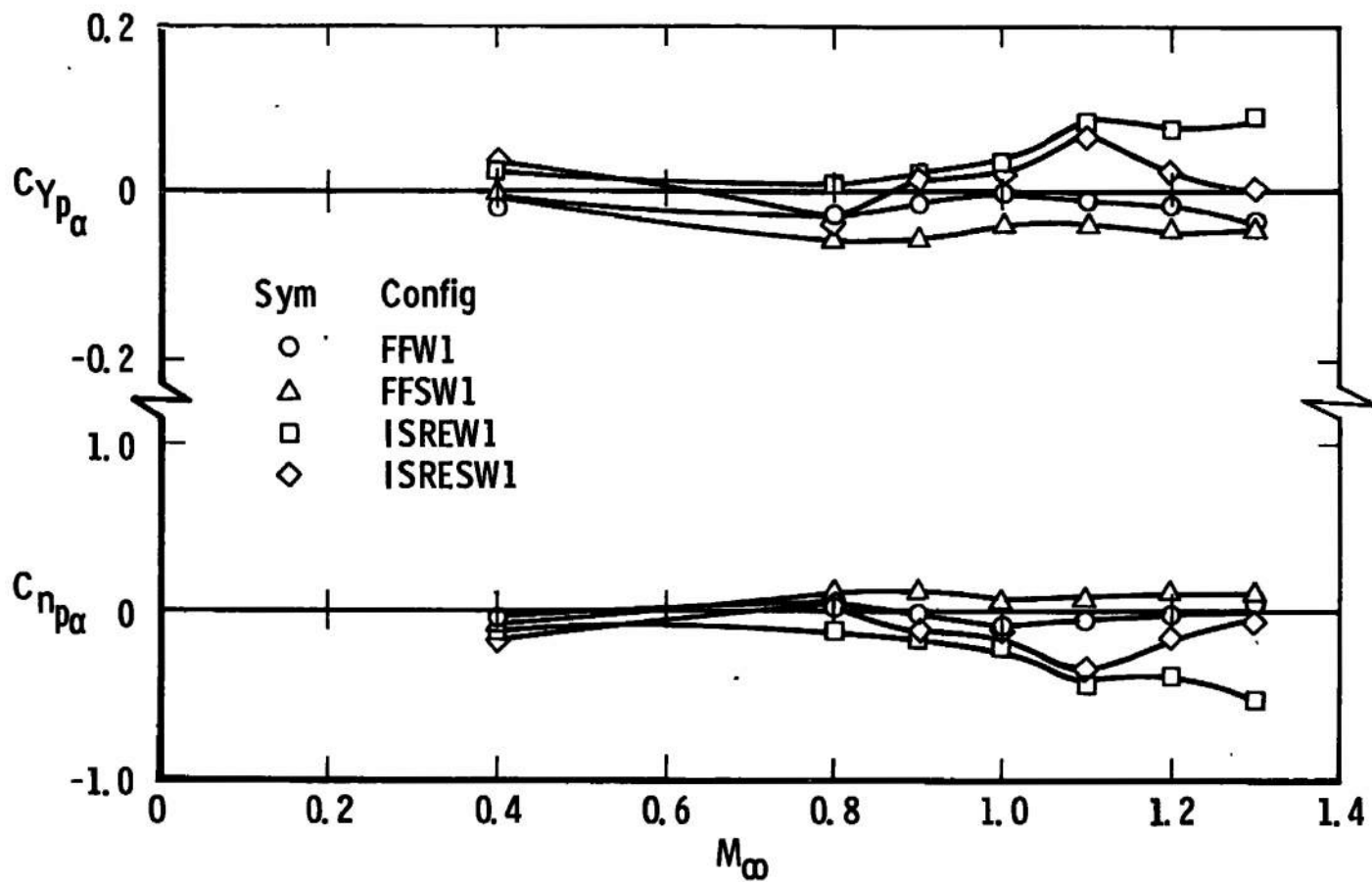
Figure 27. Variation of $C_{Y_{p_a}}$ and $C_{n_{p_a}}$ with Mach number, $a = 0$.
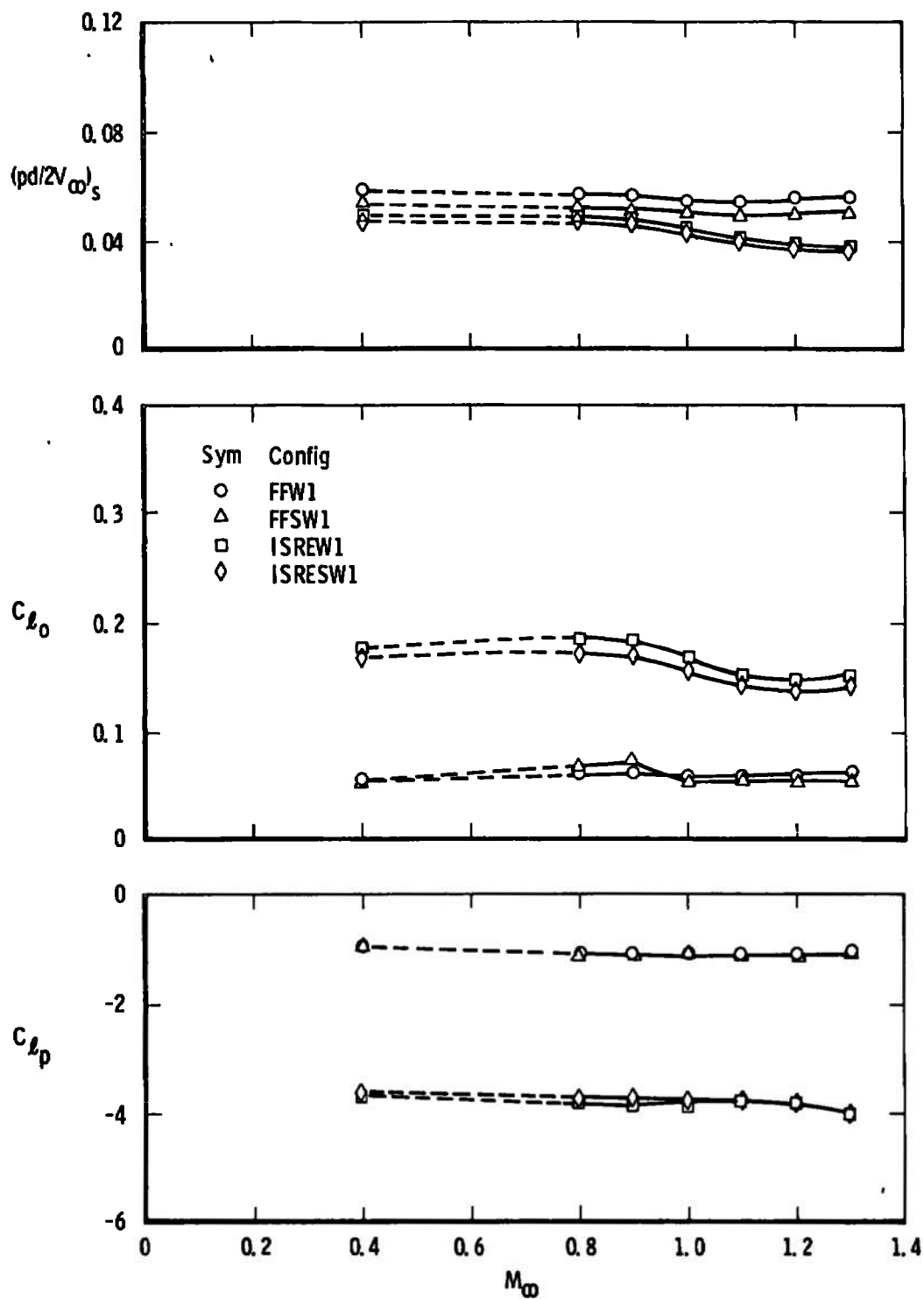
a. $a = 0$

Figure 28. Variation of $(pd/2V_\infty)_s$, C_{ℓ_0}, and C_{ℓ_p} with Mach number.
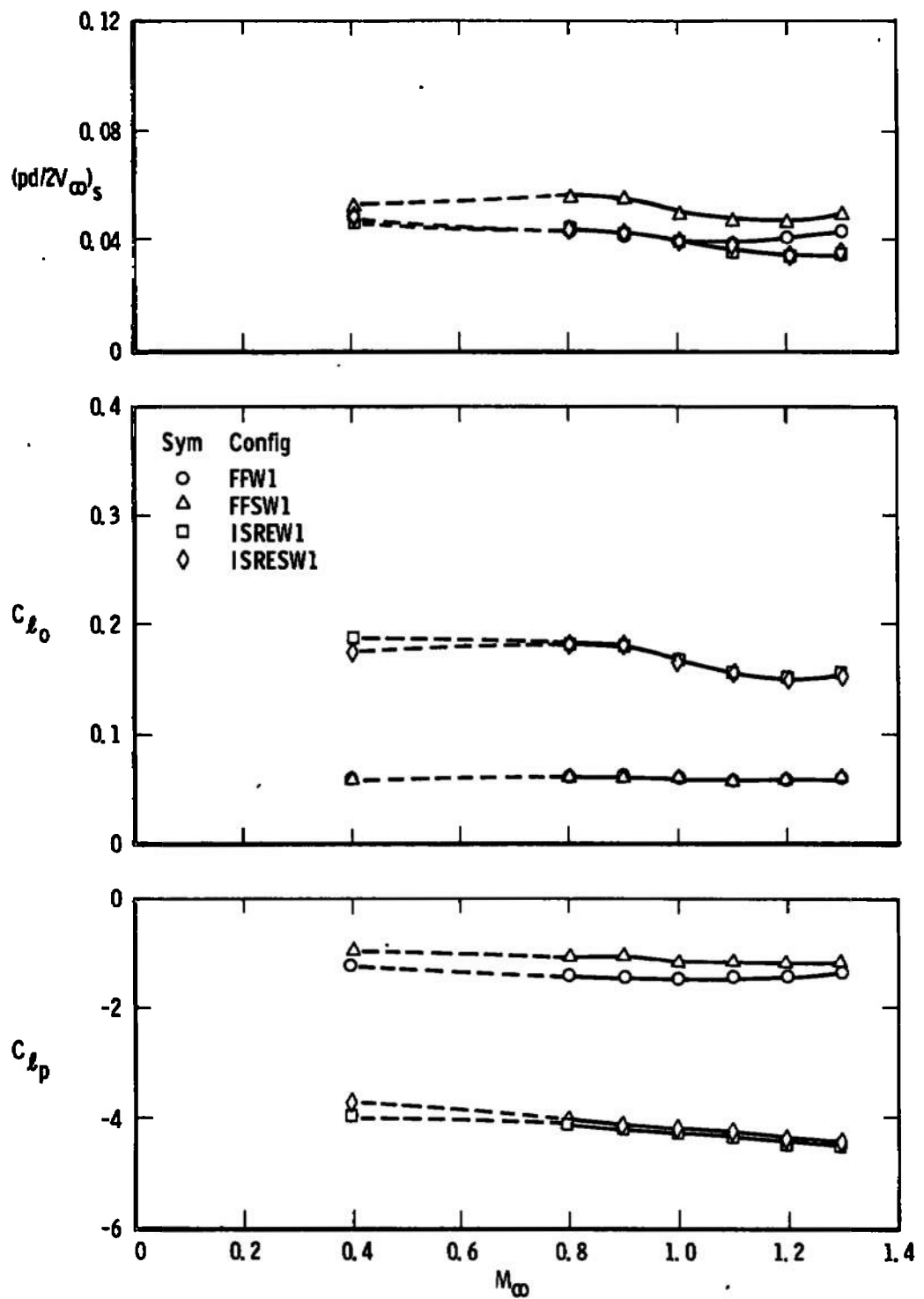
b. $a = 10$ deg
Figure 28. Continued.

135
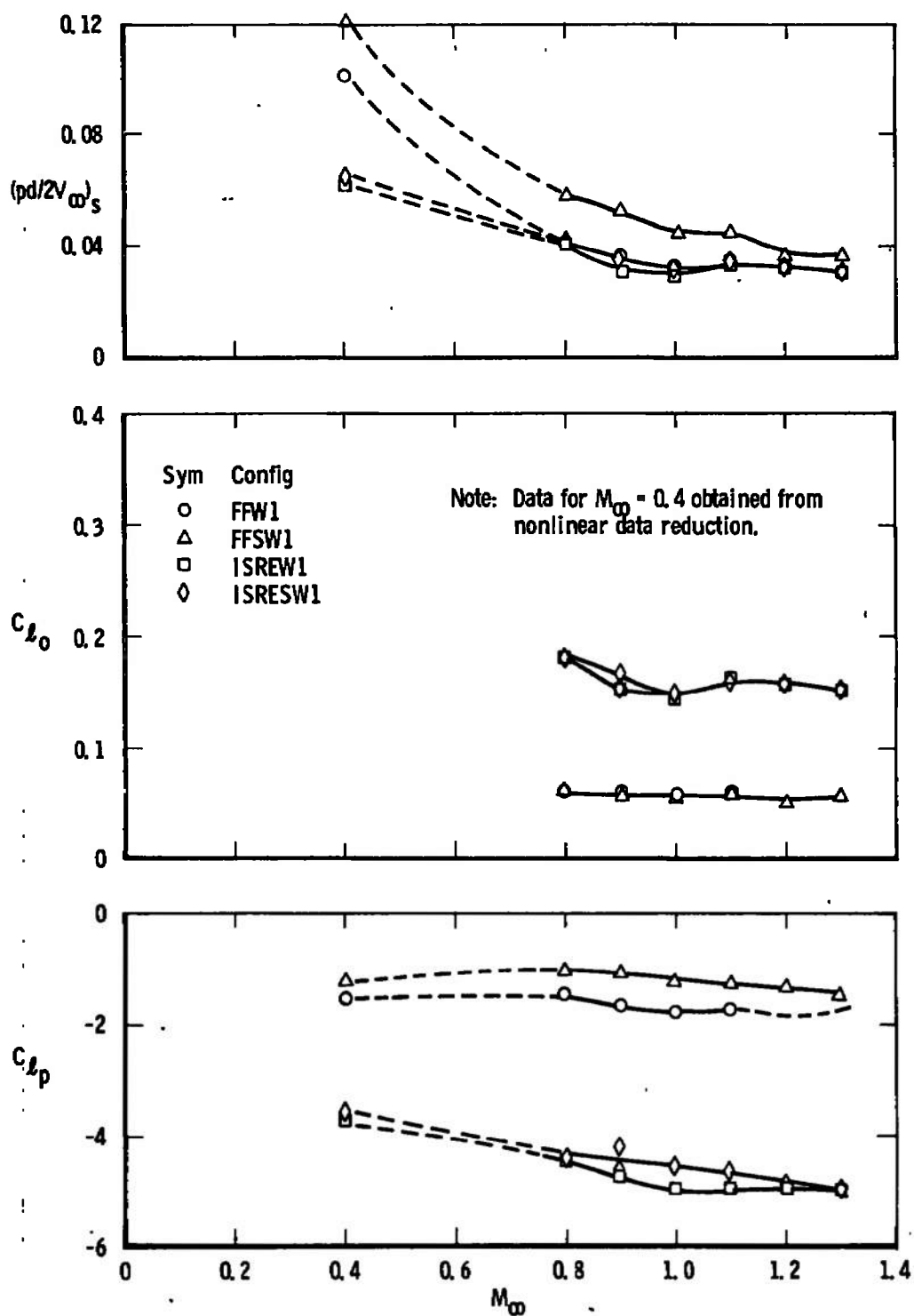
c. $a = 20$ deg

Figure 28. Concluded.

Table 1. Test Summary and Model Parameters

Configurations	Angle of Fin Wedges, deg	Fin Slots	I_x, ft-lb-sec^2	Mach Numbers Tested*
FF	0	No	0.0230	B
FFW1	15	No	0.0231	A
FFW2	25	No	0.0231	B
FFS	0	Yes	0.0229	B
FFSW1	15	Yes	0.0230	A
FFSW2	25	Yes	0.0230	B
ISRE	0	No	0.0391	B
ISREW1	15	No	0.0393	A
ISREW2	25	No	0.0395	B
ISRES	0	Yes	0.0389	B
ISRESW1	15	Yes	0.0391	A
ISRESW2	25	Yes	0.0393	B

Reference lengths and area:

d = 4.750 in.
A = 17.7205 in.^{2}

*Mach numbers tested

A, 0.4, 0.8, 0.9, 1.0, 1.1, 1.2, 1.3
B, 0.8, 1.0, 1.2

p_o = 1,200 psfa
T_o = 560°R
α = -2 to 26 deg

137

NOMENCLATURE

A Reference area, model nominal cross-sectional area, 17.7205 in.^{2}

C_ℓ Rolling-moment coefficient, rolling moment/$q_\infty Ad$

C_{ℓ_o} Rolling-moment coefficient at zero roll velocity

C_{ℓ_p} Rolling-moment coefficient attributable to roll velocity $\partial(C_\ell)/\partial(pd/2V_\infty)$ per radian

C_m Pitching-moment coefficient, pitching moment/$q_\infty Ad$

C_{m_a} Pitching-moment coefficient derivative, $\partial C_m/\partial a$, per deg (-2.5 $<$ a $<$ 2.5 deg)

C_N Normal-force coefficient, normal force/$q_\infty A$

C_{N_a} Normal-force coefficient derivative, $\partial C_N/\partial a$, per deg (-2.5 $<$ a $<$ 2.5 deg)

C_n Yawing (Magnus)-moment coefficient, yawing moment/$q_\infty Ad$

C_{n_p} Magnus-moment spin derivative coefficient, $\partial C_n/\partial(pd/2V_\infty)$, per radian, (0 $<$ $pd/2V_\infty$ $<$ 0.04)

$C_{n_{pa}}$ Magnus-moment coefficient derivative, $\partial^2 C_n/\partial(pd/2V_\infty)\partial a$, per radian^2, (-2 $<$ a $<$ 2 deg)

C_Y Side (Magnus)-force coefficient, side force/$q_\infty A$

C_{Y_p} Magnus-force spin derivative coefficient, $\partial C_Y/\partial(pd/2V_\infty)$, per radian (0 $<$ $pd/2V_\infty$ $<$ 0.04)

$C_{Y_{pa}}$ Magnus-force coefficient derivative, $\partial^2 C_Y/\partial(pd/2V_\infty)\partial a$, per radian^2, (-2 $<$ a $<$ 2 deg)

d Reference diameter, model nominal diameter, 4.750 in.

I_x Model mass moment of inertia about spin axis, ft-lb-sec^2

L Total rolling moment, ft-lb

L_o Rolling moment at zero spin rate, ft-lb

L_{o_a} L_o aerodynamic

L_{O_V} L_O balance tare in a vacuum (zero for this report)

L_p Rolling-moment derivative $\partial L/\partial p$, ft-lb-sec/radian

L_{p_a} L_p aerodynamic

L_{p_V} L_p balance tare in a vacuum (-0.0003 ft-lb-sec/radian for this report)

M_∞ Free-stream Mach number

p Model spin rate, $\partial\phi/\partial t$, (positive, clockwise viewing from the base), radians/sec

p_i Initial p at time zero

$\dot{p}$ $\partial p/\partial t$, radians/sec

p_o Tunnel stilling chamber pressure, psfa

p_∞ Free-stream dynamic pressure, psfa

$pd/2V_\infty$ Spin parameter, radians

$(pd/2V_\infty)_s$ Steady-state spin parameter, radians (zero bearing friction)

p_{ss} Steady-state spin rate, radians/sec (zero bearing friction)

q_∞ Free-stream dynamic pressure, psfa

Re_d Free-stream Reynolds number based on model diameter (d)

t Time, sec

T_o Tunnel stilling chamber temperature, °R

T_∞ Free-stream temperature, °R

V_∞ Free-stream velocity, ft/sec

$(X_{cp}/d)_N$ Center of pressure in the pitch plane in calibers from the nose (note: caliber = 4.750 in.), $X_{MR} - (C_{m_\alpha}/C_{N_\alpha})_{\alpha=0}$

$(X_{cp}/d)_Y$ Magnus center of pressure in calibers from the nose (note: caliber = 4.750 in.), $X_{MR} - (C_{n_{p_\alpha}}/C_{Y_{p_\alpha}})_{\alpha=0}$

X_{MR} — Moment reference point in calibers from the nose, 3.8661 calibers for FF configuration and 3.6440 calibers for ISRE configuration

a — Angle of attack, deg

ϕ — Roll angle, radians

ϕ_i — Initial ϕ at time zero